The University Of Sheffield.

On the dynamic stability of surface grinding: the role of the specific energy in regenerative chatter

Author:
Máté Tóth

Supervisors:
Prof Neil Sims
Dr David Curtis

A thesis submitted in partial fulfilment of the requirements for the degree of Doctor of Philosophy

Department of Mechanical Engineering
The University of Sheffield
March 2020

Acknowledgements

First of all, I would like to express my sincere gratitude to Prof Neil Sims for his encouragement and support over the past four and a half years. Your understanding and gentle yet firm communication of my strengths and weaknesses have been of tremendous value to me, not only in this project but regarding my future career as well.

I also wish to thank Dr David Curtis for his insight into the practical aspects of this research, along with Gary McKee and Andrew Winder for their assistance with the experiments. I truly appreciate your skills and commitment, which were indispensable to the completion of this work.

I am very grateful to the Industrial Doctorate Centre, the Dynamics Research Group and the Machining Dynamics Group for their ability and willingness to give me professional advice whenever I needed it. It was a pleasure to be working with you all.

And most of all, I am deeply thankful to my family and friends, including my church family both in Hungary and in England, for their constant love and presence in my life. Without you, I would not have been able to complete this research. Your support, especially in times of disappointment and discouragement, has been an invaluable source of motivation and strength.

The author acknowledges funding provided by the Engineering and Physical Sciences Research Council (EPSRC) for the Industrial Doctorate Centre (IDC) in Machining Science (Grant Reference Number: EP/L016257/1).

To God alone be the glory.

Summary

Chatter or unstable relative vibration between the cutting tool and the workpiece is a serious problem in the machining industry. It harmfully affects virtually all chip formation processes, such as turning, milling, drilling, boring and grinding. Among other negative consequences, these vibrations are responsible for deteriorating the surface quality and dimensional accuracy of the final product, reducing the lifetime of the cutting tool, and generating unpleasant noise. They are self-excited oscillations, which means that the dynamic instability of the machining process originates and develops from within itself. Avoiding chatter was tightly connected to severe limitations on productivity for a very long time, and in fact, this approach remains the regular practice of several companies to this day. Much research has been done in order to mitigate this issue by creating models capable of predicting the boundaries between stable and unstable cutting processes. One of the primary aims of such work is to avoid chatter without reducing productivity beyond what is necessary.

This thesis focuses on the dynamic stability of one chip formation process in particular, namely surface grinding, and investigates the role of the specific energy in chatter development. The specific energy is a fundamental quantity in grinding that defines a relationship between the material removal rate and the corresponding power consumption. The main novelty of this research lies in the proposal of a new mechanism by which instability can occur. The literature is clear that wheel-related chatter is a consequence of uneven wear around the circumference of the grinding wheel, which is almost exclusively modelled as uneven material loss resulting in a non-circular wheel surface. While this approach is certainly true to reality, wheel wear or grit dullness is reflected not only in a reduced wheel radius but also in an increased specific energy. In other words, based on the definition of the specific energy, a dull grain corresponds to a higher specific energy than a sharp one. This research aims to explore the effect of a wear-induced variation in specific energy on the dynamic stability of surface grinding.

The new chatter theory developed in this thesis is capable of capturing wheel-related instability as a consequence of an uneven specific energy distribution around the circumference of the grinding wheel. Stability boundaries and chatter frequencies are predicted by the model and validated by experiments. Considering the relative simplicity of the proposed theory, it provides remarkably accurate results. The main finding of this work is a chatter-free zone corresponding to high productivity with virtually no coverage in the literature, yet very promising potential in practice.

Table of Contents

List of Tables

List of Figures

Table of Nomenclature

Due to the fact that certain quantities have traditional notations in the literature (e.g. both the coefficient of friction and the mean of a probability distribution are denoted by μ), a few symbols have multiple meanings in this thesis. Avoiding duplicate notations would have been possible only at the expense of clarity, which the author has decided against. The following table highlights those instances where more than one definition corresponds to the same symbol. These are relatively rare and fairly easy to discern.

Symbol	Description
α	empirical exponent, only in Eq. (2.12)
	grinding force angle (Chapters 4 and 5)
	cutting point angle of the grain model (Figure 5.12 and Chapter 6)
β	empirical exponent
γ	empirical exponent
Γ_F	graph of the Nyquist plot
Γ_s	graph of the Nyquist contour
δ	instantaneous depth of cut
δ_0	nominal depth of cut
ε	empirical exponent (Section 2.2.4.2)
	radius of infinitesimal detours in the Nyquist contour (Figure 5.7)
ζ	damping ratio of the grinding wheel (Chapters 4, 5 and 6)
	damping ratio characterising relative stability (Chapters 5 and 6)
μ	coefficient of friction, only in Eq. (2.7)
	mean of a normal distribution (Chapter 4)
	grinding force ratio between F_t and F_n (Chapter 5)
μ_x	grinding force ratio between F_x and F_t
ξ	small perturbation on top of the forced vibration in x
ρ_j	random constant for each grit generating an irregular distribution
σ	standard deviation of a normal distribution
τ	rotation period of the workpiece (Chapter 2)
	grit-passing period (Chapter 4)
	local time coordinate fixed to the grinding zone (Chapter 5)
$\tilde{\tau}$	variable of integration in Eq. (5.17)
τ_c	actual immersion time of a single grain
$\tau_{c,0}$	quasi-steady immersion time of a single grain
τ_g	grit-passing period
τ_j	random grit-passing period corresponding to grit j

Symbol	Description
φ	angular coordinate in the grinding zone
φ_c	instantaneous contact angle
$\varphi_{c,0}$	nominal contact angle
φ_{en}	entering angle of the grinding zone
φ_{ex}	exiting angle of the grinding zone
φ_g	pitch angle between grits
φ_j	angular position of grit j on the grinding wheel
ϕ_j	pitch angle of grit j
Φ_x	Laplace transform of F_x
$\Phi_{x,a}$	Laplace transform of $F_{x,a}$
$\Phi_{x,i}$	Laplace transform of $F_{x,i}$
$\Phi_{x,w}$	Laplace transform of $F_{x,w}$
ω	angular frequency, imaginary part of s
ω_c	chatter frequency in rad/s
ω_g	rotational speed of the grinding wheel
ω_n	natural frequency of the grinding wheel in rad/s
ω_p	grit-passing frequency
a	generalised system parameter, only in Eq. (2.1)
	arbitrary constant, only in Eq. (4.48)
	index abbreviating 'arithmetic mean' (Chapter 5)
	coefficient of the fitted exponential (Chapter 6)
A	wear-flat area
b	generalised system parameter, only in Eq. (2.1)
	coefficient of the fitted exponential (Chapter 6)
c	generalised system parameter, only in Eq. (2.1)
	modal damping of the grinding wheel (Chapter 4)
C_a	time-independent part of $F_{x,a}$
C_d	dynamic cutting edge density (Chapter 2)
	coefficient of dulling (Chapter 5)
C_i	time-independent part of $F_{x,i}$
c_n	Fourier coefficients
C_n	j-independent part of c_n
C_s	static cutting edge density
C_w	time-independent part of $F_{x,w}$
D	Laplace transform of δ
D_1	empirical exponent
D_2	empirical exponent
D_3	empirical exponent
d_e	equivalent grinding wheel diameter
d_g	grain diameter
f	arbitrary function, only in Eq. (4.48)
	probability density function of a normal distribution (Chapter 4)
F	total grinding force (Figure 4.1)
	Laplace transform of f, only in Eq. (4.48)
	characteristic function (Appendix A)

Symbol	Description
F_a	characteristic function corresponding to the arithmetic mean
f_c	chatter frequency in Hz
F_i	characteristic function corresponding to $i = a$ or $i = w$
$F_{j,n}$	normal component of the cutting force acting on grit j
$F_{j,t}$	tangential component of the cutting force acting on grit j
$F_{j,x}$	x-component of the cutting force acting on grit j
f_n	natural frequency of the grinding wheel in Hz
F_n	normal component of the total grinding force
$F_{n,c}$	cutting component of the normal grinding force
$F_{n,ch}$	chip formation component of the normal grinding force
$F_{n,pl}$	ploughing component of the normal grinding force
$F_{n,sl}$	sliding component of the normal grinding force
F_t	tangential component of the total grinding force
$F_{t,c}$	cutting component of the tangential grinding force
$F_{t,ch}$	chip formation component of the tangential grinding force
$F_{t,pl}$	ploughing component of the tangential grinding force
$F_{t,sl}$	sliding component of the tangential grinding force
F_x	x-component of the total grinding force
$F_{x,a}$	F_x corresponding to the arithmetic mean of u in the grinding zone
$F_{x,d}$	dynamic part of F_x
$F_{x,i}$	F_x corresponding to one of the two averaging methods ($i = a, w$)
$F_{x,s}$	static part of F_x
$F_{x,w}$	F_x corresponding to the weighted mean of u in the grinding zone
G	structural dynamics of the system (Chapters 4 and 5)
	grinding ratio (Chapters 5 and 6)
$\hat{\mathbf{GH}}$	doubly infinite open-loop transfer function matrix
g_j	unit step function selecting whether grit j is in or out of cut
G_M	gain margin
$\hat{g}_{p,p}$	matrix elements according to Eqs. (4.55) and (4.85)
h	total chip thickness
H_a	transfer function between U and $\Phi_{x,a}$
h_d	dynamic chip thickness
H_i	transfer function between U and $\Phi_{x,i}$
h_j	total chip thickness cut by grit j
$\hat{h}_{p,q}$	matrix elements according to Eqs. (4.56) and (4.86)
h_s	static chip thickness
$h_{s,max}$	theoretical maximum of the static chip thickness
H_w	transfer function between U and $\Phi_{x,w}$
i	imaginary unit (Chapters 4 and 5)
	general index for a or w referring to the averaging method (Chapter 5)
	integer counting wheel periods, only in Figure 5.21
I	input function of the block diagram in Figure 4.5
$\mathbf{I}$	identity matrix
I_j	integrand corresponding to grit j (Section 4.1.3)
j	grit index

Symbol	Description
J	transfer function between D and U
k	modal stiffness of the grinding wheel (Chapters 4 and 6)
	Taylor index (Chapter 4)
	arbitrary integer identifying the pole-zero structure of $T_{i,o}$ (Chapter 5)
K	number of Taylor terms considered (Figure 4.11)
K_d	dynamic cutting-force coefficient
$K_{D,ch}$	chip formation coefficient in Eq. (2.13)
$K_{D,pl}$	ploughing coefficient in Eq. (2.13)
$K_{D,sl}$	sliding coefficient in Eq. (2.13)
$K_{L,ch}$	chip formation coefficient in Eq. (2.12)
$K_{L,sl}$	sliding coefficient in Eq. (2.12)
K_n	normal cutting-force coefficient
K_s	static cutting-force coefficient
K_t	tangential cutting-force coefficient
K_W	factor of proportionality in Eq. (2.9)
m	modal mass of the grinding wheel
m_1	physical mass of the grinding wheel labelled as GW-1 (Table 6.2)
m_2	physical mass of the grinding wheel labelled as GW-2 (Table 6.2)
M_k	k^{th}-order raw moment of a normal distribution
n	number of high spots on the surface of the wheel (Chapter 2)
	Fourier index (Chapter 4)
N	number of Fourier terms or harmonics considered (Chapter 4)
	number of Nyquist encirclements (Appendix A)
p	index identifying the harmonics in X
P	total grinding power (Chapter 2)
	number of poles of F encircled by Γ_s (Appendix A)
P_M	phase margin
q	cutting-force exponent (Chapter 4)
	auxiliary index defined as $q = p - n$ (Chapter 4)
Q_w	instantaneous volumetric material removal rate
$Q_{w,0}$	nominal volumetric material removal rate
r	radius of the semicircular arc in the Nyquist contour (Figure 5.7)
r_g	half-length of the base of the triangular grain model (Figure 5.12)
R_g	nominal grinding wheel radius
$R_{g,\text{after}}$	grinding wheel radius after an experiment
$R_{g,\text{before}}$	grinding wheel radius before an experiment
s	complex Laplace frequency
t	global time coordinate
T_1	s-independent part of $T_{a,o}$
T_2	s-dependent part of $T_{a,o}$
$T_{a,o}$	T_o corresponding to the arithmetic mean of u in the grinding zone
T_c	closed-loop transfer function
T_g	rotation period of the grinding wheel
$T_{i,c}$	T_c corresponding to either of the two averaging methods ($i = a, w$)
$T_{i,o}$	T_o corresponding to either of the two averaging methods ($i = a, w$)

Symbol	Description
T_o	open-loop transfer function
$\mathbf{T}_o$	open-loop transfer function matrix
u	total specific grinding energy
U	Laplace transform of u
u_c	specific cutting energy
u_{ch}	specific chip formation energy
u_{past}	effect of the past on the specific energy, defined in Eq. (5.16)
u_{pl}	specific ploughing energy
u_{pres}	effect of the present on the specific energy, defined in Eq. (5.17)
u_{sl}	specific sliding energy
v_g	circumferential speed of the grinding wheel
V_g	volume of abrasive material removed from a single grain
v_w	feed rate (linear speed of the workpiece relative to the wheel)
V_w	volume of workpiece material removed by a single grain
V'_w	specific volume of workpiece material removed by a single grain
w	grinding width (predominant meaning throughout the thesis)
	index abbreviating 'weighted mean' (Chapter 5)
W_w	Laplace transform of V_w
x	general coordinate describing the displacement of the cutting tool
X	Laplace transform of ξ (Chapter 4)
	Laplace transform of x (Chapter 5)
$\hat{\mathbf{X}}$	vector collecting the harmonics in X
x_0	steady-state displacement of the cutting tool
x_p	part of x corresponding to periodic forced vibration
$\hat{x}_p$	elements of vector $\hat{\mathbf{X}}$ according to index p
$\hat{x}_q$	elements of vector $\hat{\mathbf{X}}$ according to index q
y	general spatial coordinate, used only in Figure 6.9
z	general spatial coordinate, used only in Figure 6.9
Z	total number of grits on the wheel (Chapters 4 and 5)
	number of zeros of F encircled by Γ_s (Appendix A)

Declaration

I, the author, confirm that this thesis is my own work. I am aware of the University's guidance on the use of unfair means (`www.sheffield.ac.uk/ssid/unfair-means`). This work has not previously been presented for an award at this or any other university.

Part of this research has been published in the following conference paper:

Tóth, M., Sims, N. and Curtis, D. (2019) An analytical study of wheel regeneration in surface grinding. In: *Procedia CIRP*. 17th CIRP Conference on Modelling of Machining Operations, 13-14 Jun 2019, Sheffield, UK. Elsevier, pp. 214-219.

`https://doi.org/10.1016/j.procir.2019.04.046`

Chapter 1

Introduction to modern manufacturing

This thesis is concerned with the dynamics and stability of abrasive machining. To set the scene for the research, the present chapter summarises the modern approaches to the manufacturing of structural components, particularly focusing on the use of abrasive operations and the vibration challenges that can arise.

In general terms, manufacturing is a process through which raw materials are transformed into finished products. It is a highly versatile field of modern industry and an indispensable, yet often hidden part of life in the 21st century. The history of manufacturing goes back thousands of years, and probably originated with prehistoric man's need and desire to modify the shapes and sizes of certain materials (e.g. a stone) in order to make tools capable of performing specific functions (e.g. cutting animal hides) [1]. Manufacturing has come a long way since its inception and has grown both in productivity and in sophistication since its early days. Modern manufacturing is one of the most essential components of developed economies and societies, without which products and services expected and regarded as natural by modern man – such as mobile phones, tablets, computers, cars, aeroplanes, optical devices, prosthetic implants and pharmaceutical drugs – would be impossible. Due to the significant advancement of the manufacturing sector, especially over the past couple of centuries or so, the term 'manufacturing' has become very broad and encompasses a wide range of engineering processes today (e.g. chemical manufacturing, drug manufacturing, electronics manufacturing, etc.). Since this research is concerned with the manufacturing of structural components, unless otherwise noted, the term 'manufacturing' will be used in this particular sense throughout the rest of the thesis. However, even such a focused view of manufacturing includes a number of engineering processes in industry, therefore, it is helpful to put them into different categories for the sake of clarity and understanding. The following section continues to discuss modern manufacturing operations by classifying them according to additive, formative and subtractive procedures.

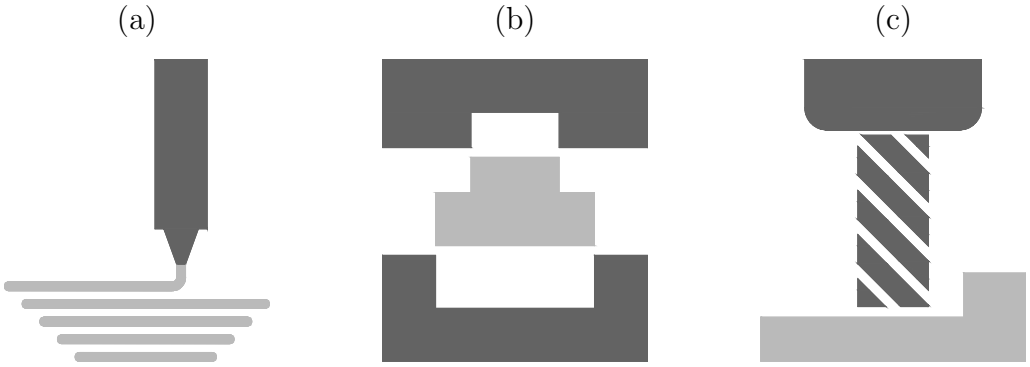

Figure 1.1: A schematic representation of modern manufacturing technologies: (a) additive, (b) formative, and (c) subtractive processes

1.1 Additive, formative and subtractive processes

Manufacturing operations today can be fundamentally divided into additive, formative and subtractive processes [2]. A schematic representation of these three categories is given in Figure 1.1. Additive manufacturing (also known as 3D printing) is a relatively modern procedure, dating back to the end of the 20th century, through which a mass of raw material is transformed into a desired shape, typically layer by layer. The particles of the starting material, most commonly in the form of a powder or a wire, are joined or solidified together with more and more material being added in order to create a finished product. 3D printing is an exceptionally diverse and versatile manufacturing operation, capable of producing highly complex parts with very little waste. Formative processes, such as bending, forging and casting, neither add material to nor remove material from the workpiece. Their aim is to modify the shape of the base material by applying mechanical forces to it (bending), or heating it up and hammering it (forging), or melting it, pouring it into a mould and allowing it to cool down and solidify (casting). Typical examples of products manufactured in formative ways are bended metal tubes, rings, flanges, gears, firefighting equipment, fire hydrants, bronze plaques, etc. Since the in-depth study of additive and formative processes is outside the scope of this work, they are mentioned only for the sake of completeness and perspective. More information on 3D printing and formative operations can be found in several technical books, such as those listed in [2–4].

The topic of this research lies within the sphere of subtractive manufacturing (also known as machining), which is a collective term for a number of processes governed by the principle of material removal, i.e., a solid block of raw material is cut by a machine tool in order to achieve a desired shape. Due to their limited line of sight, subtractive manufacturing operations are unable to create certain design features (e.g. lattices, hollow parts and very intricate, organic geometries such as those presented in [5]), and they also generate significantly more waste than additive processes, however, the physical properties (e.g. strength) of printable materials may be less desirable (or even inadequate for certain practical applications) than those of machinable materials [6]. Therefore, the overall relationship between additive and subtractive manufacturing operations is not primarily competitive but complementary [7].

Figure 1.2: Conventional (left) and abrasive (right) cutting tools

1.2 Conventional and abrasive operations

Subtractive manufacturing processes can be further divided into three categories: conventional, non-conventional and hybrid machining operations. Conventional or traditional processes are characterised by direct contact between the tool and the workpiece. Regarding the cutting tool, it is possible to distinguish between defined cutting edges (e.g. turning, milling, drilling) and non-defined cutting edges (e.g. grinding). In non-conventional or non-traditional operations, the energy that is required for material removal is transmitted without direct contact between the tool and the workpiece. Some of these processes are ultrasonic machining (USM), laser beam machining (LBM), electron beam machining (EBM), electrical discharge machining (EDM), and electrochemical machining (ECM) [8]. Hybrid operations aim to exploit the advantages of multiple machining processes, typically by combining a conventional and a non-conventional one to create a new machining operation, such as laser-assisted turning or electrochemical milling [9].

However, the terminology describing all these different categories of subtractive manufacturing tends to be rather loose in practice. For example, it is not uncommon in the context of conventional processes (as defined in the previous paragraph) to refer to machining with defined and non-defined cutting edges as conventional and abrasive operations, respectively. This means that grinding, for instance, is set apart from conventional processes and regarded as an abrasive operation. The rest of the thesis adopts this terminology in order to avoid lengthy definitions when it comes to characterising cutting tools with defined and non-defined cutting edges.

Figure 1.2 is presented to visualise the difference between these two categories. It can be seen that conventional cutting tools are typically marked by regular, well-defined shapes, whereas abrasive cutting tools are usually characterised by irregular, ill-defined geometries. In terms of their respective wear rates, abrasive tools – by virtue of being made up of small particles bonded together with pores between them – tend to be structurally weaker and thus more prone to material loss (i.e. wear) than conventional tools under

similar machining circumstances, however, actual wear rates largely depend on the tool and workpiece materials, cutting parameters, cooling conditions, etc. [10]. For example, in grinding, the ratio between the amount of material removed from the workpiece and the amount of material lost from the wheel can cover an extremely wide range of values from less than unity to more than 60 000 (according to Malkin and Guo [11], p. 287).

Some of the most common conventional machining operations are turning, milling and drilling. Turning is a process in which a single-point cutting tool plunges into and removes material from a rotating workpiece. Turning tools typically move in the axial and radial directions of a cylindrical workpiece. Milling is an operation where the rotating component is the cutting tool, which removes material by advancing into the workpiece. The feed direction in milling is usually perpendicular to the axis of the cutting tool. Drilling is a process that uses a rotating drill bit to cut a circular hole in a stationary workpiece. As opposed to milling, the feed direction in drilling is always parallel to the axis of the cutting tool. Unlike turning, milling and drilling tools often have multiple cutting edges. Typical parts machined by conventional operations are shafts, axles, pins, screws, threaded rods, camshafts, pipes, valves, flanges, etc. Further information on conventional processes can be found in a number of machining books, such as [12–14].

Examples of the most widely used abrasive operations include grinding, honing and polishing. Grinding is a collective term for machining processes that utilise small, abrasive particles called grits or grains bonded into a wheel as a cutting medium to produce parts. Each abrasive particle acts as a microscopic cutting tool with the potential to remove material from the workpiece. Of all subtractive manufacturing operations (both conventional and abrasive), this work focuses on grinding processes, therefore, a short historical overview of grinding is provided in the next section.

1.2.1 The early days of grinding

Grinding is probably the oldest machining operation in existence [16], dating back to prehistoric man and his discovery of being able to sharpen his tools by rubbing them against hard, gritty surfaces like rocks and sandstones. Metal grinding, along with the invention of the grinding wheel, originated in ancient Egypt around 2000 BC. Up until the Industrial Revolution, grinding was mainly used for sharpening and polishing tools, weapons and armour. Early concepts of grinding machines were developed by Leonardo da Vinci (1452-1519), whose famous mirror grinding machine is presented in Figure 1.3. Leonardo's ideas were not put into practice until the 19th century when the necessary grinding wheel technology became available to be effectively utilised by industrial grinding machines. The advancement of grinding technology continued in the 20th century when superabrasives, such as diamond and cu-

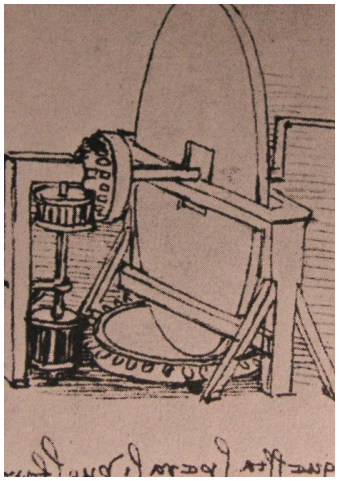

Figure 1.3: Leonardo's mirror grinding machine [15]

bic boron nitride (often abbreviated as CBN), were developed and first introduced to the machining world, pushing and expanding the boundaries of efficiency and machinability. This is a very brief account of the early days of grinding based on a short overview provided by Malkin and Guo [11], and serves the primary purpose of putting the subject at hand in a historical perspective. More detailed surveys on the origin and development of grinding can be found in the works of other authors, such as [17–21].

1.2.2 Grinding in the 21st century

As highlighted in [11], p. 1, approximately one quarter of all machining costs are attributed to grinding operations in the 21st century, which is a significant share of the manufacturing sector in developed countries. This means that more products than probably most people realise have been machined at least in part by grinding, or to put it another way, could not have been adequately manufactured without abrasive processes. The uniqueness of grinding lies in its cutting tool. Grinding wheels are made up of two main components: abrasive particles and a bonding agent or matrix. The most common abrasives today are aluminium oxide (Al_2O_3), silicon carbide (SiC), diamond and CBN, the last two being superabrasive materials. There are six general bond types for conventional abrasives: resinoid, shellac, oxychloride, rubber, silicate and vitrified, although most conventional wheels have either resinoid or vitrified bonds (according to [11], pp. 11-30). Superabrasive wheels are typically produced with three bond types: resinoid, vitrified and metal.

Grinding is commonly considered a finishing operation, capable of producing smooth surfaces and observing fine tolerances. And indeed, when it comes to precision machining, it is among the best and most widely implemented processes in industry (as stated in [11], pp. 1-2). However, grinding is not limited to delicate finishing operations alone, but is often used for stock removal as well. Such grinding processes – like creep-feed grinding (CFG) and high-efficiency deep grinding (HEDG) to name a couple of them – work with high depths of cut and low feed rates, and are able to reach such high material removal rates that can only be matched by conventional machining operations. Thus, once its full potential has been exploited, grinding is a very efficient and versatile machining process. The versatility of grinding is also demonstrated by the numerous wheel-workpiece arrangements available to the machinist. As illustrated in Figure 1.4, some of the simplest and most common configurations are external and internal cylindrical grinding, surface grinding and centreless grinding – all of which can also be either traverse or plunge grinding, depending on the applied feed direction [22]. Apart from the principal feed (i.e. the linear motion of the workpiece relative to the wheel in surface grinding, and the rotational motion of the workpiece in cylindrical and centreless grinding), two additional or secondary feed directions can be distinguished. In traverse grinding, this is the crossfeed, and it is parallel to the workpiece surface and the wheel axis as well. In plunge grinding, the secondary feed is the infeed, and it is perpendicular to the workpiece surface and the wheel axis as well. Although the terms ‘crossfeed’ and ‘infeed’ are quite descriptive of the motions that they represent, sometimes they are used interchangeably with reference to the secondary feed direction.

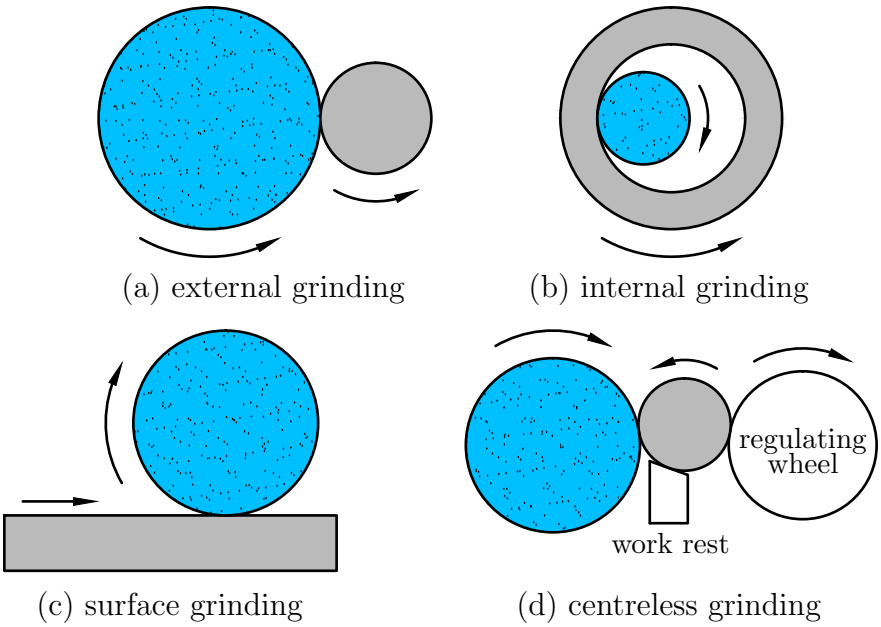

(a) external grinding (b) internal grinding

(c) surface grinding (d) centreless grinding

Figure 1.4: Common arrangements of the wheel (blue) and the workpiece (grey)

Besides achieving high material removal rates and producing outstanding surface quality and dimensional accuracy, abrasive operations also excel at cutting difficult-to-machine materials, such as hardened steels, ceramics and glasses (as asserted in [11], pp. 2-3). However, despite its many advantages, grinding is often regarded by machinists as a necessary evil rather than a potent and versatile machining operation. This is in part owing to the fact that grinding is the least understood of all machining processes due to its inherent complexities, such as the irregular geometry and significant wear of the tool, which make it especially complicated to accurately predict the behaviour of grinding operations. Much research has been done, particularly over the past few decades, in order to transform the 'black art' of grinding (learning by experience and practice) into an applied science (learning by theoretical research and practical validation) [11, 23, 24]. This work continues to improve on the predictability of grinding operations by focusing on the above-mentioned complexities and addressing them by scientific means.

In conclusion, it can be seen that grinding has a long history and has come a long way from being prehistoric man's way of sharpening his tools to becoming modern man's way of manufacturing a multitude of parts, thus enabling him to build complex machines such as gas turbines and aircraft engines.

1.3 Forced and self-excited vibrations

This research focuses on one of the most harmful phenomena in chip formation processes, namely the onset of sustained relative vibration between the workpiece and the cutting tool. Virtually all conventional and abrasive operations are affected by it, and as far as grinding is concerned – which is the primary topic of this research, these vibrations can

be either forced or self-excited in nature [25].

Forced vibrations are relatively easy to detect and suppress by locating and eliminating their sources through frequency measurements. Typical causes of forced vibrations are common machine faults, such as imbalance, misalignment, wear and looseness. The detection and elimination of such vibration sources is one of the main purposes of machine fault diagnosis and condition monitoring. More information on these topics can be found in [26–30].

Self-excited vibrations (or chatter as they are often referred to) are much more complex than forced vibrations, and suppressing them is significantly more complicated than locating and eliminating a machine fault. As Frederick Taylor famously put it in 1906, *"chatter is the most obscure and delicate of all problems facing the machinist, and [...] probably no rules or formulae can be devised which will accurately guide the machinist in taking the maximum cuts and speeds possible without producing chatter"* [31]. Machine tool chatter is indeed an especially intricate problem and has been a topic of extensive research since Taylor's day up to the present time [32–35]. The primary motivation to understand the dynamics of chatter lies in the fact that unstable relative vibration between the workpiece and the cutting tool has a strong negative effect on the entire machining process. Chatter deteriorates the surface quality and dimensional accuracy of the workpiece, reduces the lifetime of the cutting tool, generates unpleasant noise, and limits productivity on the manufacturing floor. Therefore, predicting and avoiding self-excited machine tool vibrations is of critical importance when it comes to ensuring the stability, efficiency and productivity of machining operations.

In general, there are four different types of machine tool chatter: frictional, regenerative, mode-coupling and thermomechanical [36]. These mechanisms are not independent of each other, and can generate different types of chatter at the same time. However, the most common reason for unstable machine tool vibrations is the so-called regenerative effect, which is an effect of the past, i.e., the vibrations of the system in the past influence the vibrations of the system in the present in such a way that leads to instability (according to Stépán [33], p. 136). In most machining processes, the tool removes material from the workpiece in a gradual manner. This means that the machine tool will periodically cut a workpiece surface that was already cut at some point in the past. Therefore, as a new workpiece surface is generated, or in other words, as the workpiece surface is regenerated, the effect of the past (e.g. waviness on the workpiece surface) will influence the present. For example, a wavy workpiece surface – which can be the result of tool vibration in the past due to some external perturbation – and an oscillating cutting tool in the present can produce a varying chip thickness, which ought to be constant under ideal circumstances (as graphically illustrated in Figure 1.5). This will generate a varying cutting force which will in turn disturb the tool displacement, resulting in a new, wavy workpiece surface. Under certain conditions, which have to do with the phase angle difference between two successively generated workpiece surface waves, the above-described regenerative vibration can get locked into a state of unstable growth. That is why chatter refers to self-excited vibration – the excitation of the system originates and develops from within the system itself. Investigating the conditions under which such a state of unstable self-excitation can occur constitutes a major part of this work.

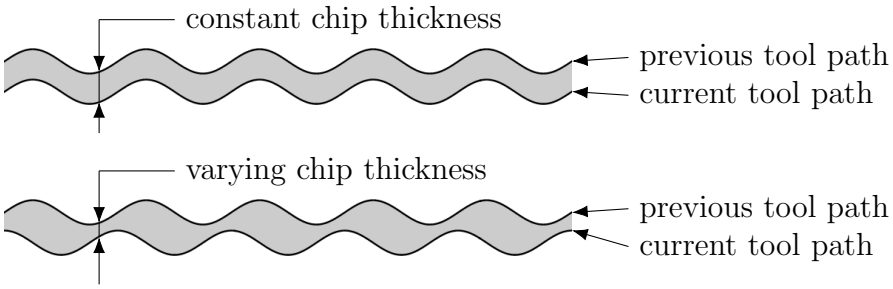

Figure 1.5: Two successively generated workpiece surface waves: in phase with a constant chip thickness (top) and out of phase with a varying chip thickness (bottom)

Similarly to conventional machining processes, grinding is also prone to regenerative chatter. More than that, in the case of grinding, self-excited vibration can be even more harmful due to the fact that grinding is often a finishing operation and thus responsible for the final state (surface quality and dimensional accuracy) of the workpiece. Therefore, grinding chatter has the potential to destroy a part at the final stage of its production. Consequently, understanding the intricate nature of grinding chatter is of crucial importance when it comes to designing grinding processes. That is what this research seeks to advance – the current knowledge of grinding with regard to dynamics and vibration in order to enhance product quality, process efficiency and machine productivity by predicting and avoiding grinding chatter.

The following chapter presents a brief overview of regenerative chatter in conventional machining operations and a detailed, chronological review of the literature's most relevant papers on the historical development of regenerative chatter theories in grinding. Each contribution is discussed and evaluated on an individual basis before it is placed in the context of grinding dynamics at large. However, before moving on to the literature review in detail, the knowledge gap and the research aims are foreshadowed in the next section in order to briefly articulate the motivation for this work and the expected outcome of the thesis.

1.4 Knowledge gap and research aims

In summary, this research is concerned with the dynamics and stability of abrasive machining in general, and the self-excited vibrations of grinding processes in particular. Combining the inherent uncertainties of machining with thousands of irregular and geometrically ill-defined cutting edges with the intricacies of modelling and predicting regenerative chatter vibrations, the resulting problem is highly complex yet very practical. That is why a significant amount of research has been dedicated already to addressing the issue of grinding chatter with the aim of avoiding or at least suppressing it as much as possible. Despite the fact that a lot has been discovered about grinding chatter as a result of persistent and hard work over many decades, the problem remains an active area of research to this day.

This thesis seeks to gain a better understanding of a fundamental aspect of grinding chatter that is scarcely addressed in the literature and therefore constitutes a gap in current knowledge, namely the specific mechanism by which wheel-related regeneration occurs and thus wheel-related instability develops. The details of this statement are presented at length in Chapters 2 and 3. Following a literature review (Chapter 2), the aims and objectives of this research are revisited and expanded upon (Chapter 3), in order to set out the original contributions of the remaining chapters.

Chapter 2

Literature review on regenerative machine tool chatter

As it was stated in Section 1.3, virtually all chip formation processes are prone to experiencing sustained relative vibration between the workpiece and the cutting tool. It has also been mentioned that, with regard to grinding – which is the main topic of this work, these harmful vibrations can be either forced or self-excited in nature [25]. This chapter is dedicated to reviewing the literature on regenerative machine tool chatter (which is the most common type of chatter in machining [33,36]) briefly for conventional processes and more thoroughly for abrasive operations.

2.1 Chatter in conventional machining

Machine tool chatter in conventional operations has been a topic of extensive research since the beginning of the 20th century. After the initial observations of Taylor [31], a number of researchers attempted to explain and describe machine tool vibrations in a systematic way [37–39], however, it was not until 1958 that a comprehensive mathematical model of machine tool chatter was developed by Tobias and Fishwick [40]. Their theory was also one of the first accurate models of self-excited vibration in orthogonal cutting, along with the works of Tlusty and Polacek [41], and Merritt [42]. These authors are among the most prominent pioneers of advanced research in machine tool chatter, having built the foundations for those coming after them. Their fruitful labour has encouraged several future researchers and initiated a substantial amount of work now published in the literature on the origin and suppression of self-excited machining vibrations. Despite Taylor's rather negative presumption that *"probably no rules or formulae can be devised which will accurately guide the machinist in taking the maximum cuts and speeds possible without producing chatter"* [31], rules and formulae have in fact been discovered, governing the behaviour of self-excited machining vibrations in a predictable way. Some of the greatest researchers in the field have written many significant books and papers to provide a physical explanation and a mathematical description for such an intricate phenomenon

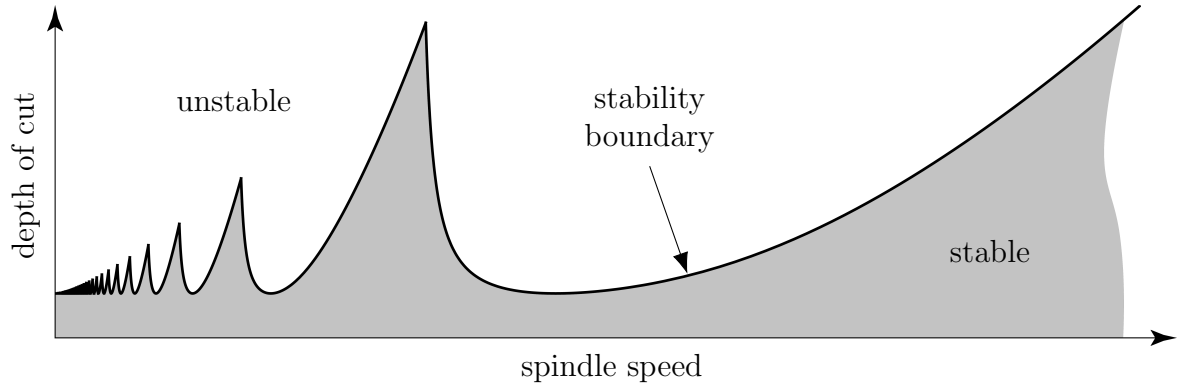

Figure 2.1: Example of a typical stability lobe diagram for turning [87]

as machine tool chatter. The most widely known and frequently cited sources include but are not limited to the works of Altintas [35, 43–47], Budak [36, 43, 45–51], Tlusty [34, 41, 52–55], Marui [56–62], Ismail [53, 54, 63–66], Insperger [67–73], Stépán [33, 67–70, 72–77], Schmitz [73, 78, 79], Tobias [32, 40, 80] and Ota [81–83]. Since the detailed discussion of these publications (which are still only a small fraction of the entire body of work on machining vibrations) is outside the scope of this research, a few large-scale reviews of the literature will be presented later in this section, in order to provide some preliminary insight into decades' worth of hard work in this area. Although the references above will not be revisited one by one, a number of them will be cited again to support the main summarising statements that the present author has made regarding the historical development and current state of research in machining dynamics.

It can be seen that the amount of work conducted in the field of machine tool chatter since Taylor's day is indeed vast. As demonstrated by the citations above, numerous in-depth studies have been published on turning [83–85], milling [43, 55, 72] and drilling operations [57, 59, 60], in order to gain a deeper understanding of the intricate nature of machining vibrations. As a result of perseverance and success in research, not only have chatter prediction and suppression techniques become widely available, but they have also been growing more and more advanced and sophisticated in recent decades [86]. Consequently, the maximum cuts and speeds possible without producing chatter have increased, which is a major improvement since Taylor's famous quote predicting the contrary. One of the most often-used ways to demonstrate progress and development in machining stability is the construction of so-called stability charts or stability diagrams. They were invented to visualise the stability properties of machine tools, and have been around since the first comprehensive chatter theories were formulated [40–42]. Because of their outstanding utility and clarity, the usage of such graphical tools is common practice in machining dynamics today [35]. Stability charts are usually two-dimensional figures that plot the stability boundaries of a machining process against two cutting parameters, such as the spindle speed and the depth of cut (an example of a typical stability lobe diagram is presented in Figure 2.1). Sometimes multiple stability boundaries are plotted in the same stability chart in order to demonstrate the effect of a third parameter under investigation. Mathematically speaking, the dynamics of machining operations is governed by so-called delay differential equations (DDEs), where the derivative of the unknown function at a certain time is given in terms of the values of the function at previous times. For example,

the general form of the DDE corresponding to Figure 2.1 can be written as

$$\ddot{x}(t) + a\dot{x}(t) + bx(t) = cx(t - \tau). \tag{2.1}$$

Similarly to the first appearance of stability lobe diagrams in the literature, a fundamentally identical variation of Eq. (2.1) was first developed by the aforementioned pioneers of rigorous chatter research, in order to capture the dynamics of machine tools by mathematical means [40–42]. In Eq. (2.1), the function $x(t)$ describes the displacement of the turning tool in time, the coefficients a, b and c are generalised system parameters, and τ denotes the time delay which is equal to the rotation period of the workpiece. The dot symbol represents the first and second derivatives of x with respect to time. It can be seen that apart from the typical terms of an ordinary differential equation (ODE), the time-delayed version of the tool displacement appears in Eq. (2.1) as well, indicating the effect of the past on the behaviour of the system in the present (as discussed earlier in Section 1.3). Although the equation of turning displayed above is considered a relatively simple DDE, the stability analysis of Eq. (2.1) is still significantly more complicated than that of an ODE [88]. The primary purpose of presenting an equation of motion so early on is to put the dynamics of machining in a mathematical context. The stability of DDEs can be assessed in a number of ways, which will be discussed in later chapters.

As mentioned earlier in this section, a few large-scale reviews of machine tool chatter are presented now in order to provide a concise yet non-exhaustive overview of the topic.

In 1997, Ehmann et al. published a summary paper on modelling the dynamics of machining processes [89]. They critically reviewed the corresponding literature and identified four general types of modelling approaches: analytical, experimental, mechanistic and numerical. They also distinguished between three existing philosophies which relate the dynamic cutting force to the instantaneous uncut chip cross section, the shear plane area, and non-linear mechanisms. Each modelling approach considers one (or more) of these philosophies in order to determine the dynamic cutting force. Citing the works of several researchers, the authors carefully and systematically presented the evolution of dynamic cutting process modelling up to 1997. They claim that, due to the complexity of machining operations, the prevailing modelling approach in the 20th century relied heavily on assuming a single, presumably dominant mechanism of the cutting process, and testing the model against experimental data. However, as a result of such significant simplification, a number of empirical coefficients were necessitated in order to make up for the intentionally neglected modelling details. This problem called for a compromise to be made between the accuracy and simplicity of the proposed model. It is also noted by the authors that a combination of various modelling approaches was yet to be realised in 1997. As a conclusion, the authors also included a brief assessment of perceived needs and potential directions of research in the future. A graphical summary of their review is presented in Figure 2.2.

In 2011, Quintana and Ciurana wrote an article in an attempt to review and summarise the state of research on machine tool chatter, including both conventional and abrasive operations [90]. The paper contains an introduction of considerable length, discussing the history and relevance of chatter in machining. It also touches on the four mechanisms of self-excitation (friction, thermomechanics, mode coupling, regeneration) and states that

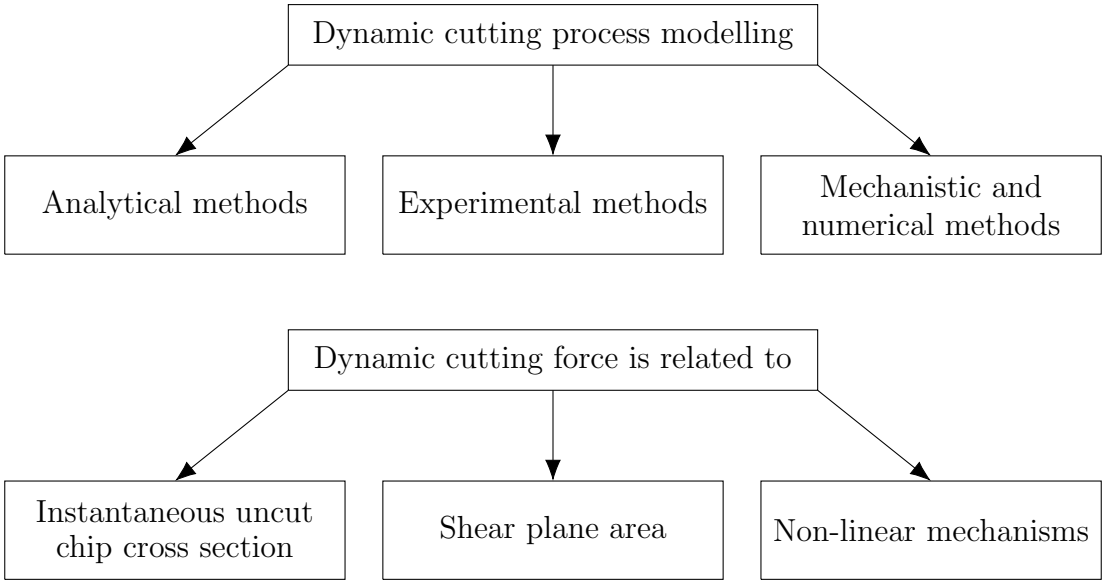

Figure 2.2: Chatter modelling approaches and philosophies as reviewed in [89]

surface regeneration is the most important cause of chatter. That is why – unless otherwise specified – 'chatter' usually refers to regenerative chatter, which is a convention that has been generally followed by the majority of publications on the subject. Concluding the first section, the identification and purpose of stability lobe diagrams are discussed in order to provide a sufficiently detailed background for the following chapters. Having reviewed a great deal of literature, the authors arrived at a classification of chatter prediction and suppression methods according to two main approaches. The first one consists of methods that ensure a stable machining operation by considering the so-called lobe effect and choosing stable cutting parameters accordingly. Regarding this group, it is possible to differentiate between out-of-process and in-process methods. Out-of-process approaches aim to identify the stability lobes and select a stable set of cutting parameters before the machining operation begins. In-process methods, however, detect chatter during the metal cutting process and correct the system parameters in order to achieve a stable manufacturing operation. The second approach includes methods that avoid chatter by changing the dynamics of the machine and thus manipulating the lobe structure of the system in order to ensure stable machining conditions for a desired set of cutting parameters. In this group, passive and active methods can be distinguished. Passive strategies rely on the modification of certain machine tool elements in order to change the dynamics of the system (e.g. variable pitch and variable helix tools). Active strategies seek to suppress chatter by introducing active elements and system modifications, such as tunable vibration absorbers and spindle speed variation. The principal lines of research as summarised by Quintana and Ciurana are presented in Figure 2.3.

In 2015, Insperger et al. presented a brief overview of the two intrinsic components of machine tool chatter modelling, namely the regenerative time delay and the parametric excitation of the cutting edges [91]. After a short introduction concerning the basics of chatter in machining (e.g. surface regeneration and stability lobe diagrams), an important qualitative difference is made between turning and milling operations in terms of their respective mathematical models. In turning, regenerative chatter can be described by

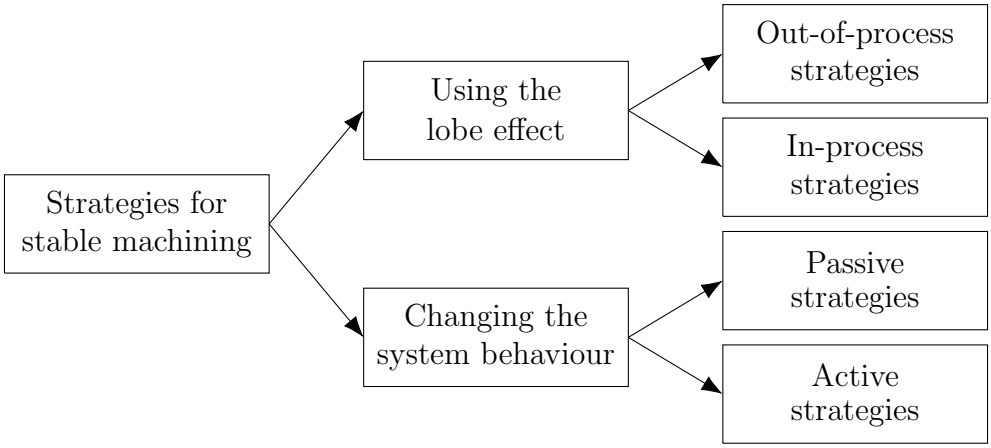

Figure 2.3: Principal lines of research on chatter suppression techniques [90]

time-invariant DDEs, i.e., the coefficients a, b and c in Eq. (2.1) are independent of time t. The stability of such systems can be assessed by the classical D-subdivision method [33]. In milling, however, surface regeneration is coupled with the parametric excitation of the cutting edges, which results in a DDE with time-periodic coefficients. This means that b and c will appear in Eq. (2.1) as periodic functions of time, where the common time period is equal to the principal period of the system, corresponding for instance to the tooth-passing period for uniform-pitch tools and to the rotation period of the cutter for variable-pitch tools. The stability analysis of milling processes is different from that of turning operations and requires the application of the Floquet theory to adequately predict the stability properties of a time-periodic system. Although – due to the presence of parametric excitation – the stability lobe diagrams cannot be determined analytically in milling, a number of numerical solutions have been formulated over the past few decades in order to deal with the mathematical complexity of milling stability analysis. Such techniques include but are not limited to the semi-discretisation method [92, 93] and the multi-frequency solution [43, 94, 95]. A graphical summary of the two intrinsic components of machine tool chatter modelling as reviewed by Insperger et al. is presented in Figure 2.4. It is an interesting question whether grinding can be affected by parametric excitation and thus the corresponding governing equation of motion can feature time-periodic coefficients. Since a grinding wheel can be thought of as a milling tool with a large number of microscopic cutting edges, the theoretical answer is yes, however the vast number of cutting points may render this phenomenon negligible in practice. This issue will be discussed later on in this thesis (Chapter 4).

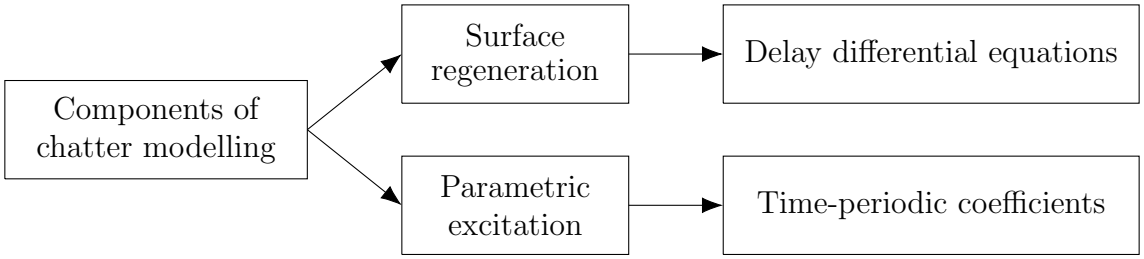

Figure 2.4: Intrinsic components of machine tool chatter modelling [91]

In 2016, a comprehensive review of chatter suppression techniques in metal cutting was presented by some of the most respected and well-known experts in the field of machining science [86]. Containing 358 references, it is potentially the most all-inclusive review on chatter prediction and suppression methods today. The paper begins with an introduction that summarises the main reasons for continued research on the subject of machine tool chatter and classifies the available solutions developed to tackle the problem of self-excited vibrations in machining processes. A graphical review of the existing chatter suppression techniques listed by the authors is given in Figure 2.5. The most suitable of these methods for a given scenario is to be selected based on three criteria: machinability (which may limit the available range of spindle speeds), the relative location of chatter in the stability diagram (which is defined by the ratio of the chatter frequency to the tooth passing frequency), and the critical elements of the system (which can be the machine tool structure, spindle, tool, toolholder, workpiece, etc.). The rest of the review elaborates in great detail on the different chatter suppression techniques listed at the beginning of the paper, and concludes with a very useful and concise table summarising the most suitable chatter suppression methods depending on the origin of vibration in the system and the qualitative location of chatter in the stability lobe diagram. Finally, the authors highlight the ongoing necessity of improving the robustness and simplicity of existing chatter suppression techniques, while acknowledging the fact that production engineers already have a wide range of working solutions to industrial chatter problems.

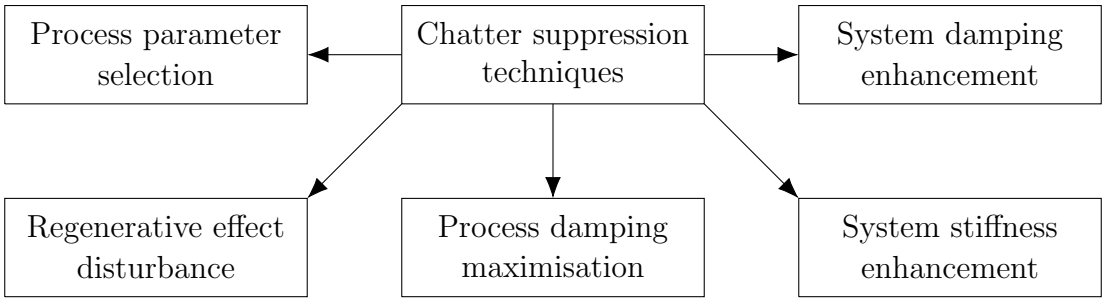

Figure 2.5: Chatter suppression techniques in metal cutting [86]

The fact that such a vast amount of research has been published in machining dynamics since Taylor's day demonstrates both the complexity of machine tool chatter and the necessity to predict and avoid it. There is still much to be discovered and understood, however, Taylor's initial presumption about a harmful yet rather elusive phenomenon without rules or formulae has been thankfully allayed by human perseverance and skill. The following section focuses on self-excited vibration in abrasive machining processes as opposed to conventional operations, and presents a detailed review of grinding chatter in particular, in order to provide an up-to-date historical background for this research.

2.2 Chatter in abrasive machining

As a result of extensive research in machining science, the 20th century brought significant advancements and improvements in grinding technology, including the complex area

of grinding dynamics. Taylor's famous work titled *On the art of cutting metals* and published at the very beginning of the century [31] was followed by a number of articles on machining dynamics, addressing the intricate nature of machine tool chatter. However, progress in understanding grinding dynamics and developing accurate chatter theories was lagging behind the findings of similar works in conventional machining operations for a number of years (as claimed by Stone [96], pp. 135-136). Again, this is in part due to the inherent complexities involved in abrasive processes (i.e., irregular tool geometry and significant tool wear), which made it difficult for grinding to keep up with conventional machining. Nevertheless, grinding chatter has been a topic of substantial research for decades, which is clearly reflected in the number and content of scientific papers available on the subject.

In order to establish an initial, rudimentary understanding of self-excited vibration in grinding, the problem is first discussed in the context of conventional chatter (reviewed briefly in Section 2.1). When it comes to the physical explanation and mathematical description of chatter, grinding exhibits some important differences from turning and milling. Based on the review of Insperger et al. [91], these differences will be investigated with regard to surface regeneration and parametric excitation. Similarly to turning and milling operations, surface regeneration is the leading cause of chatter in grinding processes as well [25]. However, due to the fact that grinding wheels wear significantly faster than conventional tools, surface waves can develop not only on the workpiece but also on the grinding wheel. This unique and rather complex phenomenon called 'double regeneration' sets grinding apart from other machining operations both physically (as described above) and mathematically (i.e., an additional time delay is necessary to describe the effect of wheel regeneration). In terms of parametric excitation, it is an interesting question whether individual grit impacts can be responsible for such an effect. The literature predominantly (if not without exception) assumes that parametric excitation is negligible in grinding. However, it is important to verify such an assumption, even if it sounds intuitive to most researchers. Since a grinding wheel can be thought of as a milling tool with many cutting edges, presumably there exists a certain number of grits above which the effect of parametric excitation or the intermittent nature of the grinding process can be neglected. Chapter 4 is dedicated to answering this question and considering its consequences. Section 2.2.1 presents some of the most pivotal chatter theories in grinding and attempts to trace the development of grinding dynamics over the past few decades.

2.2.1 Review of chatter theories

One of the first research papers addressing the issue of regenerative chatter in grinding operations was published by Hahn in the 1950s [97]. He considered a single-degree-of-freedom model of internal cylindrical grinding (illustrated in Figure 1.4b) with a perfectly wear-resistant wheel, thus allowing surface regeneration to occur only on the workpiece. Hahn also assumed a line contact between the wheel and the workpiece (instead of a finite area), therefore, in principle, his theory is equally applicable to turning processes. Hahn based his stability analysis on the proportionality between the instantaneous depth of cut and the instantaneous grinding force, and derived a second-order differential-difference

equation (or delay differential equation in modern terms) to determine the stability of the system. He showed that the time delay or the time period of the rotating workpiece has a significant impact on the distribution of stable and unstable parameter regions, and concluded that as long as the unstable zones are avoided (or the stable zones are favoured), productivity can be increased without compromising the dimensional accuracy and surface quality of the final product. Hahn's contribution is pivotal not only to the understanding of grinding chatter but also to the initiation of further in-depth research in the dynamics of abrasive machining.

Only a few years after the foundational work of Hahn, the experiments of Landberg [98] demonstrated that grinding wheels do not necessarily wear evenly over time and surface regeneration can affect not only the workpiece but the grinding wheel as well. Although his measurements clearly supported the existence of high spots or uneven wear around the circumference of the grinding wheel, he provided no physical explanation as to how such surface waves gradually develop. He proved the presence of wheel-related instability by recording a vibration frequency that was a multiple of the wheel speed and the multiplier was equal to the number of waves on the surface of the wheel. Additionally, Landberg's experiments also revealed that the amplitude growth of grinding vibrations is exponential in nature. Therefore, Landberg's work is significant, because it builds on and advances the existing understanding of grinding chatter by establishing a link between grinding dynamics and surface topography with regard to both the wheel and the workpiece.

Building on the experimental foundation laid by Landberg that grinding wheels do not necessarily wear evenly [98], Gurney postulated his theory as to how uneven wheel wear can lead to unstable vibration in grinding [99]. He called his explanatory mechanism 'surface wave instability', carefully and purposefully differentiating it from the concept of regenerative chatter for two reasons. First, the physics behind surface wave instability – Gurney states – is different from the mechanisms that govern regenerative chatter. In order to substantiate his claim, the author provides the following rationale. The initial irregularities on the surface of the grinding wheel can be expanded into a Fourier series, where each term is responsible for vibration at an integer multiple of the wheel speed. For example, considering only one Fourier term at a vibration frequency $n\omega_g$ (where n is an integer and ω_g is the wheel speed), there will be n high spots on the surface of the wheel, resulting in a periodic variation in the grinding force (n times per wheel revolution). If the maximum grinding force occurs when a high spot is cutting, then the high spot will wear more and the irregularity of the wheel surface will decrease. However, if the maximum grinding force occurs when a low spot is cutting, then the low spot will wear more and the irregularity of the wheel surface will increase. This is also a self-excited vibration, but – according to the author – it is different from surface regeneration.

The second reason Gurney gives why surface wave instability is distinct from regenerative chatter has to do with their respective time scales. While chatter builds up in a matter of seconds, surface wave instability takes minutes to develop. In his mathematical analysis, Gurney considered cylindrical plunge grinding and derived the corresponding equation of motion, which is a non-autonomous DDE with a single time delay equal to the rotation period of the workpiece. The author also presented a couple of stability diagrams depicting the 'depth of cut coefficient' or 'cutting force coefficient' against the vibration

frequency. Gurney's experiments are in acceptable agreement with his theory, and they also demonstrated a rather interesting phenomenon: as the waves on the surface of the wheel grow under unstable grinding conditions, they do not remain stationary but slowly precess around the circumference of the wheel. In terms of his explicit distinction between surface wave instability and regenerative chatter, it is an interesting but rather puzzling idea (even in light of the author's justification), therefore, it will be readdressed in the context of a different chatter theory later on in this section. Nevertheless, Gurney's work is of great significance, being one of the earliest contributions to physically explaining and mathematically describing wheel-related instability in grinding operations.

The next big step in the development of grinding chatter theories was taken by Snoeys and Brown [100], who investigated the dominating parameters in both wheel- and workpiece-related regenerative chatter. They created a mechanical model of external cylindrical plunge grinding and constructed a block diagram in order to represent the mathematical model of the problem in a graphical way. Their block scheme clearly indicates that wheel- and workpiece-related regenerative chatter are not studied separately but in relation to one another. Then the transfer function of the process is derived, which is defined as the ratio of the instantaneous depth of cut to the instantaneous infeed, in order to investigate the stability properties of the system. The main grinding parameters appearing in the transfer function and thus influencing stability are identified as the cutting stiffness, wheel wear resistance, contact stiffness and machine stiffness. Snoeys and Brown provided a set of very helpful tables summarising the dominating grinding parameters with respect to regenerative chatter along with their respective ranges of practical values. They also drew attention to a couple of geometrical limitations to grinding chatter, namely transverse feed filtering and filtering due to the finite length of contact. Transverse feed filtering happens because the actual width of contact is reduced by applying a transverse feed. Filtering due to the finite length of contact is a result of high frequency vibrations being filtered out or cut off from the surface of the wheel or the workpiece. Snoeys and Brown performed a number of experiments to verify their theoretical findings. They managed not only to validate their model but also to demonstrate – similarly to Gurney's research [99] – that wheel undulations slowly precess or travel around the circumference of the grinding wheel. Additionally, they concluded that most grinding operations take place under unstable conditions, in which case the growth rate of chatter becomes more important and more interesting than stability itself. The work of Snoeys and Brown is of central significance – it is one of the first research papers discussing both wheel and workpiece regenerative chatter in the same model.

By the end of the 1960s, the fundamental grinding parameters governing self-excited vibration had been identified, and the first chatter theories had been developed and experimentally validated. The idea of 'double regeneration' or simultaneous surface regeneration on both the wheel and the workpiece was taken further on by Thompson, who confirmed and deepened the scientific understanding of grinding chatter by several of his works [101–105]. Before the primary years of his contribution to double regeneration though, Thompson published a substantial piece of work on the dynamic behaviour of surface grinding [106, 107]. His theory predicts the possibility of unstable grinding vibrations and reveals some important facts about the frequency of these oscillations. First, the unstable vibrations of a surface grinder can occur at only one frequency. Second,

Case	Natural frequency [Hz]	Chatter frequency [Hz]	
		Theory	Experiment
#1	190.19	223.66	221.19
#2	249.87	276.61	277.36
#3	312.10	333.95	334.57

Table 2.1: Summary of Thompson's results at $\omega_g = 3000$ rpm [107]

this single chatter frequency is always higher than the system's uncoupled fundamental resonant frequency. Third, the self-excited vibrations – which correspond to surface lobes on the grinding wheel – can be represented as a sum of two frequency components: the lobe frequency and the precession frequency. The lobe frequency is always an integer multiple of the wheel speed, corresponding to the number of wheel lobes that develop under unstable cutting conditions. The precession frequency is a small part of the overall chatter frequency and describes the rate at which surface lobes travel around the circumference of the grinding wheel. In order to validate his mathematical model, Thompson performed some surface grinding experiments and recorded data for three different test conditions. His theoretically predicted and experimentally determined chatter frequencies are summarised and compared in Table 2.1. The two being in good agreement, Thompson's results are both clear and reliable, contributing to the overall understanding of wheel-related surface regeneration in grinding.

The literature on grinding chatter was thoroughly reviewed by Inasaki et al. [25]. Theirs is a pivotal paper that not only summarises and clarifies the findings of the 20th century, but also advances research and knowledge by addressing the origin and suppression of grinding chatter in a systematic way. The authors restate and emphasise the difference between forced and self-excited vibrations in order to provide a solid and clear starting point. Before getting on to the stability analysis, they draw attention to the well-known feature of grinding chatter that surface regeneration can affect both the workpiece and the wheel. Agreeing with Snoeys and Brown, they arrive at the conclusion that even though wheel-related chatter develops much more slowly than workpiece-related chatter, most grinding operations are unstable with regard to wheel-related chatter. Building on the work of Snoeys and Brown, the authors point out some of the key grinding parameters that govern process stability. After discussing the negative effects of grinding chatter on the dimensional accuracy and surface quality of the final product, they present different ways to monitor, detect and suppress chatter vibrations in grinding systems, which is one of the main accomplishments of their paper. Among other conclusions, they state that although the mechanisms of self-excited vibration in grinding have been made clear from a theoretical point of view, there are still many complications involved (such as the identification and variation of machine characteristics and grinding parameters), which make it difficult to accurately assess machining stability. Nevertheless, the paper of Inasaki et al. has been recognised as one of the most fundamental and most often-cited works in the history of grinding chatter research.

At this point, it is timely to revisit Gurney's distinction between surface wave instability and regenerative chatter [99], because interestingly, Inasaki et al. make no difference between the two. More than that, they cite Gurney's work as a publication on wheel regenerative chatter without any reference to his distinction or terminology. Inasaki presents wheel-related instability in grinding as a phenomenon that takes much longer to develop than workpiece regeneration, but is still a result of the well-known regenerative effect. The significant difference between the time scales of wheel- and workpiece-related instability was noted by Gurney as well, however, he understood it as evidence against surface regeneration. Agreeing with Inasaki, many other prominent authors also consider the regenerative effect as the most common and most important reason for wheel-related instability in grinding [100–108]. Therefore, due to a lack of sufficient literature-based conviction that there is a significant qualitative difference between surface wave instability and regenerative chatter, the two will be treated as identical in this work. This is common practice in the literature, and strong deviations (such as Gurney's) from the well-established and widely accepted theoretical models and explanatory mechanisms are relatively rare. Nevertheless, such exceptions are still welcome as they can provide fresh and valuable insight into the nature of grinding chatter.

In 2006, a new theory of wheel regenerative chatter was developed and tested by Li and Shin [108]. Summarising the experimental findings of researchers before them [107, 109,110], the authors reiterate the following well-established facts of surface grinding: (1) chatter develops very slowly and occurs even at very low feed rates; (2) at the early stages of chatter, it is not easy to differentiate it from forced vibration or to see chatter marks on the surface of the workpiece; and (3) as chatter becomes more severe, waves on the grinding wheel can be detected and chatter marks on the workpiece can be observed. The most novel contribution of Li and Shin's work is their description of the grinding force as a function of not only the instantaneous chip thickness but also the uneven grit dullness or uneven grit wear around the circumference of the grinding wheel. With the help of their new surface grinding model, the authors managed to shed light on certain measurement results in the literature that previous chatter theories were unable to explain.

Li and Shin listed five such experimental observations: (1) with regard to wheel regenerative chatter, there is no difference between continuous grinding, interrupted grinding and grinding a series of workpieces; (2) the single dominant chatter frequency is approximately an integer multiple of the wheel speed; (3) the precession of wheel undulations is very slow, i.e., the single dominant chatter frequency is almost exactly an integer multiple of the wheel speed; (4) more than one chatter frequency can appear under unstable grinding conditions, all of which are approximately integer multiples of the wheel speed; and (5) as chatter grows, harmonics of the chatter frequencies can be observed.

The model proposed by Li and Shin is numerical in nature. Their approach is similar to a finite element method, since it discretises time and thus the positions of the wheel and the workpiece as well. As it was stated before, the novel idea behind Li and Shin's theory is that the grinding force does not depend on the instantaneous chip thickness alone, but is also influenced by how dull or worn the cutting points currently are. The underlying principle is that a duller grain produces a higher grinding force, because it has a larger specific energy. The specific energy is a fundamental quantity in grinding. It defines a

relationship between the material removal rate and the corresponding power consumption. Or equivalently, it is a measure of how much energy is required to remove a unit volume of workpiece material. Practically speaking, a high specific energy is unwanted, because it is an indication of a challenging grinding process.

Considering grit dullness or grit wear when it comes to calculating the grinding force results in a more accurate and thus more realistic model of wheel regenerative chatter. Li and Shin also performed a number of surface grinding experiments and successfully validated their theory. They compared their predicted and measured chatter frequencies for a number of different grinding scenarios and found them to be in good agreement with each other. Therefore, the work of Li and Shin makes a substantial contribution to grinding dynamics, however, their paper is surprisingly undercited and lacks any real follow-up research. According to the present author's judgement, their new chatter theory not only deserves more attention and credit, but also merits further exploration and investigation. Consequently, one of the main directions of this study is to build and improve on the findings of Li and Shin. As a result of this specific focus, the trend of relevant research papers after 2006 is presented only in essence, summarising the most significant accomplishments without much regard for minor details.

Regenerative chatter in grinding is an actively studied topic of research to this day. Modern stability theories are becoming more and more accurate and sophisticated, describing and explaining the dynamics of grinding processes in greater detail than ever before. Current grinding models address more problems and offer more solutions than the 'mere' suppression of self-excited vibration. Grinding chatter today is often considered alongside a number of other complicating factors, such as non-linear behaviour [111–114], self-interrupted grinding [115], workpiece imbalance [116], and parallel grinding [117]. The list goes on, demonstrating the fact that the development of grinding dynamics models and stability theories has come a long way since Hahn first published his paper on regenerative chatter. Nevertheless, there is a real sense in which the fundamentals of grinding dynamics are still unclear. This is due to the fact that the two inherent complexities of grinding, namely the ill-defined and uncertain geometry and the significant wear of the wheel, continue to pose major challenges to researchers today. These two difficulties are considered and discussed in greater detail in the following sections.

Concluding this overview of existing chatter theories in the literature, Table 2.2 summarises the general flow of the most important accomplishments in grinding stability analysis up to Li and Shin's work at the beginning of the 21st century, which serves as a foundational paper to this research.

2.2.2 Effect of wheel wear

Before Li and Shin's work [108], chatter theories considered wheel wear as material loss from the grinding wheel resulting in a reduced wheel radius, which is exactly what happens in real life. Therefore, wheel wear is often measured by the so-called grinding ratio or G-ratio, which is defined as the volume ratio of the material removed from the workpiece to the material removed from the wheel. Material loss from the grinding wheel (or simply

Author(s)	Year(s)	Main accomplishment(s)
R. S. Hahn	1954	Workpiece regeneration described, stable and unstable parameter regions calculated
P. Landberg	1957	Wheel-related instability discovered, vibration frequencies under unstable grinding conditions observed to be integer multiples of the wheel speed, exponential growth of unstable vibrations recorded
J. P. Gurney	1965	Surface wave instability formulated, precession of wheel undulations measured
R. Snoeys, D. Brown	1969	Wheel and workpiece regeneration combined, dominating grinding parameters determined
R. A. Thompson	1971	Important stability properties of surface grinding (such as chatter frequency and lobe precession) predicted and validated
R. A. Thompson	1974-1992	Different aspects of the doubly regenerative effect (such as chatter growth, contact stiffness and wave filtering) investigated and understood
I. Inasaki et al.	2001	Origin and suppression of grinding chatter thoroughly reviewed and systematically presented
H. Li, Y. C. Shin	2006	New wheel regenerative chatter theory developed and tested: wheel-related instability can be induced by the combined effect of distributed radial wear and distributed grit dullness around the circumference of the wheel

Table 2.2: Summary of pivotal chatter theories in grinding up to Li and Shin's work

wheel wear) can generally be classified as either attritious or fracture wear [118–121].

Attritious wear is a consequence of abrasive particles rubbing against the surface of the workpiece, resulting in the flattening or dulling of the grains (as depicted in Figure 2.6a). The amount of wear – measured by the collective area of wear flats on the surface of the wheel – is directly related to the grinding forces: the duller the wheel, the higher the forces. Malkin and Cook [120] found this relationship to be linear in nature: the wear flat area is proportional to the grinding force. However, they also observed a break in this linear relationship, which they attributed to the presence of a harmful phenomenon called grinding burn. Due to the friction between the wheel and the workpiece, wear flats can generate excessive heat and cause thermal damage to the workpiece. This happens when the collective area of wear flats reaches a critically high value. Additionally, grinding

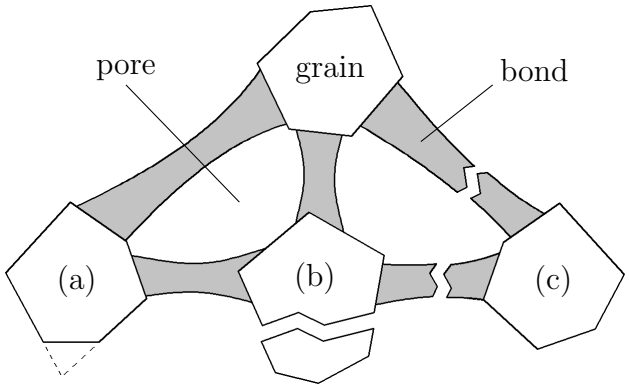

Figure 2.6: Grains affected by (a) attritious wear, (b) grain fracture, and (c) bond fracture

burn not only damages the workpiece but also significantly increases the grinding forces, which has the potential to expedite the onset of chatter. Therefore, grinding burn is to be avoided by all means. Similarly to the grinding forces, the specific energy is also affected by wheel wear – dull grains require more energy to remove the same amount of workpiece material than sharp ones do. In summary, attritious wheel wear has an overwhelmingly negative effect on the grinding process as it reduces efficiency by causing potential burn, producing high grinding forces and increasing the specific energy.

Fracture wear refers to breakage across a grain or across the bond. These two types of fracture wear are called grain fracture and bond fracture, respectively, and they are illustrated in Figures 2.6b and 2.6c. Grain fracture is partial, i.e., only part of the grain is broken off, while bond fracture is total – an entire grain is dislodged and lost as a result. When it comes to typical wear volumes, the amount of fracture wear far outweighs that of attritious wear, however, attritious wear is the most important form of wear as it is directly related to the grinding forces and workpiece burn, thus controlling both grain and bond fracture wear [121]. But unlike attritious wear which is typically undesirable, fracture wear can be beneficial. A partially fractured grain is left with new and sharp cutting edges, while an entirely dislodged grain is replaced by a new, sharp grit. In both cases, fracture wear contributes to an advantageous phenomenon called self-sharpening, a process by which the grinding wheel sharpens itself as it wears.

However, the self-sharpening effect is neither sufficient nor reliable enough to keep the wheel sharp in an accurate and controlled fashion. Therefore, another sharpening method needs to be employed in order to get rid of dull particles and expose fresh grits from the surface of the wheel. This process is called dressing, and it serves three main purposes in grinding: (1) it sharpens the wheel by dislodging worn grains and exposing sharp ones, (2) it cleans the wheel by removing built-up workpiece material from the pores, and (3) it trues the wheel by restoring its intended, original shape. Naturally, the dresser material has to be significantly harder than the wheel material. This is usually achieved with diamond dressers. There are fundamentally two types of dressing: intermittent and continuous. Intermittent dressing means that the wheel is dressed periodically, after a certain amount of grinding time and accumulated wear. Continuous dressing, however, indicates that the wheel is being dressed throughout the entire grinding process. In

this way, the cutting properties of the wheel can be kept under control and relatively constant, but the downside of it is that the wheel is consumed much faster, which means more frequent wheel changes and higher grinding costs.

When it comes to chatter models, wheel wear had only been considered as a change in grinding wheel radius until Li and Shin introduced their new theory in 2006 [108]. Even though their approach takes both wheel radius variation and grain dullness variation into account, it suggests that it is possible to model wheel wear (and thus wheel regenerative chatter) solely based on the grain dullness variation (or specific energy variation) of a perfectly circular circumference, without changing the radius of the grinding wheel. Li and Shin did not consider a self-sharpening wheel, but regarded it as continuously dulling, assuming an approximately linear relationship between the degree of wheel wear and the magnitude of the resulting grinding forces. Despite the significant potential of their new theory, it has received little to no follow-up research. Therefore, the fundamental way to go about wheel wear modelling in terms of grinding chatter has not changed significantly over the past decades. This is in part owing to the fact that old wheel wear theories are reliable and functional, and also that apart from Li and Shin's contribution, the fundamental approach to grinding chatter modelling has not seen a working alternative. However, their work shows that the common understanding of wheel wear with regard to grinding chatter is not yet complete and leaves much to be discovered. Consequently, this research aims to focus on and continue the work that Li and Shin began, in order to shed some more light on the fundamental causes of chatter in grinding.

2.2.3 Effect of wheel geometry

As it was demonstrated in Figure 1.2, unlike conventional cutting tools, abrasive wheels have no clear, well-defined geometry. Within certain limits, they are made up of randomly shaped, sized, oriented and distributed particles. However, the uncertainty of wheel geometry has been somewhat mitigated in recent years by new technologies such as grain shape control (e.g. 3M™ Cubitron™ II Abrasives) and wheel texture customisation [122]. Nevertheless, despite some remarkable advancements in abrasive tooling, the accurate modelling of wheel geometry and the resulting grinding forces remains a significant challenge to this day.

One of the complicating factors in understanding and modelling grinding at a micro level is that not all the specific grinding energy is spent on actual cutting. The total specific grinding energy is distributed among three mechanisms: sliding, ploughing and chip formation [11]. Sliding refers to wear flats rubbing against the surface of the workpiece. In this case, valuable grinding energy is consumed and wasted on heat generation, without any material being removed from the workpiece. Ploughing describes a process by which material is displaced but not removed from the workpiece. Again, grinding energy is consumed by material displacement, but no material is actually removed from the workpiece. Chip formation is the ultimate goal of grinding. It is a mechanism by which material is actually removed from the workpiece in the form of tiny chips. Therefore, as far as material removal is concerned, all the grinding energy that is spent on sliding and ploughing is essentially wasted. After Malkin and Guo (as presented in [11], p. 132), the

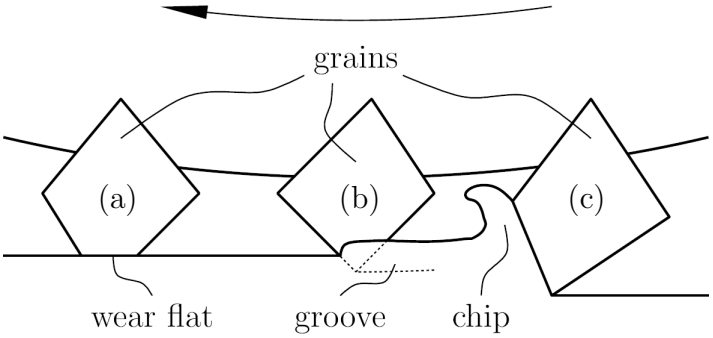

Figure 2.7: Three separate grains demonstrating the three grinding mechanisms: (a) sliding, (b) ploughing, and (c) chip formation

total specific grinding energy can be expressed as the sum of its three components, i.e., chip formation (u_{ch}), ploughing (u_{pl}) and sliding (u_{sl}):

$$u = u_{ch} + u_{pl} + u_{sl}. \tag{2.2}$$

For the sake of clarity, the three grinding mechanisms described above are presented in Figure 2.7 for three separate grains, however, one grain often contributes to all three grinding mechanisms over a single cutting path.

The complexities of the wheel geometry give rise to grinding forces that are rather difficult to predict accurately. Therefore, the next section reviews and discusses a number of existing grinding force models along with their applications to chatter theory.

2.2.4 Review of force models

The literature presents three main approaches when it comes to modelling wheel geometry and the resulting grinding forces: idealised models, empirical models and stochastic models. The terminology describing these three categories is primarily of the present author, therefore, the following subsections are dedicated to explaining and summarising them by reviewing the relevant papers and presenting the corresponding grinding force models.

2.2.4.1 Idealised models

Idealised models are built on solid theoretical foundations, but also make a number of assumptions and simplifications in order to deal with the uncertainty of grinding wheel topography. Although these models often consider micro-level grinding (e.g. chip formation, ploughing and sliding mechanisms), they tend to excessively simplify or even altogether neglect the randomness of grinding wheel geometry. They describe a deterministic system, attempting to approximate the stochastic one as closely as possible while keeping the model simple enough and relatively easy to work with. Ultimately, it is a compromise between accuracy and simplicity. Based on Malkin and Guo's theory [11],

this section presents the main steps of creating an idealised model in order to demonstrate the advantages and limitations of this approach.

As it was stated before, the total specific grinding energy is the ratio of the total grinding power to the volumetric material removal rate according to

$$u = \frac{P}{Q_w}, \tag{2.3}$$

where u is the total specific grinding energy, P is the total grinding power, and Q_w is the volumetric material removal rate. The total grinding power consists of three components, corresponding to the three grinding force components: tangential, normal and axial. However, the normal and axial contributions to the grinding power are usually negligible relative to the tangential one. Also, due to the fact that the wheel speed is typically much higher than the workpiece speed, the power consumption corresponding to the tangential contribution can be calculated by multiplying the tangential grinding force component by the circumferential speed of the grinding wheel. Thus the total grinding power can be approximated as

$$P = F_t v_g, \tag{2.4}$$

where F_t is the tangential grinding force component, and v_g is the circumferential speed of the grinding wheel. It is important to note that the total grinding power described above is always negative, as F_t always acts against v_g, hindering the grinding action and drawing power away from the grinding process. This mathematical fact simply means that electric power has to be constantly supplied to the grinding machine in order to sustain operation.

Based on experimental observations, it was proposed that the grinding force (and thus the specific energy) can be considered as a sum of cutting and sliding components [120]. The cutting force component is responsible for displacing or removing material from the workpiece, whereas the sliding force component is a result of abrasive particles rubbing against the workpiece without actually displacing or removing any material from it. Consequently, the tangential grinding force component can be expressed as a sum of the tangential cutting force component ($F_{t,c}$) and the tangential sliding force component ($F_{t,sl}$) according to

$$F_t = F_{t,c} + F_{t,sl}, \tag{2.5}$$

where $F_{t,sl}$ is dependent on the collective area of wear flats, the average contact pressure between the wear flats and the workpiece, and the coefficient of friction between the wear flats and the workpiece. Since wheel wear only affects the sliding component of the grinding force and the cutting component is constant for a given set of grinding conditions, it is possible to derive the constant cutting component of the grinding force. Combining Eqs. (2.3) and (2.4), and considering that the volumetric material removal rate Q_w is the product of the grinding width w, depth of cut δ and feed rate v_w, the cutting component of the tangential grinding force can be written as

$$F'_{t,c} = u_c \frac{v_w}{v_g} \delta, \tag{2.6}$$

where the prime symbol indicates that the specific grinding force (grinding force per unit grinding width) is used. The specific cutting energy denoted by u_c is the sum of the

specific chip formation and ploughing energies u_{ch} and u_{pl}. Equation (2.6) is one of the simplest ways to formulate the cutting component of the tangential grinding force. It was also found that, unlike $F'_{t,c}$, the cutting component of the total specific grinding energy u_c is not independent of the grinding conditions, but is a function of the specific material removal rate (material removal rate per unit grinding width). Experiments reveal that the specific cutting energy increases hyperbolically as the specific material removal rate decreases [123–125]. This is the so-called 'size effect', and suggests that only part of the specific cutting energy is actually related to chip formation. Thus there must be at least one other grinding mechanism to absorb the rest of the specific cutting energy. This is the mechanism of ploughing, and it was described in Section 2.2.3 and illustrated in Figure 2.7.

The expressions listed above are primarily concerned with the tangential component of the grinding force. However, the normal component can also be of interest, especially when it comes to determining the resultant grinding force in a specific direction. The sliding components of the tangential and normal grinding forces are connected by the coefficient of friction (μ) between the wear flats and the workpiece according to

$$\mu = \frac{F_{t,sl}}{F_{n,sl}}. \tag{2.7}$$

A similar relationship can be established between the cutting components of the tangential and normal grinding forces $F_{t,c}$ and $F_{n,c}$, however, both $F_{t,c}$ and $F_{n,c}$ consist of chip formation and ploughing components denoted by $F_{t,ch}$, $F_{t,pl}$, $F_{n,ch}$ and $F_{n,pl}$, respectively. Experiments show that the chip formation components $F_{t,ch}$ and $F_{n,ch}$ increase linearly with the specific material removal rate, while the ploughing components $F_{t,pl}$ and $F_{n,pl}$ remain approximately constant, i.e., they are independent of the specific material removal rate [123–125]. This is another way to come to the same conclusion that the specific chip formation energy u_{ch} is constant, while the specific ploughing energy u_{pl} changes hyperbolically with the specific material removal rate. Consequently, $F_{t,c}$ and $F_{n,c}$ are constant only for a given set of grinding conditions [11]. Although it is possible to establish a relationship between them, the physical meaning behind the ratio of $F_{t,c}$ to $F_{n,c}$ is not significant enough in terms of grinding chatter to be discussed in this review.

Therefore, it can be seen that an idealised approach does not consider the uncertainty of grinding wheel topography, but assumes an ideal scenario and focuses on a qualitative description of the grinding forces, rather than being concerned with individual abrasive particles. Consequently, the results are less accurate than those produced by more complex and more sophisticated methods, however, an idealised model provides a grinding force expression that is capable of describing self-excited vibration in a simple yet theoretically well-founded way.

2.2.4.2 Empirical models

Empirical models are significantly different from idealised ones. They tend to provide more accurate results than idealised models do – at the expense of relying on a number of empirical constants, often with limited understanding of the physics behind them. This

section presents the most widely accepted grinding force models in the literature, which are used to this day to assess the stability properties of grinding processes.

The following model proposed by Inasaki et al. [126] defines the tangential component of the grinding force as proportional to the specific material removal rate $v_w\delta$ according to

$$F_t' = u\left(\frac{v_w}{v_g}\delta\right)^{\varepsilon}, \tag{2.8}$$

which is very similar to the idealised force model presented before, apart from two main differences. Inasaki et al. do not consider the three grinding mechanisms separately, but describe the tangential component of the grinding force based on what they simply call the 'specific grinding energy' in one of their related articles [127]. The other difference is that the relationship between the grinding force and the specific material removal rate is no longer linear, however, the exponent of non-linearity ε in Eq. (2.8) is estimated to be 0.9 by the authors [127], which is not far from a linear relationship. The biggest advantage of this empirical model relative to the idealised one is that it is able to capture the grinding force characteristics of a non-linear system as well. Recent publications have shown little interest in Inasaki's force model, however, it is still used at times due to its relative accuracy and remarkable simplicity, especially when it comes to exploring certain aspects of grinding which are already complicated regardless of the applied force model, such as regenerative chatter in parallel grinding [117].

One of the most frequently used grinding force models was developed by Werner [128]. Articles to date demonstrate the validity and reliability of his work by successfully applying it to a number of problems in grinding dynamics [115, 129–133]. In terms of the three grinding mechanisms, Werner considered sliding and chip formation but neglected the effect of ploughing, assuming a high enough specific material removal rate for the size effect to be negligible [11]. The grinding force model proposed by Werner can be formulated as

$$F_n' = K_W C_s^{\gamma}\left(\frac{v_w}{v_g}\right)^{2\varepsilon-1} d_e^{1-\varepsilon}\delta^{\varepsilon}, \tag{2.9}$$

where d_e is the equivalent wheel diameter [11], and K_W [force/grain] is a factor of proportionality that defines the grinding force acting on a single grain. The coefficient C_s [grains/area] is the so-called static cutting edge density, denoting the number of grains over a unit area of the grinding wheel surface. The exponent γ converts the static cutting edge density to a dynamic cutting edge density (i.e. $C_d = C_s^{\gamma}$), which represents the density of active grains in the grinding process. It is important to note that active grains are not necessarily cutting grains, but grains that become cutting grains when they reach the grinding zone. Since the number of active grains can never exceed the number of all grains (i.e. $C_d \leq C_s$), the exponent γ ranges from 0 to 1. The product of K_W and C_s^{γ}, whose SI unit is [N/m^2] or [J/m^3], is closely related to the sliding and chip formation components of the specific grinding energy. The experimental parameter ε ranges from 0.5 to 1, and indicates the ratio between the sliding and chip formation mechanisms in the grinding process. It is equal to 1 when sliding is negligible compared to chip formation, and 0.5 when sliding is significantly more dominant than chip formation. Substituting these two extreme values of ε into Eq. (2.9), the resulting grinding force expressions correspond to

pure chip formation and pure sliding, respectively:

$$F'_{n,ch}(\varepsilon \to 1) = K_W C_s^{\gamma} \frac{v_w}{v_g} \delta, \tag{2.10}$$

$$F'_{n,sl}(\varepsilon \to 0.5) = K_W C_s^{\gamma} (d_e \delta)^{1/2}. \tag{2.11}$$

It can be seen that $\varepsilon = 1$ provides an expression similar to Eqs. (2.6) and (2.8), whereas in the case of $\varepsilon = 0.5$, the contact length $(d_e\delta)^{1/2}$ appears in the grinding force expression, indicating the dominance of sliding in the grinding process.

According to the results of Mishra and Salonitis [134], the empirical constants K_W, C_s and γ can be replaced by a single factor, leaving only two experimental parameters to be determined, however, this simplification does not address the issue that Werner's grinding force model does not make a clear physical distinction between sliding and chip formation. Nevertheless, Werner's formula remains one of the most often-used force models in grinding chatter theory [115, 129–133].

The problem of separating the sliding and chip formation mechanisms was resolved by Lichun et al. [135], who proposed a grinding force model similar to that of Werner:

$$F'_n = K_{L,ch} \frac{v_w}{v_g} \delta + K_{L,sl} C_s^{\beta} \left(\frac{v_w}{v_g} \right)^{\alpha} d_e^{\frac{1-\alpha}{2}} \delta^{\frac{1+\alpha}{2}}, \tag{2.12}$$

where $K_{L,ch}$ and $K_{L,sl}$ are factors of proportionality, and α and β are empirical exponents. Treating $K_{L,sl}C_s^{\beta}$ as a single parameter, three experimental coefficients remain in Eq. (2.12) instead of two as in Werner's model. Although sliding and chip formation have been successfully separated, ploughing is still not considered by the authors. Recent articles demonstrate that Lichun's grinding force expression is not a particularly widespread one, as it is barely used to study regenerative chatter. One example of Lichun's model being applied to self-excited vibration is the work of Yan et al. on plunge grinding [114].

A new grinding force model was developed by Durgumahanti et al. [136], considering all three grinding mechanisms, including ploughing:

$$F'_n = K_{D,ch} \frac{v_w}{v_g} \delta + K_{D,pl} \left(\frac{v_w}{v_g} \right)^{D_1} d_g^{D_2} \delta^{D_3} (d_e \delta)^{1/2} + K_{D,sl} \frac{v_w}{v_g} \left(\frac{\delta}{d_e} \right)^{1/2}, \tag{2.13}$$

where d_g is the grain diameter, and $K_{D,ch}$, $K_{D,pl}$, $K_{D,sl}$, D_1, D_2 and D_3 are experimental parameters. This particular grinding force model is more sophisticated than the previous three, however, it requires six empirical constants, which makes its application especially laborious in practice. Similarly to Lichun's grinding force expression, Durgumahanti's model is rarely used to study regenerative chatter, primarily because of its heavily empirical nature. Nevertheless, Yan et al. have applied it to plunge grinding [116], but they neglected the ploughing component of Eq. (2.13) and considered only sliding and chip formation to formulate their grinding force expression.

Reviewing the literature, it can be concluded that even though the grinding force models of Inasaki, Lichun and Durgumahanti are still used at times, the majority of modern research papers prefer Werner's model when it comes to investigating regenerative chatter

in grinding. However, certain publications are so focused on the intricacies of self-excited vibration that they intentionally apply the simplest grinding force models in order to concentrate more fully on chatter [137, 138].

It can be seen that empirical models – with the help of experimental constants – are able to capture something of the inherent randomness of grinding. They generally provide more accurate force results than idealised approaches, however, due to the very nature of empirical models, they are based not only on theoretical considerations but also on experimental observations. Because of this, an empirical model – although fairly accurate and reliable – is somewhat restricted in its usage when it comes to theoretical and practical applications, since the experimental constants required by the model need to be determined in advance. Despite this rather limiting difficulty, certain empirical models are still widely applied to grinding chatter theories due to the favourable trade-off they produce between accuracy and simplicity.

2.2.4.3 Stochastic models

The third and last category of grinding force models investigated in this review is that of stochastic approaches. Stochastic grinding force models are today's most sophisticated ways of connecting the grinding forces with the surface topography of the grinding wheel. The main idea behind stochastic models is the replacement of oversimplified scenarios and experimental constants (pertaining to idealised and empirical models respectively) with probability distributions. The affected parameters include the shape, size and orientation of abrasive grains and their distribution on the surface of the grinding wheel.

One of the first in-depth studies on the stochastic nature of grinding was published by Hou and Komanduri [139], who determined the number and minimum diameter of contacting and cutting grains and the average chip volume by statistical methods and compared them with experimental results reported in the literature. They did not consider the shapes and orientations of individual grains or their distribution on the surface of the grinding wheel, but focused only on the grit size distribution and its effect on other parameters, such as the number of contacting and cutting grains and the average chip volume. They found that only a small fraction of grains contribute to chip formation, and a large number of grains merely plough, slide or do not even come into contact with the workpiece at all. The analytical model developed by Hou and Komanduri is based on a number of assumptions and it is regarded by the authors as a 'first approximation' of the stochastic nature of grinding processes. Despite their important findings, no grinding force model is presented in their paper.

The random distribution of abrasive grains on the surface of the grinding wheel was considered by Chang and Wang [140]. They developed a stochastic grinding force model based on the convolution of a single-grit force expression and a random grain distribution function, and verified it by experimental methods. The grinding force model presented by Chang and Wang does not consider the shape, size and orientation distributions of individual grains, but assumes the same single-grit force expression for each grain. Practically speaking, the random grain distribution function and a couple of grinding

coefficients are to be determined by experimental means, which makes Chang and Wang's approach a semi-analytical theory.

The stochastic distribution of abrasive grains was also investigated by Stępień [141], however, his study assumes a uniform grit distribution along the axial and circumferential coordinates of the grinding wheel, and considers only the radial distribution of grains as random or irregular. The probabilistic grinding force model proposed by Stępień takes the shapes of abrasive grits into account as well, but does not consider their sizes and orientations. The parametric expression describing the profile of each abrasive grit is capable of generating an infinite number of grain shapes, however, the scenarios investigated by the author focus only on two profiles – rounded and triangular. Although the grain profile is a legitimate variable in Stępień's model, it is identical for each grit of the grinding wheel, resulting in a uniform grain shape distribution instead of a stochastic one. Additionally, the identical grit profiles are constant in time as well, i.e., grit wear is not considered by the author. Stępień's findings agree with the observation that the actual contact length between the grinding wheel and the workpiece is longer than the geometric contact length, which has been generally attributed to the presence of elastic deformation between the grinding wheel and the workpiece [142–146]. Since the paper does not focus on grinding dynamics, no force model is presented by the author.

Aslan and Budak measured the topography of the grinding wheel using an optical method [147]. Besides the number of active grains, the authors determined the shapes and orientations of abrasive grits as well. After identifying the number of active grains and measuring the rake angle and edge radius distributions of abrasive grits, a force model analogous to milling is presented. The chip formation and ploughing force components are considered, but sliding is neglected in the model. The tangential and normal components of the total grinding force are expressed as a sum of individual grain forces and validated by experimental means. The paper does not provide sufficient information whether the stochastic distribution of abrasive grits on the surface of the grinding wheel was investigated beyond measuring the number of active grains and considering the average distance between two neighbouring grits. Consequently, the grinding force model proposed by Aslan and Budak is a semi-analytical approach, because it requires the experimental identification of the grinding wheel topography.

One of the most detailed and up-to-date grinding force models was developed by the same authors, Aslan and Budak, as a continuation of their semi-analytical approach from the previous year [148]. It is described by the authors as a significant improvement compared to earlier cutting models of abrasive machining. Their theory is based on the calculation of individual grain forces by taking into account both the primary and secondary shear zones, thus modelling the chip flow and the pressure distribution on the grit rake face. Once the topography of the grinding wheel (i.e. the height, width, rake angle, oblique angle and edge radius distributions of abrasive grits) and the coefficient of friction between the chip and the grit rake face are determined, the grain forces can be calculated. The tangential and normal components of the total grinding force are obtained by integrating the individual grain forces over the number of active grits. If the distance between two neighbouring grains is smaller than the grit size, then the two grains intersect each other and a single grain with multiple cutting edges is created. The grinding model developed

Grinding force model	Characteristic approach	Accuracy	Simplicity	Application to chatter
Idealised	Simplifying assumptions	Low	High	Occasionally
Empirical	Experimental constants	Medium	Medium	Frequently
Stochastic	Probability distributions	High	Low	Rarely

Table 2.3: Three types of grinding force models

by Aslan and Budak is capable of modelling such a complex phenomenon by considering both the grain size and the distribution of abrasive grits on the surface of the wheel. Therefore, the authors take into account all the stochastic grain parameters mentioned in this section (shape, size, orientation and distribution), however, all of them are measured by experimental methods, which means that Aslan and Budak's improvement of their own theory is detailed and realistic but remains a semi-analytical grinding force model.

Stochastic models that build on solid theoretical foundations yet preserve the inherently random nature of grinding are superior to both idealised and empirical approaches in accuracy and reliability. However, when it comes to complexity and applicability to chatter theories, stochastic models are at a serious disadvantage. This is probably the main reason why they are generally avoided and replaced by simpler approaches in the literature, even though one of the core elements of a good grinding chatter theory is the applied force model.

Additional stochastic models have been developed in recent years concerning different research areas in grinding, such as grain wear [149] and microgrinding [150], however, due to the fact that modern grinding chatter theories tend to avoid stochastic grinding force models, these publications are not discussed in detail in this review.

In order to summarise the three types of grinding force models reviewed in this section, Table 2.3 presents the main characteristics of each one. In conclusion, it can be stated that the majority of research papers on grinding chatter prefer empirical approaches, Werner's force model in particular, as a good balance between accuracy and simplicity.

2.3 Summary of the literature review

In this chapter, the literature on regenerative machine tool chatter was reviewed. Although much remains to be discovered and understood still, conventional machining has been the focus of rigorous and fruitful research ever since the dangers and intricacies of self-excited vibration were first addressed at the beginning of the 20th century. Following a brief overview of regenerative chatter in conventional machining, a more thorough

review of the literature was provided on regenerative chatter in abrasive machining. Having considered the chronological development of the most pivotal chatter theories, it was found that, although much has been achieved and clarified in an absolute sense, the current understanding of regenerative chatter in abrasive processes still falls short of that in conventional operations. This is primarily due to the inherent complexities involved in abrasive machining, namely the significant wear and irregular geometry of abrasive cutting tools in general, and – as far as this thesis is concerned – grinding wheels in particular.

Therefore, these two aspects of grinding were addressed in more detail in this chapter. In terms of wheel wear, it was demonstrated that material loss from the grinding wheel can be either attritious or fracture wear, the latter of which contributes to the self-sharpening of the wheel. Since this effect alone is not enough to keep the grinding wheel sharp, an additional process called dressing is required. With regard to self-excited vibration, wheel wear results in a unique phenomenon in grinding, which sets it apart from conventional machining. This is the so-called doubly regenerative effect, which means that surface regeneration occurs not only on the workpiece but on the grinding wheel as well. It was also highlighted that the vast majority of chatter theories in the literature consider wheel-related instability to be the consequence of distributed radial wear alone. Although Li and Shin proposed an alternative approach by introducing the regenerative mechanism of distributed grit dullness [108], their contribution has received little attention. In terms of the geometry of the wheel at a micro level, the three grinding mechanisms of sliding, ploughing and chip formation were discussed and related to chatter theory.

Furthermore, since the wear and geometry of the wheel have a direct impact on the grinding force (which is of critical importance in chatter research), a number of grinding force models were reviewed. They were classified according to three categories (idealised, empirical and stochastic models) and evaluated according to four properties (characteristic approach, accuracy, simplicity, and frequency of application in chatter research). Depending on the level of accuracy required and the degree of complexity tolerated, different grinding force models are at the researcher's disposal.

Based on the present literature review, the following chapter elaborates on the gap in knowledge that was briefly articulated in Section 1.4, and presents the aims and objectives of the thesis in detail.

Chapter 3

Aims and objectives of the thesis

As it was demonstrated by the works of previous authors in Section 2.2.1, grinding chatter has been the subject of careful and extensive research since the 1950s. Somewhat lagging behind conventional machining operations due to its inherently more complex nature, grinding chatter is an actively pursued area of academic and industrial interest to this day. Much has been accomplished over the past 70 years in the field of grinding dynamics in terms of predicting and suppressing chatter vibrations, nevertheless, the complexity of the problem leaves much to be discovered still – even at a fundamental level. Therefore, instead of following the research trend set by recent papers on grinding chatter and considering the problem alongside some other complicating factor (such as workpiece imbalance or non-linear behaviour), this work goes back to the fundamental mechanisms responsible for regenerative chatter in grinding in order to understand them better. It focuses on a particular explanation for the origin of unstable grinding vibrations that has received little attention ever since it was articulated and published in 2006 by Li and Shin [108]. As it was discussed in detail in Section 2.2.1, these authors went beyond the classical understanding of wheel-related grinding chatter, namely that wheel-related instability is a result of distributed radial wear quantified by physical surface waves around the circumference of the grinding wheel. They argued that besides this well-established principle, there is another mechanism responsible for the onset of chatter vibrations in grinding. This mechanism is associated with distributed grit dullness quantified by specific energy waves around the circumference of the grinding wheel. Li and Shin's new approach, although closely related to the idea of radial wear, is fundamentally different from previous grinding chatter theories published in the literature.

3.1 Proposal of a new regenerative mechanism

Figure 3.1 presents three approaches to describing the mechanism behind chatter in grinding. It can be seen that the primary difference between them is the mechanism by which regeneration progresses and instability develops.

In the classical case, physical surface waves are forming and growing on the wheel under

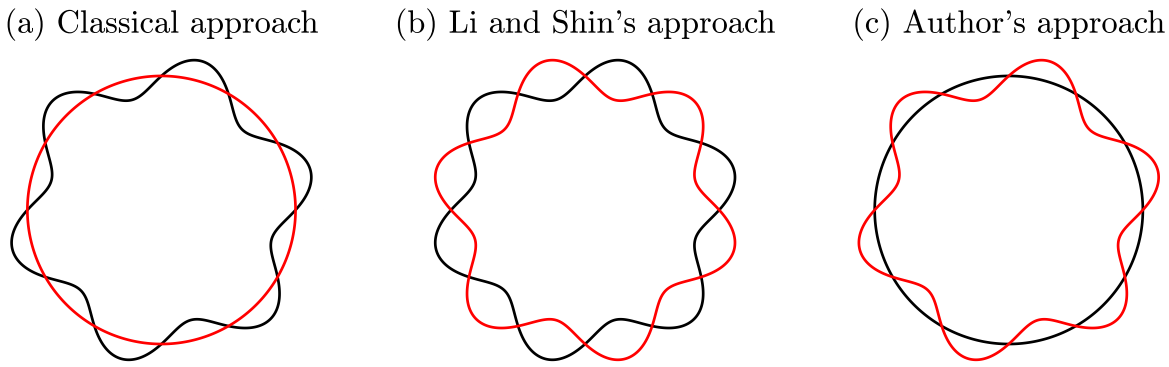

Figure 3.1: Three approaches describing the regenerative mechanism leading to chatter: — physical wheel surface, — specific energy distribution

unstable circumstances, so the periodic grinding force variation necessary for chatter to occur is generated by a non-circular wheel surface producing a varying depth of cut or chip thickness – depending on the applied grinding force model. Even if the specific energy is constant and evenly distributed around the circumference of the grinding wheel, instability can still develop solely as a result of the physical shape of the wheel being uneven and wavy. This is the classical approach to wheel-related grinding chatter modelling, and it is depicted in Figure 3.1a.

The novelty of Li and Shin's idea lies in the fact that instability can be generated in another way as well. According to their new theory, not only the radial wear but also the grit dullness can be described as a quantity distributed around the circumference of the grinding wheel. Therefore, besides physical surface waves, specific energy waves can be forming and growing under unstable circumstances as well, so the grinding force variation necessary for chatter to occur can be generated by a combination of two phenomena: a varying chip thickness and a varying specific energy. It is fairly straightforward to conclude that the phase difference between the physical surface waves and the specific energy waves cannot be arbitrary, since a more worn section of the wheel corresponds to both increased radial wear and increased grit dullness. Therefore, due to the fact that severe wear is indicated by valleys in the physical surface waves and peaks in the specific energy waves, the two are treated as constantly out of phase in Li and Shin's model, according to Figure 3.1b. As for the relative dominance of these two mechanisms, the original authors refer to [120, 151] and state that the effects of radial wear and grit dullness on the grinding forces are comparably significant.

However, neither of their references is concerned with grinding chatter in particular, therefore, the relative significance of these two mechanisms with regard to chatter has not been established until now. Although it is possible to compare some classical approaches with Li and Shin's theory and assess the relative significance of distributed radial wear and distributed grit dullness in a preliminary fashion, a rigorous analysis comparing the two mechanisms has not been performed yet. This is the first main gap in knowledge that has been exposed by the literature review. Filling this gap would provide the researcher with valuable information as to which regenerative mechanism is more dominant in a given grinding scenario, and whether one is negligible relative to the other.

Furthermore, since Li and Shin formulated their new theory considering both distributed radial wear and distributed grit dullness, the significance of distributed grit dullness alone (i.e. in an absolute sense, isolated from distributed radial wear) has not been assessed yet either. This is the second main gap in knowledge exposed by a thorough review of the literature. Similarly to the first one, it is possible to collect some preliminary information regarding the dominance of distributed grit dullness by comparing a few classical theories with Li and Shin's model, but, as of today, a meticulous analysis that considers distributed grit dullness in isolation from distributed radial wear cannot be found in the literature. Filling this gap would provide valuable insight into the significance of distributed grit dullness as a wheel regenerative mechanism, which is not part of mainstream grinding chatter research to this day.

In summary, two main gaps in knowledge have been exposed by the literature review. No rigorous analysis has been published until now that can provide clear and reliable information on:

1. The relative significance of distributed radial wear and distributed grit dullness with regard to process stability.
2. The dominance of distributed grit dullness and its capacity to generate wheel-related instability on its own.

This thesis addresses the second gap. It begins to investigate the effect of distributed grit dullness alone, and aims to determine its significance with regard to grinding chatter – whether it is a mechanism strong enough to generate wheel-related instability on its own or it merely supports and contributes to the effect of distributed radial wear as a secondary mechanism. In order to test this, the effect of distributed radial wear is disregarded in this study by assuming a perfectly circular wheel throughout the entire grinding process. Only the specific energy is allowed to change around the circumference of the wheel according to Figure 3.1c. Therefore, the primary aim of this thesis is to formulate and test this new regenerative mechanism in such a way that the final piece of work is both clear and repeatable.

3.2 Selection of a suitable grinding process

In order to isolate the problem of wheel-related instability induced by specific energy waves around the circumference of the grinding wheel, single-pass surface grinding is considered to eliminate the potential for workpiece regeneration as much as possible. Using surface grinding instead of cylindrical grinding removes the regenerative effect associated with the rotating workpiece. Also, considering only a single wheel pass instead of multiple ones prevents a kind of workpiece regeneration that is initiated by recutting the same workpiece surface multiple times. This type of workpiece regeneration is similar to that in cylindrical grinding, but it is interrupted rather than continuous, which is typically a hindrance to chatter development, but it can still lead to instability. Therefore, using single-pass surface grinding instead of any other grinding operation immediately eliminates two potential sources of workpiece regeneration from the system, however, a

third one remains inherently in the process. Theoretically speaking, single-pass surface grinding is capable of experiencing workpiece regeneration and workpiece-related instability in the same way as a milling process can, i.e., through one tooth cutting a wavy workpiece surface left behind by the previous tooth. Although this kind of workpiece regeneration is unlikely to occur in grinding due to the large number of cutting edges inherently involved in the process, it is still useful not only to keep it in mind but also to confirm that it is truly negligible for all practical purposes. This investigation is another objective of this work.

3.3 Summary of aims and objectives

The aim of this research is to develop a new grinding chatter theory based on the wheel regenerative mechanism of distributed grit dullness alone, apart from any effect of distributed radial wear, and calculate its stability predictions for single-pass surface grinding.

The objectives of this work are to:

1. Confirm the predominant assumption of the literature according to which the effect of parametric excitation on grinding stability is negligible due to the large number of cutting edges. This objective is equivalent to checking whether workpiece regeneration is truly negligible in single-pass surface grinding.

2. Construct a mechanical model that is capable of describing distributed grit dullness as the sole regenerative mechanism in the grinding system.

3. Develop a mathematical model of the problem by deriving the equation of motion that governs the dynamics of the grinding process.

4. Determine the stability properties of the governing equation of motion and present the results in the form of stability diagrams and, in the case of instability, chatter frequencies.

5. Perform enough surface grinding experiments to test the theoretical model against experimental data in such a way that is repeatable and informative with regard to the validity of the proposed model.

6. Compare and discuss the theoretical and experimental results with reference to their novelty, impact and the future work to which they potentially lead.

3.4 Structure of the rest of the thesis

The two main objectives presented in Sections 3.1 and 3.2 – namely exploring the possibility of workpiece regeneration in single-pass surface grinding, and formulating a new chatter theory based on the wheel regenerative mechanism of distributed grit dullness

	Workpiece regeneration	Wheel regeneration	Research question to be answered
Chapter 4	Considered	Neglected	Can workpiece-related instability occur?
Chapter 5	Neglected	Considered	Can wheel-related instability occur?

Table 3.1: Theoretical investigations for single-pass surface grinding

alone – constitute the theoretical backbone of this work and define the topics of the following two chapters as well. Therefore, Chapter 4 is dedicated to investigating the possibility of workpiece regeneration in single-pass surface grinding, while Chapter 5 contains the analytical formulation of a chatter theory based on the new regenerative mechanism proposed in Section 3.1. These two theoretical scenarios are summarised in Table 3.1 in order to articulate the main objectives of this research in a clear and concise fashion. After all the theoretical work, Chapter 6 presents a detailed report on a number of surface grinding experiments performed to test the validity of the proposed chatter theory. The thesis is concluded in Chapter 7 with a comprehensive discussion about the obtained results and a list of potential opportunities for future work.

Chapter 4

Workpiece regeneration in single-pass surface grinding

As it was stated in Chapter 3, the primary objective of this chapter is to answer the question whether single-pass surface grinding can be affected by workpiece regeneration in such a way that leads to stability issues in practical applications. Having eliminated two potential sources of workpiece regeneration from the process by considering surface grinding instead of cylindrical grinding and a single pass instead of multiple passes, the only remaining possibility for workpiece regeneration to occur is to have rapid surface regeneration take place in the grinding zone as one cutting edge machines the workpiece surface left behind by another, just like it happens in milling [43, 46, 47]. Although such a phenomenon is unlikely to develop due to the large number of grains on the wheel, this chapter is dedicated to providing a mathematically well-founded argument for this suspicion.

In order to simplify the problem under consideration, wheel wear and thus wheel regeneration are neglected in this study, and the grinding wheel is assumed to behave like a milling tool with many cutting edges. Because of this assumption, an important distinction can be made right at the start with regard to the distribution of grains around the circumference of the grinding wheel: they can be either regular (evenly spaced) or irregular (randomly spaced). Therefore, the rest of this chapter is divided into two main parts accordingly. Although a regular grit distribution describes an impractical scenario, as grains are typically randomly spaced on the wheel, it is still helpful to consider the simpler case first and build the more complicated theory on that. After investigating these two scenarios, the chapter is concluded with a summary of the main results.

4.1 Regular grain distribution

Therefore, for the sake of simplicity, a regular grain distribution is considered first. The flow of this particular investigation is as follows. In order to assess whether workpiece

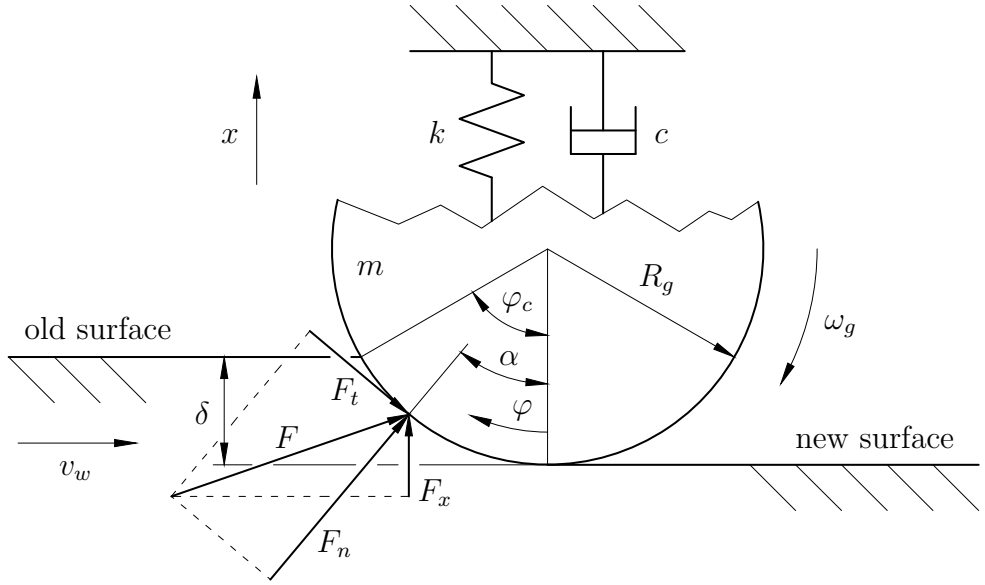

Figure 4.1: A two-dimensional, single-degree-of-freedom mechanical model of single-pass surface grinding (up-grinding)

regeneration can lead to instability in single-pass surface grinding, the equation of motion of the system has to be derived. The formulation of the equation of motion depends heavily on the force expression employed, however, since the grinding wheel is modelled as a milling tool in this study, the typical force models reviewed in Section 2.2.4 cannot be used here. This is not a big issue though, as milling force models are well established in the literature [35]. They are based on the chip thickness (whereas grinding force models usually rely on the depth of cut), which can vary according to the oscillations of the cutting tool. Therefore, researchers differentiate between static and dynamic chip thicknesses [35]. The static chip thickness corresponds to steady-state machining conditions, so it is unaffected by the unwanted vibrations of the cutting tool, while the dynamic chip thickness is the part of the total chip thickness that is originating from tool vibration. Thus the total chip thickness is a sum of its static and dynamic components. Consequently, in order to derive the equation of motion of the system for the purpose of assessing process stability, the chip thickness has to be determined first, then the cutting force second. Therefore, the structure of this section follows the flow described above, starting with the formulation of the chip thickness expression.

4.1.1 Mechanical model

Before constructing the mathematical representation of the problem, a mechanical model has to be created that is capable of capturing the phenomenon under investigation. Thus the mechanical model serves the purpose of simplifying the system to the greatest possible degree suitable for analysing workpiece regeneration in single-pass surface grinding. Therefore, a single-degree-of-freedom mechanical model of the system is considered and presented in Figure 4.1. It can be seen that the grinding wheel of radius R_g is allowed to oscillate relative to the workpiece only in the direction of the depth of cut. The dis-

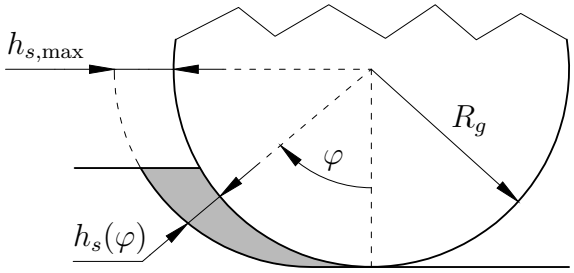

Figure 4.2: Variation of the static chip thickness in the grinding zone

placement of the centre of the wheel is described by the general coordinate x, and it is zero when the spring force is zero. The modal parameters of the grinding wheel, namely its modal mass, modal damping and modal stiffness, are denoted by m, c and k, respectively. Since the damping and stiffness characteristics of the wheel are described by a single constant each, it can be seen that both of them are assumed to be linear in the proposed model. The workpiece is fed to the wheel at a depth of cut of δ and a feed rate of v_w. Due to the fact that single-pass surface grinding is considered, the length of the workpiece is assumed to be infinite. The wheel rotates at a speed of ω_g in a clockwise direction, so combined with the direction of the feed rate, the resulting configuration is up-grinding (i.e. the circumferential speed of the wheel is opposite to the linear speed of the workpiece). The variables corresponding to the contact zone will be addressed and explained later. It is important to note at this stage that a possible way to improve the proposed mechanical model is to extend it to multiple degrees of freedom.

4.1.2 Mathematical model

The mathematical model of the system is constructed in four stages, corresponding to the following four subsections. First, the static chip thickness is formulated based on steady-state machining conditions, then, considering the potential vibrations of the grinding wheel, the dynamic chip thickness is derived. Combining the two yields the total chip thickness, which is necessary to determine the grinding force. Once the grinding force has been obtained, the equation of motion can be formulated with relative ease.

4.1.2.1 Static chip thickness

The variation of the static chip thickness in the grinding zone is presented in Figure 4.2. It can be seen that the change is sinusoidal with respect to the angular coordinate φ, which describes the angular location of a particular chip thickness on the workpiece relative to the point where the grains enter the grinding zone (as shown in Figure 4.1 as well). Therefore, the static chip thickness cut by a single grit can be approximated as

$$h_s(\varphi) = h_{s,\max} \sin \varphi, \tag{4.1}$$

where $h_{s,\max}$ corresponds to the theoretical maximum of the static chip thickness at $\varphi = \pi/2$, and it can be determined by calculating the distance travelled by the workpiece

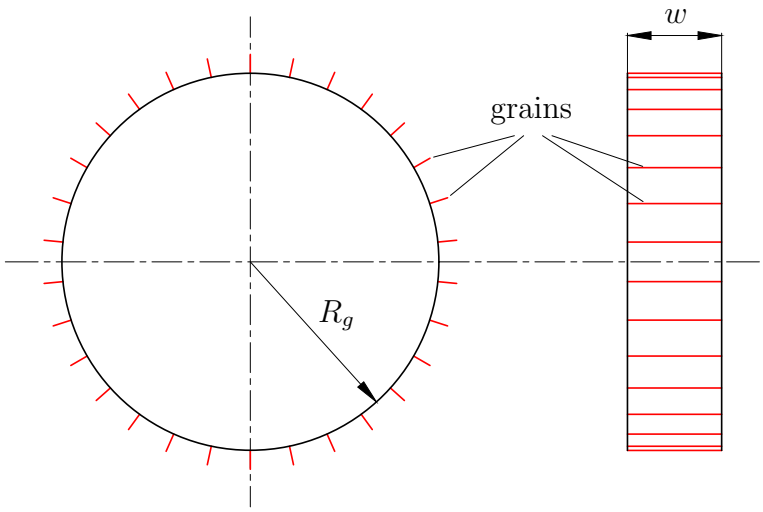

Figure 4.3: Modelling grains on the wheel as teeth on a straight-fluted milling tool

over one grit-passing period τ. Since the grains are assumed to be evenly distributed around the circumference of the wheel, the grit-passing period is constant and can be simply calculated as the wheel period T_g divided by the number of grits Z, where the grain density corresponds to a two-dimensional model of the grinding wheel, according to Figure 4.3. Therefore, the theoretical maximum of the static chip thickness is

$$h_{s,\max} = v_w \tau = v_w \frac{T_g}{Z} = \frac{2\pi v_w}{\omega_g Z}. \tag{4.2}$$

Substituting Eq. (4.2) into Eq. (4.1), the variation of the static chip thickness in the grinding zone can be obtained as

$$h_s(\varphi) = \frac{2\pi v_w}{\omega_g Z} \sin\varphi. \tag{4.3}$$

4.1.2.2 Dynamic chip thickness

Considering Figure 4.2, it is fairly easy to see that if the grinding wheel moves upward (i.e. in the positive x-direction), then the chip thickness decreases, but if it moves downward (i.e. in the negative x-direction), then the chip thickness increases. Therefore, the dynamic chip thickness can increase in two ways. First, the grinding wheel is displaced in the negative x-direction at the current time t, and second, the grinding wheel was displaced in the positive x-direction one grit-passing period before the current time, i.e., at $t - \tau$. Therefore, the dynamic chip thickness can be written as

$$h_d(x, \varphi) = (x(t - \tau) - x(t)) \cos\varphi, \tag{4.4}$$

where the cosine term projects the vibration of the wheel into the direction of the chip thickness. Thus the dynamic chip thickness varies with φ just as the static component, however, the two are 90 degrees out of phase with each other – when one is zero, the other reaches its minimum or maximum value and vice versa. There is a significant

difference between the static and dynamic components of the chip thickness though – the static chip thickness is independent of time, while the dynamic chip thickness is time dependent through the vibration of the grinding wheel.

For the sake of completeness, it is noted that the vibration of the grinding wheel changes not only the chip thickness but also the angles at which the cutting edges enter and exit the grinding zone (and consequently the contact angle φ_c as well, according to Figure 4.1). However, taking this rather complex effect of arguably minor importance into account at this stage is outside the scope of this investigation. That is because the primary mechanism potentially responsible for workpiece regeneration in single-pass surface grinding is the variation of the chip thickness in the grinding zone, not the variation of the grinding zone itself. Therefore, the angles characterising the contact zone are assumed to be constant throughout this study.

Adding Eqs. (4.3) and (4.4) together, the total chip thickness – accounting for both steady-state grinding and wheel vibration – becomes

$$h(x,\varphi) = \frac{2\pi v_w}{\omega_g Z}\sin\varphi + (x(t-\tau) - x(t))\cos\varphi. \tag{4.5}$$

4.1.2.3 Grinding force

According to the classical milling theory [43, 46, 47], the force acting on a single tooth depends on four main factors: (1) the chip thickness, (2) the chip width, (3) the so-called normal and tangential cutting-force coefficients, and (4) whether the tooth under consideration is in or out of cut – this is typically controlled by a unit step function that is equal to one when the tooth is in cut and zero when it is out of cut. In order to apply a milling force model to grinding, the grits on the wheel have to be considered like the teeth of a straight-fluted milling tool according to Figure 4.3. Granted that the grains are assumed to be straight and elongated in the axial direction so that the wheel looks like a milling tool with many small cutting edges, the normal and tangential components of the total force acting on a single grit can be formulated as

$$F_{j,n}(t) = g_j(t) K_n w h_j^q(t), \tag{4.6}$$

$$F_{j,t}(t) = g_j(t) K_t w h_j^q(t), \tag{4.7}$$

where the general subscript j identifies each grain and thus runs from one to the total number of grits on the wheel. The potentially non-linear dependence of the grinding force on the total chip thickness is indicated by the cutting-force exponent q. The chip width is denoted by w, and it is identical to the grinding width according to Figure 4.3 (depending on how much of the wheel is engaged, the grinding width can be less than or equal to the wheel width). The normal and tangential cutting-force coefficients K_n and K_t are well-established quantities in milling and define a relationship between the chip cross section and the cutting forces. The unit step function selecting whether grit j is in or out of cut is denoted by g_j and defined as

$$g_j(t) = \begin{cases} 1 & \text{if } \varphi_{en} \leq \varphi_j(t) \bmod 2\pi \leq \varphi_{ex}, \\ 0 & \text{otherwise,} \end{cases} \tag{4.8}$$

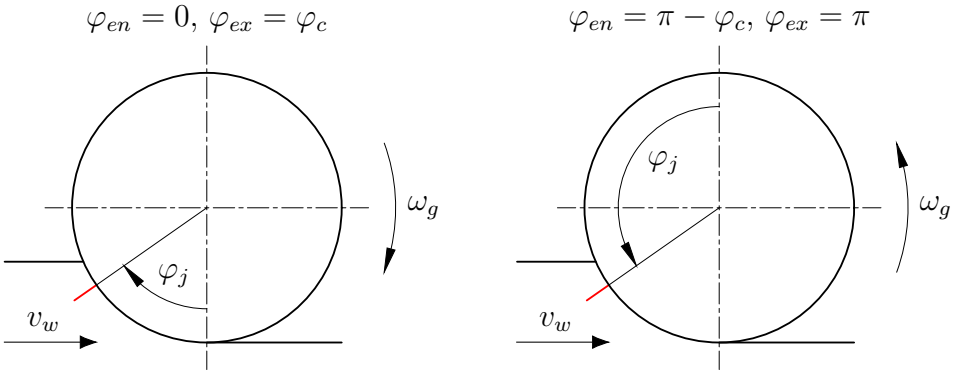

Figure 4.4: Defining φ_j for up-grinding (left) and down-grinding (right)

where φ_{en} and φ_{ex} are the entering and exiting angles, i.e., the angles at which the grains enter and exit the grinding zone. It is important to note that, although φ_{en} and φ_{ex} are simple to calculate, they differ for up-grinding and down-grinding. This difference is graphically illustrated in Figure 4.4. The instantaneous angular position of grain j around the circumference of the grinding wheel is φ_j and can be obtained as

$$\varphi_j(t) = \omega_g t + j\frac{2\pi}{Z}. \tag{4.9}$$

It can be seen that φ_j increases linearly with time, therefore, the modulo operation is required to determine whether grit j is in or out of cut. This is denoted by 'mod' in Eq. (4.8).

Depending on whether up-grinding or down-grinding is considered, the coordinate systems corresponding to φ and φ_j may differ. Keeping in mind that φ is used to describe the variation of the chip thickness in the grinding zone and φ_j identifies the angular location of grit j around the circumference of the wheel, the traditional way of defining the origin of φ_j is presented in Figure 4.4 for up-grinding and down-grinding. This is a typical convention for milling [93], and will be used for grinding as well. Therefore, considering Figure 4.4, it is easy to see that the relationship between φ and φ_j can be established according to

$$\varphi = \begin{cases} \varphi_j & \text{for up-grinding,} \\ \pi - \varphi_j & \text{for down-grinding,} \end{cases} \tag{4.10}$$

which means that, substituting Eq. (4.10) into the trigonometric expressions in Eq. (4.5) and utilising the well-known identities

$$\sin(\pi - \varphi_j) = \sin\varphi_j, \tag{4.11}$$
$$\cos(\pi - \varphi_j) = -\cos\varphi_j, \tag{4.12}$$

the total chip thickness cut by grit j becomes

$$h_j(t) = \frac{2\pi v_w}{\omega_g Z}\sin\varphi_j(t) \pm (x(t-\tau) - x(t))\cos\varphi_j(t), \tag{4.13}$$

where the $\pm$ symbol corresponds to up-grinding and down-grinding, respectively. This notation will be used throughout this chapter. It can be seen that, although the total

chip thickness still depends on the angular location of grain j in the grinding zone, this angular dependence has been replaced by time dependence through the rotational speed of the grinding wheel.

In order to describe the vibrations of the wheel in the x-direction, the x-component of the grinding force needs to be calculated by projecting the normal and tangential components into the direction of the depth of cut. It is important to note that, although the normal component of the grinding force always points towards the centre of the wheel, the tangential component always acts against the rotation of the wheel and therefore its direction depends on whether up-grinding or down-grinding is considered. Paying careful attention to these details, the grit force in the x-direction can be obtained as

$$F_{j,x}(t) = \pm F_{j,n}(t)\cos\varphi_j(t) \mp F_{j,t}(t)\sin\varphi_j(t), \tag{4.14}$$

where the top and bottom signs correspond to up-grinding and down-grinding, respectively. Substituting Eqs. (4.6) and (4.7) into Eq. (4.14), the grit force in the x-direction becomes

$$F_{j,x}(t) = \pm g_j(t) w h_j^q(t)(K_n\cos\varphi_j(t) - K_t\sin\varphi_j(t)). \tag{4.15}$$

Summarising the individual grit forces, it is possible to obtain the total grinding force in the x-direction:

$$F_x(t) = \pm w\sum_{j=0}^{Z-1} g_j(t) h_j^q(t)(K_n\cos\varphi_j(t) - K_t\sin\varphi_j(t)). \tag{4.16}$$

It can be seen that the grains are summarised not from one to the total number of grits but from zero to the total number minus one. That is because this formulation ensures that the angular position of the first grain at the beginning of each simulation is zero regardless of the total number of cutting points. In other words, this little mathematical manoeuvre provides a constant and consistent reference point for future calculations.

4.1.2.4 Equation of motion

The equation of motion of the single-degree-of-freedom oscillatory system presented in Figure 4.1 can be formulated as

$$m\ddot{x}(t) + c\dot{x}(t) + kx(t) = F_x(t), \tag{4.17}$$

where the dot symbol indicates the time derivatives of $x(t)$. Dividing both sides by the modal mass of the grinding wheel, it is possible to get

$$\ddot{x}(t) + 2\zeta\omega_n\dot{x}(t) + \omega_n^2 x(t) = \frac{1}{m}F_x(t), \tag{4.18}$$

where $\zeta = c/(2m\omega_n)$ and $\omega_n = \sqrt{k/m}$ are the damping ratio and natural angular frequency of the wheel, respectively. It is important to recognise that Eq. (4.18) is a non-linear delay differential equation with respect to x, because the grinding force is a non-linear function of the chip thickness whose dynamic component depends on the

vibration of the grinding wheel. Therefore, in order to prepare the equation of motion for a linear stability analysis, the chip thickness has to be linearised around the steady-state oscillations of the system. To separate the steady-state solution from all other sources of vibration, the displacement of the grinding wheel is assumed to have the form

$$x(t) = x_p(t) + \xi(t), \tag{4.19}$$

where $x_p(t)$ is a τ-periodic function corresponding to forced vibration caused by the periodic excitation of the cutting edges, and $\xi(t)$ is a small perturbation having the potential to grow into unstable self-excited vibration (i.e. chatter). This decomposition is a well-established method in classical milling stability theory [93].

Therefore, the chip thickness is to be linearised around the steady-state solution $x_p(t)$, or equivalently, around $\xi(t) \equiv 0$. Substituting Eq. (4.19) into Eq. (4.13) and utilising the fact that $x_p(t)$ is τ-periodic, i.e., $x_p(t) \equiv x_p(t-\tau)$, the chip thickness expression becomes

$$h_j(t) = \frac{2\pi v_w}{\omega_g Z} \sin\varphi_j(t) \pm (\xi(t-\tau) - \xi(t)) \cos\varphi_j(t). \tag{4.20}$$

Calculating the linear approximation, i.e. the first order Taylor expansion of $h_j^q(t)$ around $\xi(t) \equiv 0$, it is possible to obtain

$$h_j^q(t) \approx \left(\frac{2\pi v_w}{\omega_g Z} \sin\varphi_j(t)\right)^q \pm q \left(\frac{2\pi v_w}{\omega_g Z} \sin\varphi_j(t)\right)^{q-1} (\xi(t-\tau) - \xi(t)) \cos\varphi_j(t). \tag{4.21}$$

Substituting Eq. (4.21) into the grinding force expression in Eq. (4.16), it is clear that – similarly to the chip thickness – the grinding force will also have static and dynamic components. Therefore, the linearised grinding force in the x-direction can be decomposed as

$$F_x(t) = F_{x,s}(t) + F_{x,d}(t), \tag{4.22}$$

where the static and dynamic grinding force expressions are

$$F_{x,s}(t) = \pm \left(\frac{2\pi v_w}{\omega_g Z}\right)^q w \sum_{j=0}^{Z-1} g_j(t) (\sin\varphi_j(t))^q (K_n \cos\varphi_j(t) - K_t \sin\varphi_j(t)), \tag{4.23}$$

$$\begin{aligned} F_{x,d}(t) = q \left(\frac{2\pi v_w}{\omega_g Z}\right)^{q-1} w \sum_{j=0}^{Z-1} g_j(t) (\sin\varphi_j(t))^{q-1} (K_n \cos\varphi_j(t) - K_t \sin\varphi_j(t)) \times \\ \times (\xi(t-\tau) - \xi(t)) \cos\varphi_j(t). \end{aligned} \tag{4.24}$$

It can be seen that the static force is independent of the small perturbation ξ, while the dynamic force depends on it. This is in fact the basis on which the static and dynamic grinding force components have been separated.

Substituting Eqs. (4.19) and (4.22) into Eq. (4.18), the linearised equation of motion becomes

$$\ddot{x}_p(t) + 2\zeta\omega_n \dot{x}_p(t) + \omega_n^2 x_p(t) + \ddot{\xi}(t) + 2\zeta\omega_n \dot{\xi}(t) + \omega_n^2 \xi(t) = \frac{1}{m}(F_{x,s}(t) + F_{x,d}(t)). \tag{4.25}$$

Due to the fact that instability is caused by the perturbation term ξ and not the periodic motion x_p, the periodic solution can be detached from Eq. (4.25) without altering the

stability properties of the system. Considering the steady-state part of the equation of motion, i.e. $\xi(t) \equiv 0$ and thus $F_{x,d}(t) \equiv 0$, the undisturbed oscillations of the structure are described by the equation

$$\ddot{x}_p(t) + 2\zeta\omega_n\dot{x}_p(t) + \omega_n^2 x_p(t) = \frac{1}{m}F_{x,s}(t). \tag{4.26}$$

Therefore, subtracting Eq. (4.26) from Eq. (4.25), the unwanted vibrations of the grinding wheel – expressed purely as a function of ξ – have the form

$$\ddot{\xi}(t) + 2\zeta\omega_n\dot{\xi}(t) + \omega_n^2\xi(t) = K_s K_d(t)(\xi(t-\tau) - \xi(t)), \tag{4.27}$$

where K_s and K_d are the static and dynamic cutting-force coefficients respectively, defined as follows:

$$K_s = \frac{wq}{m}\left(\frac{2\pi v_w}{\omega_g Z}\right)^{q-1}, \tag{4.28}$$

$$K_d(t) = \sum_{j=0}^{Z-1} g_j(t)(\sin\varphi_j(t))^{q-1}\cos\varphi_j(t)(K_n\cos\varphi_j(t) - K_t\sin\varphi_j(t)). \tag{4.29}$$

It is important to note that, as their names suggest, the static cutting-force coefficient is constant, while the dynamic cutting-force coefficient is a τ-periodic function of time. Also, comparing Eqs. (4.23) and (4.24), it can be seen that the static grinding force is dependent on whether up-grinding or down-grinding is considered (i.e. the $\pm$ signs remain in the force expression), however, the dynamic grinding force is independent of the surface grinding configuration (i.e. the $\pm$ signs cancel out). Therefore, up-grinding and down-grinding differ only in terms of the entering and exiting angles as far as surface grinding stability is concerned.

Concluding the derivation of the equation of motion, it can be seen that Eq. (4.27) is a delay differential equation with time-periodic coefficients, reflecting a combination of workpiece regeneration and parametric excitation in the system (more information on this complex phenomenon can be found in Section 2.1 and Figure 2.4).

4.1.3 Stability analysis

The stability properties of Eq. (4.27) are investigated in this section. Due to the complexity of the equation of motion – i.e. surface regeneration coupled with parametric excitation, resulting in a delay differential equation with time-periodic coefficients – Eq. (4.27) has no analytical solution in its current form. The problem can be reduced to a delay differential equation with constant coefficients if the parametric excitation of the cutting edges is negligible. This is usually the case when the number of cutting edges is high and the radial immersion is large [93]. In grinding, the number of cutting edges is very high indeed, however, the radial immersion can be very low, which means that neglecting the intermittent nature of the process by replacing the time-periodic term with a constant is not always justified. Therefore, further analysis is warranted.

The primary issue presented by Eq. (4.27) can be mitigated by approximating the time-periodic coefficient $K_d(t)$ by its Fourier series. Depending on the number of harmonics or Fourier terms considered, a desired ratio between the accuracy and simplicity of the solution can be obtained in a controlled fashion. This is a well-established method when it comes to assessing the stability of time-periodic systems [35]. Therefore, the dynamic cutting-force coefficient can be represented by its Fourier series in the form

$$K_d(t) = \sum_{n=-N}^{N} c_n e^{i\frac{2\pi n t}{\tau}}, \tag{4.30}$$

where N is the number of harmonics considered, and the Fourier coefficients denoted by c_n can be calculated as

$$c_n = \frac{1}{\tau}\int_0^{\tau} K_d(t) e^{-i\frac{2\pi n t}{\tau}} dt. \tag{4.31}$$

Due to the fact that the Fourier coefficients play a key role in the stability analysis of the system, they have to be calculated explicitly by evaluating the integral in Eq. (4.31). Therefore, substituting Eq. (4.29) into Eq. (4.31), the Fourier coefficients become

$$c_n = \frac{1}{\tau}\int_0^{\tau} \sum_{j=0}^{Z-1} g_j(t)(\sin\varphi_j(t))^{q-1}\cos\varphi_j(t)(K_n\cos\varphi_j(t) - K_t\sin\varphi_j(t))e^{-i\frac{2\pi n t}{\tau}} dt. \tag{4.32}$$

Since the grit index j does not appear between the integral and the sum, i.e. inside the integral yet outside the sum, the order of integration and summation does not change the value of c_n. Therefore, swapping the integral and the sum, the same Fourier coefficients can also be obtained as

$$c_n = \frac{1}{\tau}\sum_{j=0}^{Z-1} \int_0^{\tau} g_j(t)(\sin\varphi_j(t))^{q-1}\cos\varphi_j(t)(K_n\cos\varphi_j(t) - K_t\sin\varphi_j(t))e^{-i\frac{2\pi n t}{\tau}} dt. \tag{4.33}$$

The difficulty of evaluating the integral above lies in the fact that the general coordinate $\varphi_j(t)$ and thus the integrand itself is different for each j. This problem can be visualised by replacing the integrand with the symbol $I_j(t)$ corresponding to a particular grain and expanding the first few terms of the sum according to

$$c_n = \frac{1}{\tau}\int_0^{\tau} I_0(t)dt + \frac{1}{\tau}\int_0^{\tau} I_1(t)dt + \frac{1}{\tau}\int_0^{\tau} I_2(t)dt + \frac{1}{\tau}\int_0^{\tau} I_3(t)dt + \dots \tag{4.34}$$

In order to obtain an explicit expression for the Fourier coefficients, the sum of the integrals above has to be calculated, which is currently hindered by the fact that the integrands are different in each term of the sum. However, considering Eq. (4.9), it can be seen that the general coordinates $\varphi_j(t)$ and thus the integrands $I_j(t)$ are merely offset versions of one another. Therefore, since the offset between two neighbouring grits is constant as long as a regular grain distribution is assumed, the integrands can be made identical by shifting the limits of integration in each term. The main idea is that – according to Eq. (4.9) – grit $j+1$ is always one grit-passing period ahead of grit j, i.e., $\varphi_{j+1}(t) = \varphi_j(t+\tau)$. This mathematical manipulation transforms Eq. (4.34) into

$$c_n = \frac{1}{\tau}\int_0^{\tau} I_0(t)dt + \frac{1}{\tau}\int_{\tau}^{2\tau} I_0(t)dt + \frac{1}{\tau}\int_{2\tau}^{3\tau} I_0(t)dt + \frac{1}{\tau}\int_{3\tau}^{4\tau} I_0(t)dt + \dots \tag{4.35}$$

Considering every term of the sum, the Fourier coefficients become

$$c_n = \frac{1}{\tau}\int_0^{\tau} I_0(t)dt + \cdots + \frac{1}{\tau}\int_{(Z-1)\tau}^{Z\tau} I_0(t)dt = \frac{1}{\tau}\int_0^{Z\tau} I_0(t)dt = \frac{1}{\tau}\int_0^{T_g} I_0(t)dt. \quad (4.36)$$

Changing the variable of integration from t to $\varphi_0(t)$, where the relationship between the two is established by Eq. (4.9), i.e. $\varphi_0(t) = \omega_g t$, it is possible to get

$$c_n = \frac{1}{\omega_g \tau}\int_0^{2\pi} I_0(\varphi_0)d\varphi_0 = \frac{Z}{2\pi}\int_0^{2\pi} I_0(\varphi_0)d\varphi_0. \quad (4.37)$$

Substituting the integrand back into Eq. (4.37), the Fourier coefficients can be written as

$$c_n = \frac{Z}{2\pi}\int_0^{2\pi} g_0(\varphi_0)(\sin\varphi_0)^{q-1}\cos\varphi_0(K_n\cos\varphi_0 - K_t\sin\varphi_0)e^{-inZ\varphi_0}d\varphi_0. \quad (4.38)$$

And finally, applying the effect of $g_0(\varphi_0)$ to Eq. (4.38), the Fourier coefficients can be obtained in the explicit form

$$c_n = \frac{Z}{2\pi}\int_{\varphi_{en}}^{\varphi_{ex}} (\sin\varphi_0)^{q-1}\cos\varphi_0(K_n\cos\varphi_0 - K_t\sin\varphi_0)e^{-inZ\varphi_0}d\varphi_0. \quad (4.39)$$

Based on the number of harmonics or Fourier terms considered in Eq. (4.30), the literature distinguishes between zero-frequency ($N = 0$) and multi-frequency ($N \geq 1$) solutions [35], which are discussed in detail in Sections 4.1.3.1 and 4.1.3.2.

4.1.3.1 Zero-frequency solution

The simplest way to assess the stability properties of Eq. (4.27) is to consider only the constant term of the Fourier series of the dynamic cutting-force coefficient. According to Eq. (4.30), that is $K_d(t) \equiv c_0$. As long as the depth of cut is large enough, this is a good approximation for grinding, since the intermittent nature of the cutting process is negligible. In order to simplify the system even further, the relationship between the chip thickness and the grinding force is assumed to be linear, i.e., the cutting-force exponent q is considered to be one in Eqs. (4.6) and (4.7). Since the exact value of the cutting-force exponent is of no major concern in this particular investigation, this is a reasonable simplification. However, it is important to note that as a result of this assumption, the feed rate v_w is not going to feature in the stability analysis. That is because the static cutting-force coefficient expressed in Eq. (4.28), which contains the feed rate for $q \neq 1$, reduces to w/m for $q = 1$. Therefore, substituting $K_d(t) \equiv c_0$ and $q = 1$ into Eq. (4.27), the equation of motion of the system can be simplified to

$$\ddot{\xi}(t) + 2\zeta\omega_n\dot{\xi}(t) + \omega_n^2\xi(t) = \frac{wc_0}{m}(\xi(t-\tau) - \xi(t)), \quad (4.40)$$

where the constant Fourier term is identical to the zeroth Fourier coefficient:

$$\begin{aligned} c_0 &= \frac{Z}{2\pi}\int_{\varphi_{en}}^{\varphi_{ex}} \cos\varphi_0(K_n\cos\varphi_0 - K_t\sin\varphi_0)d\varphi_0 = \\ &= \frac{Z}{4\pi}(K_n(\varphi_c + \cos\varphi_c\sin\varphi_c) \mp K_t(\sin\varphi_c)^2), \end{aligned} \quad (4.41)$$

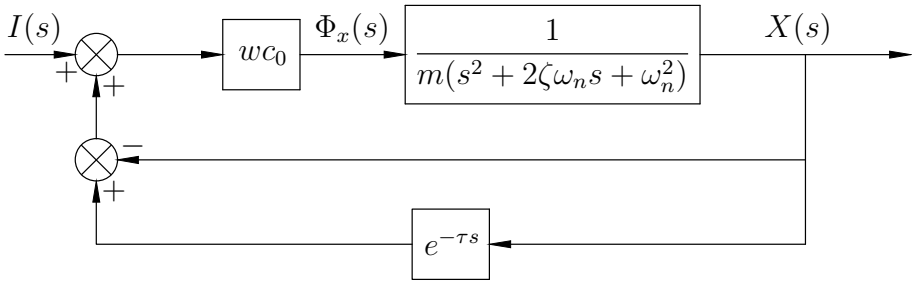

Figure 4.5: Block diagram representation of Eq. (4.42)

and the $\mp$ symbol corresponds to up-grinding and down-grinding, respectively. Since the parametric excitation of the cutting edges has been eliminated, the stability analysis of Eq. (4.40) is fairly straightforward. It can be carried out using the Nyquist criterion (discussed in detail in Appendix A), which determines the stability of a system in the frequency domain. Therefore, taking the Laplace transform of Eq. (4.40) with zero initial conditions, the frequency domain representation of the equation of motion reads as

$$(s^2 + 2\zeta\omega_n s + \omega_n^2)X(s) = \frac{wc_0}{m}(e^{-\tau s} - 1)X(s), \tag{4.42}$$

where s is the complex Laplace frequency, and $X(s)$ is the Laplace transform of $\xi(t)$. The block diagram representation of Eq. (4.42) is given in Figure 4.5, where the Laplace transform of the grinding force is denoted by $\Phi_x(s)$, and the input function $I(s)$ – normally describing the forced vibration of the system – is set to zero in order to investigate the stability properties of the regenerative process. Considering the fact that Figure 4.5 depicts a positive feedback system, the open-loop transfer function of the corresponding negative feedback system can be written as

$$T_o(s) = \frac{wc_0(1 - e^{-\tau s})}{m(s^2 + 2\zeta\omega_n s + \omega_n^2)}. \tag{4.43}$$

Applying the Nyquist criterion to Eq. (4.43), the stability boundaries of the system can be calculated. Before that however, the multi-frequency solution is derived in order to present the two sets of results together.

4.1.3.2 Multi-frequency solution

The multi-frequency solution considers a number of harmonics in Eq. (4.30), therefore, it is inherently more accurate and more complex than the zero-frequency solution. Substituting Eq. (4.30) into Eq. (4.27), and continuing to assume a linear relationship between the chip thickness and the grinding force, i.e. $q = 1$, the equation of motion becomes

$$\ddot{\xi}(t) + 2\zeta\omega_n\dot{\xi}(t) + \omega_n^2\xi(t) = \frac{w}{m}(\xi(t-\tau) - \xi(t)) \sum_{n=-N}^{N} c_n e^{i\frac{2\pi nt}{\tau}}, \tag{4.44}$$

where the Fourier coefficients can be calculated as

$$c_n = \frac{Z}{2\pi} \int_{\varphi_{en}}^{\varphi_{ex}} \cos\varphi_0(K_n \cos\varphi_0 - K_t \sin\varphi_0)e^{-inZ\varphi_0} d\varphi_0. \tag{4.45}$$

Although the integral above can be evaluated in closed form, the result is rather lengthy, therefore, it is not presented here. Similarly to the zero-frequency solution, the stability analysis of Eq. (4.44) can be carried out using the Nyquist criterion. Therefore, taking the Laplace transform of Eq. (4.44) with zero initial conditions, it is possible to get

$$\frac{X(s)}{G(s)} = \int_0^\infty \left(w(\xi(t-\tau) - \xi(t)) \sum_{n=-N}^{N} c_n e^{i\frac{2\pi n t}{\tau}} \right) e^{-st} dt, \tag{4.46}$$

where $G(s) = 1/(m(s^2 + 2\zeta\omega_n s + \omega_n^2))$ is the transfer function of the structural dynamics of the system, defining a relationship between the grinding force and the wheel vibration in the frequency domain according to Figure 4.5. The right-hand side of Eq. (4.46) can be rearranged to obtain

$$\frac{X(s)}{G(s)} = w \sum_{n=-N}^{N} c_n \left(\int_0^\infty \xi(t-\tau) e^{i\frac{2\pi n t}{\tau}} e^{-st} dt - \int_0^\infty \xi(t) e^{i\frac{2\pi n t}{\tau}} e^{-st} dt \right). \tag{4.47}$$

Utilising the frequency shifting property of the Laplace transform, according to which

$$\int_0^\infty f(t) e^{at} e^{-st} dt = F(s-a), \tag{4.48}$$

where a is arbitrary and $F(s)$ is the Laplace transform of $f(t)$, it is possible to get

$$\frac{X(s)}{G(s)} = w \sum_{n=-N}^{N} c_n \left(e^{-\tau\left(s - i\frac{2\pi n}{\tau}\right)} X\left(s - i\frac{2\pi n}{\tau}\right) - X\left(s - i\frac{2\pi n}{\tau}\right) \right), \tag{4.49}$$

which can be further simplified to

$$\frac{X(s)}{G(s)} = w(e^{-\tau s} - 1) \sum_{n=-N}^{N} c_n X\left(s - i\frac{2\pi n}{\tau}\right). \tag{4.50}$$

Although Eq. (4.50) defines a closed-form expression for the wheel vibration X, the corresponding open-loop transfer function is not straightforward to calculate, because the arguments of X are not identical, but offset versions of one another. Therefore, in order to obtain the open-loop transfer function from Eq. (4.50), further mathematical manipulations are required. The following steps are largely based on the harmonic transfer function approach introduced by Sims to determine the stability of variable helix tools [152].

Introducing the grit-passing frequency $\omega_p = 2\pi/\tau = Z\omega_g$, and substituting $s = i\omega$, which gives the Fourier transform or frequency response of the system, Eq. (4.50) can be rearranged as

$$X(i\omega) = w\left(e^{-2\pi i\frac{\omega}{\omega_p}} - 1\right) G(i\omega) \sum_{n=-N}^{N} c_n X(i\omega - in\omega_p). \tag{4.51}$$

It can be seen in Eq. (4.51) that the wheel vibration X at any frequency ω contains components from a number of harmonics. In other words, the wheel vibration at any frequency depends on the same vibration at a number of other frequencies as well. Therefore,

generalising Eq. (4.51) by substituting $\omega = \omega + p\omega_p$, the frequency response of the system can be calculated at any harmonic according to

$$X(i\omega + ip\omega_p) = w\left(e^{-2\pi i\frac{\omega+p\omega_p}{\omega_p}} - 1\right) G(i\omega + ip\omega_p) \sum_{n=-N}^{N} c_n X(i\omega + ip\omega_p - in\omega_p). \quad (4.52)$$

Introducing $q = p - n$, so that $n = p - q$, it is possible to get

$$X(i\omega + ip\omega_p) = w\left(e^{-2\pi i\frac{\omega+p\omega_p}{\omega_p}} - 1\right) G(i\omega + ip\omega_p) \sum_{p-q=-N}^{N} c_{p-q} X(i\omega + iq\omega_p). \quad (4.53)$$

Using the index notations

$$\hat{x}_p(i\omega) = X(i\omega + ip\omega_p), \quad (4.54)$$

$$\hat{g}_{p,p}(i\omega) = w\left(e^{-2\pi i\frac{\omega+p\omega_p}{\omega_p}} - 1\right) G(i\omega + ip\omega_p), \quad (4.55)$$

$$\hat{h}_{p,q} = c_{p-q}, \quad (4.56)$$

$$\hat{x}_q(i\omega) = X(i\omega + iq\omega_p), \quad (4.57)$$

Eq. (4.53) can be written in the compact form

$$\hat{x}_p(i\omega) = \hat{g}_{p,p}(i\omega) \sum_{p-q=-N}^{N} \hat{h}_{p,q}\hat{x}_q(i\omega), \quad (4.58)$$

where both p and q run from $-\infty$ to $+\infty$. For the sake of clarity and understanding, Eq. (4.58) is presented in matrix form as well:

$$\begin{bmatrix} \vdots \\ \hat{x}_{-1} \\ \hat{x}_0 \\ \hat{x}_1 \\ \vdots \end{bmatrix} = \begin{bmatrix} \ddots & \vdots & \vdots & \vdots & \iddots \\ \cdots & \hat{g}_{-1,-1} & 0 & 0 & \cdots \\ \cdots & 0 & \hat{g}_{0,0} & 0 & \cdots \\ \cdots & 0 & 0 & \hat{g}_{1,1} & \cdots \\ \iddots & \vdots & \vdots & \vdots & \ddots \end{bmatrix} \begin{bmatrix} \ddots & \vdots & \vdots & \vdots & \iddots \\ \cdots & \hat{h}_{-1,-1} & \hat{h}_{-1,0} & \hat{h}_{-1,1} & \cdots \\ \cdots & \hat{h}_{0,-1} & \hat{h}_{0,0} & \hat{h}_{0,1} & \cdots \\ \cdots & \hat{h}_{1,-1} & \hat{h}_{1,0} & \hat{h}_{1,1} & \cdots \\ \iddots & \vdots & \vdots & \vdots & \ddots \end{bmatrix} \begin{bmatrix} \vdots \\ \hat{x}_{-1} \\ \hat{x}_0 \\ \hat{x}_1 \\ \vdots \end{bmatrix}. \quad (4.59)$$

It can be seen that $\hat{x}_p(i\omega)$ and $\hat{x}_q(i\omega)$ represent the same column vector with different indices. Therefore, a new closed-form expression has been derived for the wheel vibration X, but this time, the arguments of X are identical. The cost of this transformation was that $\hat{\mathbf{GH}}(i\omega) = \hat{g}_{p,p}(i\omega)\hat{h}_{p,q}$, which is the open-loop transfer function of the positive feedback system, is now a doubly infinite matrix. Although this is a major increase in complexity, Sims lays out a number of ways to simplify $\hat{\mathbf{GH}}(i\omega)$, such as exploiting its periodicity and symmetry, and truncating it based on the high-frequency behaviour of $G(i\omega)$. These are not presented here at length, the details are provided in [152].

Having derived the open-loop transfer function of the system for both the zero-frequency and the multi-frequency solutions, the following section presents and discusses the stability results obtained by these two approaches.

m [kg]	ζ [%]	f_n [Hz]	K_n [N/m^2]	K_t [N/m^2]	R_g [mm]
5	5	200	2×10^8	6×10^8	110

Table 4.1: Modal and cutting parameters corresponding to Figures 4.6 and 4.7

4.1.4 Stability results

The stability boundaries corresponding to a regular grain distribution are presented in Figures 4.6 and 4.7 for two rather extreme depths of cut (0.02 and 6 mm) in order to demonstrate the effect of radial immersion on process stability. Every other parameter is identical in the two cases. These constants are summarised in Table 4.1, where $f_n = \omega_n/(2\pi)$ is the natural frequency of the grinding wheel in Hertz. The normal and tangential cutting-force coefficients were chosen based on the ones reported in [153] for milling. The only parameter that varies in each subplot is the number of cutting edges: three values have been considered (50, 100 and 500), all of which are much lower than what is expected in practice. However, they were selected in this way for a reason, i.e., to demonstrate the overall effect of Z as clearly as possible. It can be seen that increasing the number of cutting edges stabilises the process relatively quickly. Although the absolute stability limit (corresponding to a width of cut below which the process is stable irrespective of the wheel speed) moves slightly downwards, the biggest lobe rises and moves to the left, resulting in an overall increase in stability. Therefore, considering the general trend demonstrated by each subplot in Figures 4.6 and 4.7, it can be concluded that single-pass surface grinding is always stable with respect to workpiece regenerative chatter, due to the fact that the number of cutting edges is in the order of thousands or even tens of thousands in practice.

Although the primary objective of this section has been achieved, it is interesting to note the effect of radial immersion on process stability. It can be seen that for a low depth of cut, there is a significant difference between the zero-frequency and multi-frequency solutions. That is because for a low radial immersion, the intermittent nature of the grinding process cannot be neglected, i.e., the effect of parametric excitation is so dominant that approximating the dynamic cutting-force coefficient by the constant term of its Fourier series yields a highly inaccurate result. However, for a low depth of cut, there is no major difference between up-grinding and down-grinding operations – the stability diagrams are nearly identical in the two scenarios. Considering the high radial immersion case, the difference between the zero-frequency and multi-frequency solutions is not very significant, indicating the fact that the effect of parametric excitation is negligible, i.e., assuming a constant dynamic cutting-force coefficient gives a fairly accurate result. In this case, however, there is a more prominent difference between up-grinding and down-grinding – the former is a more stable configuration. Furthermore, low immersion grinding is significantly more stable with respect to workpiece regeneration than high immersion grinding (note the scales of the width of cut axes in Figures 4.6 and 4.7). But since the overall conclusion of this section is that workpiece-related instability does not affect single-pass surface grinding in practice, the stability results summarised in Figures 4.6 and 4.7 are not discussed in any further detail.

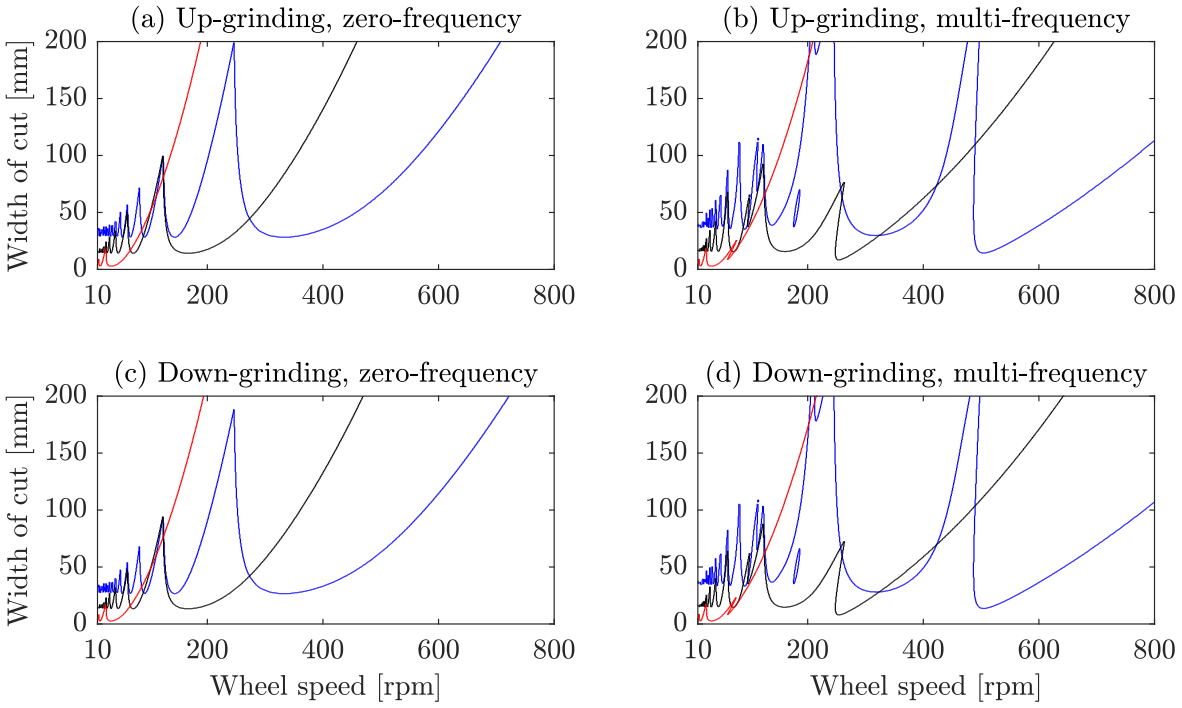

Figure 4.6: Stability boundaries corresponding to a regular grain distribution for a depth of cut of 0.02 mm: —— $Z = 50$, —— $Z = 100$, —— $Z = 500$

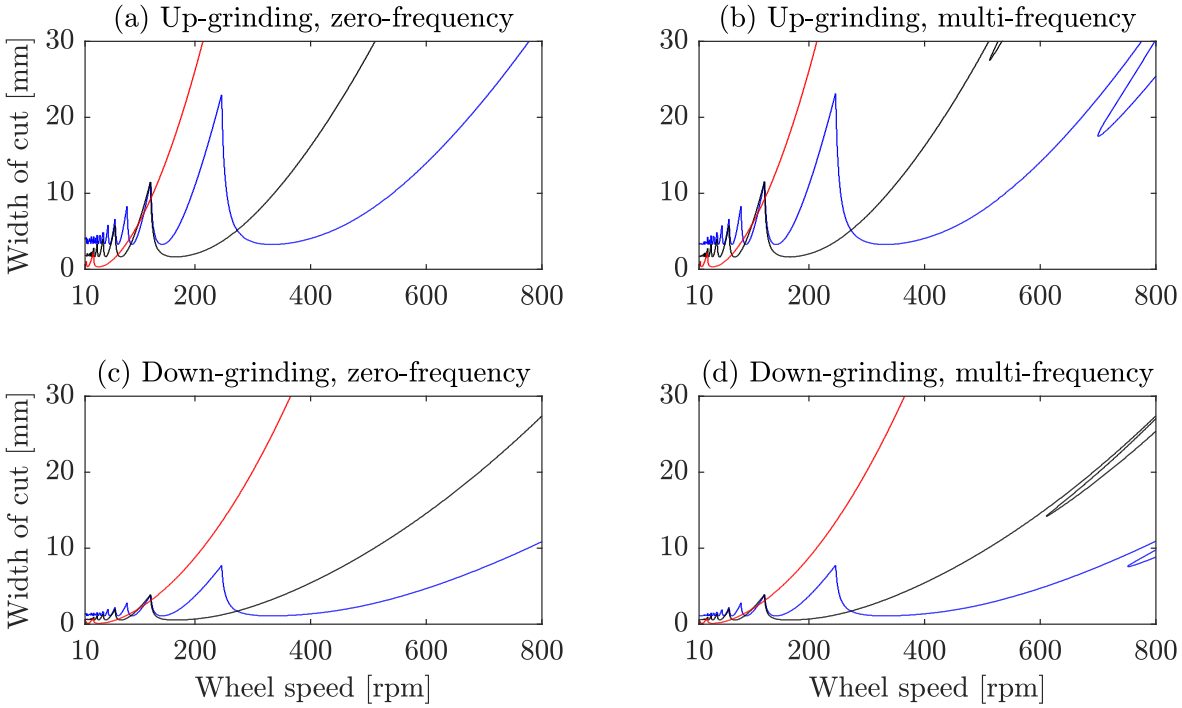

Figure 4.7: Stability boundaries corresponding to a regular grain distribution for a depth of cut of 6 mm: —— $Z = 50$, —— $Z = 100$, —— $Z = 500$

Although an irregular grain distribution certainly disturbs the regenerative effect and increases stability even further, it is presented in the next section for the sake of completeness and practical understanding, as it provides much more realistic insight into the inherently random nature of grinding than a regular grain distribution model does.

4.2 Irregular grain distribution

This investigation follows the same flow of thought as that corresponding to a regular grain distribution. Since the mechanical models are identical in the two cases (i.e. Figure 4.1 can describe both regular and irregular grain distributions), the mathematical model of the problem is considered right away.

4.2.1 Mathematical model

Due to the fact that the derivation of the equation of motion was presented at length in Section 4.1, the following analysis focuses on explaining the differences between the two scenarios instead of repeating the same steps in detail. Based on Eq. (4.27), the equation of motion corresponding to an irregular grain distribution can be formulated as

$$\ddot{\xi}(t) + 2\zeta\omega_n\dot{\xi}(t) + \omega_n^2\xi(t) = K_s \sum_{j=0}^{Z-1} K_d(t)(\xi(t-\tau_j) - \xi(t)), \tag{4.60}$$

where the static and dynamic cutting-force coefficients, K_s and $K_d(t)$, are defined as

$$K_s = \frac{wq}{m}\left(\frac{2\pi v_w}{\omega_g Z}\right)^{q-1}, \tag{4.61}$$

$$K_d(t) = g_j(t)(\sin\varphi_j(t))^{q-1}\cos\varphi_j(t)(K_n\cos\varphi_j(t) - K_t\sin\varphi_j(t)). \tag{4.62}$$

There are three main differences between Eqs. (4.27) and (4.60). First, the time delay is no longer uniform but stochastic across the cutting edges. Second, as a result of this, the difference of the current and delayed positions of the grinding wheel cannot be taken out of the sum. And third, the instantaneous angular position of grain j becomes

$$\varphi_j(t) = \omega_g t + j\frac{2\pi}{Z} + \rho_j, \tag{4.63}$$

where ρ_j is a random constant for each grain, which can be generated according to a number of probability distributions, such as uniform or normal. Chosen from the symmetric interval $\rho_j \in (-\pi/Z, +\pi/Z)$, the total range of ρ_j is equal to the pitch angle between two grits corresponding to a regular grain distribution, i.e., $2\pi/Z$.

4.2.2 Stability analysis

Similarly to the regular grain distribution case, Eq. (4.60) has no analytical solution in its current form, but this problem can be resolved by considering the Fourier series approxi-

mation of the dynamic cutting-force coefficient again, which is a T_g-periodic function now due to the stochastic distribution of the cutting edges around the circumference of the grinding wheel. Therefore, taking the Fourier series approximation of $K_d(t)$, it is possible to get

$$K_d(t) = \sum_{n=-N}^{N} c_n e^{i\frac{2\pi nt}{T_g}}, \tag{4.64}$$

where the Fourier coefficients can be found in the form

$$c_n = \frac{1}{T_g}\int_0^{T_g} K_d(t) e^{-i\frac{2\pi nt}{T_g}} dt. \tag{4.65}$$

Substituting Eq. (4.62) into Eq. (4.65), the Fourier coefficients can be calculated as

$$c_n = \frac{1}{T_g}\int_0^{T_g} g_j(t)(\sin\varphi_j(t))^{q-1}\cos\varphi_j(t)(K_n\cos\varphi_j(t) - K_t\sin\varphi_j(t))e^{-i\frac{2\pi nt}{T_g}} dt. \tag{4.66}$$

Changing the variable of integration from t to φ_j, where the relationship between the two is established by Eq. (4.63), it is possible to get

$$c_n = \frac{1}{\omega_g T_g}\int_{j\frac{2\pi}{Z}+\rho_j}^{2\pi+j\frac{2\pi}{Z}+\rho_j} g_j(\varphi_j)(\sin\varphi_j)^{q-1}\cos\varphi_j \ldots$$
$$\ldots (K_n\cos\varphi_j - K_t\sin\varphi_j)e^{-in\left(\varphi_j - j\frac{2\pi}{Z} - \rho_j\right)} d\varphi_j. \tag{4.67}$$

The current limits of integration show that each grain (regardless of its starting point) is to be considered for one full revolution of the grinding wheel. Due to the fact that $g_j(\varphi_j) = 0$ unless $\varphi_{en} \leq \varphi_j \bmod 2\pi \leq \varphi_{ex}$, it is possible to write

$$c_n = \frac{e^{in\left(j\frac{2\pi}{Z}+\rho_j\right)}}{2\pi}\int_{\varphi_{en}}^{\varphi_{ex}} (\sin\varphi_j)^{q-1}\cos\varphi_j(K_n\cos\varphi_j - K_t\sin\varphi_j)e^{-in\varphi_j} d\varphi_j. \tag{4.68}$$

For the sake of clarity with regard to future calculations, the Fourier coefficients are represented from now on in the short form

$$c_n = C_n e^{in\left(j\frac{2\pi}{Z}+\rho_j\right)}, \tag{4.69}$$

where the parameter C_n is independent of j and stands for

$$C_n = \frac{1}{2\pi}\int_{\varphi_{en}}^{\varphi_{ex}} (\sin\varphi_j)^{q-1}\cos\varphi_j(K_n\cos\varphi_j - K_t\sin\varphi_j)e^{-in\varphi_j} d\varphi_j. \tag{4.70}$$

It can be seen that the Fourier coefficients are dependent on j for an irregular grain distribution, while Eq. (4.39) shows that they were independent of j in the regular case. Based on the number of harmonics or Fourier terms considered, one can again distinguish between zero-frequency and multi-frequency solutions.

4.2.2.1 Zero-frequency solution

Neglecting all harmonics and considering the constant Fourier term alone, the equation of motion becomes

$$\ddot{\xi}(t) + 2\zeta\omega_n\dot{\xi}(t) + \omega_n^2\xi(t) = \frac{wc_0}{m}\sum_{j=0}^{Z-1}(\xi(t-\tau_j) - \xi(t)), \tag{4.71}$$

where the relationship between the chip thickness and the grinding force has been assumed to be linear again, so the constant Fourier coefficient can be calculated as

$$\begin{aligned} c_0 &= \frac{1}{2\pi}\int_{\varphi_{en}}^{\varphi_{ex}} \cos\varphi_j(K_n\cos\varphi_j - K_t\sin\varphi_j)d\varphi_j = \\ &= \frac{1}{4\pi}(K_n(\varphi_c + \cos\varphi_c\sin\varphi_c) \mp K_t(\sin\varphi_c)^2), \end{aligned} \tag{4.72}$$

which is exactly the same as Eq. (4.41), except for the multiplication by Z, which is retained in Eq. (4.71) in the form of a sum. Similarly to the regular grain distribution case, the stability of the system will be assessed by the Nyquist criterion. Therefore, taking the Laplace transform of Eq. (4.71), it is possible to get

$$(s^2 + 2\zeta\omega_n s + \omega_n^2)X(s) = \frac{wc_0}{m}\left(\sum_{j=0}^{Z-1} e^{-\tau_j s} - Z\right)X(s). \tag{4.73}$$

Therefore, the open-loop transfer function of the negative feedback system reads as

$$T_o(s) = \frac{wc_0\left(Z - \sum_{j=0}^{Z-1} e^{-\tau_j s}\right)}{m(s^2 + 2\zeta\omega_n s + \omega_n^2)}. \tag{4.74}$$

Comparing Eqs. (4.43) and (4.74), it can be seen that the main difference between the two transfer functions lies in the exponential term that contains the time delay. Similarly to the regular grain distribution case, the stability results corresponding to Eq. (4.74) will be presented together with those of the multi-frequency solution.

4.2.2.2 Multi-frequency solution

Considering multiple harmonics in Eq. (4.64) and substituting it back into Eq. (4.60), the equation of motion of the system has the form

$$\ddot{\xi}(t) + 2\zeta\omega_n\dot{\xi}(t) + \omega_n^2\xi(t) = \frac{w}{m}\sum_{j=0}^{Z-1}\sum_{n=-N}^{N} c_n e^{i\frac{2\pi nt}{T_g}}(\xi(t-\tau_j) - \xi(t)), \tag{4.75}$$

where the cutting-force exponent q has been assumed to be one again. Substituting Eq. (4.69) and rearranging Eq. (4.75), it is possible to get

$$\ddot{\xi}(t) + 2\zeta\omega_n\dot{\xi}(t) + \omega_n^2\xi(t) = \frac{w}{m}\sum_{n=-N}^{N} C_n\sum_{j=0}^{Z-1} e^{in\left(j\frac{2\pi}{Z}+\rho_j\right)}e^{in\omega_g t}(\xi(t-\tau_j) - \xi(t)). \tag{4.76}$$

Taking the Laplace transform of Eq. (4.76), and substituting $G(s) = 1/(m(s^2 + 2\zeta\omega_n s + \omega_n^2))$ for the structural dynamics of the system again, the equation of motion becomes

$$\frac{X(s)}{G(s)} = \int_0^\infty \left(w \sum_{n=-N}^{N} C_n \sum_{j=0}^{Z-1} e^{in\left(j\frac{2\pi}{Z}+\rho_j\right)} e^{in\omega_g t} (\xi(t-\tau_j) - \xi(t)) \right) e^{-st} dt. \tag{4.77}$$

Taking all the time-independent terms out of the integral, Eq. (4.77) can be written as

$$\begin{aligned} \frac{X(s)}{G(s)} = w \sum_{n=-N}^{N} C_n \sum_{j=0}^{Z-1} e^{in\left(j\frac{2\pi}{Z}+\rho_j\right)} \dots \\ \dots \left(\int_0^\infty \xi(t-\tau_j) e^{in\omega_g t} e^{-st} dt - \int_0^\infty \xi(t) e^{in\omega_g t} e^{-st} dt \right). \end{aligned} \tag{4.78}$$

Utilising the frequency shifting property of the Laplace transform again, the integrals above can be evaluated such that Eq. (4.78) becomes

$$\frac{X(s)}{G(s)} = w \sum_{n=-N}^{N} C_n \sum_{j=0}^{Z-1} e^{in\left(j\frac{2\pi}{Z}+\rho_j\right)} (e^{-\tau_j(s-in\omega_g)} X(s - in\omega_g) - X(s - in\omega_g)). \tag{4.79}$$

Substituting $s = i\omega$ in order to get the Fourier transform, i.e., the frequency response of the system, it is possible to obtain

$$\begin{aligned} X(i\omega) = wG(i\omega) \sum_{n=-N}^{N} C_n \sum_{j=0}^{Z-1} e^{in\left(j\frac{2\pi}{Z}+\rho_j\right)} \dots \\ \dots (e^{-\tau_j(i\omega - in\omega_g)} X(i\omega - in\omega_g) - X(i\omega - in\omega_g)). \end{aligned} \tag{4.80}$$

Factoring out $X(i\omega - in\omega_g)$, Eq. (4.80) can be further simplified to

$$X(i\omega) = wG(i\omega) \sum_{n=-N}^{N} C_n X(i\omega - in\omega_g) \sum_{j=0}^{Z-1} e^{in\left(j\frac{2\pi}{Z}+\rho_j\right)} (e^{-\tau_j(i\omega - in\omega_g)} - 1). \tag{4.81}$$

Substituting $\omega = \omega + p\omega_g$, Eq. (4.81) can be generalised according to

$$\begin{aligned} X(i\omega + ip\omega_g) = wG(i\omega + ip\omega_g) \dots \\ \dots \sum_{n=-N}^{N} C_n X(i\omega + ip\omega_g - in\omega_g) \sum_{j=0}^{Z-1} e^{in\left(j\frac{2\pi}{Z}+\rho_j\right)} (e^{-\tau_j(i\omega + ip\omega_g - in\omega_g)} - 1). \end{aligned} \tag{4.82}$$

Introducing $q = p - n$ again, so that $n = p - q$, it is possible to get

$$\begin{aligned} X(i\omega + ip\omega_g) = wG(i\omega + ip\omega_g) \dots \\ \dots \sum_{p-q=-N}^{N} C_{p-q} X(i\omega + iq\omega_g) \sum_{j=0}^{Z-1} e^{i(p-q)\left(j\frac{2\pi}{Z}+\rho_j\right)} (e^{-\tau_j(i\omega + iq\omega_g)} - 1). \end{aligned} \tag{4.83}$$

Using the index notations

$$\hat{x}_p(i\omega) = X(i\omega + ip\omega_g), \tag{4.84}$$

$$\hat{g}_{p,p}(i\omega) = wG(i\omega + ip\omega_g), \tag{4.85}$$

$$\hat{h}_{p,q}(i\omega) = C_{p-q} \sum_{j=0}^{Z-1} e^{i(p-q)\left(j\frac{2\pi}{Z}+\rho_j\right)} (e^{-\tau_j(i\omega+iq\omega_g)} - 1), \tag{4.86}$$

$$\hat{x}_q(i\omega) = X(i\omega + iq\omega_g), \tag{4.87}$$

Eq. (4.83) can be written in the compact forms

$$\hat{x}_p(i\omega) = \hat{g}_{p,p}(i\omega) \sum_{p-q=-N}^{N} \hat{h}_{p,q}(i\omega)\hat{x}_q(i\omega), \tag{4.88}$$

$$\hat{\mathbf{X}}(i\omega) = \hat{\mathbf{GH}}(i\omega)\hat{\mathbf{X}}(i\omega), \tag{4.89}$$

where, similarly to the regular grain distribution case, the open-loop transfer function $\hat{\mathbf{GH}}(i\omega)$ is a doubly infinite matrix that can be simplified according to the principles mentioned in Section 4.1 and described in greater detail in [152].

4.2.3 Results and observations

The stability boundaries corresponding to an irregular grain distribution are presented in Figure 4.8 for the same grinding parameters as those listed in Section 4.1.4. These calculations are computationally expensive, significantly more than the regular grain distribution case, that is why the stability diagrams are presented for only one depth of cut and that is why the resolution of the stability boundaries is noticeably lower than that corresponding to a regular grain distribution. Nevertheless, the overall conclusion that can be drawn from Figure 4.8 is the same as that pertaining to Figures 4.6 and 4.7, i.e., increasing the number of cutting points to practical values stabilises the process to such an extent that workpiece regeneration cannot be the source of instability in single-pass surface grinding.

Additionally, the presented theory is in agreement with the well-known stabilising effect of an irregular cutting edge distribution. In milling, for example, the stability of the process can be improved by using variable pitch tools [50, 51, 154], which is fundamentally the same idea – the regenerative effect is disrupted by an uneven distribution of cutting points around the circumference of the tool. The difference in stability between a regular and an irregular grain distribution is presented in Figure 4.9. It can be seen that an irregular grain distribution results in a significantly more stable process than a regular one.

Thirdly, the author has noticed that increasing the number of irregularly distributed cutting edges gives more consistent stability boundaries. In other words, two randomly generated grain distributions produce two different stability diagrams, and increasing the number of cutting points reduces the difference between these two sets of stability boundaries. This somewhat intuitive result is demonstrated in Figure 4.10. However, the

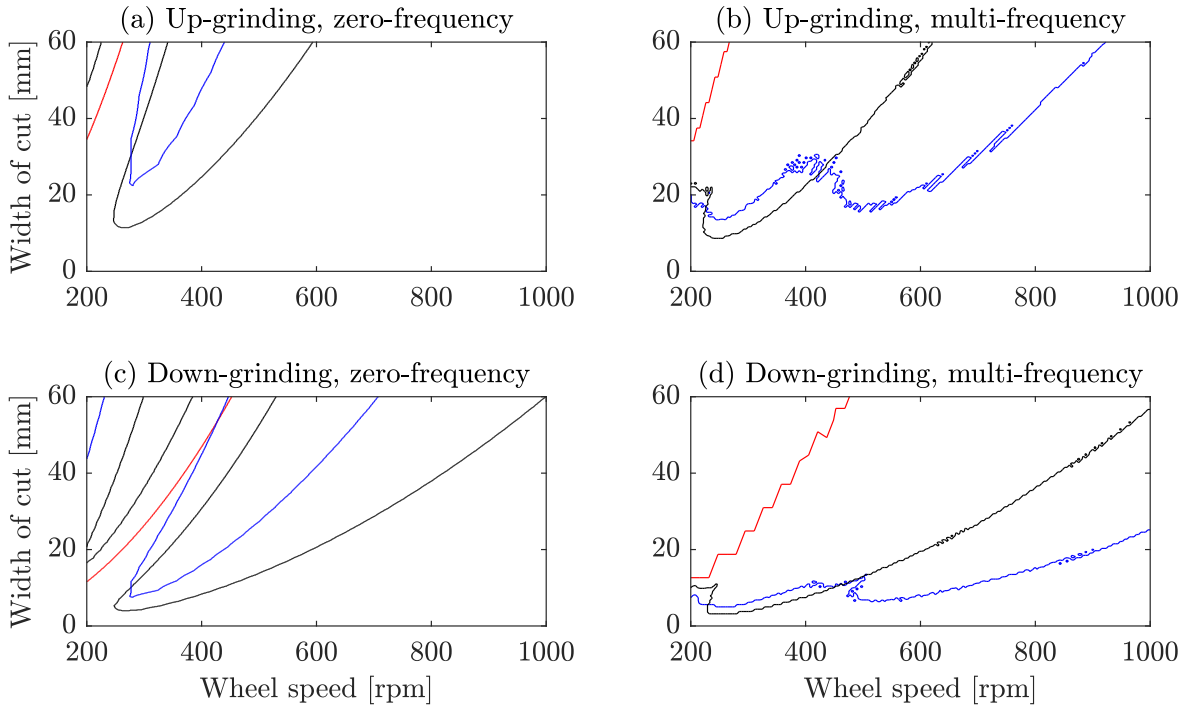

Figure 4.8: Stability boundaries corresponding to an irregular grain distribution for a depth of cut of 6 mm: —— $Z = 50$, —— $Z = 100$, —— $Z = 500$

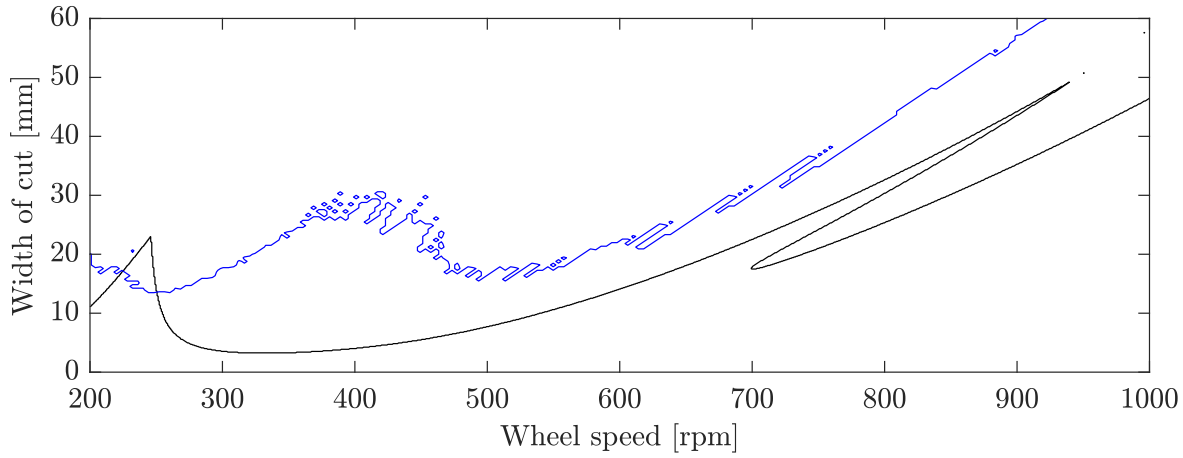

Figure 4.9: Stability boundaries for $Z = 50$ (up-grinding, multi-frequency): —— regular grain distribution, —— irregular grain distribution

fact that a higher number of grits corresponds to more consistent stability boundaries suggests that, for a large enough number of cutting edges, the stability of the process no longer depends on the actual layout of grains, but can be characterised solely by the statistical parameters of the normal distribution from which the individual samples are randomly drawn. Recognising this, it is possible to avoid having to generate a specific layout of cutting edges before each simulation. This would favourably impact the amount of resources necessary to perform computationally expensive calculations. Therefore, although this is somewhat of a tangent since the main point of this chapter has already been established, this idea is briefly explored now, because the application of stochastic

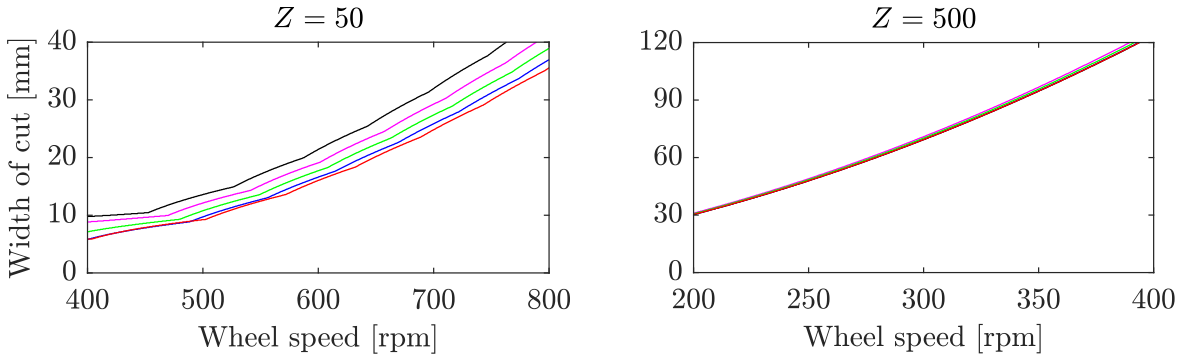

Figure 4.10: Stability diagrams for two different grain densities – the different colours indicate different random realisations corresponding to the same pitch angle distribution parameters: $\mu = 2\pi/Z$, $\sigma = \pi/Z$ (up-grinding, zero-frequency)

time delays is much broader than grinding. Taking the simpler case, i.e. the zero-frequency solution, the stochastic sum in Eq. (4.74) can be manipulated in such a way that the statistical parameters of the random distribution will eventually appear in the open-loop transfer function of the system. Considering the fact that the randomness of the grain distribution is characterised by $\tau_j = \phi_j/\omega_g$, where ϕ_j is the pitch angle of grit j, the stochastic sum in Eq. (4.74) can be expanded into a Taylor series according to

$$\sum_{j=0}^{Z-1} e^{-\frac{\phi_j}{\omega_g}s} = \sum_{j=0}^{Z-1}\sum_{k=0}^{\infty} \frac{(-\phi_j s)^k}{\omega_g^k k!} = \sum_{k=0}^{\infty} \frac{(-s)^k}{\omega_g^k k!} \sum_{j=0}^{Z-1} \phi_j^k \approx Z \sum_{k=0}^{\infty} \frac{(-s)^k}{\omega_g^k k!} M_k(\mu, \sigma^2), \tag{4.90}$$

where $M_k(\mu, \sigma^2)$ is the k^{th}-order non-central or raw moment of the normal distribution characterised by its mean μ and variance σ^2. The above expansion of the exponential function was calculated at $s = 0$, which corresponds to the midpoint of the numerical Nyquist contour (as presented in Appendix A) and therefore is a reasonable location for the Taylor series. The approximation at the end of Eq. (4.90) is accurate if the number of samples (i.e. cutting edges) is large enough, which is always true for realistic grinding processes. If the probability density function of the normal distribution is in the form

$$f(\phi_j \,|\, \mu, \sigma^2) = \frac{1}{\sqrt{2\pi\sigma^2}} e^{-\frac{(\phi_j - \mu)^2}{2\sigma^2}}, \tag{4.91}$$

then the formal definition of the k^{th}-order non-central or raw moment reads as

$$\frac{1}{Z}\sum_{j=0}^{Z-1} \phi_j^k \approx M_k(\mu, \sigma^2) = \int_{-\infty}^{\infty} f(\phi_j \,|\, \mu, \sigma^2)\, \phi_j^k \, d\phi_j. \tag{4.92}$$

These moments can be calculated relatively easily with the help of symbolic software such as Wolfram Mathematica. The description of random time delays as presented here has promising theoretical and practical implications when it comes to determining the stability of stochastic systems in general. Therefore, the solution of the stochastic delay problem as defined by Eqs. (4.90) to (4.92) is explored briefly in the following section.

k	$M_k(\mu, \sigma^2)$	$\frac{(-s)^k}{\omega_g^k k!} M_k(\mu, \sigma^2)$
0	1	1
1	μ	$\frac{-s}{\omega_g}\mu$
2	$\mu^2 + \sigma^2$	$\frac{s^2}{2\omega_g^2}(\mu^2 + \sigma^2)$
3	$\mu^3 + 3\mu\sigma^2$	$\frac{-s^3}{6\omega_g^3}(\mu^3 + 3\mu\sigma^2)$
4	$\mu^4 + 6\mu^2\sigma^2 + 3\sigma^4$	$\frac{s^4}{24\omega_g^4}(\mu^4 + 6\mu^2\sigma^2 + 3\sigma^4)$

Table 4.2: The first few terms of the infinite series in Eq. (4.93)

4.2.4 Solution of the stochastic delay problem

According to the final observation of the previous section, the solution of the stochastic delay problem is presented here. Substituting Eq. (4.90) into Eq. (4.74), the open-loop transfer function of the system corresponding to the zero-frequency solution becomes

$$T_o(s) = \frac{wc_0 Z \left(1 - \sum_{k=0}^{\infty} \frac{(-s)^k}{\omega_g^k k!} M_k(\mu, \sigma^2)\right)}{m(s^2 + 2\zeta\omega_n s + \omega_n^2)}, \tag{4.93}$$

where the constant Fourier coefficient c_0 is given in Eq. (4.72). In order to visualise the infinite series in Eq. (4.93), its first few terms are summarised in Table 4.2. Therefore, the open-loop transfer function can be expanded as

$$\begin{aligned} T_o(s) = &- \frac{wc_0 Z \frac{-s}{\omega_g}\mu}{m(s^2 + 2\zeta\omega_n s + \omega_n^2)} - \frac{wc_0 Z \frac{s^2}{2\omega_g^2}(\mu^2 + \sigma^2)}{m(s^2 + 2\zeta\omega_n s + \omega_n^2)} - \\ &- \frac{wc_0 Z \frac{-s^3}{6\omega_g^3}(\mu^3 + 3\mu\sigma^2)}{m(s^2 + 2\zeta\omega_n s + \omega_n^2)} - \frac{wc_0 Z \frac{s^4}{24\omega_g^4}(\mu^4 + 6\mu^2\sigma^2 + 3\sigma^4)}{m(s^2 + 2\zeta\omega_n s + \omega_n^2)} - \dots \end{aligned} \tag{4.94}$$

Due to the fact that the infinite series is a result of a Taylor expansion, $T_o(s)$ is expected to converge to its analytical form as more and more terms are considered. However, when it comes to numerical calculations, the infinite series in Eq. (4.94) has to be truncated after a certain number of terms. Figure 4.11 presents several stability boundaries corresponding to different lengths of truncation, i.e., to different degrees of accuracy.

It can be seen that the rate of convergence depends on the standard deviation σ. Decreasing σ increases the rate of convergence, i.e., the number of Taylor terms necessary for an acceptable solution is lower. Also, the overall speed of convergence seems to be rather slow, which is indicated by the fact that considering more terms noticeably alters the solution. This suggests that many more Taylor terms would be required to obtain an accurate solution. However, comparing Figures 4.8a and 4.11, it is clear that the author's new approach provides a qualitatively good result without having to generate an actual layout of abrasive grits. This saves a lot of time and computational resources. Since this particular problem is not part of the main topic of this work, it is not investigated here

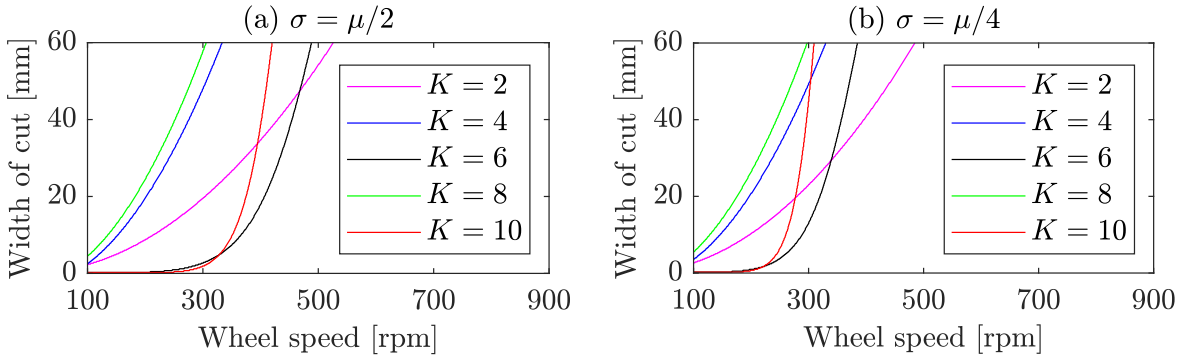

Figure 4.11: Stability boundaries calculated by the author's new approach for $Z = 500$ and $\mu = 2\pi/Z$, considering the first K terms of the infinite series in Eq. (4.94) (irregular grain distribution, up-grinding, zero-frequency)

any further but reserved for future research instead. Nevertheless, it has been shown that the stochastic delay problem can be solved, and the proposed method is a promising way to calculate the dynamic stability of stochastic time-delay systems in general.

4.3 Summary of results

The primary aim of this chapter was to answer the question whether workpiece-related instability or workpiece-related regenerative chatter can occur in single-pass surface grinding. In terms of the layout of the cutting edges around the circumference of the grinding wheel, two fundamental cases were investigated: regular and irregular grain distributions.

As for the regular grain distribution, two rather extreme radial immersion values were considered. One was very small, the depth of cut was 0.02 mm for a wheel radius of 110 mm, which is typical of finishing operations in grinding. The other was fairly large, the depth of cut was 6 mm for the same wheel radius, which is not unusual in creep-feed grinding (CFG) and high-efficiency deep grinding (HEDG). The effect of parametric excitation was clearly visible in the low depth of cut case, however, in terms of process stability, it was concluded that the very high number of cutting edges makes it impossible for single-pass surface grinding to experience workpiece-related regenerative chatter in practice.

Concerning the stability properties of an irregular grain distribution, the obtained results were not unexpected. Due to the fact that the uniformity of the time delay (and therefore the regenerative effect) has been disrupted by a random layout of cutting edges, the system is more stable with regard to workpiece regeneration than the one corresponding to a uniform grit distribution. Additionally, grinding is a stochastic process by nature, so an irregular grain distribution provides a more realistic description of the problem as well. Considering these two consequences of stochastic modelling, the conclusion drawn from the regular grain distribution case was confirmed again: single-pass surface grinding cannot experience workpiece-related instability, as long as practically realistic grinding parameters are considered.

In summary, it can be stated that workpiece regenerative chatter (the type that occurs in milling) cannot develop in practical grinding processes due to the very high number of cutting points on the wheel. Although this result may be somewhat intuitive, perhaps even obvious to experts in the field of machining vibrations, the author deemed the presentation of a robust mathematical analysis of the problem necessary to make sure that workpiece regeneration is truly negligible in single-pass surface grinding. Furthermore, considering the stochastic nature of grinding and approaching it by probabilistic means has opened the door to new possibilities in chatter modelling, including a potential direction for the future of this work.

Consequently, for the purposes of this investigation, there is no need to consider and model each grain individually. This simplification will fundamentally affect the grinding force, because it will no longer be calculated as a sum of chip-thickness-based grit forces, but it will depend on the depth of cut, according to the vast majority of grinding force models in the literature (as presented in Section 2.2.4). Therefore, the next chapter neglects workpiece regeneration altogether and focuses entirely on wheel regeneration based on the new regenerative mechanism proposed in Section 3.1.

Chapter 5

Wheel regeneration in single-pass surface grinding

No grinding wheel is perfectly wear resistant in real life. Even the hardest superabrasives experience some level of wear after a certain amount of grinding time. Therefore, wheel wear is a natural phenomenon in grinding, and can be especially extensive when conventional abrasives are used. And where there is wheel wear, there is a possibility of wheel regeneration as well. Having concluded in Chapter 4 that workpiece regeneration cannot cause instability in single-pass surface grinding, this chapter focuses on wheel regeneration based on the new regenerative mechanism proposed in Section 3.1.

When it comes to the literature of wheel-related grinding chatter, wheel wear has been modelled in one of two ways so far: as distributed radial wear around the circumference of the grinding wheel in the vast majority of cases [25, 100, 106, 107], and as a combination of distributed radial wear and distributed grit dullness by Li and Shin [108]. More information on these papers can be found in Section 2.2.1. Although considering wheel wear in these two ways has been partially successful in predicting wheel-related chatter in grinding, the isolated effect of distributed grit dullness – for the main purpose of assessing its dominance in chatter development – has not yet been studied to such an extent as to produce a well-known and often-cited research article. Therefore, the new grinding chatter theory presented in this chapter – isolating the regenerative mechanism of distributed grit dullness and considering its effect on process stability – is the author's primary contribution to knowledge in this thesis.

Although the graphical representation of the mechanical model is identical to that in Figure 4.1, there are three important differences between the two models, which are highlighted in Sections 5.1.1, 5.1.2 and 5.1.3. They address the grinding force model (as it is no longer chip thickness based but depends on the depth of cut), the wheel wear model (explaining how the regenerative mechanism of distributed grit dullness is implemented), and the wheel vibration model (describing how the new regenerative mechanism can lead to instability). Having established these three important aspects of the new theory, the mathematical model of the problem is derived, starting with the relationships between individual variables and combining them all together in order to obtain the governing

equation of motion of the system. Then process stability is assessed using the Nyquist criterion, followed by a detailed discussion of the obtained results and a brief summary of the most important findings of this investigation.

5.1 Mechanical model

The mechanical model of the system is identical to the one presented in Figure 4.1, apart from three main differences regarding the ways in which the grinding force, the wheel wear and the wheel vibration are considered. These new models are discussed in detail in the following three subsections.

5.1.1 Grinding force model

Based on the findings and conclusions of Chapter 4, the cutting edges no longer need to be modelled individually in order to study chatter in single-pass surface grinding. This provides an opportunity for simplifying the grinding force significantly. Instead of calculating it as a sum of chip-thickness-based grit forces, it can be expressed as a function of the depth of cut, according to the vast majority of grinding force models in the literature. In order to keep the theory as simple as possible, an idealised model will be used, which is one of the most basic ways to describe the grinding force (as discussed in detail in Section 2.2.4.1). Additionally, as an attempt to simplify the model even further, the three grinding mechanisms (sliding, ploughing and chip formation) are not separated either, but treated as a single variable characterising the entire cutting action. Therefore, the grinding force model employed in this chapter can be expressed as

$$F_t = wu\frac{v_w}{v_g}\delta, \tag{5.1}$$

where F_t is the tangential component of the total grinding force, w is the grinding width, u is the specific energy, v_w is the feed rate, v_g is the circumferential speed of the wheel, and δ is the depth of cut. Considering Figure 4.1, the x-component of the total grinding force can be calculated as

$$F_x = F_n \cos\alpha \mp F_t \sin\alpha, \tag{5.2}$$

where the $\mp$ symbol corresponds to up-grinding and down-grinding, respectively, and α is the so-called grinding force angle, indicating the angular position of the resultant grinding force in the cutting zone, where the actual grinding force is distributed in reality. The grinding force angle can be calculated by imagining the contact arc as a curved beam loaded with a sinusoidal distributed force system corresponding to the static chip thickness distribution in the cutting zone (as shown in Figure 4.2). Integrating and equating the distributed force on the two sides of $\varphi = \alpha$, it is possible to formulate an expression for the grinding force angle. Mathematically speaking, the resultant of the distributed force between 0 and α has to be equal to the resultant of the same distributed force between α and φ_c, in order to find the angular position of the concentrated force

that is equivalent to the distributed one. This can be written as

$$\int_0^{\alpha} \sin\varphi \, d\varphi = \int_{\alpha}^{\varphi_c} \sin\varphi \, d\varphi. \tag{5.3}$$

Evaluating the two integrals, it can be seen that the grinding force angle depends on the contact angle alone:

$$\alpha = \arccos\left(\cos^2 \frac{\varphi_c}{2}\right). \tag{5.4}$$

Introducing the grinding force ratio $\mu = F_t/F_n$, which is closely related to the coefficient of friction, the x-component of the total grinding force can also be expressed as

$$F_x = F_t \left(\frac{1}{\mu}\cos\alpha \mp \sin\alpha\right). \tag{5.5}$$

It can be seen that the terms within the parentheses connect the x-component and the tangential component of the total grinding force, such that a new force ratio can be introduced according to $\mu_x = F_x/F_t$. Substituting Eq. (5.1) into Eq. (5.5), the x-component of the grinding force becomes

$$F_x = \mu_x w u \frac{v_w}{v_g}\delta. \tag{5.6}$$

According to the experiments of Malkin and Guo in [11], p. 126, the grinding force ratio μ (and consequently μ_x as long as α does not change) remains approximately constant up to the point of burn as the grinding wheel wears. Therefore, the grinding force model to be employed in this chapter has been established in Eq. (5.6). It is no longer based on the chip thickness, but depends on the depth of cut. This is a fundamental deviation from Li and Shin's theory, whose grinding force model is based on the chip thickness and analogous to milling with a large number of cutting edges [108].

5.1.2 Wheel wear model

As it was stated at the beginning of this chapter, the proposed chatter theory considers wheel wear as grit dullness without radial wear, which can be captured by the specific energy. This is because the specific energy describes how much energy is required to remove a unit volume of workpiece material. Consequently, it is lower for sharper grains and higher for duller grains. Due to the fact that grit dullness is the sole mechanism responsible for the regenerative effect in this model, the variation of the specific energy needs to be quantified both in space (around the circumference of the grinding wheel) and in time (as it develops during grinding). This results in a two-variable description of the specific energy, which constitutes a rather complex mathematical problem when coupled with the stability analysis of a delay differential equation. However, the system can be simplified, because the spatial and temporal variables of the specific energy function are not independent of one another. Time is the only truly independent variable in the model, because space (i.e. the angular coordinate running along the circumference of the grinding wheel) depends on time through the constant rotational speed of the wheel. Therefore, the two variables of the specific energy can be reduced to one. This can be achieved by losing the spatial coordinate altogether and specifying that the specific energy u at time

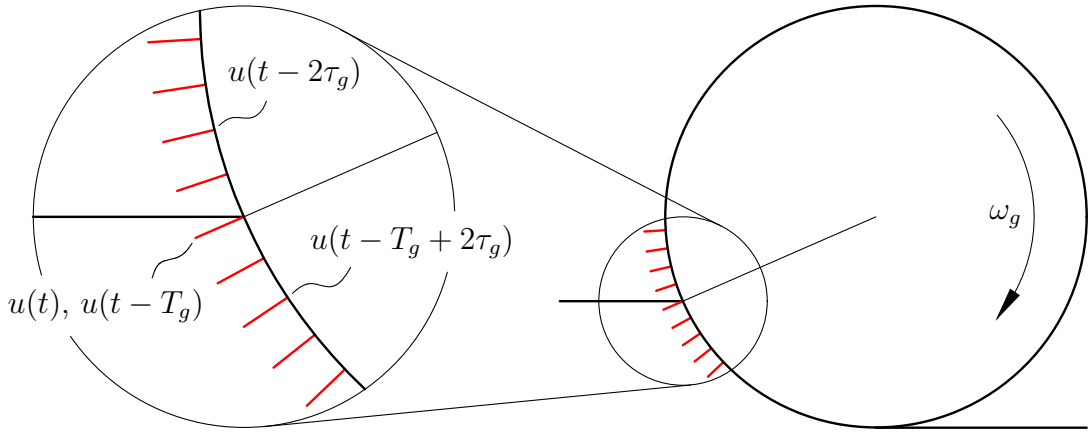

Figure 5.1: Defining the specific energy u around the circumference of the wheel (assuming a regular grain distribution, the grit-passing period is denoted by τ_g)

t corresponds to the point (or grit) on the grinding wheel that is just leaving the cutting zone. This convention is illustrated in Figure 5.1. It can be seen that the specific energy at any other angular location on the wheel can be obtained by shifting $u(t)$ in time. In simple terms, as far as $u(t)$ is concerned, whatever comes right after the angular location where the grains exit the cut is in the 'immediate past', and whatever comes right before it is in the 'distant past'. Therefore, it naturally follows that the spatial distribution of the specific energy around the entire circumference of the grinding wheel can be obtained by considering $u(t)$ over a complete wheel rotation period.

Therefore, the wheel wear model has been established: grit dullness is captured by the specific energy that is described by the solely time-dependent function $u(t)$. Regarding the specific energy, the following assumptions are made. First, due to the high density of cutting edges on the wheel and the rapid rate at which they leave the grinding zone, the specific energy is assumed to be a continuous function of time. Second, as far as the axial direction is concerned, the specific energy is assumed to be constant along the width of the wheel. This is a reasonable approximation for the scenario under study, where the feed direction is perpendicular to the axial direction. However, in the case of crossfeed, where the feed direction is parallel to the axial direction, the variation in wear along the width of the wheel cannot be neglected. And third, the specific energy is assumed to increase inside the grinding zone as a result of wear, and remain constant outside. In other words, no grain gets sharper during grinding, which means that the self-sharpening property of grinding wheels is not considered in the proposed model.

5.1.3 Wheel vibration model

One of the most crucial aspects of the proposed chatter theory is the modelling of how the new regenerative mechanism, i.e. the variation of the specific energy in space and time, influences the displacement of the grinding wheel in such a way that the wheel vibration in turn affects the specific energy, creating a closed loop.

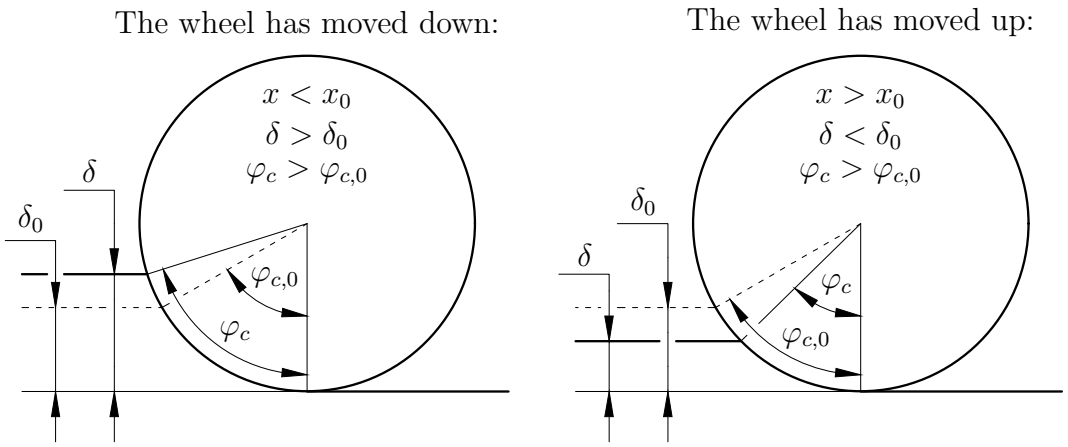

Figure 5.2: Depth-of-cut-based wheel vibration model (x, δ and φ_c are instantaneous parameters, while x_0, δ_0 and $\varphi_{c,0}$ correspond to steady-state grinding)

It is clear that the displacement of the grinding wheel changes both the chip thickness and the depth of cut in reality. As it was stated in Section 5.1.1, the grinding force model is based on the depth of cut, not the chip thickness, since there is no need to consider individual cutting edges for the practical purposes of this investigation. Therefore, the effect of wheel vibration on the chip thickness is neglected in the model. Furthermore, the displacement of the grinding wheel is assumed to disturb the nominal depth of cut in such a way that the entering angle for up-grinding and the exiting angle for down-grinding remain constant, and the exiting angle for up-grinding and the entering angle for down-grinding change as a result of wheel vibration. This concept is visualised in Figure 5.2. It is important to note that this is a significant simplification in the model, which means that, in terms of improving the accuracy of the proposed theory, reconsidering this particular assumption is of high priority.

Consequently, the regenerative effect occurs in this model as follows. As a result of some external disturbance, the grinding wheel begins to oscillate relative to the workpiece. This changes the nominal depth of cut and thus the material removal rate in such a way that both of these parameters will vary in time. Since the material removal rate is not constant anymore, different parts of the grinding wheel will remove different amounts of workpiece material. This leads to different levels of wear around the circumference of the wheel, which is quantified by the specific energy as described in Section 5.1.2. Due to the fact that the grinding force depends on the specific energy, a varying specific energy results in varying grinding forces, which lead to a time-dependent variation in wheel displacement (i.e. wheel vibration) according to the dynamics of the structure. This creates a closed loop: some initial disturbance in the displacement of the grinding wheel causes it to vibrate again. Depending on the magnitude and phase difference between the oscillations of the wheel, the grinding process can be either self-attenuating (stable) or self-amplifying (unstable).

The following section establishes five mathematical relationships between the grinding parameters mentioned above, i.e., between the wheel vibration, depth of cut, material removal rate, specific energy, grinding force and wheel vibration again. From this, the

governing equation of motion of the system is determined for the purpose of assessing the stability of the grinding process.

5.2 Mathematical model

Having established the grinding force, wheel wear and wheel vibration models, the mathematical model of the system can be formulated. Five relationships are derived in this section, all of which are necessary to obtain the equation of motion and determine the stability of the process. These five relationships are established between (1) the wheel vibration and the depth of cut, (2) the depth of cut and the material removal rate, (3) the material removal rate and the specific energy, (4) the specific energy and the grinding force, and (5) the grinding force and the wheel vibration. The following subsections discuss these five relationships in detail.

5.2.1 Wheel vibration and depth of cut

The relationship between the displacement of the grinding wheel and the variation of the depth of cut can be established as

$$\delta(t) = \delta_0 - x(t), \tag{5.7}$$

where $\delta(t)$ is the variation of the depth of cut in time, δ_0 is the desired or nominal depth of cut corresponding to steady-state grinding, and $x(t)$ describes the displacement or vibration of the grinding wheel in time. It can be seen that the origin of the general coordinate x is set in such a way that $x(t) \equiv 0$ corresponds to steady-state grinding. This is a convention chosen by the author to simply the analysis. Since the spring depicted in Figure 4.1 is assumed to be linear (hence the characterisation of it by a single constant), the origin of x can be offset freely without affecting the accuracy of the model. Therefore, the displacement of the grinding wheel is always measured relative to stable, chatter-free machining.

5.2.2 Depth of cut and material removal rate

The amount of workpiece material that has just been removed by the grain exiting the current cut at time t is denoted by $V_w(t)$. Therefore, similarly to the definition of the specific energy described in Section 5.1.2, the time-dependent material removal rate also corresponds to different grains as they are constantly leaving the grinding zone. It can be calculated by integrating the static chip thickness cut by a single grain along the entire contact length characterised by the constant grinding wheel radius and the time-varying contact angle between the wheel and the workpiece. (Note that the chip thickness is assumed to be unaffected by wheel vibration. Wheel vibration is accounted for by the time-varying contact angle.) Since the entering angle is assumed to be zero for up-grinding

regardless of the displacement of the grinding wheel, the exiting angle is always equal to the contact angle. Also, due to the fact that the amount of workpiece material removed by a single grit is independent of the grinding configuration, it can be formulated as

$$V_w(t) = w \int_0^{\varphi_c(t)} h_s(\varphi) R_g d\varphi \tag{5.8}$$

for both up-grinding and down-grinding. The grinding width is denoted by w, and the static chip thickness $h_s(\varphi)$, visualised in Figure 4.2, is expressed in Eq. (4.3). The remaining variables featuring in Eq. (5.8) are defined according to Figure 4.1. Evaluating the integral in Eq. (5.8), it is possible to get

$$V_w(t) = w v_w \tau_g R_g (1 - \cos \varphi_c(t)), \tag{5.9}$$

where τ_g is the constant grit-passing period, assuming a regular grain distribution around the circumference of the grinding wheel. The product $v_w \tau_g$ is the so-called feed per grit, a term equivalent to the feed per tooth in milling. Substituting the time-dependent contact angle

$$\varphi_c(t) = \cos^{-1}\left(1 - \frac{\delta(t)}{R_g}\right) \tag{5.10}$$

into Eq. (5.9), the amount of workpiece material removed by a single grain over one grinding wheel revolution becomes

$$V_w(t) = w v_w \tau_g \delta(t). \tag{5.11}$$

Therefore, the relationship between the depth of cut and the material removal rate has been established. When $\delta(t) < \delta_0$ (i.e. the grinding wheel has moved up), the material removal rate is less than nominal. When $\delta(t) > \delta_0$ (i.e. the grinding wheel has moved down), the material removal rate is greater than nominal. When $\delta(t) = \delta_0$ (i.e. the grinding wheel is in its steady-state position), the material removal rate is nominal.

Due to the fact that a 2D model is considered and thus no grinding parameter changes in the axial direction, the specific material removal rate (material removal rate per unit grinding width) is introduced in such a way that the specific material removed by a single grit over one grinding wheel revolution can be calculated as

$$V'_w(t) = \frac{V_w(t)}{w} = v_w \tau_g \delta(t), \tag{5.12}$$

where the prime symbol indicates that the quantity in question is divided by the grinding width. It is important to point out that, although the grinding force model is based on the depth of cut, the material removal rate requires the chip thickness as well, because it corresponds to a single grain. That is why the grit-passing period remains in Eq. (5.12).

5.2.3 Material removal rate and specific energy

Although, logically speaking, there is an intermediate step between the material removal rate and the specific energy, i.e. the extent of wheel wear and its connection to each

of these two quantities, it is possible to formulate a direct relationship between the material removal rate and the specific energy if the increase in specific energy over one grinding wheel revolution is expressed as a direct function of the material removal rate. As the grinding wheel rotates and the cutting edges exit the grinding zone continually and periodically, the specific energy of each exiting grain can be formulated as a sum of two terms: (1) the specific energy corresponding to the same grain one wheel rotation period earlier, and (2) an increase in specific energy caused by grit wear in the grinding zone. The mathematical representation of this modelling approach can be written as

$$u(t) = u(t - T_g) + \Delta u(t), \tag{5.13}$$

where the specific energy increase is a function of the current time, because it corresponds to the exiting angle, where the current time is measured.

Assuming a linear relationship between the material removal rate and the specific energy increase supported by the experiments of Li and Shin [108], the evolution of the specific energy can be expressed as

$$u(t) = u(t - T_g) + C_d V'_w(t), \tag{5.14}$$

where C_d, introduced by the present author, is the so-called coefficient of dulling. It measures the rate at which the specific energy increases as a result of material removal. It is important to remember that both u and V'_w pertain to individual grains, nevertheless, they are assumed to be continuous functions of time due to the large number of cutting edges on the wheel. The reason V'_w is used in Eq. (5.14) instead of V_w is that increasing the grinding width (and thus the material removal rate) does not increase the specific energy that characterises the entire grinding width at a particular angular location on the wheel. That is because the wider the cut, the more cutting edges are engaged, so the additional wear resulting from an increase in grinding width (and material removal rate) will be distributed among a higher number of cutting edges. This leads to an approximately constant specific energy distribution along the axial direction of the grinding wheel, just as it was assumed in Section 5.1.2. Therefore, the relationship between the material removal rate and the specific energy has been established.

5.2.4 Specific energy and grinding force

Since the different grains in the grinding zone can be worn to different degrees, their respective specific energies can be different as well. Not only that, but the specific energy changes in time as well, as the grits become duller. This creates the potential for a time-varying specific energy distribution in the grinding zone. Therefore, in order to derive a relationship between the specific energy and the grinding force, the specific energy distribution in the grinding zone has to be determined at every instant of time. That is because the grinding force depends on the specific energy according to Eq. (5.6). Therefore, formulating the time-varying specific energy distribution in the grinding zone and integrating it along the entire contact length, it is possible to calculate the instantaneous grinding force. In order to describe the specific energy distribution in the grinding zone at the current time, an additional independent variable needs to be introduced. While

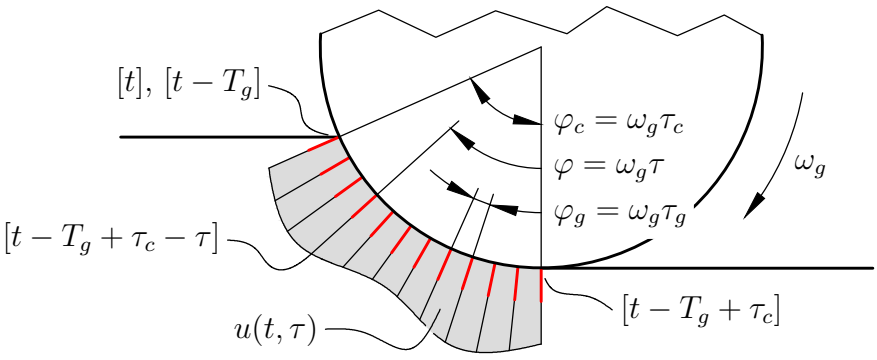

Figure 5.3: Specific energy distribution $u(t, \tau)$ in the grinding zone – the time delays corresponding to three different cutting edges are indicated in square brackets

it would be natural to use an angular coordinate such as φ in Figure 4.1, another time coordinate will be employed for this task. That is because the compatibility thus achieved between the global time coordinate t and the new, local time coordinate τ will simplify future calculations. (It is very important to note the difference between τ and τ_g in this chapter: τ is a local time coordinate fixed to the grinding zone, and τ_g is the constant grit-passing period assuming a regular grain distribution.) Therefore, the specific energy distribution in the grinding zone at the current time will be described by the two-variable function $u(t, \tau)$. This concept is illustrated in Figure 5.3. Since the new time coordinate is local, i.e., it measures the time elapsed since a grain currently in cut entered the grinding zone, it can assume any value between 0 and τ_c, where τ_c denotes the amount of time the currently exiting grain has taken to pass through the grinding zone.

It is clear that τ_c is state dependent in reality, because wheel vibration changes the depth of cut and consequently the contact length as well. It can be calculated as $\tau_c = \varphi_c / \omega_g$, where φ_c is the state-dependent contact angle and ω_g is the constant rotational speed of the grinding wheel. The current model does not take the practical variation of τ_c into account, but considers a quasi-steady cutting time instead, denoted by $\tau_{c,0}$, which corresponds to the steady-state contact angle $\varphi_{c,0}$ and the steady-state depth of cut δ_0. This is to simplify the time delay in the system from being both distributed and state dependent to being distributed only. This is a reasonable simplification assuming that the oscillations of the grinding wheel are small enough so that $\tau_c \approx \tau_{c,0}$ for each grain.

The cutting edges in the grinding zone are worn in different measures as a result of two causes – one is an effect of the past, the other is an effect of the present. On the one hand, the grains left the grinding zone at different times and removed different amounts of workpiece material during the previous cut – this is an effect of the past. On the other hand, depending on their instantaneous locations in the grinding zone at the current time, the grits have removed different amounts of workpiece material during the current cut – this is an effect of the present. Both of these causes need to be taken into account, therefore, $u(t, \tau)$ can be formulated as a sum of two terms according to

$$u(t, \tau) = u_{\text{past}}(t, \tau) + u_{\text{pres}}(\tau), \tag{5.15}$$

where $u_{\text{past}}(t, \tau)$ carries all the information pertaining to the previous cut, and $u_{\text{pres}}(\tau)$ represents all the wear accumulated during the current cut.

The effect of the past can be established by considering the fact that each grain currently in cut left the grinding zone at different times during the previous cut. According to Figure 5.3, it can be calculated as

$$u_{\text{past}}(t,\tau) = u(t - T_g + \tau_{c,0} - \tau). \tag{5.16}$$

As explained earlier, it can be seen that the state-dependent τ_c has been replaced by its quasi-steady equivalent $\tau_{c,0}$ to simplify the time delay.

The effect of the present can be formulated as a function of the local time coordinate alone. It does not depend on the global time coordinate, because it only measures the increase in specific energy as a result of grit wear accumulated during the current cut, which can be quantified by the local time coordinate alone. Therefore, the effect of the present can be determined as the coefficient of dulling times the amount of workpiece material removed by a single grain up to its current location in the grinding zone:

$$u_{\text{pres}}(\tau) = C_d \int_0^{\tau} h_s(\omega_g \tilde{\tau}) R_g \omega_g d\tilde{\tau} = C_d v_w \tau_g R_g (1 - \cos(\omega_g \tau)). \tag{5.17}$$

Therefore, substituting Eqs. (5.16) and (5.17) back into Eq. (5.15), the time-varying distribution of the specific energy in the grinding zone can be written in the form

$$u(t,\tau) = u(t - T_g + \tau_{c,0} - \tau) + C_d v_w \tau_g R_g (1 - \cos(\omega_g \tau)). \tag{5.18}$$

One of the simplest ways to determine the grinding force is to consider the average of the specific energy distribution in the grinding zone and substitute it into Eq. (5.6), so that

$$F_{x,a}(t) = \mu_x w \left(\frac{1}{\tau_{c,0}} \int_0^{\tau_{c,0}} u(t,\tau) d\tau \right) \frac{v_w}{v_g} \delta(t), \tag{5.19}$$

where $\tau_c \approx \tau_{c,0}$ has been assumed again in order to simplify the time delay. Substituting Eq. (5.18) into Eq. (5.19), the average grinding force can be calculated as

$$F_{x,a}(t) = \frac{\mu_x w v_w \delta(t)}{v_g \tau_{c,0}} \int_0^{\tau_{c,0}} u(t - T_g + \tau_{c,0} - \tau) d\tau + C_a, \tag{5.20}$$

where C_a is the time-independent part of the average grinding force and contains the constants coming from $u_{\text{pres}}(\tau)$. It is interesting to see, therefore, that the effect of the present as described earlier in this section has no dynamic impact on the system – it merely offsets the time-varying part of the average grinding force, which does not change the dynamic behaviour of the system provided that the stiffness of the wheel (represented by a spring in Figure 4.1) is linear. That is because τ_c has been replaced by $\tau_{c,0}$, which is a reasonable simplification in the model. Consequently, the constant C_a will be dropped for future calculations.

It can be seen that Eq. (5.20) is non-linear as a result of containing the depth of cut δ and the specific energy u, both of which ultimately depend on the wheel vibration x. Therefore, in order to simplify this complexity, the depth of cut is assumed to stay nominal in the grinding force expression. It is important to note that the wheel vibration that disturbs the depth of cut still changes the material removal rate which in turn affects the

specific energy. Therefore, the grinding force is still varied by the wheel vibration, but this variation occurs through the specific energy alone. In other words, the regenerative effect has not been eliminated by this assumption. So, replacing $\delta(t)$ with δ_0, the simplified grinding force expression becomes

$$F_{x,a}(t) = \frac{\mu_x w v_w \delta_0}{v_g \tau_{c,0}} \int_0^{\tau_{c,0}} u(t - T_g + \tau_{c,0} - \tau) d\tau + C_a. \tag{5.21}$$

Another way to calculate the resultant grinding force is to consider the weighted average of the specific energy distribution in the grinding zone. The weight function is the distribution of the material removal rate, since a higher material removal rate corresponds to a greater grinding force, provided that the specific energy does not change. Therefore, in order to determine the resultant grinding force, the weight function has to be formulated first. The infinitesimal material removal rate can be written as

$$dQ_w(\varphi) = w v_w \sin\varphi R_g d\varphi. \tag{5.22}$$

Substituting $\varphi = \omega_g \tau$ into Eq. (5.22), it is possible to obtain the weight function

$$dQ_w(\omega_g \tau) = w v_w \sin(\omega_g \tau) v_g d\tau. \tag{5.23}$$

Thus, considering that $Q_w = w v_w \delta$, the corresponding grinding force expression becomes

$$F_{x,w}(t) = \frac{\mu_x}{v_g} \int_0^{Q_{w,0}} u(t, \tau) dQ_w, \tag{5.24}$$

where $Q_{w,0} = w v_w \delta_0$ is the nominal material removal rate. Using the steady-state quantity instead of the instantaneous one corresponds to the assumption that $\tau_c \approx \tau_{c,0}$. Substituting Eq. (5.23) into Eq. (5.24), the resultant grinding force reads as

$$F_{x,w}(t) = \mu_x w v_w \int_0^{\tau_{c,0}} u(t, \tau) \sin(\omega_g \tau) d\tau. \tag{5.25}$$

And finally, substituting Eq. (5.18) into Eq. (5.25), it is possible to get

$$F_{x,w}(t) = \mu_x w v_w \int_0^{\tau_{c,0}} u(t - T_g + \tau_{c,0} - \tau) \sin(\omega_g \tau) d\tau + C_w, \tag{5.26}$$

where – similarly to Eq. (5.20) – C_w is the time-independent part of the grinding force. Although Eq. (5.26) is linear just like Eq. (5.21), the integral is more complicated to evaluate. Therefore, two relationships have been established between the specific energy and the grinding force, corresponding to two averaging methods: the arithmetic mean and the weighted mean.

5.2.5 Grinding force and wheel vibration

The relationship between the grinding force and the wheel vibration is identical to Eq. (4.18), so it can be written as

$$\ddot{x}(t) + 2\zeta\omega_n \dot{x}(t) + \omega_n^2 x(t) = \frac{1}{m} F_{x,i}(t), \tag{5.27}$$

where $i = a, w$ indicates the averaging method of the applied grinding force model. Therefore, the relationship between the grinding force and the wheel vibration has been established according to the classical Newtonian equation of motion.

5.2.6 Equation of motion

Combining Eqs. (5.7), (5.12), (5.14), (5.21), (5.26) and (5.27) together, it is possible to obtain the equation of motion of the system. Due to the fact that the concentrated and distributed time delays appear in the specific energy, it is easier to formulate the equation of motion for this variable instead of the wheel vibration, which would be the more conventional approach. The wheel vibration and its derivatives featuring in Eq. (5.27) can be expressed as relatively simple functions of the specific energy and its derivatives, assuming a linear relationship between x and u. This assumption follows directly from Eqs. (5.7), (5.12) and (5.14). Since two alternative grinding force expressions have been derived, two equations of motion can be formulated as well. Considering the arithmetic mean of the specific energy distribution in the grinding zone, the equation of motion is

$$\ddot{u}(t) + 2\zeta\omega_n\dot{u}(t) + \omega_n^2 u(t) = \ddot{u}(t-T_g) + 2\zeta\omega_n\dot{u}(t-T_g) + \omega_n^2 u(t-T_g) - \\ - \frac{\mu_x C_d w v_w^2 \tau_g \delta_0}{m v_g \tau_{c,0}} \int_0^{\tau_{c,0}} u(t-T_g+\tau_{c,0}-\tau)d\tau, \tag{5.28}$$

while the weighted mean approach gives the equation

$$\ddot{u}(t) + 2\zeta\omega_n\dot{u}(t) + \omega_n^2 u(t) = \ddot{u}(t-T_g) + 2\zeta\omega_n\dot{u}(t-T_g) + \omega_n^2 u(t-T_g) - \\ - \frac{\mu_x C_d w v_w^2 \tau_g}{m} \int_0^{\tau_{c,0}} u(t-T_g+\tau_{c,0}-\tau)\sin(\omega_g\tau)d\tau. \tag{5.29}$$

It can be seen that there are two time delays in the system. One is a concentrated long delay denoted by T_g, which is equal to the rotation period of the grinding wheel. The other is a distributed short delay denoted by $\tau_{c,0}$, which is equal to the contact time under steady-state grinding conditions, measuring the amount of time a grain takes to pass through the contact zone.

It is important to recognise that the new chatter theory can distinguish between up- and down-grinding configurations only through the grinding force ratio μ_x. That is because the grinding force model presented in Section 5.1.1 is based not on the chip thickness (unlike the one in Chapter 4) but on the depth of cut (according to the vast majority of grinding force models in the literature). Therefore, the grinding configuration (i.e. up- or down-grinding) does not feature in the equation of motion apart from the aforementioned parameter μ_x. The effect of the grinding configuration on this particular parameter is presented in Figure 5.4, which plots the change in μ_x as a function of the contact angle φ_c for both up- and down-grinding. These graphs were calculated based on Eqs. (5.4) and (5.5). It can be seen that the grinding force ratio corresponding to the up-grinding configuration is always below its down-grinding counterpart. This is because μ_x measures the ratio between F_x and F_t, and the x-component of F_t always acts against the x-component of F_n in up-grinding, whereas in down-grinding the x-component of F_t always acts in the same direction as the x-component of F_n. Consequently, the x-component of the total grinding force (F_x) is always smaller in up-grinding than in down-grinding, which is reflected in Figure 5.4 in graphical form. Due to the fact that μ_x is only a constant multiplier in the grinding force, it does not produce a qualitative difference in stability between the two configurations. Therefore, only one of them, namely up-grinding, will be considered in the rest of this chapter.

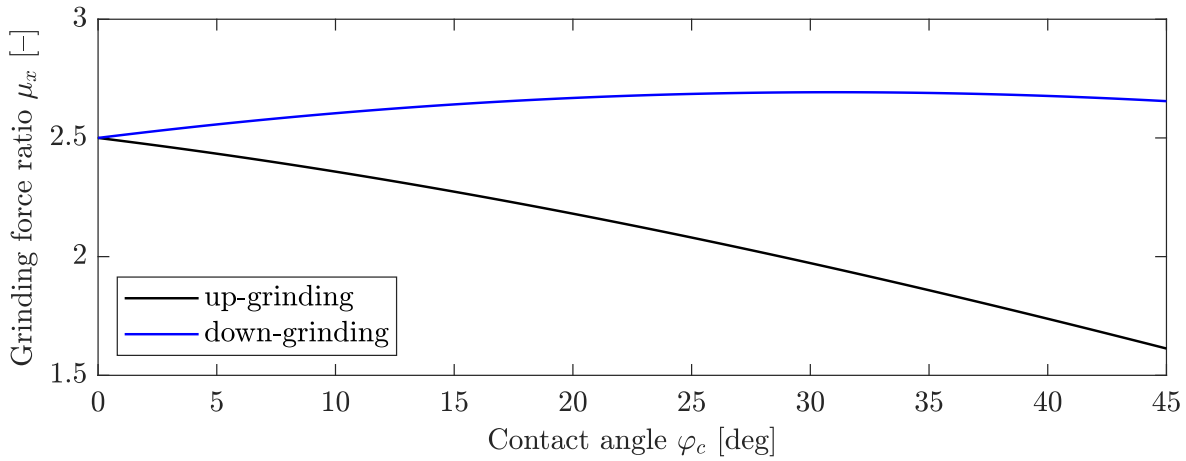

Figure 5.4: The grinding force ratio as a function of the contact angle for $\mu = 0.4$

The following section discusses the stability analysis of the system and presents the main results of the proposed theory.

5.3 Stability analysis

The stability of the system will be assessed by the Nyquist criterion (more details concerning this approach are provided in Appendix A). Therefore, the Laplace transform of each relationship derived in Section 5.2 is required in order to construct a block diagram and determine the open-loop transfer function of the system. The following subsections discuss these steps in detail.

5.3.1 Laplace transforms

The Laplace transforms of the five state variables are denoted by $\mathcal{L}\{x\}(s) = X(s)$, $\mathcal{L}\{\delta\}(s) = D(s)$, $\mathcal{L}\{V'_w\}(s) = W'_w(s)$, $\mathcal{L}\{u\}(s) = U(s)$ and $\mathcal{L}\{F_{x,i}\}(s) = \Phi_{x,i}(s)$, where s is the complex Laplace frequency. The relationships between these state variables can be established in the frequency domain as follows. Taking the Laplace transforms of Eqs. (5.7), (5.12), (5.14), (5.21), (5.26) and (5.27) respectively, gives:

$$D(s) = \frac{\delta_0}{s} - X(s), \tag{5.30}$$

$$W'_w(s) = v_w \tau_g D(s), \tag{5.31}$$

$$U(s) = e^{-T_g s} U(s) + C_d W'_w(s), \tag{5.32}$$

$$\Phi_{x,a}(s) = \frac{\mu_x w v_w \delta_0 e^{-T_g s}(e^{\tau_{c,0} s} - 1)}{v_g \tau_{c,0} s} U(s) + \frac{C_a}{s}, \tag{5.33}$$

$$\Phi_{x,w}(s) = \frac{\mu_x w v_w e^{-T_g s}(e^{\tau_{c,0} s}\omega_g - \omega_g \cos(\omega_g \tau_{c,0}) - s \sin(\omega_g \tau_{c,0}))}{s^2 + \omega_g^2} U(s) + \frac{C_w}{s}, \tag{5.34}$$

$$(s^2 + 2\zeta\omega_n s + \omega_n^2)X(s) = \frac{1}{m}\Phi_{x,i}(s), \tag{5.35}$$

where steady-state initial conditions have been assumed, i.e., $x(0) = \dot{x}(0) = 0$. Having established these relationships between the state variables in the frequency domain, the block diagram of the system can be constructed.

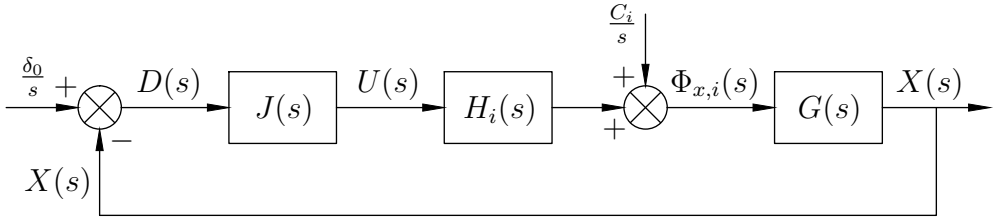

Figure 5.5: Block diagram describing wheel regeneration in single-pass surface grinding

5.3.2 Block diagram

Combining Eqs. (5.30) to (5.35), the block diagram of the system can be created according to Figure 5.5, where the transfer functions $J(s)$, $H_i(s)$ and $G(s)$ are defined as follows. Between the depth of cut and the specific energy:

$$J(s) = \frac{U(s)}{D(s)} = \frac{C_d v_w \tau_g}{1 - e^{-T_g s}}, \tag{5.36}$$

between the specific energy and the grinding force:

$$H_a(s) = \frac{\Phi_{x,a}(s) - \frac{C_a}{s}}{U(s)} = \frac{\mu_x w v_w \delta_0 e^{-T_g s}(e^{\tau_{c,0} s} - 1)}{v_g \tau_{c,0} s}, \tag{5.37}$$

$$H_w(s) = \frac{\Phi_{x,w}(s) - \frac{C_w}{s}}{U(s)} = \frac{\mu_x w v_w e^{-T_g s}(e^{\tau_{c,0} s}\omega_g - \omega_g \cos(\omega_g \tau_{c,0}) - s \sin(\omega_g \tau_{c,0}))}{s^2 + \omega_g^2}, \tag{5.38}$$

and between the grinding force and the wheel vibration:

$$G(s) = \frac{X(s)}{\Phi_{x,i}(s)} = \frac{1}{m(s^2 + 2\zeta\omega_n s + \omega_n^2)}. \tag{5.39}$$

Therefore, the open- and closed-loop transfer functions of the negative feedback system depicted in Figure 5.5 can be written as

$$T_{i,o}(s) = J(s)H_i(s)G(s), \tag{5.40}$$

$$T_{i,c}(s) = \frac{T_{i,o}(s)}{1 + T_{i,o}(s)}, \tag{5.41}$$

where the denominator of Eq. (5.41) is the characteristic function, such that

$$F_i(s) = 1 + T_{i,o}(s) = 0 \tag{5.42}$$

is the characteristic equation of the system.

	Poles	**Zeros**
$J(s)$	$s = ki\omega_g,\ k \in \mathbb{Z}$	None
$H_a(s)$	$s = 0$	$s = 2\pi ki/\tau_{c,0},\ k \in \mathbb{Z}$
$H_w(s)$	$s = \pm i\omega_g$	No closed-form solution
$G(s)$	$s = -\zeta\omega_n \pm \omega_n\sqrt{\zeta^2 - 1}$	None

Table 5.1: Poles and zeros of each term in $T_{i,o}(s)$

5.3.3 Nyquist criterion

The stability of the grinding system is assessed by the Nyquist criterion, which is described in Appendix A. The pole-zero structure of the open-loop transfer function $T_{i,o}(s)$, which is required for the Nyquist criterion, is summarised in Table 5.1. Since $T_{i,o}(s)$ is a product of three individual transfer functions, its poles and zeros can be obtained by calculating the poles and zeros of each of its terms separately. It can be seen that the zeros of $H_w(s)$ cannot be expressed in closed form. However, this is not a major issue, since the zeros of $T_{i,o}(s)$ are not strictly required for the Nyquist criterion, only its poles (as it is indicated in Eq. (5.42), the poles of $T_{i,o}(s)$ and the poles of the characteristic function $F_i(s)$ are identical). In other words, the Nyquist contour is allowed to pass through any zero of $T_{i,o}(s)$, it only has to bypass its poles (the zeros of $T_{i,o}(s)$ and $F_i(s)$ are different). Although the pole-zero structure of either open-loop transfer function is suitable for stability analysis by the Nyquist criterion, only one of the two will be looked at in detail in this thesis. Due to the fact that the grinding force expression corresponding to the arithmetic mean of the specific energy distribution in the grinding zone is the simpler of the two, only $T_{a,o}(s)$ will be considered from now on. The detailed analysis of the other force expression and open-loop transfer function (corresponding to the weighted mean) is outside the scope of this work. Nevertheless, a brief numerical simulation is presented in Appendix B to compare the results provided by the two grinding force expressions.

A visual representation of the pole-zero structure of $T_{a,o}(s)$ is shown in Figure 5.6. Since the Nyquist contour cannot pass through any pole of $T_{a,o}(s)$, the ones located on the imaginary axis are bypassed in such a way that they are excluded from the right half-plane enclosed by the Nyquist contour according to Figure 5.7. Therefore, since the poles of $T_{a,o}(s)$ and $F_a(s)$ are identical (as shown in Appendix A), the number of poles of $F_a(s)$ encircled by the Nyquist contour is zero. Consequently, the criterion for assessing stability is relatively simple: if the Nyquist plot of $T_{a,o}(s)$ encircles the $(-1, 0)$ point in a clockwise direction, then the system is unstable – if it does not, the system is stable. The Nyquist plot of $T_{a,o}(s)$ cannot encircle the $(-1, 0)$ point in an anticlockwise direction, because the number of zeros of $F_a(s)$ encircled by the Nyquist contour cannot be negative.

Due to the so-called filtering effect [100], vibrations and corresponding wave patterns with a wavelength shorter than the contact length between the workpiece and the grinding wheel are strongly attenuated and thus are unlikely to form. Therefore, the purely imaginary frequencies of the Nyquist contour are considered only between $-2\pi i/\tau_{c,0}$ and

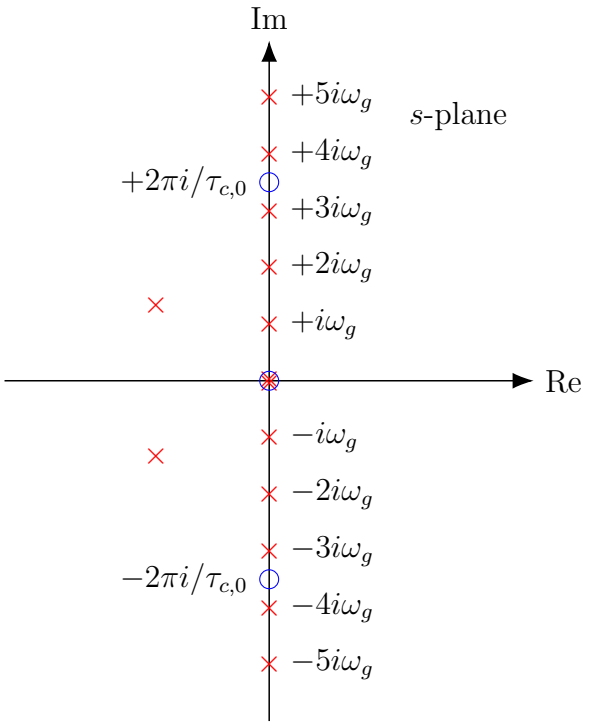

Figure 5.6: Poles (×) and zeros (○) of $T_{a,o}(s)$

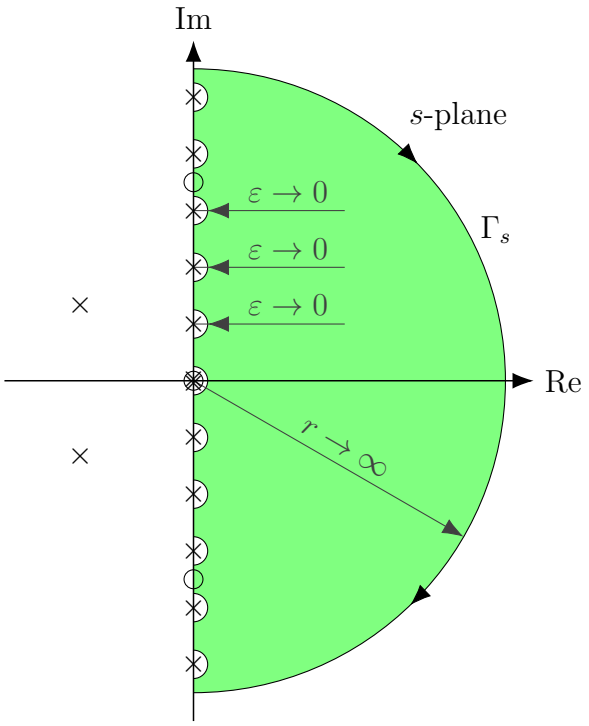

Figure 5.7: Definition of the Nyquist contour Γ_s

$+2\pi i/\tau_{c,0}$. According to [155], pp. 632-633, the infinite semicircle part of the Nyquist contour typically maps to a single point, therefore, it is disregarded in numerical simulations.

Figures 5.8 and 5.9 present two Nyquist plots of $T_{a,o}(s)$ for two different spindle speeds – every other parameter is identical in the two cases. The image of a semicircular arc of infinitesimal radius in the s-plane appears to be a semicircular arc of infinite radius in the $T_{a,o}(s)$-plane, although this cannot be stated as a fact without sufficient mathematical proof. However, it is not necessary to know the actual shape of these sections of the Nyquist plot, as long as the starting and finishing points are known. What matters is that the starting and finishing points are connected at infinity in a known direction. But for the sake of simplicity and convenience, they will be called semicircles, keeping in mind that this term is an approximation. Considering the fact that a pole bypassed by the Nyquist contour indicates an asymptote in the Nyquist plot, it is relatively straightforward to conclude that the two endpoints of each infinite semicircle are exactly 180° apart.

Since each semicircle of the Nyquist plot is infinite in radius regardless of their presented radii in Figures 5.8 and 5.9, each closed semicircle covers half of the $T_{a,o}(s)$-plane, i.e., encircles either the $(-1, 0)$ or the $(+1, 0)$ point in a clockwise direction. Consequently, the primary way to assess stability is defined by the angular orientation of each semicircle. If at least one of them encircles the $(-1, 0)$ point, the system is unstable, otherwise it is stable. This concept is visually illustrated in Figure 5.10.

It can be seen in Figure 5.8 that none of the infinite semicircles encircles the $(-1, 0)$

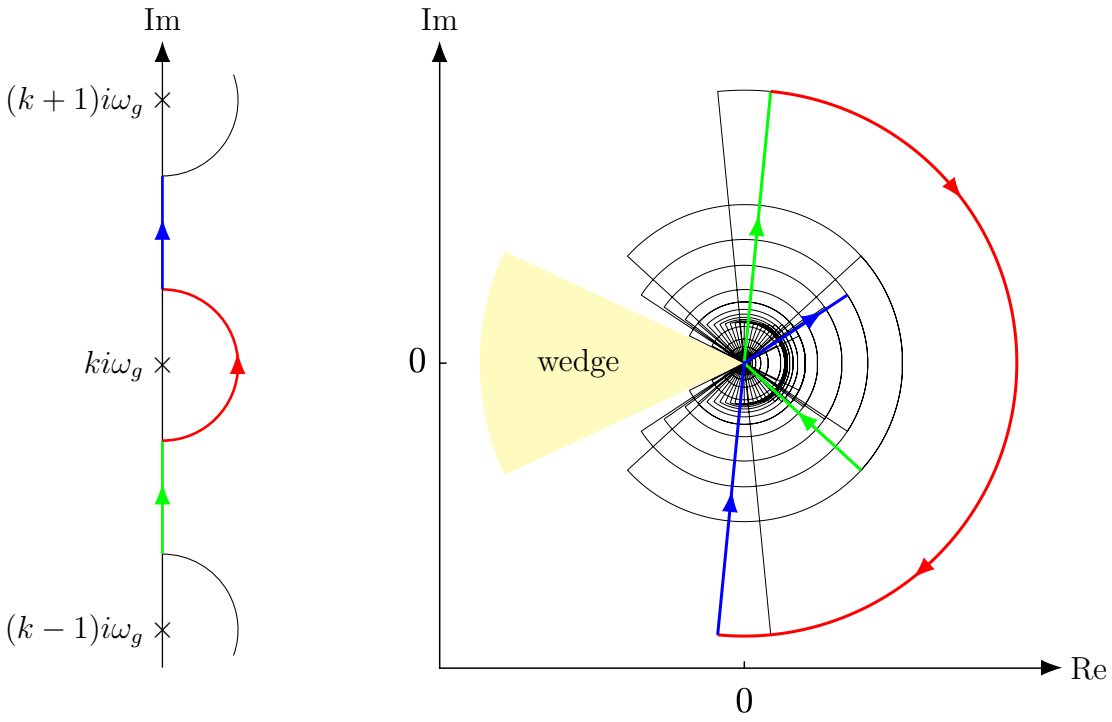

Figure 5.8: Stable grinding process – Nyquist contour (left) and Nyquist plot (right) for $\delta_0 = 3$ mm, $R_g = 100$ mm, $\zeta = 0.05$, $\omega_n = 300$ Hz, $\omega_g = 1500$ rpm, $\mu_x = 1$, $w = 20$ mm, $v_w = 56$ mm/min, $m = 1$ kg, $Z = 10\,000$

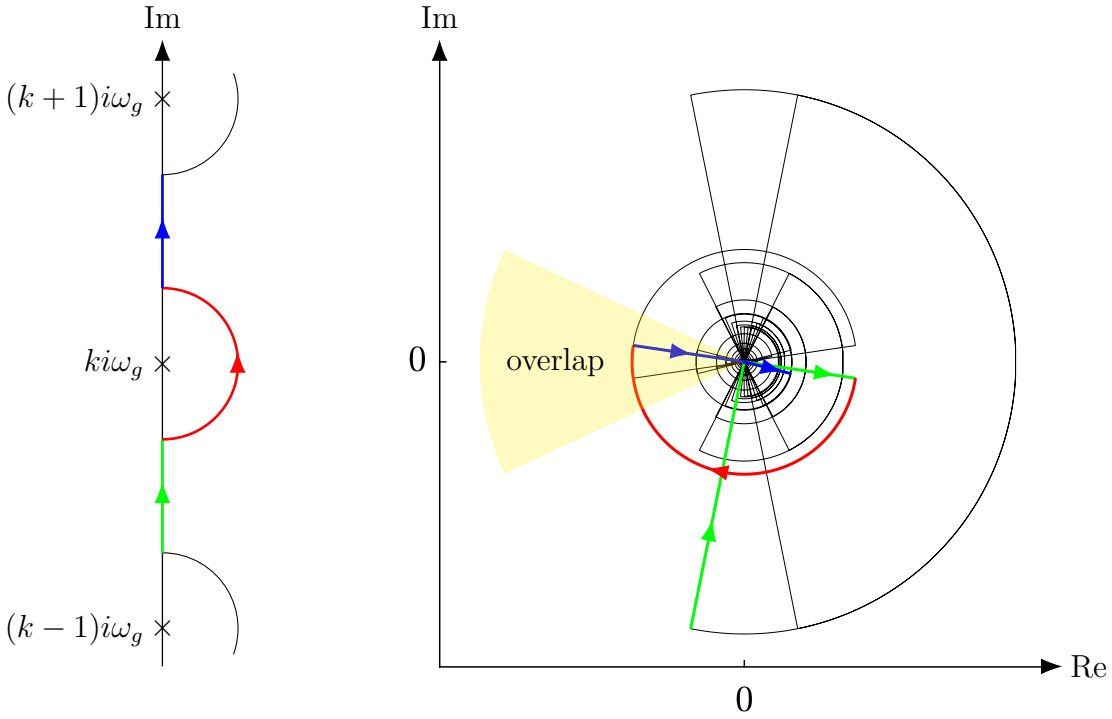

Figure 5.9: Unstable grinding process – Nyquist contour (left) and Nyquist plot (right) for $\delta_0 = 3$ mm, $R_g = 100$ mm, $\zeta = 0.05$, $\omega_n = 300$ Hz, $\omega_g = 2500$ rpm, $\mu_x = 1$, $w = 20$ mm, $v_w = 56$ mm/min, $m = 1$ kg, $Z = 10\,000$

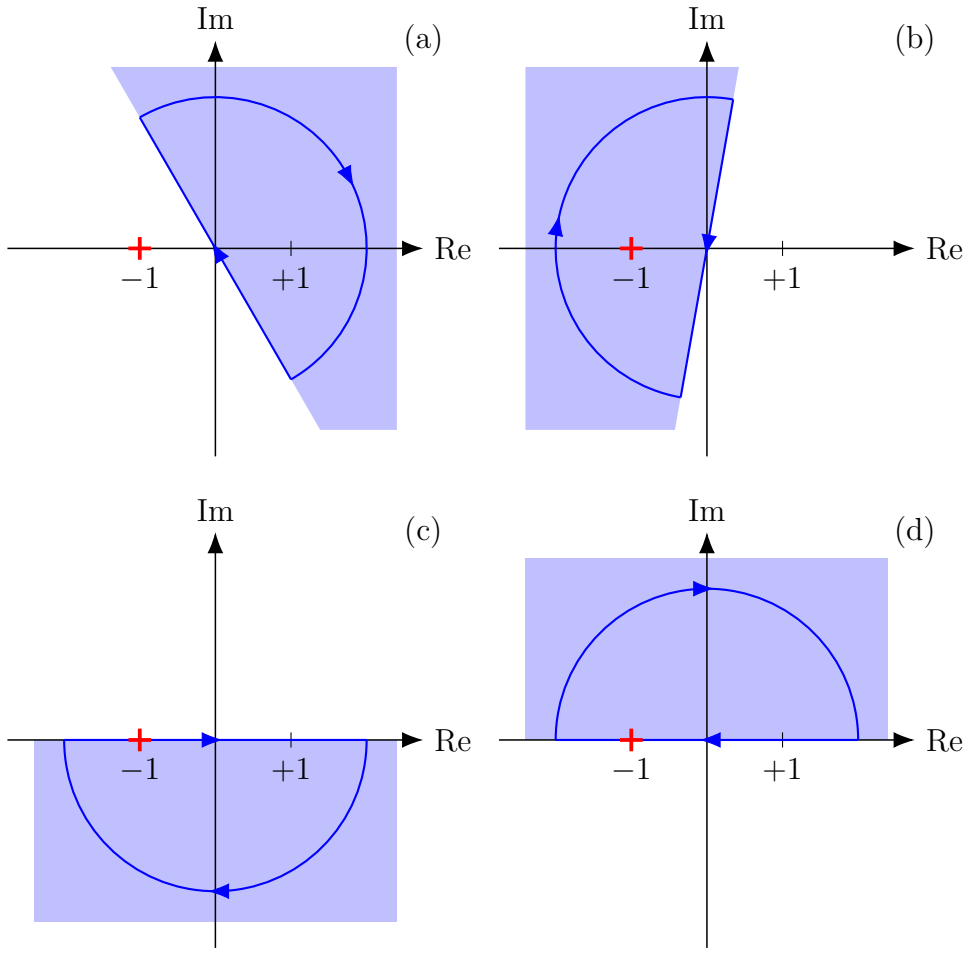

Figure 5.10: Stability according to the angular orientation of a single infinite semicircle in the $T_{a,o}(s)$-plane: the $(-1, 0)$ point is not encircled, the system is stable (a); the $(-1, 0)$ point is encircled, the system is unstable (b); the infinite semicircle passes through the $(-1, 0)$ point, the system is marginally stable (c,d)

point – the Nyquist plot of $T_{a,o}(s)$ forms a 'wedge' in the direction of the $(-1, 0)$ point. Therefore, the system parameters corresponding to Figure 5.8 result in a stable grinding process. Figure 5.9 presents a scenario where a number of infinite semicircles encircle the $(-1, 0)$ point – the wedge corresponding to the stable process turns into an 'overlap' of infinite semicircles in the direction of the $(-1, 0)$ point. Therefore, the system parameters corresponding to Figure 5.9 result in an unstable grinding process. It can be concluded from Figures 5.8 and 5.9 that there exists a limit case between the stable and unstable scenarios, where one pair of infinite semicircles are touching (i.e. closing the wedge without overlapping) and every other pair forms a wedge. This special case corresponds to a marginally stable process.

It is important to note that up to this point the stability of the system has been assessed based on the infinite semicircles of the Nyquist plot alone, hence the absence of axis scales in Figures 5.8 and 5.9. However, that is not the only way to encircle the $(-1, 0)$ point. Process instability can also occur as a result of the finite parts of the Nyquist plot encircling the $(-1, 0)$ point, which – in the absence of infinite encirclements – is the only

way for the system to become unstable. In order for this to happen, certain grinding conditions (reflected in the grinding parameters) need to be satisfied. Therefore, the following section investigates how different grinding parameters influence the Nyquist plot, and consequently, process stability in general. (The reason infinite semicircles were considered separately from the finite sections of the Nyquist plot is that they cannot be treated as truly infinite in numerical simulations.)

5.3.4 Parameter study

In order to study the effects of different grinding parameters on process stability, it is helpful to see them all in the open-loop transfer function:

$$T_{a,o}(s) = \frac{\mu_x C_d w v_w^2 \tau_g \delta_0 e^{-T_g s}(e^{\tau_{c,0} s} - 1)}{m v_g \tau_{c,0} s(1 - e^{-T_g s})(s^2 + 2\zeta\omega_n s + \omega_n^2)}. \tag{5.43}$$

Substituting $\tau_g = T_g/Z$, $\delta_0 = R_g(1 - \cos\varphi_{c,0})$, $v_g = \omega_g R_g$, $\varphi_{c,0} = \omega_g \tau_{c,0}$ and $\omega_g = 2\pi/T_g$ into Eq. (5.43), it is possible to get

$$T_{a,o}(s) = \frac{\mu_x C_d w v_w^2 T_g^2 \left(1 - \cos\left(2\pi \frac{\tau_{c,0}}{T_g}\right)\right) e^{-T_g s}(e^{\tau_{c,0} s} - 1)}{2\pi m \tau_{c,0} Z s(1 - e^{-T_g s})(s^2 + 2\zeta\omega_n s + \omega_n^2)}. \tag{5.44}$$

The grinding parameters featuring in Eq. (5.44) can be divided into two main categories. The first group contains the constant multipliers of $T_{a,o}(s)$, such as w, v_w and Z. These parameters can only scale the Nyquist plot without altering its shape. The second group of variables belong to the s-dependent part of $T_{a,o}(s)$ in such a way that they cannot be separated from every s. These parameters, e.g. ζ, ω_n and T_g, can not only scale the Nyquist plot, but they can also change its shape. For the sake of clarity, these two groups of variables can be written in the form $T_{a,o}(s) = T_1(\text{first group of parameters}) \times T_2(s, \text{second group of parameters})$, where the product of the two functions T_1 and T_2 make up the total open-loop transfer function $T_{a,o}(s)$. It can be seen that T_1 is independent of s, while T_2 depends on it.

As it was stated in Section 5.3.3, the grinding system can become unstable through not only infinite but also finite encirclements of the $(-1, 0)$ point. It is clear that scaling the Nyquist plot, i.e. changing any parameter in the first group, has no effect on the stability of the system with respect to infinite encirclements. These sections of the Nyquist plot can alter stability only through the second group of grinding parameters. This theoretical result has important practical implications: if a process is unstable through infinite encirclements, then certain grinding parameters (including the width of cut and the feed rate) are ineffective to stabilise the system. Parameters from the second group (such as the wheel speed and the depth of cut) have to be modified in order to achieve stable operation. However, this does not mean that the parameters in the first category have no influence on stability at all. Since they can scale the Nyquist plot, they can alter process stability through finite encirclements. Figure 5.11 demonstrates this idea. It shows the effect of the coefficient of dulling C_d, which is from the first group, on the Nyquist plot. It can be seen that increasing this parameter beyond a certain threshold destabilises the system through finite encirclements.

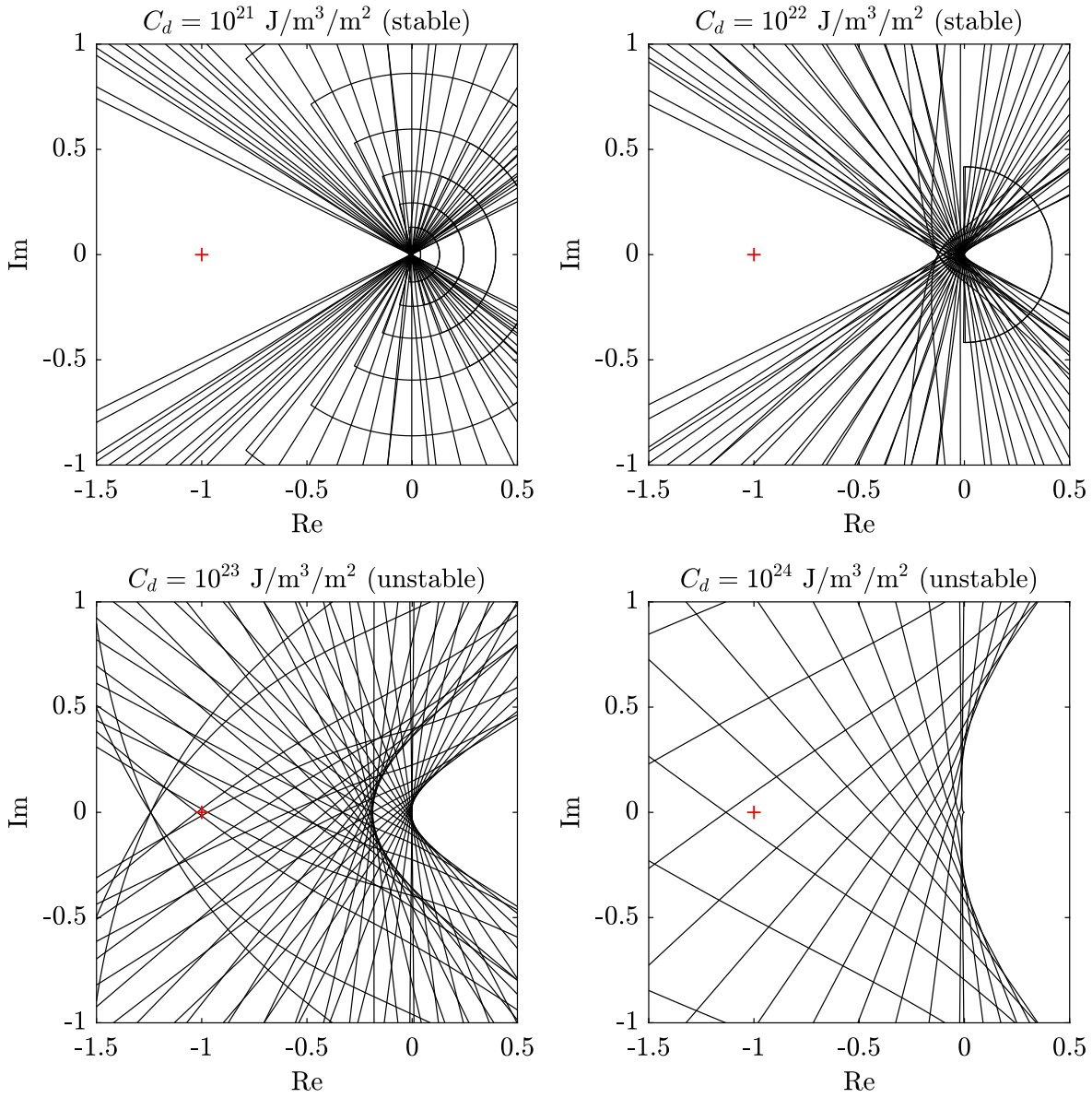

Figure 5.11: Effect of C_d on the Nyquist plot and thus process stability for $\delta_0 = 3$ mm, $R_g = 100$ mm, $\zeta = 0.05$, $\omega_n = 300$ Hz, $\omega_g = 1500$ rpm, $\mu_x = 1$, $w = 20$ mm, $v_w = 56$ mm/min, $m = 1$ kg, $Z = 10\,000$

The practical values of the grinding parameters in Eq. (5.44) are either known or relatively easy to estimate, except for one. The coefficient of dulling is a new quantity introduced by the author to describe grit wear, i.e., to define a relationship between the material removal rate and the specific energy. However, due to the novelty of this parameter, the practical values of C_d are still unknown. Therefore, the rest of this section is dedicated to deriving a formula for the coefficient of dulling that is able to provide some insight into the realistic values of this parameter. According to Eqs. (5.13) and (5.14), the coefficient of dulling has been defined as

$$\Delta u = C_d V_w'. \tag{5.45}$$

It is important to note that in this section V_w' no longer corresponds to a single wheel

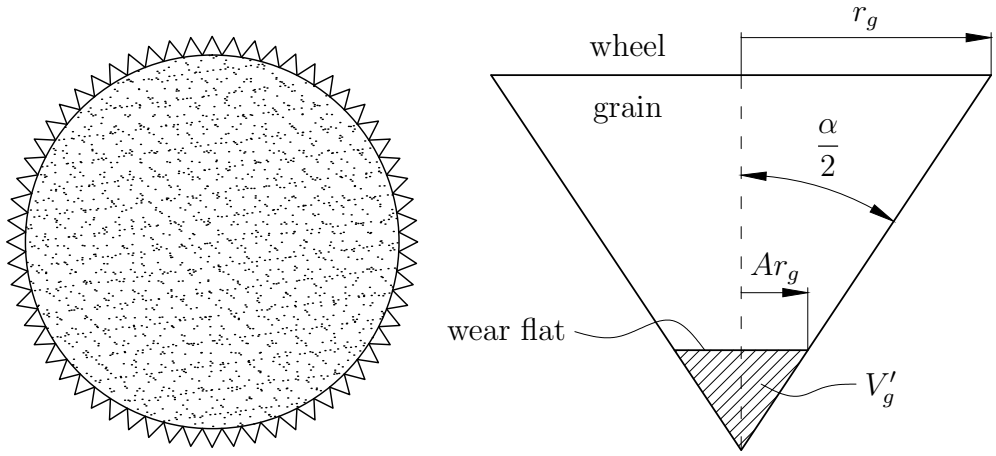

Figure 5.12: Two-dimensional wheel (left) and grain (right) models

rotation (note that the time dependence has been dropped on both sides). That is because the primary goal here is to obtain a relationship between a certain amount of workpiece material removed by a single grain (V'_w) and the resulting specific energy increase on that grain (Δu). Since the relationship between these two quantities is assumed to be linear, the coefficient of proportionality (C_d) will not be affected. Therefore, in order to estimate the practical values of C_d, an experimental relationship has to be established between the material removal rate and the specific energy. Although the author is not familiar with such a direct experimental relationship in the literature, it is fairly common to measure the relationship between the wear-flat area and the specific energy. The wear-flat area is a fraction measuring the total area of wear flats relative to the total wheel surface area (i.e. circumference $\times$ width). According to the experiments presented by Malkin and Guo (in Figure 5-19 on p. 142 of [11]), there is a linear relationship between the wear-flat area A [%] and the specific energy u [J/mm^3]. Considering these grinding experiments, $\Delta A \approx 0.6\%$ produces $\Delta u \approx 178$ J/mm^3. This is an important result, because the relationship between the wear-flat area and the material removal rate is fairly straightforward to establish. In order to obtain this relationship (between the wear-flat area and the material removal rate), the grinding wheel and its cutting edges are modelled according to Figure 5.12. Since the wear-flat area is a fractional or relative value, it is possible to apply it to a single grain. Considering a regular grain distribution and a triangular grain shape (straight and elongated in the axial direction), it is possible to determine the amount of material removed from a single grain that corresponds to a given wear-flat area. This quantity, divided by the grinding width, is denoted by V'_g and can be formulated as

$$V'_g = \frac{A^2 r_g^2}{\tan(\alpha/2)}. \tag{5.46}$$

Again, this parameter does not correspond to a single wheel revolution, but measures the accumulated wear on a single grain of a given wear-flat area. Therefore, multiplying V'_g by the grinding ratio G, the accumulated workpiece material removed by a single grain becomes

$$V'_w = \frac{G A^2 r_g^2}{\tan(\alpha/2)}. \tag{5.47}$$

m [kg]	1	R_g [mm]	100	C_d [J/m^3/m^2]	4×10^{21}
ζ [%]	1	w [mm]	20	μ [–]	0.4
f_n [Hz]	300	Z [–]	10 000	v_w [mm/min]	56

Table 5.2: Numerical parameters used to determine process stability in this chapter

Substituting Eq. (5.47) into Eq. (5.45), the coefficient of dulling can be calculated as

$$C_d = \frac{\Delta u \tan(\alpha/2)}{(\Delta A)^2 G r_g^2}. \tag{5.48}$$

It is important to remember that $\Delta A \approx 0.6\%$ producing $\Delta u \approx 178$ J/mm^3 is specific to a given grinding process, therefore, these two values are not absolute. Nevertheless, as an initial approximation, these two numbers provide a realistic estimate of C_d. Substituting $\alpha = 60°$, $G = 100$ and $r_g = 0.08$ mm into Eq. (5.48), a typical value is 4.46×10^{21} J/m^3/m^2.

Therefore, a more practical understanding of the process variables has been established. The numerical parameters that will be used to determine the stability properties of the system in Section 5.3.6 are summarised in Table 5.2. However, before moving on to analysing process stability in detail, the definition and calculation of the chatter frequency will be discussed in the following section to pave the way for the construction of stability charts and frequency diagrams.

5.3.5 Chatter frequencies

The chatter frequency is a fundamental concept in machining dynamics. It is the vibration frequency of a marginally stable system occurring at the boundary of stability. Such oscillations are characterised by a constant amplitude and, depending on the specific machining operation considered, one or more vibration frequencies (e.g. there is a single, well-defined chatter frequency in unstable turning, while multiple chatter frequencies can arise in unstable milling [68]). In unstable grinding, both a single and multiple chatter frequencies have been reported in the literature [106–108].

Although the chatter frequency is formally understood as the vibration frequency of a marginally stable system, it is possible to define it in unstable processes as well. In fact, what is typically meant by the term 'chatter frequency' in practice is the vibration frequency of an unstable system. The main difference between these two states of stability is found in their respective vibration amplitudes: while marginally stable oscillations are characterised by a constant amplitude, the magnitude of unstable vibrations grows exponentially. However, according to elementary vibration theory (e.g. [156], pp. 28-33), the degree of stability or instability of a linear dynamical system, which is characterised by the damping ratio, has no significant effect on the vibration frequency as long as the absolute value of the damping ratio is small. Therefore, since the literature is clear that the absolute value of the damping ratio is very small with respect to wheel-related instability

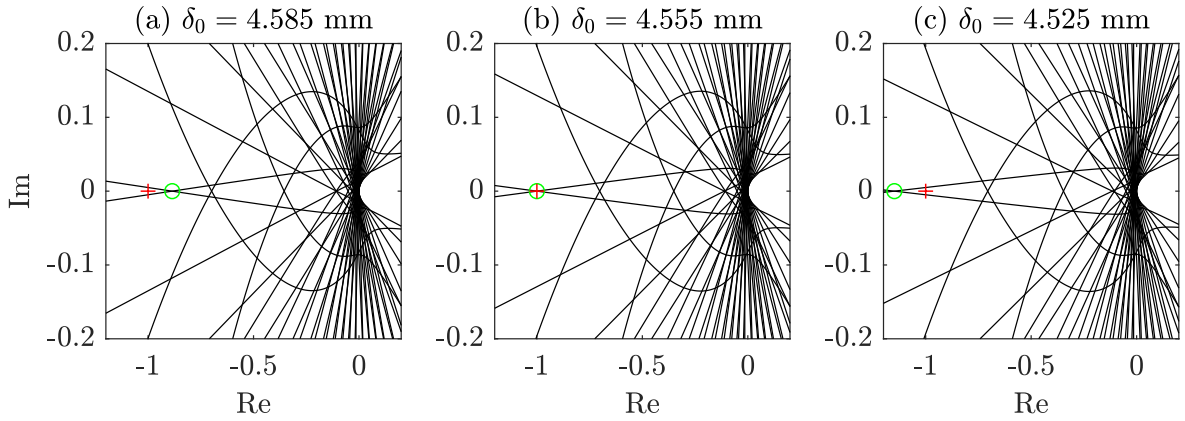

Figure 5.13: Nyquist plots corresponding to (a) stable, (b) marginally stable and (c) unstable grinding operations ($\omega_g = 2000$ rpm, every other parameter is identical to the ones listed in Table 5.2)

in grinding (i.e. self-excited vibration takes a long time to develop [25]), the concept of the chatter frequency will be, as it usually is, applied to unstable processes as well. Nevertheless, the rest of this subsection discusses the numerical process of calculating the chatter frequency using the formal definition, i.e., considering marginally stable grinding operations alone.

According to the Nyquist criterion, the marginally stable system is such that the Nyquist plot passes through the $(-1, 0)$ point any number of times without actually encircling it. In order to visualise this idea, three Nyquist plots corresponding to stable, marginally stable and unstable grinding are presented in Figure 5.13. It can be seen that in the marginally stable case (Figure 5.13b), the Nyquist plot passes through the $(-1, 0)$ point twice. These two crossings correspond to a pair of complex conjugate frequencies of the Nyquist contour with zero real parts, since the Nyquist plot is always symmetric about the real axis (as it is mapped from the Nyquist contour shown in Figure 5.7), and the infinite semicircle part of the Nyquist contour has been disregarded in numerical simulations (according to the justification given in Section 5.3.3). Therefore, the frequencies to which these two crossings belong are in fact one and the same physical frequency, however, in the Nyquist plot they appear as one positive and one negative frequency with the same absolute value. This is the chatter frequency of the system at the boundary of stability. For a given set of numerical parameters that result in a marginally stable process, the chatter frequency can be determined with relative ease: first, every point of the Nyquist plot that is located on the real axis (where the imaginary part is zero) has to be collected along with their respective frequencies, then the one with the lowest real part (which will be -1) has to be selected. The frequency associated with this point is the chatter frequency. For the scenario corresponding to Figure 5.13b, it is $f_c = 333.74$ Hz.

Note: Considering the three examples given in Figure 5.13, it is possible to determine the stability of the system based on the point marked by a green circle in each Nyquist plot. This point satisfies two conditions: (1) its imaginary part is zero, i.e., it is located on the real axis, and (2) its real part is the lowest of all points satisfying the first condition, i.e., it is located farthest to the left of the origin. The location of this point indicated

by a green circle relative to the $(-1, 0)$ position marked by a red cross can be used to determine not only absolute stability, but relative stability as well. If the green circle is situated to the right of the red cross (i.e., the system is stable), the distance between these two points provides information on how stable the process is or how quickly it reaches steady-state cutting conditions again after perturbed. A longer distance corresponds to a greater degree of stability and a faster settling time. If the green circle is located to the left of the red cross (i.e., the system is unstable), the distance between these two points provides information on how unstable the process is or how quickly it loses stability after perturbed. A longer distance corresponds to a greater degree of instability and a faster loss of stability. The idea of determining relative stability in this way is fundamentally identical to the concept of the gain margin (as presented in [155], pp. 643-650). Furthermore, the phase margin can also be extracted and used to determine the relative stability of the system (according to the previous reference). These two methods (i.e. calculating relative stability based on the gain and phase margins) will be revisited in Sections 5.3.6 and 6.5 for further investigation.

Therefore, the concept of the chatter frequency has been established, and the numerical process of determining it has been explained. The following section presents the main theoretical predictions of the proposed model in the form of absolute and relative stability charts and frequency diagrams.

5.3.6 Stability charts and frequency diagrams

Figure 5.14 presents the stability diagram of the system as a function of the wheel speed and the depth of cut, along with three Nyquist plots corresponding to three points of different stability properties. It can be seen that there are two sets of stability boundaries. The stable and unstable areas are indicated by grey and white colours, respectively. The stability boundary that separates two unstable regions implies a change in the nature of instability due to a qualitative difference between the Nyquist plots on the two sides of this stability boundary. On the outer side (marked by point A), the process is unstable through at least one infinite encirclement of the $(-1, 0)$ position. The area between this stability boundary and the stable zone (where point B lies) is also unstable, however, this kind of instability is the result of finite encirclements of the $(-1, 0)$ position. Whatever lies in the grey region (e.g. point C) is stable, i.e., the Nyquist plot does not encircle the $(-1, 0)$ position at all. These three points will be used later on as examples of qualitative differences between 'infinitely unstable' (A), 'finitely unstable' (B), and stable (C) parameter regions.

In order to have a deeper understanding of the dynamics of the grinding process, it is helpful to consider the chatter frequencies as well, which also translate into lobes or surface waves on the wheel. Figure 5.15 presents a stability chart in colour, differentiating between the same three kinds of stability areas as those shown in Figure 5.14: (1) a colour map of infinitely unstable grinding operations, (2) the region of finitely unstable processes in dark grey, and (3) the stable zone in light grey. Since the infinite encirclements of the $(-1, 0)$ point are related to integer multiples of the wheel speed in the s-plane (as shown in Figure 5.9), the chatter frequencies in the infinitely unstable region will

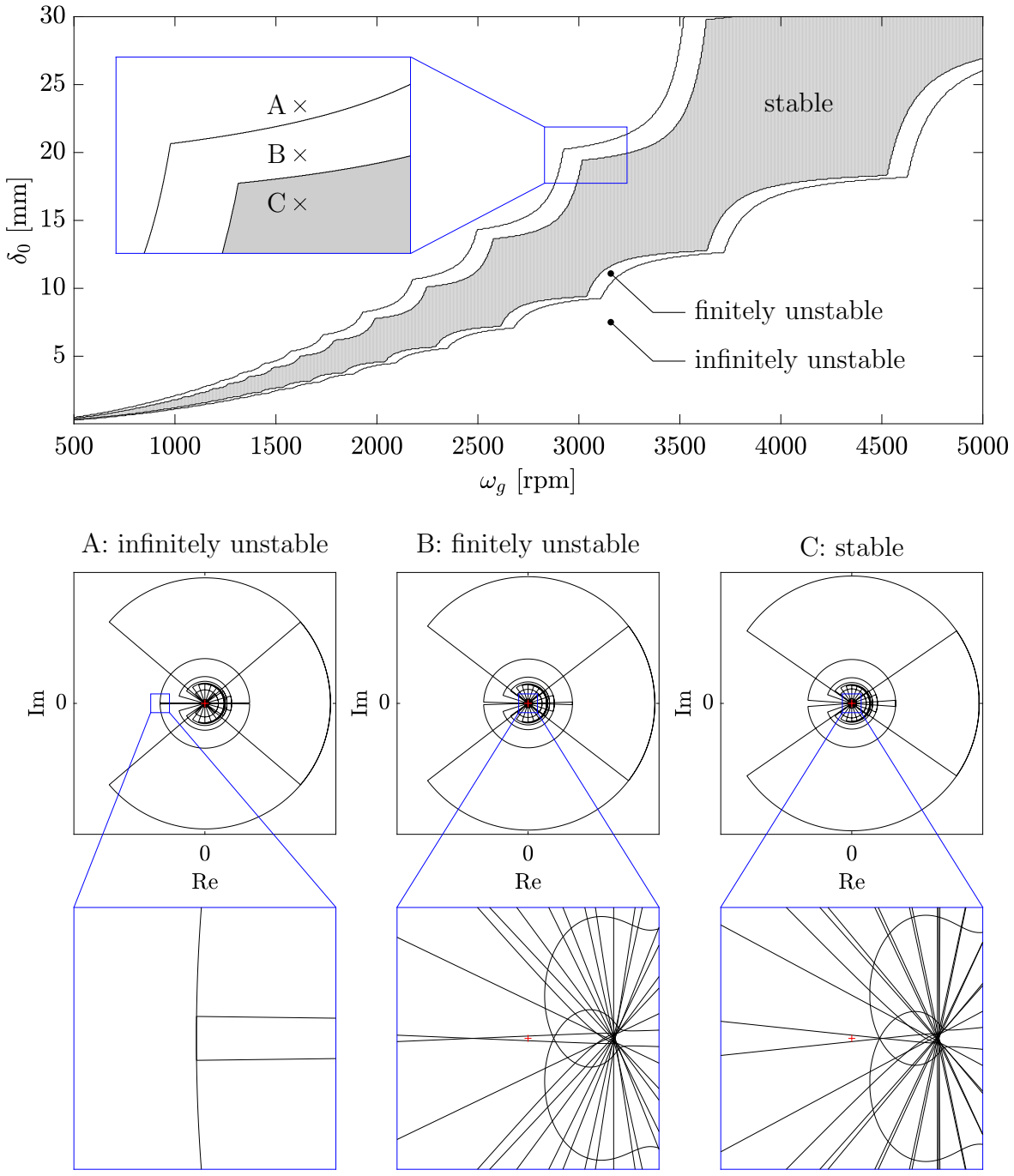

Figure 5.14: Stability chart and Nyquist plots for three test points of different stability properties: A($\omega_g = 3100$ rpm, $\delta_0 = 21$ mm), B($\omega_g = 3100$ rpm, $\delta_0 = 20$ mm) and C($\omega_g = 3100$ rpm, $\delta_0 = 19$ mm)

be approximately integer multiples of the wheel speed as well. Therefore, the number of specific energy waves on the wheel corresponding to a particular chatter frequency, which can be calculated as chatter frequency per wheel speed, will be an approximately integer number. A few of these lobe numbers are indicated in Figure 5.15. It can be seen that the structure of the colour map is disrupted around the top left quarter of the stability diagram – the infinitely unstable zone that is smoothly connected to the stability

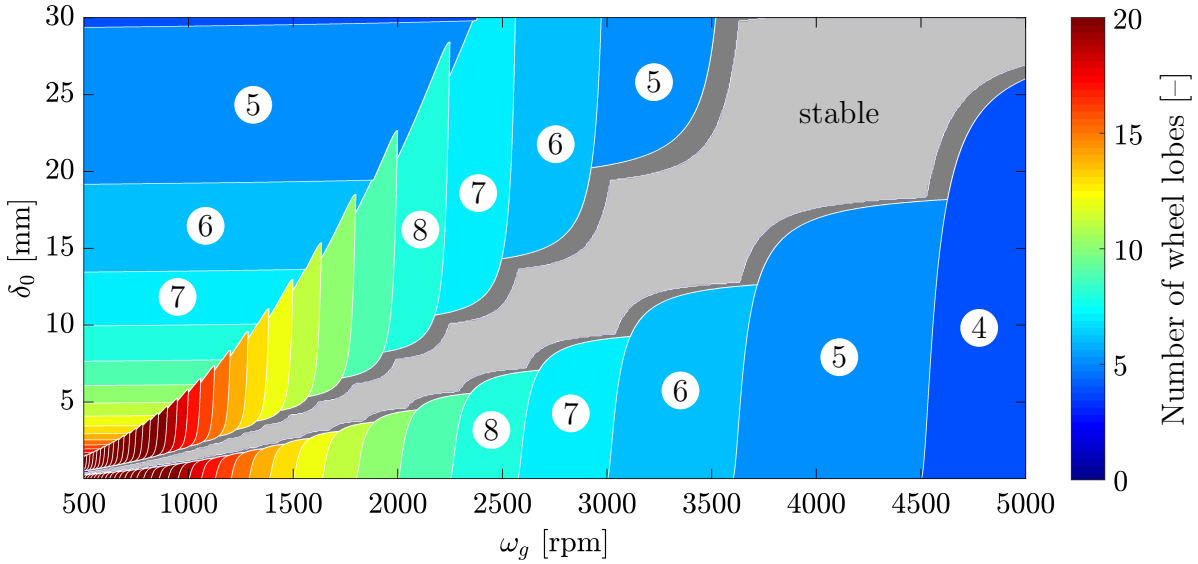

Figure 5.15: Stability chart presenting three types of stability regions: infinitely unstable (colour map), finitely unstable (dark grey), and stable (light grey)

boundaries and consists of vertically elongated regions of constant lobe numbers changes to horizontally elongated ones. Not only that, but the number of unstable lobes in this area is also reduced relative to the expected pattern. This is a result of the filtering effect, which prevents the formation of wheel lobes with a wavelength shorter than the contact length between the workpiece and the grinding wheel [100]. The filtering effect is stronger (i.e. the filter attenuates a wider range of frequencies) when a particular grain spends more time in the grinding zone. This can happen in two ways: (1) the contact length is bigger, which is equivalent to the depth of cut being larger for a given wheel radius, and (2) the spindle speed is lower. Therefore, the filtering effect has the biggest impact when the depth of cut is large and the spindle speed is low. Since these are the parameters that define the top left corner of Figure 5.15, the expected pattern of the colour map is disrupted there. The dark grey area corresponds to instability through finite encirclements, therefore, the vibration frequencies at the onset of chatter are not necessarily integer multiples of the spindle speed in this region.

Another important aspect of stability analysis in general is the calculation of the chatter frequencies at the absolute stability boundary. Due to the fact that the stable zone is defined by an upper and a lower stability boundary, two frequency diagrams demonstrate the chatter frequencies of the marginally stable system: one corresponding to the upper boundary and another corresponding to the lower boundary. Furthermore, the chatter frequencies can be displayed in two different ways: relative to the natural frequency (Figure 5.16) and relative to the wheel speed (Figure 5.17). Two main observations can be made regarding these diagrams. First, Figure 5.16 shows that the chatter frequencies are slightly below/above the natural frequency when the system becomes unstable through the upper/lower stability boundary. Second, Figure 5.17 demonstrates that the chatter frequencies are approximately integer multiples of the wheel speed, and the lobes of the stability diagram correspond to different wave patterns on the grinding wheel. Decreasing the wheel speed increases the number of lobes forming on the wheel, which is consistent

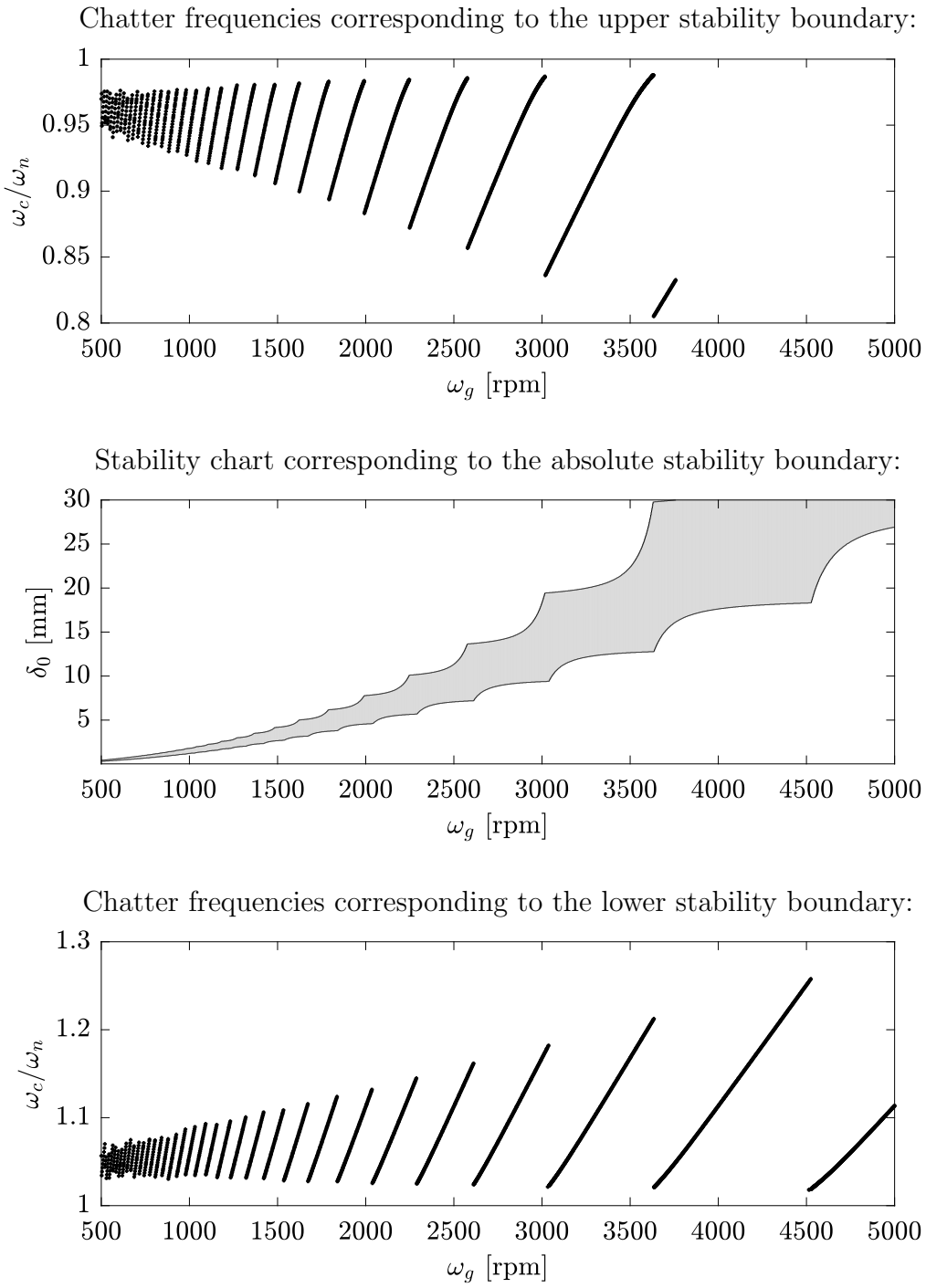

Figure 5.16: Chatter frequencies relative to the natural frequency ($\omega_n = 1885$ rad/s)

with the first observation, namely that the chatter frequencies do not deviate largely from the natural frequency of the system. It is worth noting that the expected number of wheel lobes remains approximately constant within each stability lobe, and jumps to another approximately integer value at the points where the stability lobes are connected. The fact that the chatter frequencies are not exactly integer multiples of the wheel speed (or the wheel lobes are not exactly integer numbers) is probably owing to the presence of 'wheel lobe precession' first measured by Gurney in 1965 [99] and first modelled by

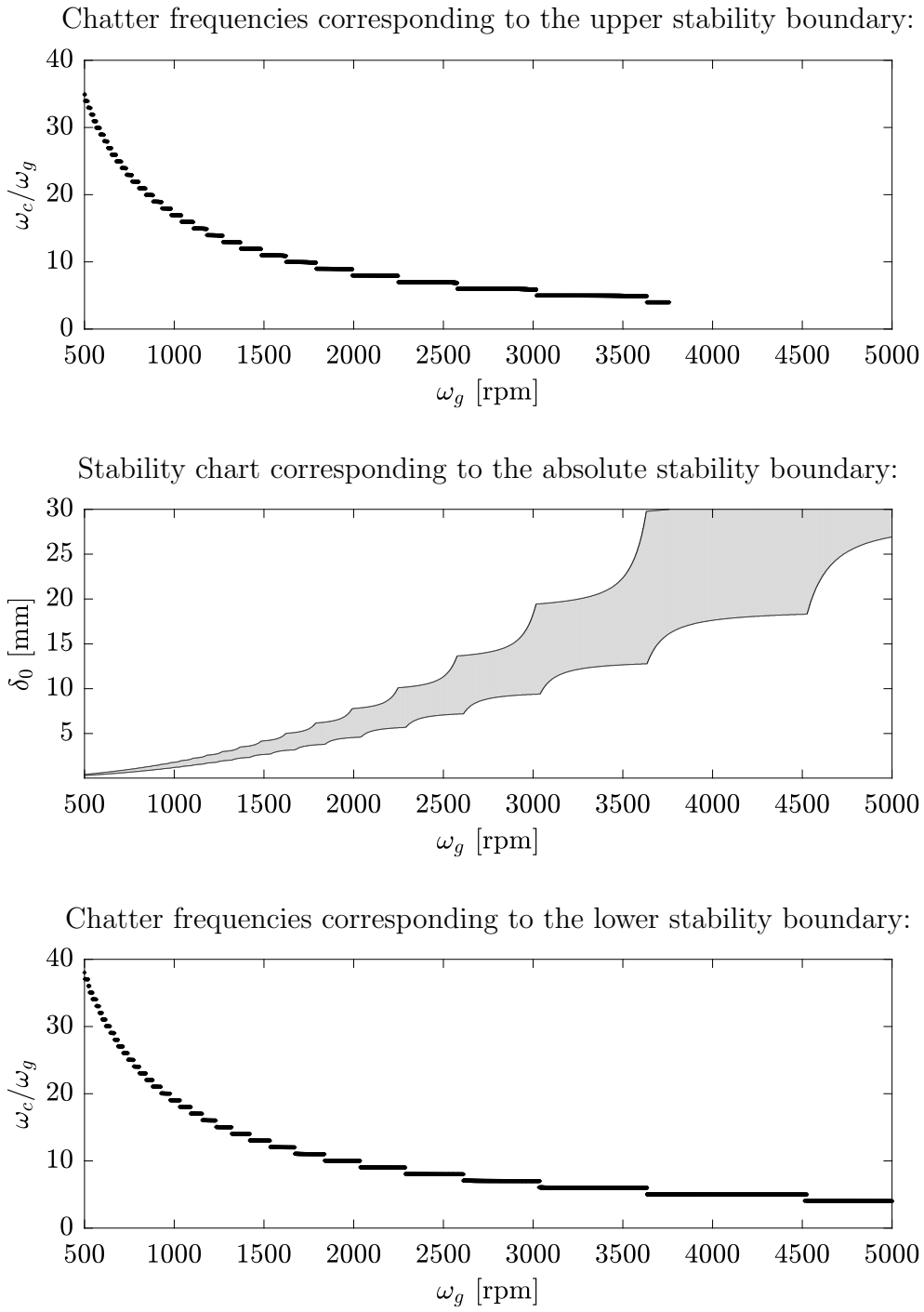

Figure 5.17: Chatter frequencies relative to the wheel speed

Thompson a few years later [106, 107]. According to this phenomenon, the waves on the wheel under unstable grinding conditions do not remain stationary, but slowly precess or travel around the circumference of the wheel. The precession frequency is typically very low, so the overall chatter frequency is nearly an integer multiple of the wheel speed in practice.

Figures 5.16 and 5.17 are also clear that only one chatter frequency is expected for a

given scenario. This result is in agreement with Thompson's theoretical and experimental findings [106, 107]: his model predicted that surface grinding vibration can occur at only one frequency, and his measurements demonstrated the truth of this result, as in each case the grinding vibrations consisted almost entirely of a single pure tone. However, Li and Shin's numerical model – considering both distributed radial wear and distributed grit dullness – predicted a number of chatter frequencies around the natural frequency of the system, all being integer multiples of the wheel speed, which were also verified by grinding experiments [108]. Since the new chatter theory presented in this thesis does not predict more than one chatter frequency, it is in disagreement with Li and Shin's model in this regard. However, it is important to remember Thompson's findings as well and point out that the literature reports not only theories but also experiments that produce different results – some predict and measure only one frequency, others more. Therefore, it appears that the number of chatter frequencies arising at the onset of chatter depends on the grinding process itself. The deeper analysis of this variation is outside the scope of this work, but constitutes a potential direction for future research.

As it was noted in Section 5.3.5, the relative stability of a second-order system (e.g. a mass-spring-damper system such as the one under investigation) can be calculated based on the gain and phase margins in the Nyquist plot. This concept is revisited now for further study. The gain margin (G_M) indicates the amount of gain by which the open-loop transfer function can be increased in order for the closed-loop system to become marginally stable. It is usually expressed in decibels. Therefore, if the gain margin is greater/less than zero, the process is stable/unstable, respectively. The phase margin (P_M) marks the amount of open-loop phase lag the closed-loop system can tolerate before becoming marginally stable. It is usually expressed in degrees. If the phase margin is greater/less than zero, the process is stable/unstable, respectively. The gain and phase margins are formally defined and graphically presented in a number of textbooks (e.g. [155], pp. 643-650), therefore, they are not discussed here in any more detail.

A colour map of the gain margin distribution for a number of wheel speeds and depths of cut is presented in Figure 5.18 along with the absolute stability boundary indicated in white. It can be seen that the gain margin increases towards the centre of the stable zone, and connects seamlessly to the finitely unstable region. However, the gain margin jumps in two places: (1) between infinite and finite encirclements, i.e., at the stability boundary between points A and B in Figure 5.14, and (2) in the infinitely unstable zone, where the dominant infinite encirclement (i.e. the biggest one relative to the others) switches to another one. This switch happens at the same numerical parameters at which the number of wheel lobes changes in Figure 5.15, because the dominant infinite encirclement played a key role in determining the number of lobes forming on the wheel under infinitely unstable grinding conditions. It is very important to note that in the infinitely unstable zone, the gain margin should theoretically be negative infinity. It is only because of the numerical scheme employed (i.e. $\varepsilon > 0$ in Figure 5.7) that the gain margins corresponding to this region appear to be finite. This means that in the infinitely unstable zone, the gain margin alone cannot provide sufficient information on the relative stability of the process – the phase margin is necessary as well.

A colour map of the phase margin distribution is given in Figure 5.19 for the same

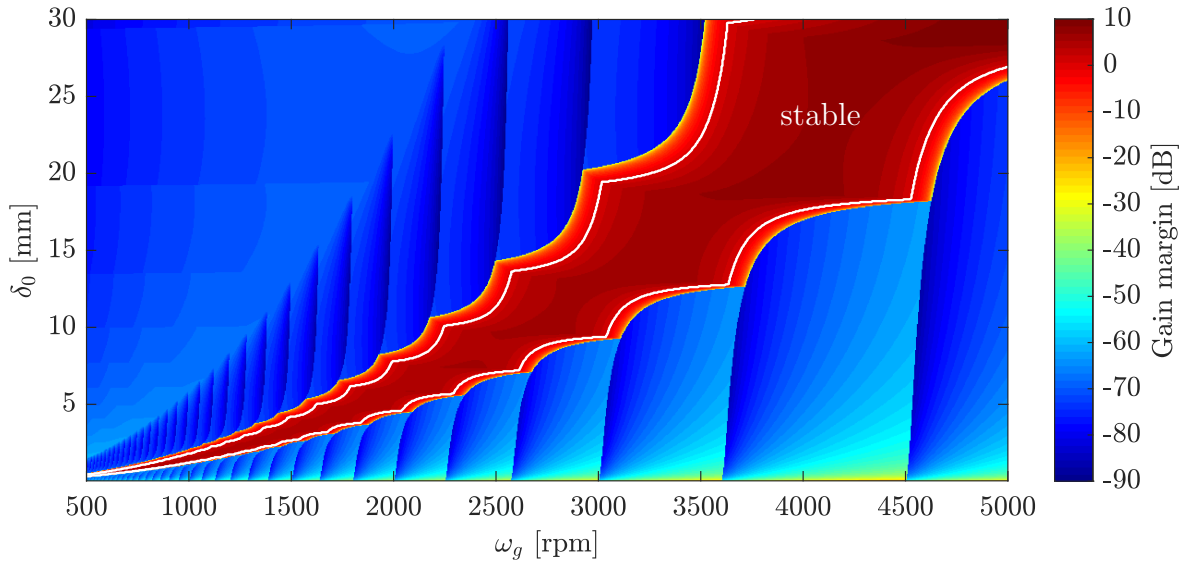

Figure 5.18: Gain margin distribution in the stability diagram

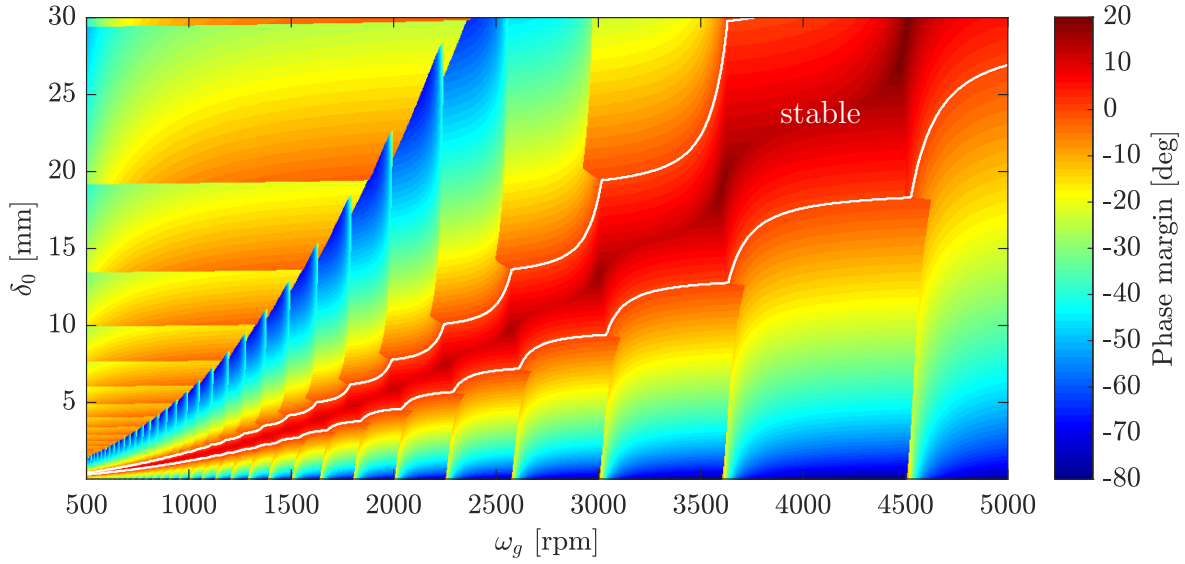

Figure 5.19: Phase margin distribution in the stability diagram

numerical parameters. Similarly to Figure 5.18, the absolute stability limit is marked in white. It can be seen that the phase margin increases towards the centre of the stable region and decreases away from it. Both of these gradients result in a smooth relative stability map – jumps only occur when the dominant infinite encirclement switches to a new one. These jumps in phase margin happen in the same places as those in lobe number (Figure 5.15) and gain margin (Figure 5.18). Due to the fact that the phase margin calculated in the infinitely unstable zone, unlike the gain margin, is unaffected by the issue that ε (as defined in Figure 5.7) cannot be truly zero in numerical simulations, it provides a reliable measure of relative stability even in this computationally challenging region. Furthermore, the phase margin (P_M) is closely related to the damping ratio (ζ) of the process. The relationship between these two quantities can be approximated as $P_M = 100\zeta$ (according to [155], p. 648), where the phase margin has to be substituted in

degrees. Since the damping ratio of a real grinding process is relatively easy to measure, this approximation provides a simple way to compare theoretical and experimental results. Therefore, the concept of relative stability in general and the phase margin approach in particular will be put to practical use in the context of grinding experiments in Chapter 6.

5.3.7 Numerical validation

In order to test the theoretical validity of the frequency-domain solution discussed in Section 5.3, a number of time-domain simulations are presented here. Applying the central difference scheme to the equation of motion, Eq. (5.28) can be solved for a given set of grinding parameters. Figure 5.20 shows three numerical simulations corresponding to the three grinding scenarios marked by points A, B and C in Figure 5.14.

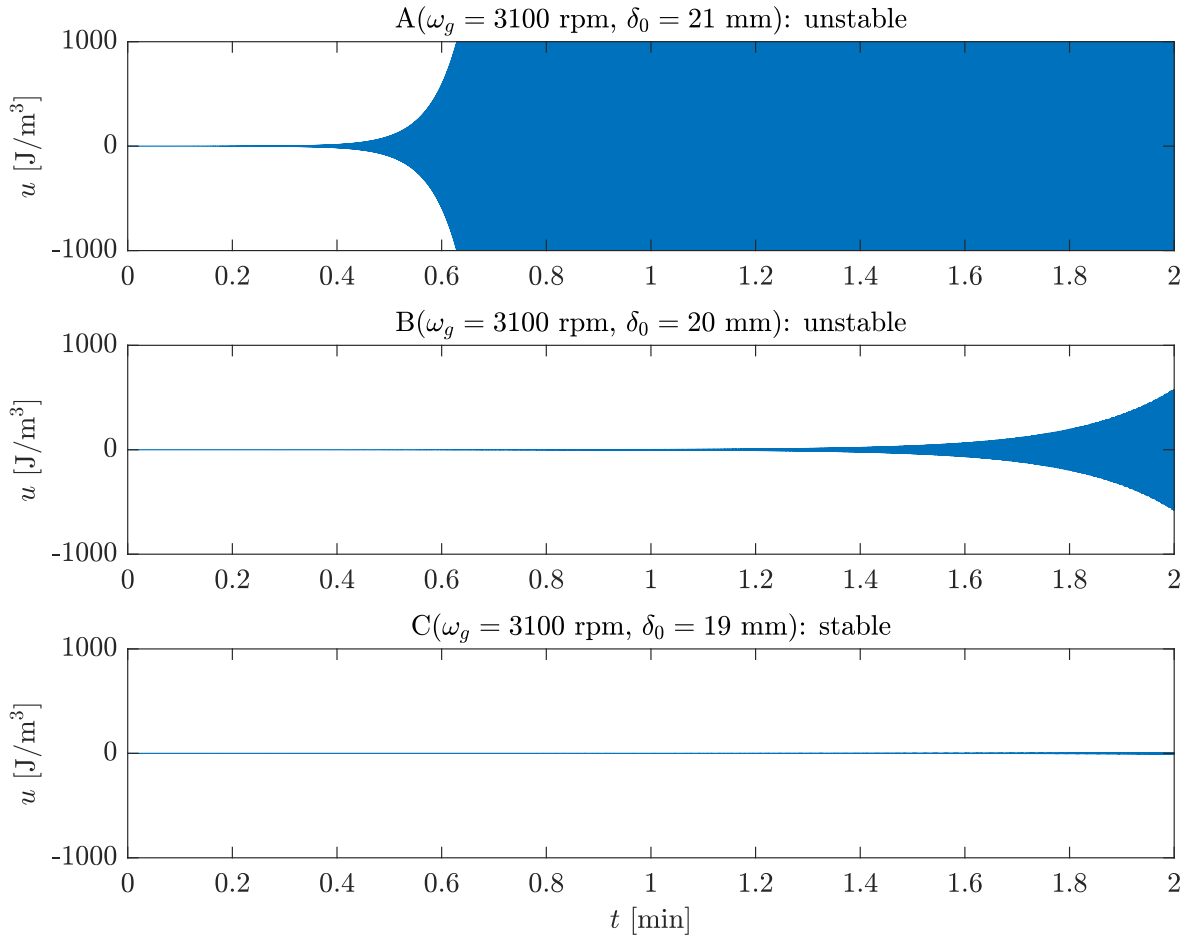

Figure 5.20: Numerical simulations corresponding to three different grinding scenarios

It can be seen that the grinding process identified by point C is stable, while the other two cases are unstable. Furthermore, scenario A is more unstable than scenario B, because A loses stability faster than B, i.e., A reaches a higher variation in specific energy than B over the same amount of grinding time (or equivalently, A reaches the same variation in specific energy as B over a shorter amount of grinding time). Also, according to

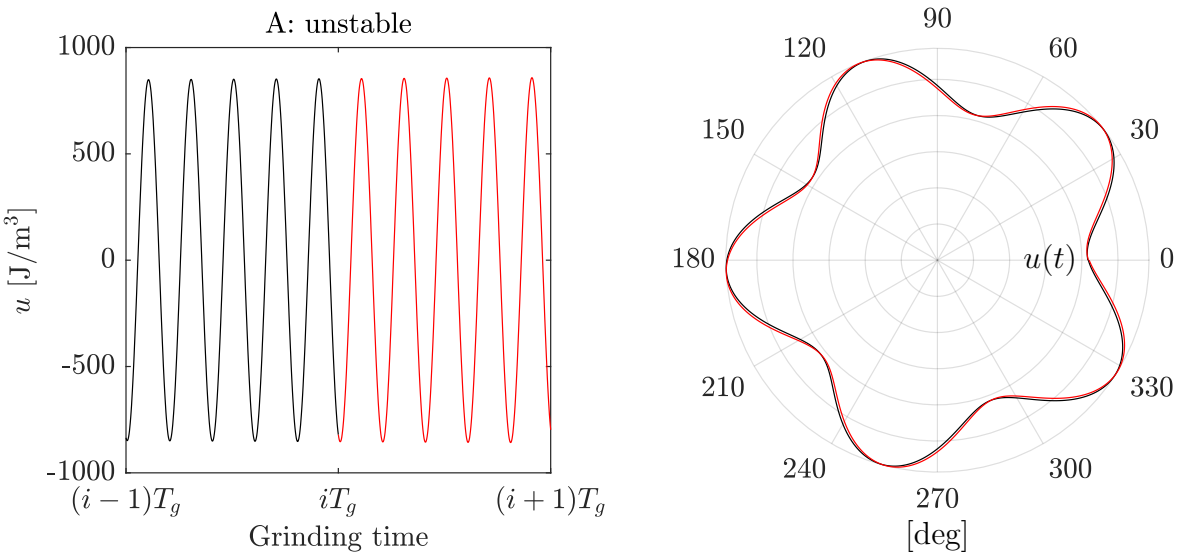

Figure 5.21: Linear (left) and polar (right) plots of the specific energy variation for two successive grinding wheel rotations depicted in different colours

Figure 5.15, the grinding process corresponding to point A is predicted to be unstable with five specific energy waves around the circumference of the wheel. The numerical simulation in Figure 5.20a verifies this result, which can be visualised by plotting the specific energy variation onto the surface of the grinding wheel in the form of a polar diagram. Considering the simulated specific energy variation in time along with the rotational speed of the grinding wheel, the number of specific energy waves on the wheel is illustrated in Figure 5.21. Two observations can be made regarding this diagram: (1) the number of wheel lobes is indeed five, according to the analytical prediction shown in Figure 5.15, and (2) the specific energy distribution on the grinding wheel is not identical for two successive wheel rotations. In other words, the specific energy waves do not remain stationary, but travel around the circumference of the grinding wheel. This phenomenon has been discussed before as 'wheel lobe precession'. Therefore, what has been merely suggested by non-integer lobe numbers, has now been verified by numerical simulations: the specific energy waves slowly precess or travel around the circumference of the wheel during grinding, and the proposed model is capable of capturing this phenomenon.

Furthermore, to compare the analytical and numerical results for a larger number of grinding processes, Figure 5.22 presents the analytical stability boundary along with several numerical simulations, indicating stability and instability with green and red colours, respectively. It can be seen that, as far as the theoretical model is concerned, the frequency- and time-domain results are in agreement, which means that the numerical simulations have validated the analytical analysis.

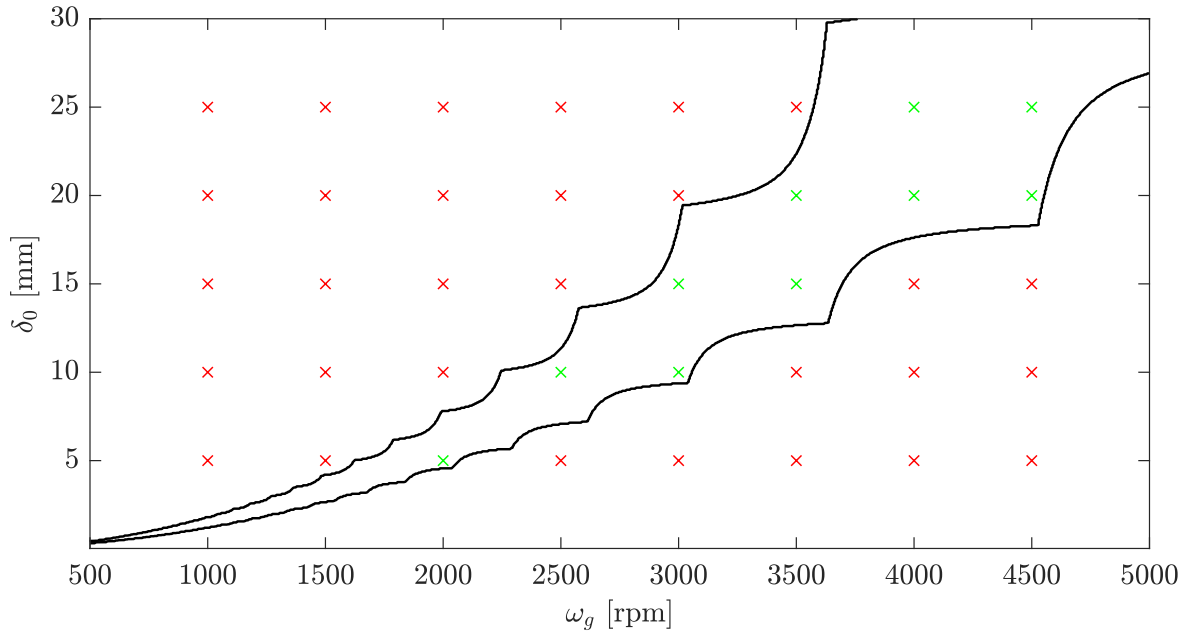

Figure 5.22: Comparison between analytical and numerical results: —— analytical stability boundary, × stable numerical simulation, × unstable numerical simulation

5.4 Summary of results

A new grinding chatter theory has been formulated in this chapter, focusing on wheel regeneration and wheel-related instability in single-pass surface grinding. Having established the mechanical and mathematical models, the Nyquist criterion was employed to assess the stability properties of the system. The primary results of this analysis were stability boundaries and chatter frequencies, which were presented in stability charts and frequency diagrams.

Considering the fact that grinding is described in the literature as typically unstable with respect to wheel regeneration [25], the most important result of the new model is the prediction of a stable region, which is rather narrow for low wheel speeds and depths of cut, but grows wider as these two grinding parameters increase. However, the depths of cut for which the proposed chatter theory predicts stable machining are quite high (certainly too high for finishing operations), which means that even if the presented model is tested and found to be valid, the stable depths of cut may be too large for practical processes, including roughing operations. When the radial immersion is low, which is typical of finishing cuts, the new chatter theory predicts grinding to be unstable with respect to wheel regeneration. This is in accordance with the predominant stance of the relevant literature. However, if the grinding parameters corresponding to the theoretically stable region turn out to be practically feasible, then the predictions of this new model are very promising indeed in terms of chatter-free grinding.

The chatter frequencies predicted by the proposed theory are in agreement with classical chatter theories in machining, both conventional and abrasive. That is to say that the theoretical chatter frequencies produced by the presented model are around the natural

frequency of the system and slightly above it for the lower stability boundary. Practically speaking, the upper stability boundary is of lesser interest due to machine limitations, nevertheless, the chatter frequencies predicted at this boundary are slightly below the natural frequency of the system. It was also noted that the chatter frequencies are approximately integer multiples of the wheel speed, and the lobes of the stability diagram govern the number of specific energy waves forming on the surface of the grinding wheel. Within each stability lobe, the chatter frequencies change in such a way that, combined with the corresponding variation in wheel speed, the chatter frequency remains approximately the same integer multiple of the current wheel speed. At the points where the stability lobes connect, the expected number of specific energy waves forming on the wheel jumps to a different value. The overall trend is that decreasing the wheel speed increases the number of specific energy waves on the surface of the grinding wheel. This is consistent with the fact that the chatter frequency remains close to the natural frequency of the system.

In summary, the new grinding chatter theory proposed in this chapter gives very promising results regarding the stability of surface grinding processes. The stable region predicted by the model can be of great benefit to the manufacturing sector. Although this result is potentially exciting, it is nevertheless based on a large number of assumptions. For the sake of completeness, these are re-listed in Appendix B.

All the theoretical results in Chapters 4 and 5 – such as stability boundaries, chatter frequencies and numerical simulations – have been obtained with the help of MATLAB. The code that the author wrote and used in this chapter to determine the stability boundaries of single-pass surface grinding is provided in Appendix C.

The following chapter presents and discusses a number of surface grinding experiments in order to test the validity of the new chatter model developed in this thesis.

Chapter 6

Surface grinding experiments

For the purpose of testing the new chatter theory formulated in Chapter 5, some surface grinding experiments were performed on a Makino G7 5-axis horizontal machining centre, which is illustrated in Figure 6.1. In six main parts, this chapter describes the experimental procedure and signal processing methodology designed and implemented to collect, analyse and evaluate data from a number of surface grinding experiments, and discusses the obtained results in detail.

The first section deals with the modal analysis of the structure. The grinding machine was tap tested in order to determine its modal parameters, which are necessary for calculating its stability properties. The second part of this chapter presents the preparations leading up to the actual experiments. A sensitivity analysis was performed in order to assess how process stability changes in response to different system parameters being varied. The third and fourth sections are of primary importance as they discuss the core experiments designed to test the validity of the proposed chatter theory, based on two main aspects of grinding dynamics: chatter frequencies and stability boundaries. The fifth part of this chapter is concerned with the concept of relative instability. The negative damping ratios of a number of unstable surface grinding experiments are calculated and compared with the corresponding theoretical predictions. The sixth and final section summarises all the practical results reported in this work.

6.1 Modal analysis of the structure

Modal analysis is the study of the dynamic properties of a system in the frequency domain. It is based on the response of a mechanical structure to a given form of excitation. The response of the system can be recorded as a displacement, velocity or acceleration signal, while the source of excitation is typically a force signal. The outcome of modal analysis is the ratio between the input and output signals, also known as the frequency response function (FRF), which defines a frequency-dependent relationship between two points of a structure. In other words, the FRF provides valuable information as to how the system behaves at different frequencies of excitation. Depending on the response signal, FRFs

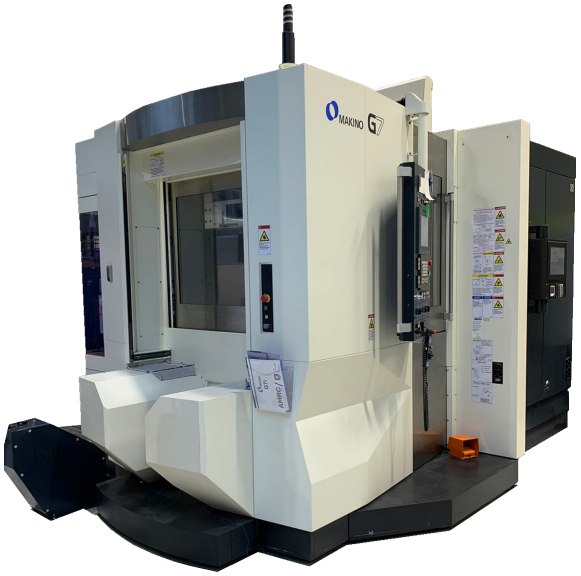

Figure 6.1: Makino G7 machining centre

can be classified as receptance (displacement per force), mobility (velocity per force) or inertance (acceleration per force).

One of the most common and widely applied methods of modal analysis is tap testing or impact hammer testing. In the simplest case, the structure is excited with an impulse hammer recording the force signal at one point, while another sensor captures the response of the system at another point. The ratio of the output signal to the input signal constitutes the FRF of the structure between those two points. This is the approach that was employed to obtain the modal parameters of the Makino G7 grinder (i.e. natural frequencies, damping ratios and modal masses). Therefore, this section is dedicated to describing the tap testing procedure and summarising its results.

6.1.1 Equipment

The tap testing equipment consisted of four main components:

1. Hammer: Kistler 9722A500 + soft PVC tip (Sensitivity: 11.63 mV/N)
2. Accelerometer: Kistler 8776A50M1 (Sensitivity: 101 mV/g)
3. Data acquisition system: National Instruments 9234
4. Computer + software: CutPro Tap Testing and Modal Analysis Modules (more information on these two modules is available at `www.malinc.com`)

6.1.2 Setup

The tap testing setup is presented in Figure 6.2. It can be seen that the accelerometer

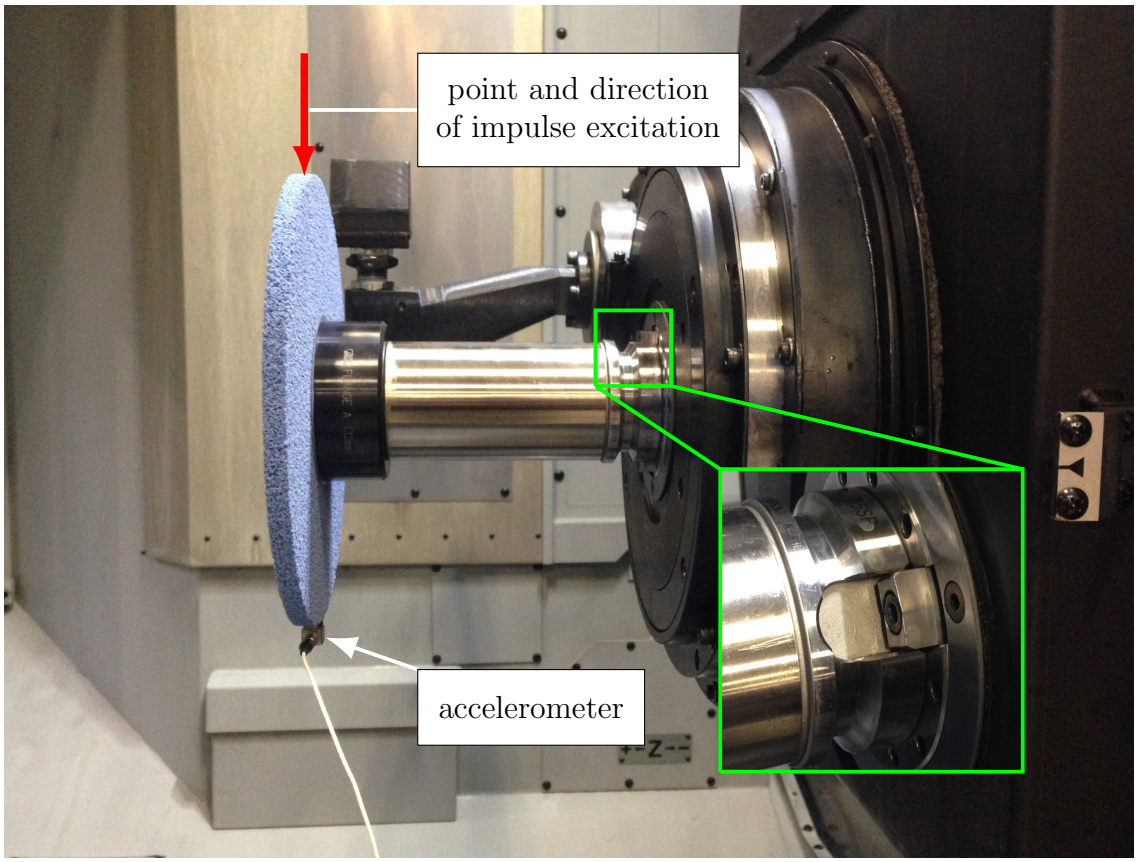

Figure 6.2: Tap testing setup

was attached to the bottom (or 6 o'clock position) of the grinding wheel, while the point of impulse excitation was chosen to be at the top (or 12 o'clock position) of the grinding wheel. Two 3M™ Cubitron™ II wheels were tested, the physical properties of which are summarised in Table 6.1.

Because of the two diametrically opposite grooves in the tool holder, also known as 'dogs' (highlighted in Figure 6.2), which are used to align the tool holder and prevent it from slipping inside the spindle, the modal properties of the structure were expected to be somewhat different depending on the alignment of these grooves. Therefore, as shown in Figure 6.3, the tap testing procedure was performed for a horizontal and a vertical alignment as well, in order to capture this potential difference.

Wheel identifier	Outer ⌀ [mm]	Inner ⌀ [mm]	Width [mm]	Grit number	Mass [kg]
GW-1	220	32	15	60/80	0.847
GW-2	220	32	10	60/80	0.551

Table 6.1: Physical properties of two 3M™ Cubitron™ II grinding wheels

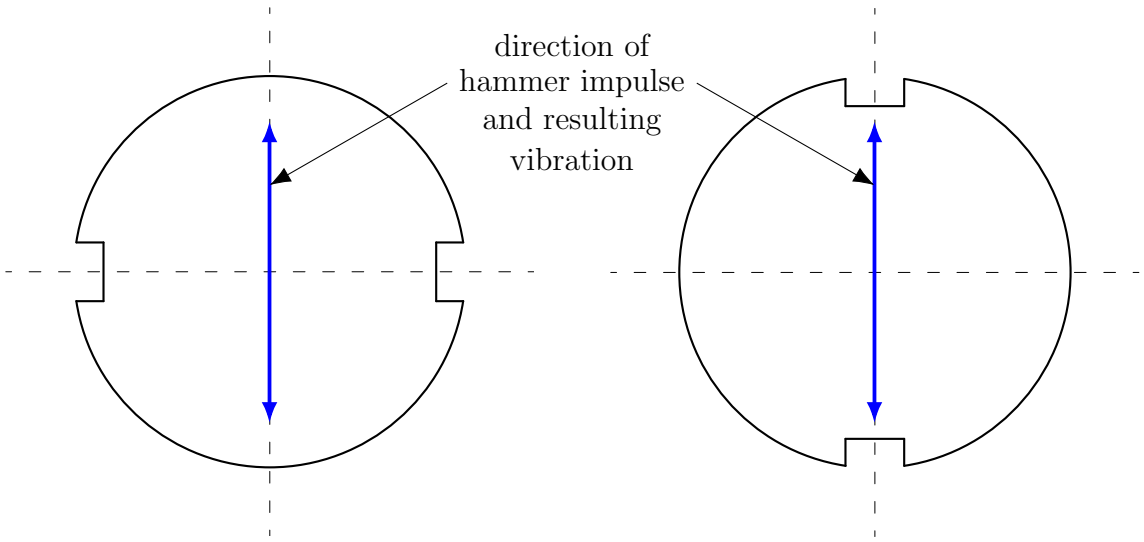

Figure 6.3: Cross section of the tool holder at the grooves:
horizontal (left) and vertical (right) alignments

As it was mentioned earlier in Section 6.1.1, CutPro was used for recording and analysing the data. Five tests were averaged in each case in order to reduce measurement errors and improve accuracy. The frequency range was set between 10 and 5000 Hz along with a sampling rate of 51,200 Hz and a frequency resolution of 0.5 Hz. CutPro calculates the window size for the fast Fourier transform (FFT) based on the sampling rate and the frequency resolution, and applies an exponential window function, which typically decays from unity to 0.05 in the total sample time (according to the work of Altintas [35], p. 98, upon which CutPro is based).

6.1.3 Results

In order to establish the fact that the dynamics of the structure consisting of the spindle, tool holder and grinding wheel can be accurately characterised by a single set of modal parameters, a coherence chart is presented in Figure 6.4 corresponding to one of the tap testing scenarios. The coherence can be used to estimate the causality between the input and output signals. In other words, the coherence provides a quantifiable measure of reliability: when the coherence is close to one, the results are reliable, but when it is far from one, the causality between the input and output signals is inadequate. Figure 6.4 indicates the reliable range of data between two red lines, along with three reliable peaks, the highest of which is clearly the dominant mode. Consequently, it is a reasonable simplification to characterise the dynamics of the system by a single set of modal parameters related to the highest peak.

The dominant modal parameters of the structure corresponding to two grinding wheels and two spindle positions are summarized in Table 6.2, where f_n is the single dominant natural frequency of the system, and ζ, k and m are the corresponding damping ratio, modal stiffness and modal mass, respectively.

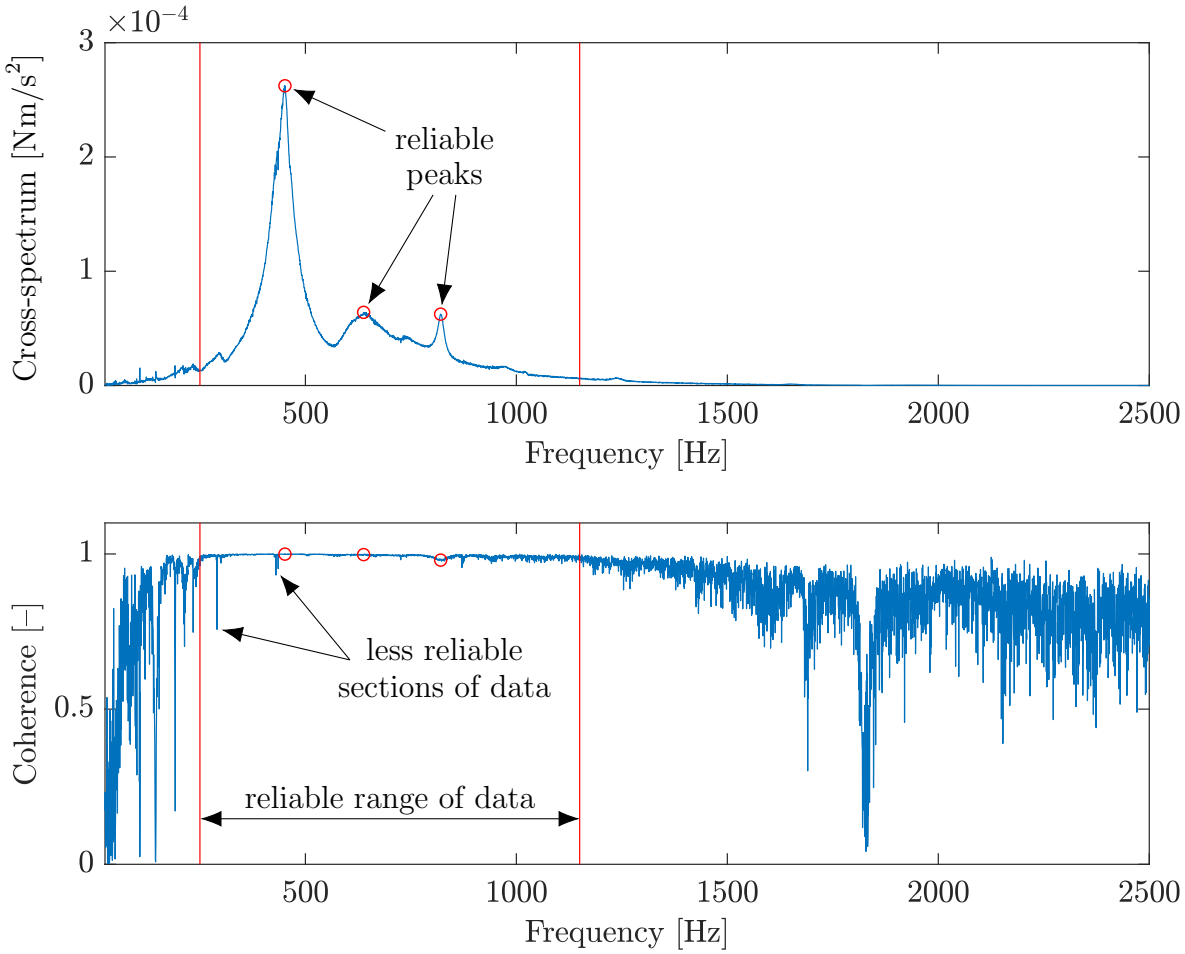

Figure 6.4: Cross-spectrum and coherence diagrams corresponding to GW-2 and a horizontal alignment of tool holder grooves

Based on the differences in second moment of area between the two spindle positions and in mass between the two grinding wheels, the following predictions can be made even before tap testing the structure: (1) a horizontal alignment of tool holder grooves produces a higher second moment of area in the direction of excitation and therefore a higher bending stiffness, resulting in a higher natural frequency than a vertical alignment, and (2) a heavier grinding wheel acts as a bigger lumped mass at the end of the tool holder, resulting in a lower natural frequency than a lighter wheel. Both of these predictions are clearly supported by the measurement results recorded in Table 6.2. The natural frequency of the structure corresponding to the heavier wheel (i.e. GW-1) is lower for both spindle positions. Also, a horizontal alignment of tool holder grooves results in a higher natural frequency for each wheel due to a higher bending stiffness. It is interesting to note that for the vertical alignment (i.e. when the structure is more compliant), the weight of the wheel has a more significant impact on the dominant natural frequency of the system. This observation is rather intuitive, however, the numerical difference between the two scenarios is quite substantial. The four natural frequencies corresponding to the two grinding wheels and the two alignments of tool holder grooves are summarised in Table 6.3, along with the difference in natural frequency between the two wheels for each alignment of tool holder grooves.

Horizontal	GW-1	GW-2
f_n [Hz]	445.55	449.81
ζ [%]	4.52	4.24
k [N/m]	4.06×10^7	3.79×10^7
m [kg]	5.176	4.750

Vertical	GW-1	GW-2
f_n [Hz]	432.31	445.71
ζ [%]	5.06	4.67
k [N/m]	3.26×10^7	3.29×10^7
m [kg]	4.416	4.191

Table 6.2: Modal parameters corresponding to two grinding wheels ($m_1 = 0.847$ kg, $m_2 = 0.551$ kg) and two spindle positions (according to Figure 6.3)

f_n [Hz]	GW-1	GW-2	Difference
Horizontal	445.55	449.81	4.26
Vertical	432.31	445.71	13.40

Table 6.3: Natural frequencies corresponding to the four test cases

Due to the fact that the proposed chatter theory is based on a single-degree-of-freedom model of surface grinding and requires a set of modal parameters (natural frequency, damping ratio, modal mass) that are independent of the angular position of the spindle, the variation of the modal parameters with respect to the angular position of the spindle will be neglected. Similarly, the modal properties of the spindle are affected by the mass of the grinding wheel as well. However, for the sake of simplicity, this variation in spindle dynamics is also neglected. Therefore, in order to obtain the necessary modelling parameters, the four sets of tap testing results corresponding to different grinding wheels and spindle positions (Table 6.2) are replaced by their average values (Table 6.4). These modal parameters will be used later on to predict stability boundaries and chatter frequencies that belong to the Makino G7 grinder.

However, it is important to keep in mind that these two simplifications concerning the angular position of the spindle and the weight of the grinding wheel will introduce some modelling inaccuracies into the theory, the extent of which is difficult to assess at this stage. Therefore, in case of a significant discrepancy between the theoretical and practical results, these two modelling assumptions are to be revisited for further consideration.

6.2 Preparation for grinding experiments

In order to conduct some experiments that are capable of testing the presented theory in a reliable way, the dynamic behaviour of the grinding system under investigation must be assessed. This includes two main sets of studies: a stability analysis and a number of sensitivity analyses corresponding to different modal and grinding parameters. The stability analysis consists in a stability diagram specific to the dynamics of the Makino

f_n [Hz]	ζ [%]	k [N/m]	m [kg]
443.34	4.62	3.60×10^7	4.633

Table 6.4: Modal parameters obtained by averaging the ones listed in Table 6.2

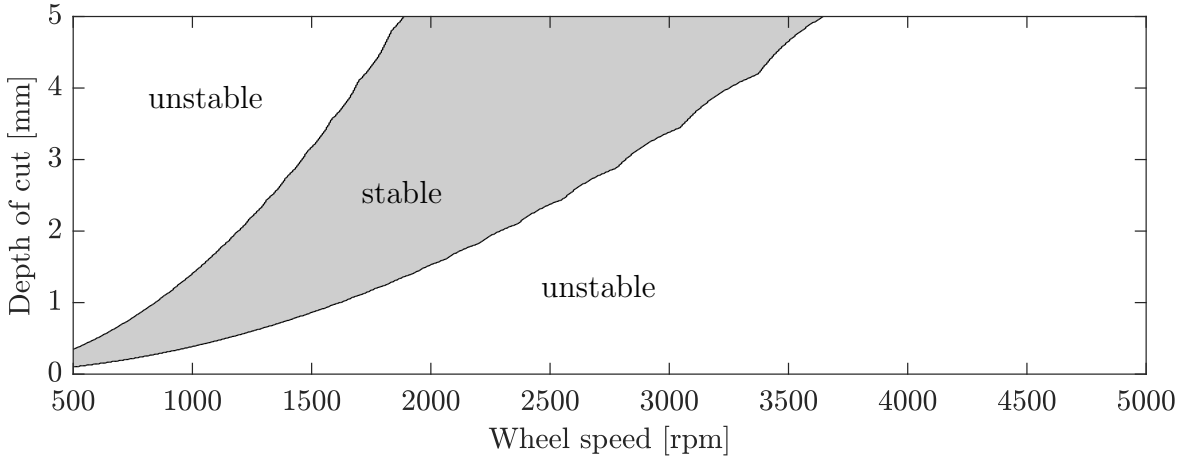

Figure 6.5: Stability map of the Makino G7 grinder for $R_g = 110$ mm, $v_w = 250$ mm/min and $G = 100$

G7 grinder, and it serves the purpose of determining some test points that can be used to check the validity of the proposed chatter theory. The sensitivity analyses are performed to confirm whether the stability properties of these test points (i.e. the ones obtained from the stability analysis) are robust enough to remain approximately unchanged in the face of small variations in certain modal and grinding parameters.

6.2.1 Stability of the Makino G7 grinder

Based on the modal parameters measured and reported in Section 6.1, the stability diagram of the Makino G7 grinder corresponding to a certain set of grinding parameters is presented in Figure 6.5. This chart is a relatively accurate representation of the stability properties of the G7, however, certain cutting parameters – such as the grinding ratio and the feed rate – can assume a very wide range of values in practice, and thus have a significant impact on the stability boundaries. The effects of these parameters are demonstrated in Section 6.2.2.

6.2.2 Sensitivity of the Makino G7 grinder

Four parameters are expected to undergo different degrees of variation: the natural frequency, the wheel radius, the grinding ratio and the feed rate. The natural frequency can change for a number of reasons – it is affected by the alignment of the tool holder grooves, the mass of the wheel, and it can also change slightly as a result of removing and

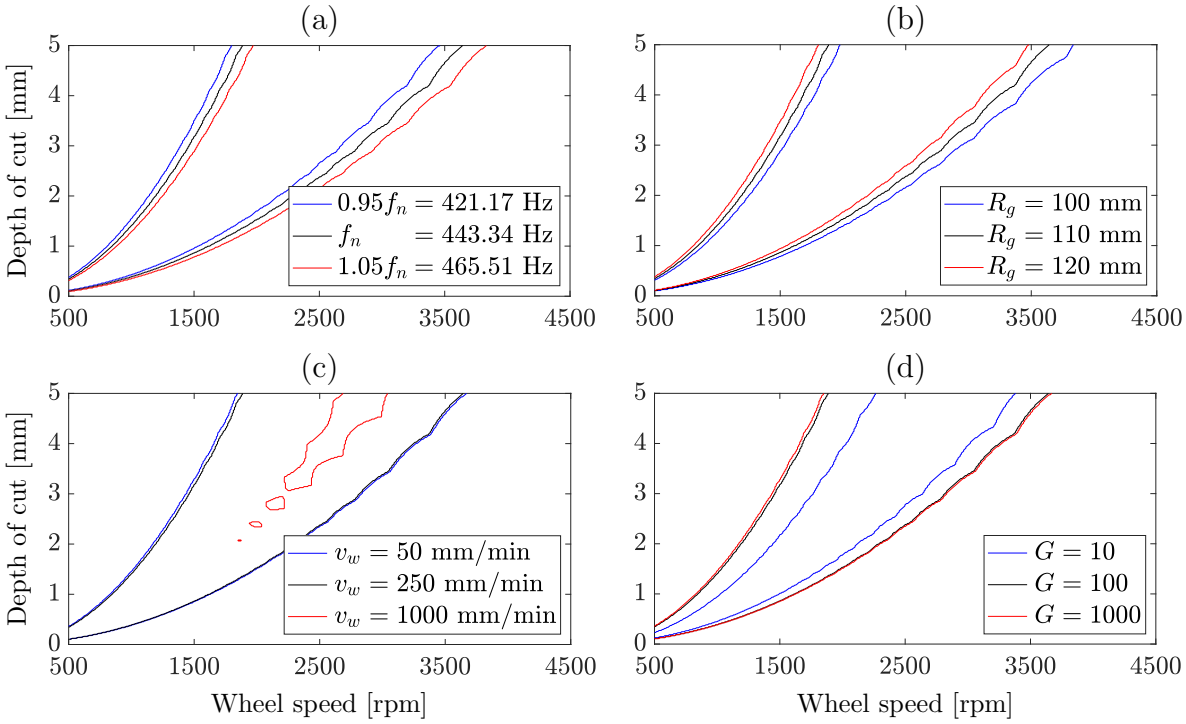

Figure 6.6: Sensitivity of the stability boundaries to the (a) natural frequency, (b) wheel radius, (c) feed rate and (d) grinding ratio – unless otherwise noted, every figure corresponds to $f_n = 443.34$ Hz, $R_g = 110$ mm, $v_w = 250$ mm/min and $G = 100$

reclamping the same grinding wheel, as it modifies the contact conditions between the spindle and the tool holder. The wheel radius changes due to dressing and wheel wear, the latter of which is tightly connected to the grinding ratio. Depending on the grinding conditions and the material properties of the wheel and the workpiece, the grinding ratio can vary from less than unity to tens of thousands in practice, which covers an extremely wide range of possible values. The feed rate is another one of those grinding parameters that can assume a very wide range of values based on the particular grinding operation employed. In creep-feed grinding, it can be as low as 50 mm/min, whereas in speed-stroke grinding, it can be as high as 120 000 mm/min. The following paragraphs discuss four sensitivity studies corresponding to these four parameters.

Figure 6.6a presents the sensitivity of the stability boundaries to the natural frequency of the grinding system. Having performed a modal analysis of the structure, it is possible to estimate the amount of variation expected in the natural frequency. Therefore, a deviation of 5% from the average natural frequency was selected, which is a significantly wider range than the one defined by its actual variation recorded in Table 6.2. Nevertheless, the variation in process stability as a result of a 5% variation in natural frequency – although clearly detectable – is not substantial. Consequently, taking into account the fact that the expected variation in natural frequency is less than 3%, the stability properties of the system predicted for $f_n = 443.34$ Hz are robust and reliable.

Figure 6.6b presents the sensitivity of the stability boundaries to the radius of the grinding wheel. The reasoning behind the selection of a wheel radius range of ±10 mm is the

reverse of that corresponding to the natural frequency. This is the wheel radius range that yields an admissible variation in process stability. Therefore, considering the fact that the initial radius of the grinding wheels tested in this study was 110 mm, it was important to remember that as the wheel radius decreased due to dressing and wear, it had to be kept above 100 mm at all times by implementing new grinding wheels on demand. This was to ensure that the stability properties of the system did not change significantly as the wheel size decreased during experiments.

Figure 6.6c presents the sensitivity of the stability boundaries to the feed rate, which can cover an extremely wide range of values depending on the particular grinding operation implemented. One of the things that is immediately noticeable here is the nature of the effect that the feed rate has on the stability boundaries. While the natural frequency and the wheel radius merely shifted the boundaries, the feed rate can shrink and expand the stable zone. It is also important to note that at the lower end of practical feed rates, the actual value of the feed rate has little impact on the stability boundaries. However, considering a certain range of wheel speeds and depths of cut, there exists a feed rate at which the stable region disappears completely. Therefore, the feed rate has the potential to substantially alter the stability boundaries, which means that the grinding process is rather sensitive to this particular parameter.

Figure 6.6d presents the sensitivity of the stability boundaries to the grinding ratio. Similarly to the feed rate, the grinding ratio also shrinks and expands the stable zone, however, the overall effect of the grinding ratio is opposite to that of the feed rate: decreasing the grinding ratio reduces process stability. It can also be seen that for high grinding ratios, i.e. when the wear resistance of the grinding wheel is high, the stability boundaries are almost entirely independent of the grinding ratio. In fact, they seem to be tending to a specific set of boundaries independent of the grinding ratio itself. However, this is a rather unreasonable observation, since $G \to \infty$ is indicative of a perfectly wear-resistant grinding wheel, in which case no wheel regeneration and thus no wheel-related instability can occur. This train of thought suggests an increasing stable zone for an increasing grinding ratio.

Since Figure 6.6d seems to contradict this line of reasoning, the stability boundaries of the system were calculated for a number of extremely high grinding ratios as well in order to see if there is any improvement in process stability. The results are presented in Figure 6.7a. It can be seen that the widening part of the stable zone (also shown in Figure 6.6d) is almost unchanged, however, a new stability feature develops as the grinding ratio reaches extremely high values: a lobe-like stability structure arises from the horizontal axis resembling that of conventional machining depicted in Figure 2.1. Endlessly increasing the grinding ratio to unrealistically high values causes the stable zone to expand through these lobes, eventually covering the entire domain of simulated grinding parameters. Therefore, Figure 6.7a is evidence that the original conviction of $G \to \infty$ resulting in an ever-expanding stable zone was correct.

It is important to note that Figure 6.7a holds some interesting prospects for superabrasives with extremely high grinding ratios. Stable regions that do not feature for lower G-ratios (i.e. for conventional abrasives) seem to appear above $G = 1000$. The further

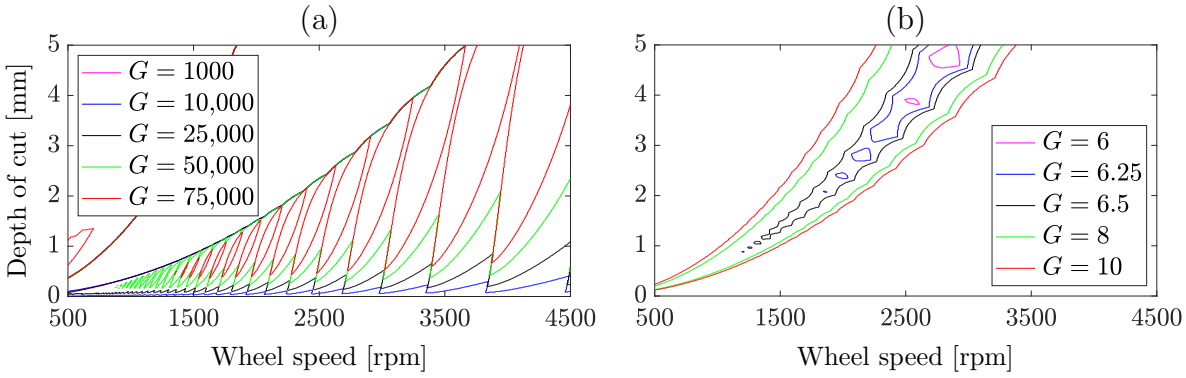

Figure 6.7: Stability boundaries corresponding to extreme grinding ratios – other parameters are $f_n = 443.34$ Hz, $R_g = 110$ mm and $v_w = 250$ mm/min

investigation of this particular topic is outside the scope of this study, but potentially constitutes a branch of this research that is worth pursuing in the future. The other feature clearly visible in Figure 6.6d has to do with the lower end of grinding ratios: when the G-ratio is small, the stability of the system depends heavily on the actual value of the grinding ratio, as it is demonstrated in Figure 6.7b for $G \leq 10$. It can be seen that the stable region begins to rapidly disappear around $G = 6.5$. Between 6.5 and 6, it almost completely vanishes from the simulated domain of grinding parameters. Therefore, for a wheel that is soft relative to the workpiece, the stability boundaries are not robust even against a small variation in the grinding ratio. Consequently, the stability diagram of the system may need to be recalculated depending on the actual value of the grinding ratio, however, Figure 6.6d provides some valuable insight into the system's overall sensitivity to realistic grinding ratios.

Since all these sensitivity studies focused on a single parameter, it is important to remember that they may influence one another. In other words, changing one of these parameters may affect the sensitivity of the system to another parameter. Therefore, it is crucial to keep in mind that the sensitivity analyses above are rudimentary studies, and further stability diagrams need to be constructed based on the real parameters corresponding to the actual grinding experiments.

6.2.3 Test plan for grinding experiments

There are two main aspects of process stability that need to be considered when it comes to checking the validity of the grinding chatter model proposed in this thesis: chatter frequencies and stability boundaries. That is because the presented theory predicts both chatter frequencies for unstable grinding scenarios and stability boundaries separating stable and unstable parameter domains. Therefore, in order to test the proposed model, both of these areas need to be addressed in the experiments. Sections 6.3 and 6.4 provide detailed reports on these two aspects of grinding stability.

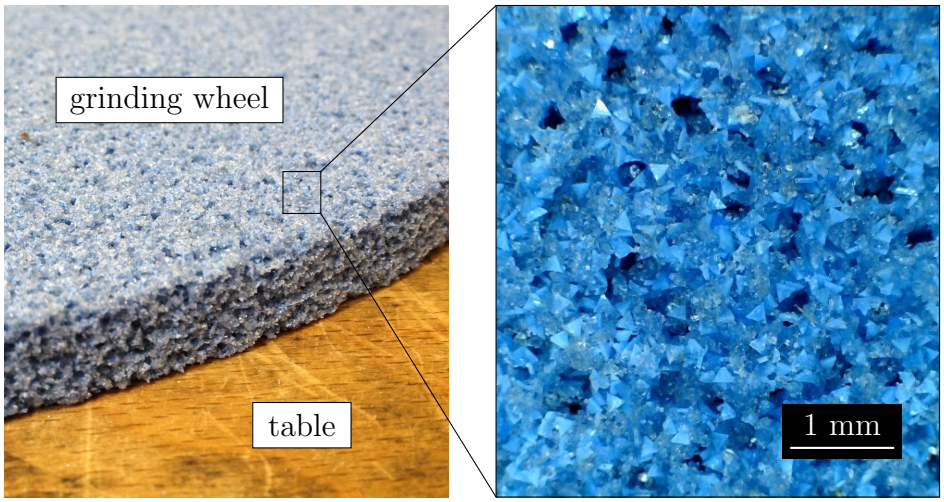

Figure 6.8: 3M™ Cubitron™ II grinding wheel and its abrasive grits

6.2.3.1 Equipment

Apart from the G7 itself, the primary piece of equipment used in the experiments was a force dynamometer (Kistler Type 9129AA). That is because the main signal to be recorded was the grinding force between the wheel and the workpiece. The theoretical model presented in this thesis captures the regenerative effect through the variation of the grinding force as a result of wheel wear, therefore, measuring the grinding force in the experiments provides a direct relationship between the model and the experiments. The grinding power is automatically monitored and recorded by the G7, however, it is not used in this work, as it is secondary to the grinding force in terms of reliability when it comes to testing the proposed chatter model. In other words, a peak in the power signal has a significantly larger number of potential sources than a peak in the force signal does, which means that the grinding power provides less clear and less specific information with regard to process dynamics than the grinding force does. Similarly to the modal analysis of the structure, the appropriate hardware (computer-based data acquisition system) and software (DynoWare) are included in the measurement kit.

The cutting tool employed in the experiments was a 3M™ Cubitron™ II grinding wheel with the physical parameters of GW-1 listed in Table 6.1. It is important to note that this wheel contains a large number of triangular grains (as shown in Figure 6.8), which corresponds to the theoretical model of the grinding wheel presented in Figure 5.12. The tested workpiece materials were Inconel 718 (nickel-chromium-based superalloy) and Custom 465 (stainless steel). The workpieces were prepared as 100 × 50 × 15 mm blocks in order for them to stay within the measurement range of the dynamometer.

The Makino G7 was equipped with RBM's Intelligent Fluid Delivery and Recycling system (IFDR). The programmable coolant nozzle (35 mm wide with an aperture width of 1.5 mm) allowed the machine to make full use of its VIPER grinding capabilities. The application of the coolant was available at different pump pressures (from 30 to 70 bar) through a range of nozzle configurations. The coolant temperature was kept between 18

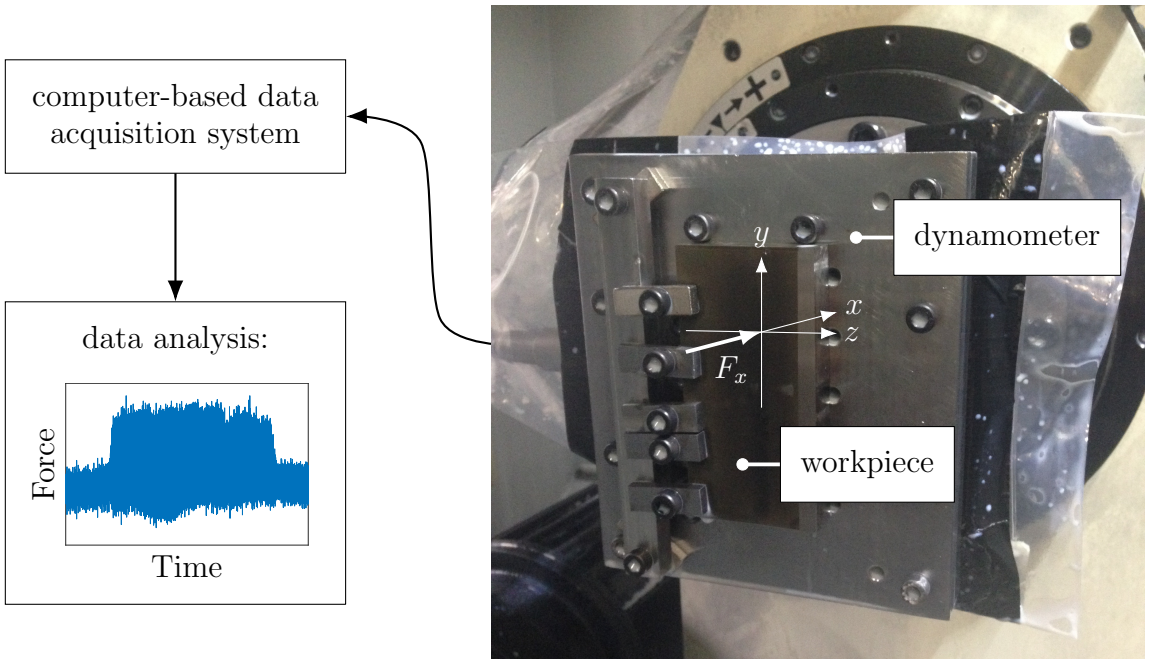

Figure 6.9: Experimental setup for recording and analysing the grinding force

and 22 °C. For the experiments discussed in this chapter, Master Chemical's TRIM C272 coolant emulsion was used and held at a concentration between 6 and 8%. The filtration of the coolant was integrated into the RBM system itself by means of hydrocyclone technology.

The dressing configuration was unidirectional, i.e., the circumferential speed of the grinding wheel was in the same direction as that of the dressing roll. The wheel was dressed on a flat diamond crush roll (150 mm in diameter, manufactured by Tyrolit) at a dressing roll speed of 3000 rpm, with a dressing speed ratio of 0.8 (roll to wheel), using a dressing feed rate of 0.0012 mm/rev.

6.2.3.2 Setup

Once the force dynamometer is installed and the workpiece is fixed, the test setup looks relatively simple as it can be seen in Figure 6.9. The dynamometer was connected to a computer-based data acquisition system, from which the grinding force signal was taken to MATLAB for further analysis. In accordance with the theoretical model, the grinding force component to be analysed is F_x, which is perpendicular to the workpiece surface. As indicated in Figure 6.9, it is positive if the workpiece is pressed against the dynamometer. Therefore, the term 'grinding force' will refer to this direction and sign convention throughout the rest of this chapter.

According to the fact that the chatter model proposed in Chapter 5 was considered in an up-grinding configuration, the experiments were performed in an up-grinding configuration as well, i.e., the circumferential velocity of the grinding wheel was opposite to the

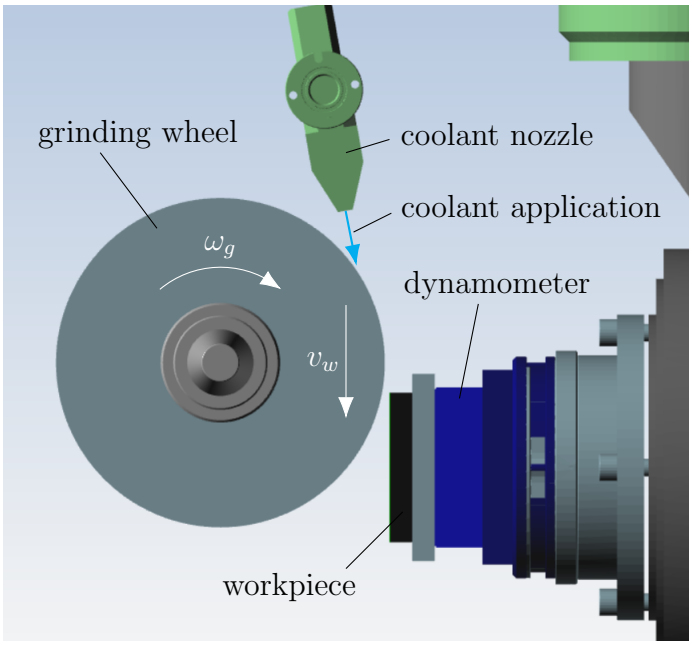

Figure 6.10: A schematic representation of the experimental setup (up-grinding configuration, the feed motion is performed by the grinding wheel)

feed velocity of the workpiece. This is shown in Figure 6.10, which presents a schematic drawing of the experimental setup and demonstrates how the test cuts were performed.

6.3 Tests for chatter frequencies

One of the most common ways to test a machine tool vibration model is to compare the theoretical chatter frequencies predicted by the model with experimental results, primarily because of the accuracy and simplicity of measuring vibration frequencies in practice. Therefore, the first line of argument for or against the validity of the new theory presented in Chapter 5 will be based on a comparison between predicted and measured chatter frequencies. This section summarises a number of machining experiments in an attempt to put the proposed grinding dynamics model to the test.

Three sets of experiments have been carried out and organised into the following three subsections. The first one presents a brief report on some initial grinding experiments that served the main purpose of generating detectable chatter in the first place. These tests proved to be informative yet unsuccessful in terms of identifying chatter frequencies in a reliable manner. The details of these experiments are summarised in Section 6.3.1. The other two sets of experiments described in Sections 6.3.2 and 6.3.3 were able to produce detectable chatter vibrations and thus yielded useful results. Due to the facts that chatter takes time to develop and the measurement range of the dynamometer is limited, it was necessary to perform interrupted grinding, i.e., to take multiple cuts or wheel passes. This opens up two possibilities with regard to machining: the workpiece surface can be ground with or without recutting the workpiece surface that was machined

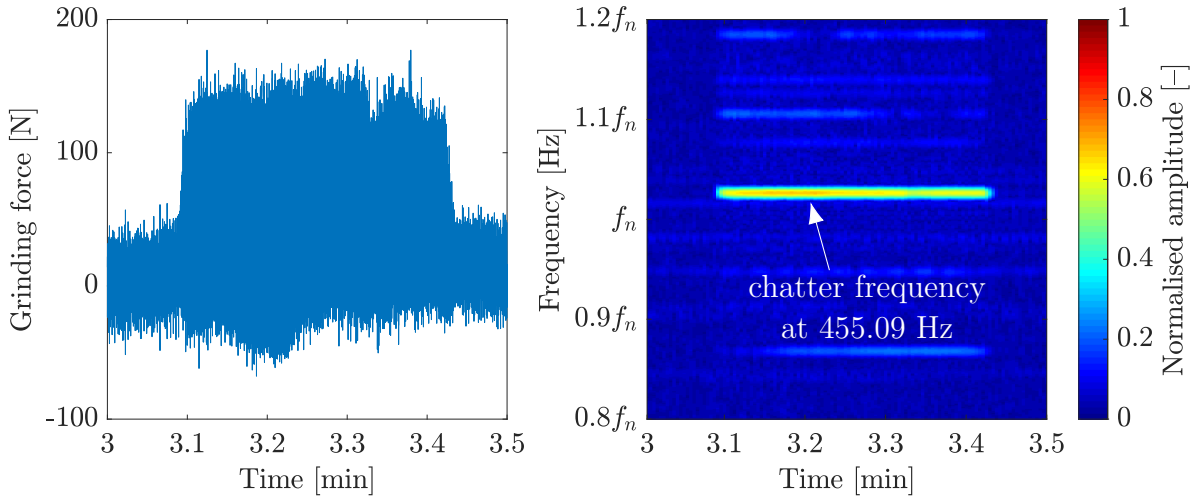

Figure 6.11: Time-domain (left) and spectrogram (right) representations of the grinding force corresponding to an unstable experiment (labelled as CFG-1 later on in this section), and the identification of the measured chatter frequency

during the previous wheel pass. Grinding with and without recutting the same workpiece surface will be referred to as regular surface grinding and creep-feed grinding, respectively. The term creep-feed grinding – being the name of an industrially recognised grinding process – indicates that not only is there a difference in cutting strategy and machining configuration, but the feed rates are lower and the depths of cut are higher as well compared to regular surface grinding. The following three subsections present these three sets of grinding experiments in detail.

However, before discussing the process of finding the most suitable methodology designed by the author to test the theoretical chatter frequencies, it is helpful to provide an example of an unstable experiment where the measured chatter frequency is clearly visible. Figure 6.11 is given for this purpose and shows the typical pattern of instability in a spectrogram. The spectrogram presents the evolution of the grinding force spectrum in time, where the third dimension is a colour map, corresponding to the normalised amplitude, which is defined relative to the zero-frequency component or average grinding force.

6.3.1 Brief report on unsuccessful experiments

The first set of experiments performed was meant to be an initial, rudimentary experiment, aiming to assess the most suitable methodology for generating and detecting chatter in surface grinding. In an attempt to accelerate the development of self-excited vibrations, Inconel 718 was chosen to be machined at a feed rate of 300 mm/min and at different depths of cut between 1 and 3 mm. Two wheel speeds were tested: 3000 and 4000 rpm. Considering the diameter of the grinding wheel (220 mm), the corresponding cutting speeds were 35 and 46 m/s, respectively. This workpiece material coupled with the above-mentioned choice of grinding parameters proved to be unsuccessful in producing and detecting chatter, because such a scenario was too aggressive for the grinding wheel

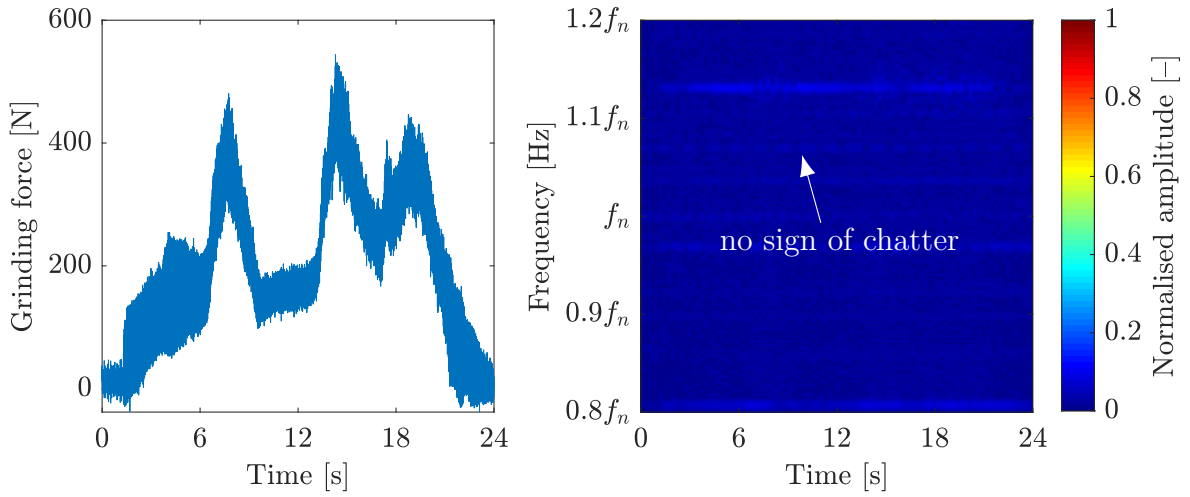

Figure 6.12: Time-domain (left) and spectrogram (right) representations of the grinding force over a single wheel pass ($\omega_g = 4000$ rpm, $\delta_0 = 3$ mm, $v_w = 300$ mm/min)

($Q'_w = 5 \ldots 15$ mm^2/s). As a result, the wheel was continually wearing, breaking down and self-sharpening at such a rapid rate that the wheel surface had no time to regenerate, and thus chatter development was stalled. It can be seen in the time-domain representation of the signal (presented in Figure 6.12) that the grinding force varies significantly even within a single wheel pass. It increases as the wheel wears, then decreases as the wheel breaks down and new cutting edges are exposed. This cycle repeats itself multiple times over a single wheel pass, disrupting the regenerative effect and thus preventing self-excited vibrations from developing. The spectrogram shows this clearly: there is no sign of chatter, even though it is expected to occur and exponentially grow in time around $1.07 f_n = 476$ Hz according to the proposed model. Although the applied grinding conditions did not produce chatter, which is beneficial from a practical point of view, the result is ultimately unfavourable, because the deterioration of the grinding wheel surface was neither controllable nor predictable during the process. In the end, these initial experiments – although unsuccessful in terms of generating and detecting chatter – proved to be informative and helpful in preparing the following set of experiments reported and discussed in Sections 6.3.2 and 6.3.3.

6.3.2 Regular surface grinding (RSG)

Building on the informative findings reported in Section 6.3.1, the second set of grinding experiments was performed using a different, more easily machinable workpiece material (Custom 465 instead of Inconel 718) and taking significantly lower depths of cut (from 0.01 to 0.03 mm instead of 1 to 3 mm), in order to create an environment that is less hostile to the grinding wheel. A higher feed rate of 5000 mm/min was chosen to ensure efficient grinding conditions, because if the material removal rate is too low, the so-called size effect causes the specific energy to become extremely large, and the dominant grinding mechanism will no longer be chip formation but ploughing [11]. In order to avoid such an unfavourable scenario, a high enough feed rate had to be chosen, so that even at low

depths of cut, the material removal rate may stay high enough for the size effect to remain negligible. The width of cut was kept constant at 5 mm (i.e. at one third of the entire wheel width) throughout the experiments in order to save workpiece material and reduce the grinding forces.

These grinding experiments were still exploratory, which means that the methodology presented in this section does not yet fit with an important assumption of the proposed theory. The chatter model developed and documented in this work assumes continuous grinding, where it is not possible to recut a workpiece surface that has already been ground. Yet the grinding experiments reported in this section were performed by recutting the same workpiece surface multiple times. Theoretically speaking, this particular setup allows for workpiece regeneration to occur, which the proposed model does not take into account. Being aware of this important difference, the second set of machining experiments – termed regular surface grinding (RSG) – takes another step forward in the pursuit of generating and detecting self-excited grinding vibrations in a controlled and repeatable fashion. Nevertheless, it is essential to keep in mind that the grinding setup described in this section does not exactly correspond with the theory to be tested, and therefore must be treated with caution when it comes to comparing its results with the model.

The test points of the RSG experiments are summarised in Table 6.5, where v_g is the circumferential speed of the wheel, δ_0 is the incremental depth of cut (the total depth of cut is 3 mm in all six cases), Q'_w is the specific material removal rate, $R_{g,\text{before}}$ and $R_{g,\text{after}}$ are the wheel radii before and after each experiment, ω_g is the rotational speed of the wheel, and G is the grinding ratio. In terms of theoretical stability, the grinding process is predicted to be unstable for every test point listed in Table 6.5. In fact, considering wheel speeds ranging from 500 to 5000 rpm and depths of cut ranging from 0 to 5 mm, no stable region can be found. That is why no stability diagram is presented here.

The rest of this section is divided into two parts: the first half considers the first case (i.e. RSG-1) in detail, while the second half summarises the main results of all six without repeating a meticulous analysis for each scenario.

Case identifier	v_g [m/s]	δ_0 [mm] × № of passes	Q'_w [mm^2/s]	$R_{g,\text{before}}$ [mm]	$R_{g,\text{after}}$ [mm]	ω_g [rpm]	G [–]
RSG-1	23	0.01 × 300	0.83	109.208	109.079	2011	3.391
RSG-2	34	0.01 × 300	0.83	106.264	106.148	3055	3.876
RSG-3	23	0.02 × 150	1.67	105.642	105.386	2079	1.768
RSG-4	34	0.02 × 150	1.67	108.109	107.865	3003	1.812
RSG-5	23	0.03 × 100	2.5	105.022	104.678	2091	1.324
RSG-6	34	0.03 × 100	2.5	106.881	106.561	3038	1.398

Table 6.5: Test cases corresponding to regular surface grinding discussed in Section 6.3.2

6.3.2.1 Results of RSG-1

The first RSG experiment was performed at a circumferential wheel speed of 23 m/s and an incremental depth of cut of 0.01 mm (further details corresponding to this experiment are given in Table 6.5). Since the total depth of material removed was 3 mm, this particular test case included 300 wheel passes. The evolution of the grinding force in time is presented in Figure 6.13, capturing $F_x(t)$ near the beginning and the end of the experiment. It can be seen that the grinding force significantly increases as a result of wheel wear: the maximum force between 2 and 3 minutes of grinding time is around 80 N, whereas between 15 and 16 minutes, it is about 120 N – one and a half times higher.

In order to investigate the evolution of the frequency content of the grinding force in time, the FFT of every 35th pass has been calculated and presented in Figure 6.14 in the form of a waterfall diagram (1 pass is equivalent to 100 mm of grinding length and 1.2 s of grinding time). Selecting every 35th pass has the advantage of covering almost the entire range of 300 passes with a sampling density that is both informative and clear. It can be observed that a single frequency is dominant among all the other peaks. The magnitude of this frequency component is not constant in time, but shows a significant variation as the grinding wheel wears and its topography changes. In order to gain more insight into the evolution of this frequency in time, Figure 6.15 is presented to see the variation of its magnitude on a much finer scale. Every recorded wheel pass has been considered in this diagram, except for those corresponding to either incomplete or inconsistent time signals. Such passes (namely 1, 97, 98, 198, 199, 200, 235 and 295) were counted as anomalies, unable to provide an accurate frequency peak that is representative of the grinding process at that particular point in time. Therefore, each data point corresponds to a single wheel pass, resulting in nearly 300 samples altogether, based on which the amplitude variation of the frequency component in question can be more accurately determined. Three features are especially noteworthy in Figure 6.15:

1. Up to about pass 175, the magnitude of the investigated frequency (i.e. 468.75 Hz according to Figure 6.14) exhibits an approximately exponential increase, which is indicative of the fact that the frequency component under consideration is the chatter frequency of the grinding process. This observation agrees well with Thompson's work on grinding chatter [106,107], who documented – both theoretically and experimentally – the presence of a single chatter frequency in surface grinding that is always higher than the system's uncoupled resonant frequency (in this case 443.34 Hz). The ratio of the chatter frequency to the natural frequency is $468.75/443.34 = 1.0573$, which is of the same order of magnitude as those recorded by Thompson in Table 2.1.

2. There is a clear decline in the magnitude of the chatter frequency after pass 175. This phenomenon is possibly caused by wheel self-sharpening. In other words, as the wheel wears and unstable lobes form around its circumference, the self-sharpening property of the grinding wheel can work against the progression of instability, slowing it down by exposing a new wheel surface in place of the old one. Since this is a possible explanation instead of a definite one, the declining side of the data is not investigated any further.

3. There are waves in the signal, disturbing the monotonic nature of both the increasing

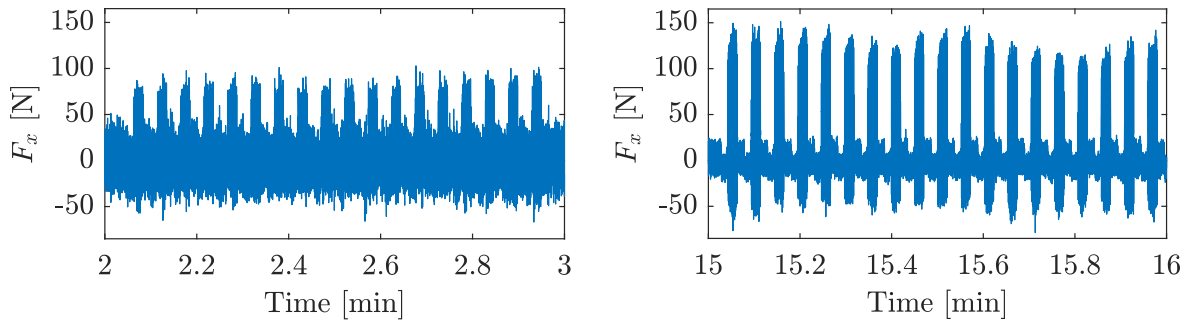

Figure 6.13: Grinding force near the beginning and the end of RSG-1

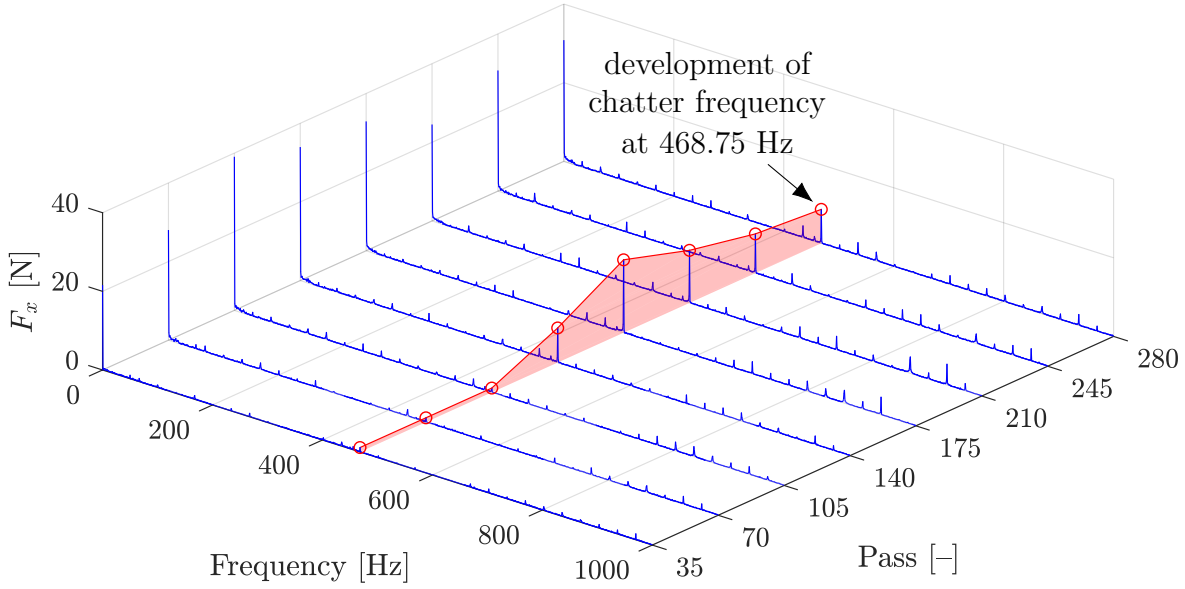

Figure 6.14: Evolution of the grinding force in the frequency domain for RSG-1

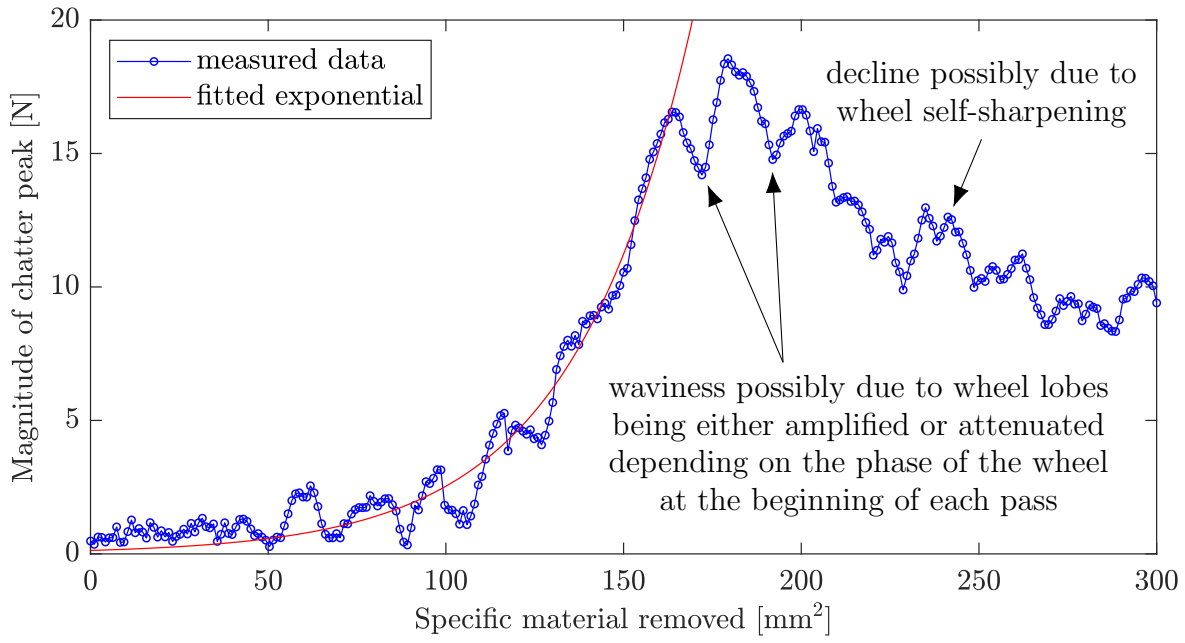

Figure 6.15: Variation in the magnitude of the chatter frequency component for RSG-1

and the declining sections of the recorded data. This is probably due to the fact that the phase of the grinding wheel was not identical at the beginning of each pass. As a result of such an irregularity in the process, the wheel lobes can be either amplified or attenuated, depending on the angular position of the grinding wheel at the moment of each wheel-workpiece engagement. Therefore, instability can be either accelerated or decelerated by taking multiple cuts instead of grinding continuously. Consequently, the rate at which the system loses its stability – as it is defined by the fitted exponential in Figure 6.15 – is only a rudimentary value influenced by a number of irregular wheel-workpiece engagements and therefore cannot be used to accurately determine the relative stability of the system.

6.3.2.2 Summary of RSG cases

Having discussed the results of RSG-1 in detail, the aim of this section is to summarise all six RSG cases listed in Table 6.5 with regard to the chatter frequency and its development in time. Figure 6.16 presents the magnitude of the chatter-frequency component as a function of the specific material removed for each RSG case, along with the magnitude of the zero-frequency component (which corresponds to the average grinding force) in order to provide a quantifiable measure of comparison to determine whether the chatter-frequency component is large enough for the grinding process under investigation to be characterised as unstable. The evolution of the chatter-frequency component is represented by a blue line, the variation of the zero-frequency component is indicated by a dotted line, and the exponential fitted to each chatter peak curve is plotted in red. Due to the fact that the total depth of cut is 3 mm in each case and one data point corresponds to one pass in Figure 6.16, the resolution of the chatter-frequency curves decreases as the incremental depth of cut increases (i.e. the total number of passes decreases). This is clearly visible in Figure 6.16: RSG-1 and RSG-2 have a significantly higher resolution than RSG-5 and RSG-6, with RSG-3 and RSG-4 situated halfway between them.

It can be seen that four cases out of six, namely RSG-1, RSG-2, RSG-4 and RSG-6, exhibit chatter development characteristics that are very clearly exponential in nature. In terms of the other two cases, RSG-3 and RSG-5, growth in chatter amplitude is unmistakable, however, the exponential nature of the growth is less obvious. There is an unusual jump in RSG-3 between two successive grinding passes, which is an anomalous phenomenon compared with the other cases, and it makes the fitted exponential a relatively coarse approximation of the increasing section of the chatter-frequency curve. In RSG-5, it is difficult to judge the extent of the supposedly exponential part of the chatter-frequency curve, which means that the quality of the fitted exponential – similarly to RSG-3 – is substandard with regard to the actual curve to which it is fitted. Nevertheless, it can be stated that the general trend of each chatter-frequency curve is very similar to that of RSG-1 discussed in detail in Section 6.3.2.1.

It is crucial to keep in mind that all RSG cases hold the potential for workpiece regeneration and thus workpiece-related instability, which cannot be taken into account by the proposed chatter model. Consequently, the RSG cases take a step further from the first set of grinding experiments described in Section 6.3.1, but they are still only part of the

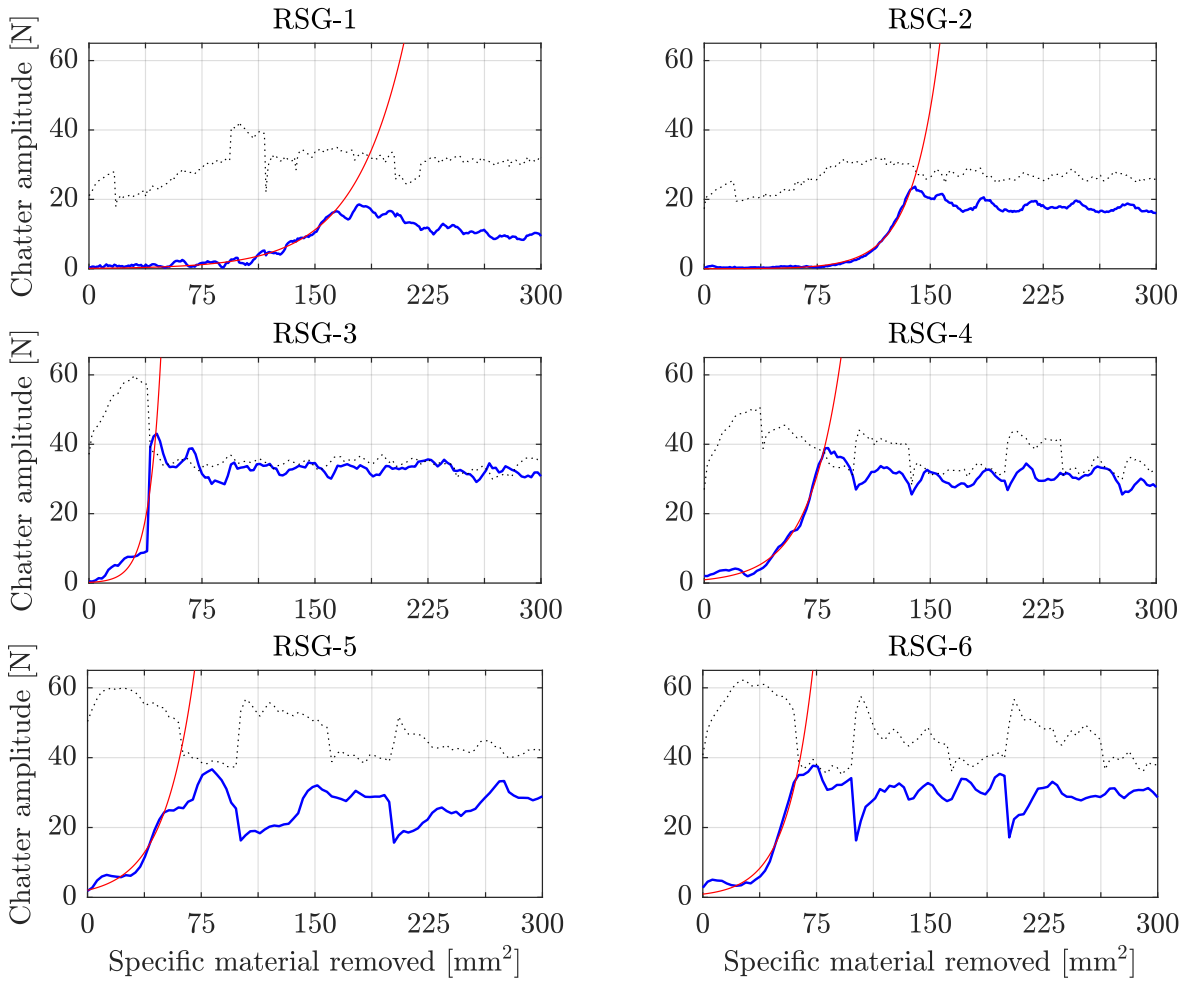

Figure 6.16: Variation in chatter amplitude for all RSG cases: ····· amplitude variation of the zero-frequency component, —— amplitude variation of the chatter-frequency component, —— exponential fitted to the chatter-frequency curve

process aiming to develop a suitable methodology for generating and detecting chatter in surface grinding. Therefore, the RSG cases presented in this section cannot yet provide a satisfactory point of comparison between theoretical and experimental results due to their inherent potential to be affected by workpiece regeneration. Nevertheless, the difference between the predicted and measured chatter frequencies is summarised in Table 6.6 for the sake of completeness. It can be seen that the differences between the theoretical and experimental chatter frequencies vary from rather small to relatively large.

Two cases stand out from the rest, namely RSG-1 and RSG-5, because the predicted chatter frequencies are not only further from the experimental values, but they also deviate in the negative direction. Furthermore, the theoretical chatter frequency in RSG-1 is almost exactly the natural frequency, while in RSG-5, it is clearly below the natural frequency. This kind of behaviour goes against fundamental and well-established regenerative chatter theory [25], and in fact against the proposed model itself (for small depths of cut, the chatter frequencies are expected to be higher than the natural frequency, according to Figure 5.16). The author suspects the following reason for this discrepancy. Figures 6.6c

Case identifier	Chatter frequency			Peak ratio [–]
	Theory [Hz]	Experiment [Hz]	Difference [%]	
RSG-1	443.66	468.75	−5.35	0.33
RSG-2	463.78	457.76	1.31	0.67
RSG-3	456.61	450.44	1.37	1.00
RSG-4	459.85	450.44	2.09	1.00
RSG-5	430.26	452.88	−4.99	0.75
RSG-6	464.20	455.32	1.95	0.75

Table 6.6: Comparison between theoretical and experimental chatter frequencies (RSG)

and 6.6d show that the combination of a relatively high feed rate and an extremely low grinding ratio produces a highly unstable grinding process. Consequently, the numerical simulations (such as those presented in Figure 5.20) corresponding to these highly unstable cases lose stability very quickly. As a matter of fact, MATLAB runs out of its numerical capacities and starts producing infinite results after 5 to 14 seconds of grinding time, depending on the actual RSG case considered. Therefore, it is possible that highly unstable processes combined with MATLAB's numerical limitations are responsible for the inaccurate chatter frequencies. Later findings (such as those reported in Table 6.8) seem to support this suspicion, as less unstable grinding simulations give theoretically admissible and experimentally expected frequency values. On the other hand, RSG-4 and RSG-6 are more unstable than RSG-1 (as far as the feed rate and the grinding ratio are concerned), yet these two scenarios provide relatively accurate theoretical predictions of the chatter frequency. As this is a counterexample to the explanation given above, the author remains unconvinced of the exact reason for the discrepancy regarding RSG-1 and RSG-5. Therefore, further study is warranted, but since this issue does not persist in the third and final experimental methodology (presented in Section 6.3.3), it is not investigated any further in this work.

Another important property of the chatter-frequency curve is the ratio of its steady-state magnitude (after the exponential trend is broken) to that of the zero-frequency component (i.e. the average grinding force), or equivalently, the steady-state value of the normalised amplitude (first introduced in Figure 6.11). Based on this quantity (termed as 'peak ratio' in Table 6.6), it is possible to assess the severity of instability in relation to the average grinding force. Although the author is aware of no established threshold of the peak ratio published in the literature separating stable and unstable processes, it gives a quantifiable measure of instability that can be used to judge the intensity of chatter in the grinding process. Also, if the peak ratio is 'small enough' (the in-depth analysis of which is outside the scope of this work), then the grinding process can be characterised as stable. For the purposes of this particular study, the measured peak ratios are assessed on a case by case basis for lack of a well-established standard. All six peak ratios listed in Table 6.6, ranging from 1/3 to 1, are considered by the author to be indicative of unstable grinding operations with different levels of chatter vibration.

In summary, the RSG cases serve as the next step after the first set of grinding experiments described in Section 6.3.1 to develop a suitable methodology for generating and detecting chatter in surface grinding. However, they are not yet satisfactory in terms of their capacity to provide an adequate point of comparison between theoretical and experimental findings. This is owing to the fact that the RSG experiments are inherently exposed to workpiece regeneration, which the proposed chatter model does not take into account. The following section presents the next and final step in the pursuit of a suitable experimental methodology that is able to eliminate workpiece regeneration from the grinding process.

6.3.3 Creep-feed grinding (CFG)

The elimination of the potential for workpiece regeneration from the grinding process can be achieved by machining the workpiece without recutting the same surface. This was carried out by preparing the workpiece in such a way that each pass can be done on a fresh, smooth surface. Due to the fact that only one third of the total wheel width was used for grinding in order to save more workpiece material and decrease the grinding forces, a number of steps were prepared on the workpiece to keep the passive or non-cutting section of the wheel width from interacting with any other part of the workpiece. This methodology provides a way to approximate the single-pass grinding scenario modelled by the proposed chatter theory even more accurately, as the potential for workpiece regeneration has been eliminated. The interrupted nature of the grinding process – which is the only main difference now remaining between the theoretical model and the experimental setup – has been shown to be inconsequential in terms of significantly suppressing wheel-related grinding chatter [108]. Therefore, this approach has been judged by the author as an adequate method to test the chatter frequencies predicted by the presented model.

Due to the fact that the number of steps that can be prepared on the workpiece is limited (leaving enough space for clamping and using 5 mm of the total wheel width, the maximum number of steps along the width of a $100 \times 50 \times 15$ mm block is eight), the depth of cut had to be increased in order to keep the total amount of workpiece material removed approximately the same as in regular surface grinding for the sake of consistency. Therefore, the depths of cut were increased from $0.01 \ldots 0.03$ mm to $0.25 \ldots 0.5$ mm. In order to remain consistent in terms of the specific material removal rate as well, the feed rate was reduced from 5000 mm/min to 300 mm/min.

Similarly to the structure of Section 6.3.2, the rest of this section is divided into two parts: the first one analyses one case in detail, and the second one summarises the results of all six grinding scenarios listed in Table 6.7. In terms of theoretical stability, no stable region can be found for the parameter domain $\omega_g = 500 \ldots 5000$ rpm and $\delta_0 = 0 \ldots 5$ mm.

Case identifier	v_g [m/s]	δ_0 [mm] × № of passes	Q'_w [mm^2/s]	$R_{g,\text{before}}$ [mm]	$R_{g,\text{after}}$ [mm]	ω_g [rpm]	G [–]
CFG-1	23	0.25 × 8	1.25	104.492	104.266	2102	1.349
CFG-2	34	0.25 × 8	1.25	103.770	103.669	3129	3.039
CFG-3	23	0.375 × 8	1.875	103.120	102.875	2130	1.892
CFG-4	34	0.375 × 8	1.875	102.476	102.325	3168	3.088
CFG-5	23	0.5 × 8	2.5	101.831	101.495	2157	1.864
CFG-6	34	0.5 × 8	2.5	101.180	100.949	3209	2.727

Table 6.7: Test cases corresponding to creep-feed grinding discussed in Section 6.3.3

6.3.3.1 Results of CFG-1

The first CFG experiment was carried out at a circumferential wheel speed of 23 m/s and an incremental depth of cut of 0.25 mm (further details regarding this experiment are provided in Table 6.7). As it was stated before, every CFG test case involved 8 wheel passes, therefore, the total depth of workpiece material removed in CFG-1 was 8×0.25 mm = 2 mm (1 pass is equivalent to 100 mm of grinding length and 20 s of grinding time). The evolution of the grinding force in time is presented in Figure 6.17, capturing $F_x(t)$ during the first two and last two passes of the grinding wheel. It can be seen that there is no significant increase in the magnitude of the grinding force as there was in regular surface grinding, however, it is noteworthy that the grinding force becomes more even with time.

In terms of the frequency content of the grinding force, two important features need to be mentioned with reference to regular surface grinding – one similarity and one difference. Figure 6.18 highlights the evolution of two dominant frequency components in the signal, where the first is larger than the second. Similarly to regular surface grinding, the larger frequency component exhibits an approximately exponential increase before it breaks off and settles, indicating that this frequency component is in fact the chatter frequency of the system under the specified grinding conditions. A higher-resolution graph of the chatter peak variation is presented in Figure 6.19 in order to further justify this conclusion. However, with regard to the frequency content of the grinding force, there is a significant difference between the results corresponding to creep-feed grinding and regular surface grinding. In Figure 6.18, another frequency component arises at exactly two times the chatter frequency. This is the second harmonic of the chatter frequency, which was present in some of the RSG cases as well, although it certainly was not as dominant there as it is here in creep-feed grinding. Observing harmonics of the chatter frequency as instability grows is not a novel discovery, however, according to Li and Shin, it is a phenomenon that was unexplained in grinding prior to their new wheel regenerative chatter theory [108].

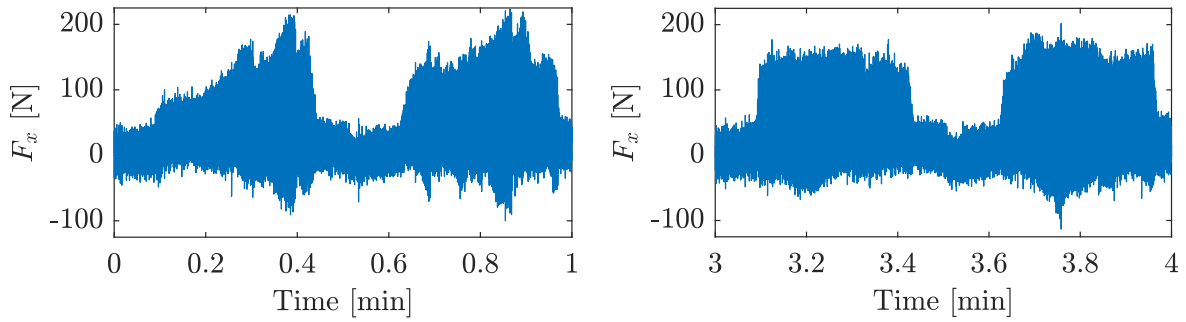

Figure 6.17: Grinding force during the first two and last two wheel passes in CFG-1

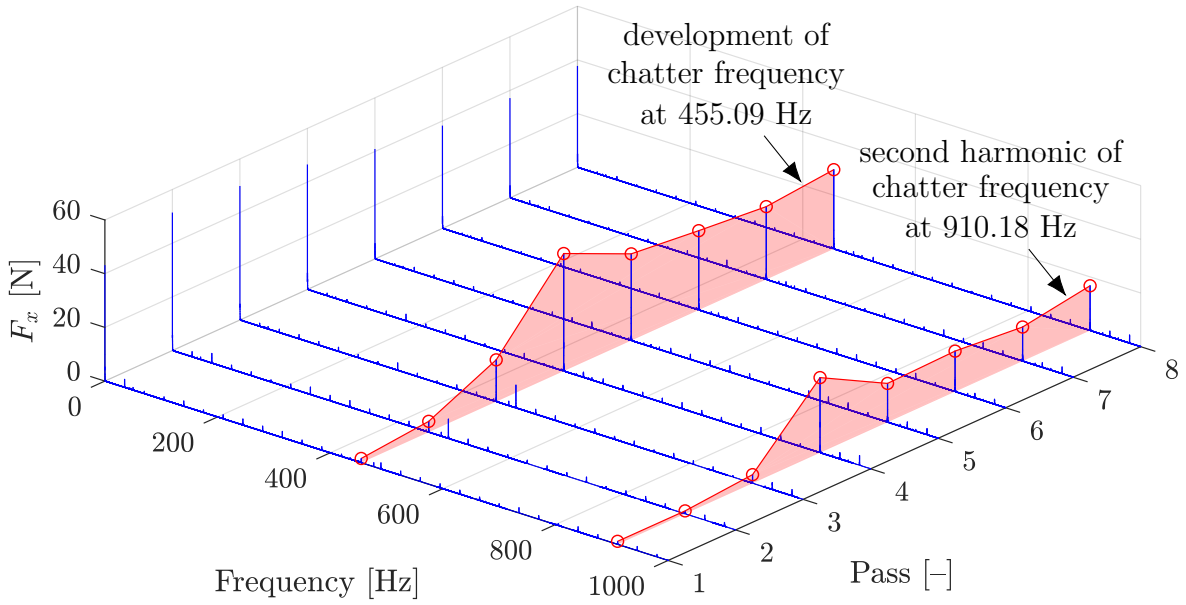

Figure 6.18: Evolution of the grinding force in the frequency domain for CFG-1

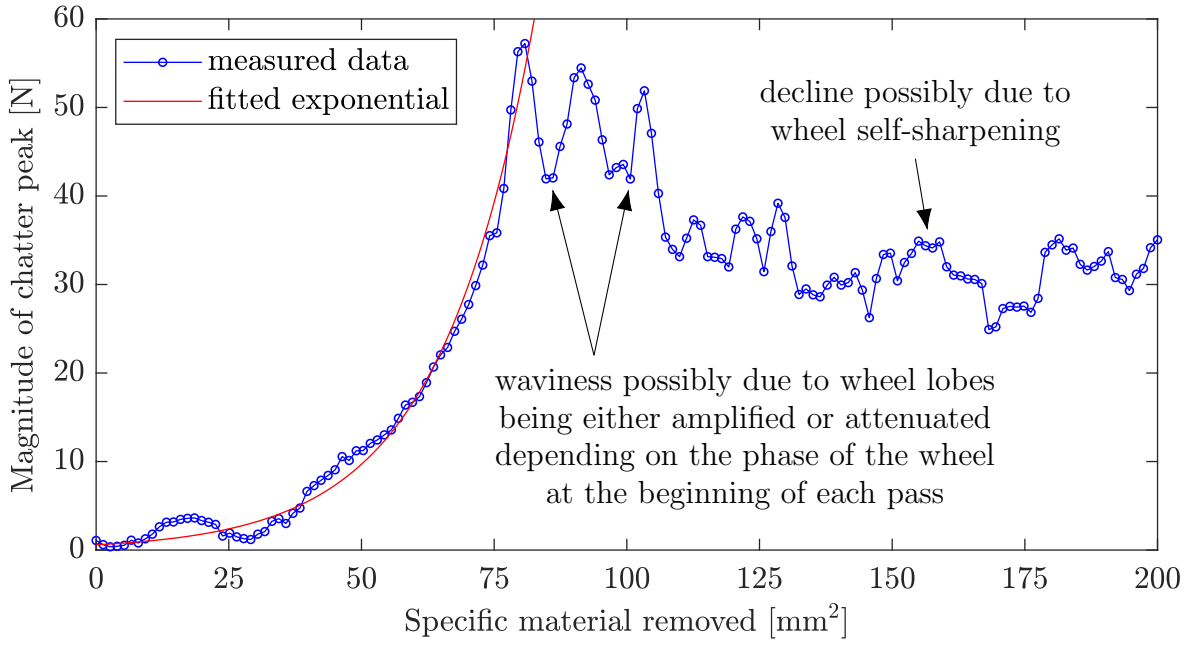

Figure 6.19: Variation in the magnitude of the chatter frequency component for CFG-1

The three observations discussed in Section 6.3.2.1 regarding the evolution of the chatter peak hold true for creep-feed grinding as well, therefore, they are not repeated in this section.

6.3.3.2 Summary of CFG cases

Similarly to the RSG cases, Figure 6.20 shows the magnitude of the chatter-frequency component along with the magnitude of the zero-frequency component (or the average grinding force) as a function of the specific material removed for each CFG scenario. However, unlike in the case of regular surface grinding, the resolution of the chatter-frequency curves remains the same for each depth of cut due to the fact that one data point always corresponds to one second of grinding time. The vertical grid lines are drawn in such a way that they separate individual wheel passes, therefore, the horizontal axis is divided into eight sections in each case.

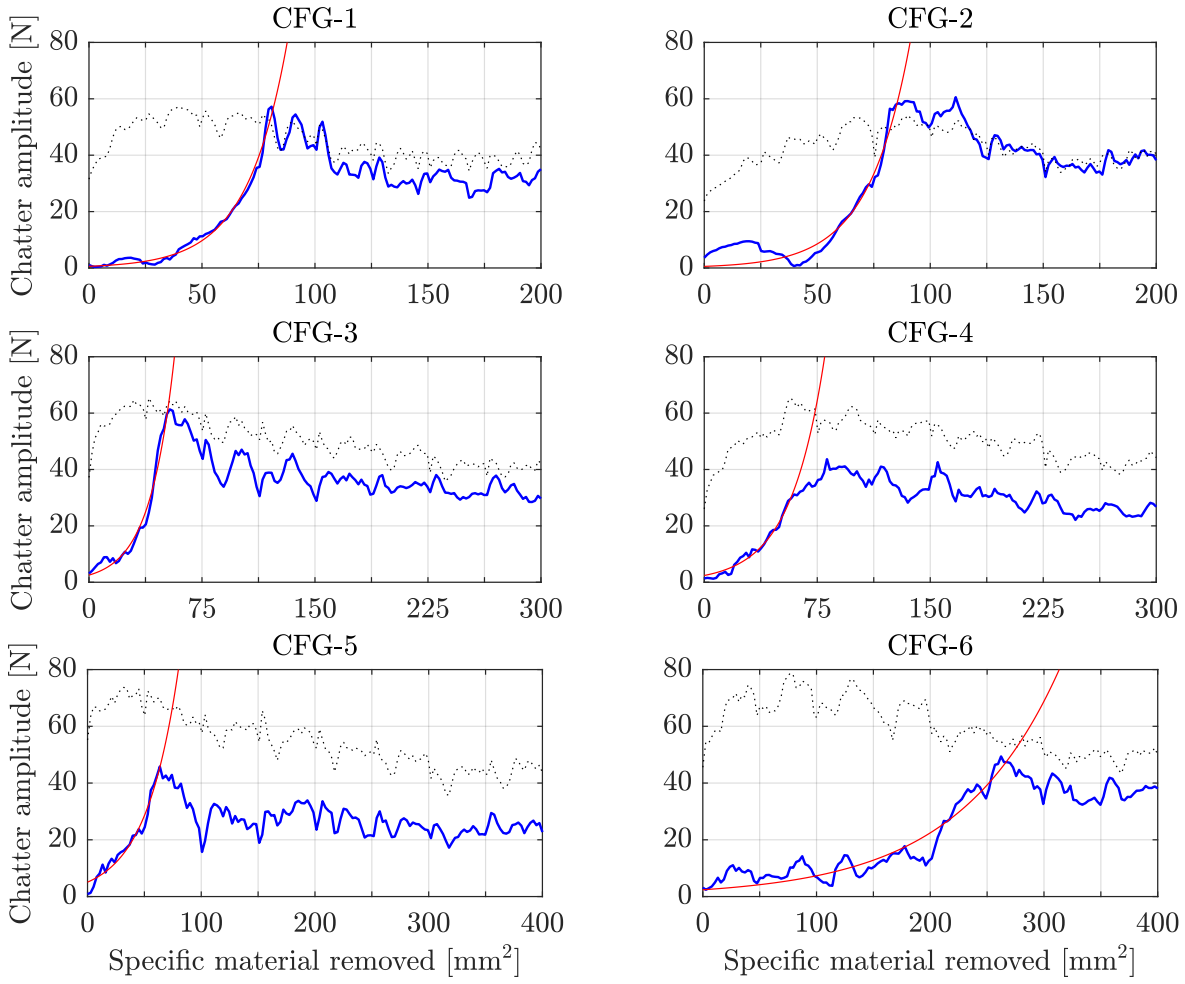

Figure 6.20: Variation in chatter amplitude for all CFG cases: ····· amplitude variation of the zero-frequency component, —— amplitude variation of the chatter-frequency component, —— exponential fitted to the chatter-frequency curve

It can be seen in Figure 6.20 that the magnitude of the chatter-frequency component is significant in each grinding scenario, indicating the presence of unstable vibrations. Theoretically speaking, the growth of these unstable vibrations is expected to be exponential in nature, and this is in fact clearly visible in all cases, although one experiment seems to lack the same degree of clarity that the others have. The last scenario, namely CFG-6, appears to be an anomaly compared with the other cases, as chatter – although certainly present – not only takes a significantly longer time to manifest but also develops after a series of variations in its amplitude, which is an unusual phenomenon in light of the other five cases. This waviness is probably owing to the same effect as that noted in Figures 6.15 and 6.19, namely that wheel lobes (i.e. specific energy waves) can be either amplified or attenuated depending on the phase of the grinding wheel at the beginning of each pass. Therefore, since instability took such a long time to set off, it is possible that the phase of the wheel during the first three or four passes was such that chatter development was hindered rather than facilitated by the interrupted nature of the grinding process. However, it works somewhat against this line of reasoning that the changes in chatter amplitude occur not only at the beginning of passes but during grinding as well. Nevertheless, the exponential increase in the chatter-frequency component is visible in CFG-6 as well, but it is less clear and less smooth than in the other cases.

It is important to note that (apart from CFG-6) the rate at which visible instability developed is quite similar in each case in terms of how much workpiece material had to be removed for chatter to become clear. This was not the case in regular surface grinding, where the differences were more significant between the first two and the last four sets of grinding experiments.

It is also important to remember that, unlike in the RSG cases, the potential for workpiece regeneration and workpiece-related instability has been eliminated from the CFG setup. Therefore, the chatter frequencies corresponding to the CFG scenarios (listed in Table 6.8) are more reliable when it comes to testing the proposed chatter model than those belonging to regular surface grinding. It can be seen that the differences between the predicted and measured chatter frequencies are around 1%, which is strong evidence for the validity of the presented theory. Also, there are no anomalies this time, every CFG case follows the same pattern, namely a small difference between the theoretical and experimental results with the predicted chatter frequencies being slightly higher than the measured ones.

The peak ratios (discussed in Section 6.3.2.2 and defined as the ratio between the steady-state magnitudes of the chatter- and zero-frequency components) are similar to those corresponding to regular surface grinding, therefore, the author considers them indicative of unstable grinding operations again with different levels of self-excited vibration.

In summary, it can be concluded that the grinding chatter theory developed in Chapter 5 is supported by the experimental chatter frequencies reported in this section. Therefore, in terms of the predicted chatter frequencies, the presented model is both accurate and reliable.

Case identifier	Chatter frequency			Peak ratio [–]
	Theory [Hz]	Experiment [Hz]	Difference [%]	
CFG-1	460.07	455.09	1.09	0.75
CFG-2	470.75	468.90	0.39	1.00
CFG-3	465.95	460.82	1.11	0.75
CFG-4	476.88	474.55	0.49	0.60
CFG-5	472.17	466.54	1.21	0.53
CFG-6	483.48	480.73	0.57	0.75

Table 6.8: Comparison between theoretical and experimental chatter frequencies (CFG)

6.4 Tests for stability boundaries

Another widespread method for testing the validity of a chatter model is to compare the stability boundaries predicted by the model with experimental results. Therefore, this will be the second line of argument for or against the reliability of the proposed chatter theory. The concept of the peak ratio will be critical here, as it will be the primary way of quantifying the difference between stability and instability. Although, as it was mentioned before, the author is aware of no peak-ratio-based theory published in the literature that establishes a clear and well-founded difference between stable and unstable grinding operations, differentiating between the two is typically fairly straightforward.

As it was stated in Section 6.3, the peak ratio is the steady-state value of the normalised chatter amplitude, which is the ratio between the chatter- and zero-frequency components of the grinding force spectrum. While in the previous section the stability analysis was based on tracking the magnitudes of these two frequency components in time, this section introduces a change in illustration methodology. Instead of looking at only two frequency components of the grinding force spectrum, all frequencies are going to be presented in a predetermined vicinity of the natural frequency, where the chatter frequency is expected to show up if the process is unstable. The magnitude of each frequency component will be normalised by the average grinding force, resulting in the normalised amplitude mentioned earlier. All of these frequencies will be plotted in time, producing a spectrogram such as that in Figure 6.11. This change in illustration methodology is introduced for the following reasons: (1) the spectrogram is more general than the previous approach, because a wide range of frequencies are visible (and thus available for inspection) at the same time instead of just a few components, (2) the spectrogram can be quickly generated and easily automated, whereas the first methodology proved to be slow and cumbersome, which is far from ideal, especially when it comes to assessing the stability properties of several grinding experiments on the spot, and (3) it is faster and easier not only to create a spectrogram but also to draw conclusions from it by simple visual inspection. Therefore, once the analyst understands and recognises the spectral signs of grinding chatter, the spectrogram is a more practical tool for stability analysis

than looking at individual frequency components separately. In terms of the waterfall diagrams, such as those presented in Figures 6.14 and 6.18, the spectrogram is simply a two-dimensional representation of the same information, where the third dimension has been replaced by a colour map. One disadvantage of the spectrogram is that the trend of chatter development is not as clearly visible as in the case of the waterfall diagram. Overall, however, the arguments in favour of the spectrogram outweigh those against it. For this reason, the author will predominantly use spectrograms for data analysis throughout the rest of this chapter.

This section is divided into two parts: the first half presents a brief report on some unsuccessful experiments, while the second half summarises a number of grinding experiments set up in a CFG configuration. Regular surface grinding experiments (as defined in Section 6.3.2) were not performed in this case, since creep-feed grinding has already been established in Section 6.3.3 as the more capable approach when it comes to testing the presented chatter theory.

6.4.1 Brief report on unsuccessful experiments

Shifting the focus from the chatter frequencies to the stability boundaries, a new experimental methodology was employed as well, primarily as an attempt to save more workpiece material. Instead of preparing eight steps on the workpiece as before, which does indeed waste a significant amount of workpiece material, the following experimental strategy was implemented by the author: besides the test wheel, a so-called cleaning wheel was used as well with the sole purpose of cleaning the workpiece surface after every pass of the test wheel in order to remove any potential waves from the workpiece surface and thus eliminate the possibility of workpiece regeneration. Using this approach, the workpiece required no meticulous preparation whatsoever, and the whole experiment was much simpler as a result. Due to the fact that a different parameter domain was necessary to test the predicted stability boundaries (i.e. different from the one used for testing the chatter frequencies), the depth of cut had to be increased to $0.75 \ldots 1.75$ mm. Therefore, in order to keep the specific material removal rate consistent with the previous experiments, the feed rate was reduced to 100 mm/min.

Figure 6.21 shows eight pairs of grinding parameters (wheel speeds and depths of cut) that were tested for stability. It is important to note that, as it was concluded in Section 6.2.2 and presented in Figure 6.7b, the stability boundaries are very sensitive to low values of the grinding ratio. This observation is confirmed again in Figure 6.21, which presents two sets of stability boundaries corresponding to the minimum and maximum values of the grinding ratio (0.986 and 3.857) measured for the eight experiments under discussion. As it is clearly visible, the stable and unstable regions can vary significantly depending on the actual value of the grinding ratio. Therefore, in order to accurately compare the theoretical and practical results, each experiment would have to be marked in a slightly different stability diagram defined by the specific grinding ratio corresponding to that experiment. However, since the main point of this particular section (i.e. why these experiments were unsuccessful) can be articulated without such a detailed analysis, the presentation of the results in Figure 6.21 is not refined any further. Nevertheless, it is

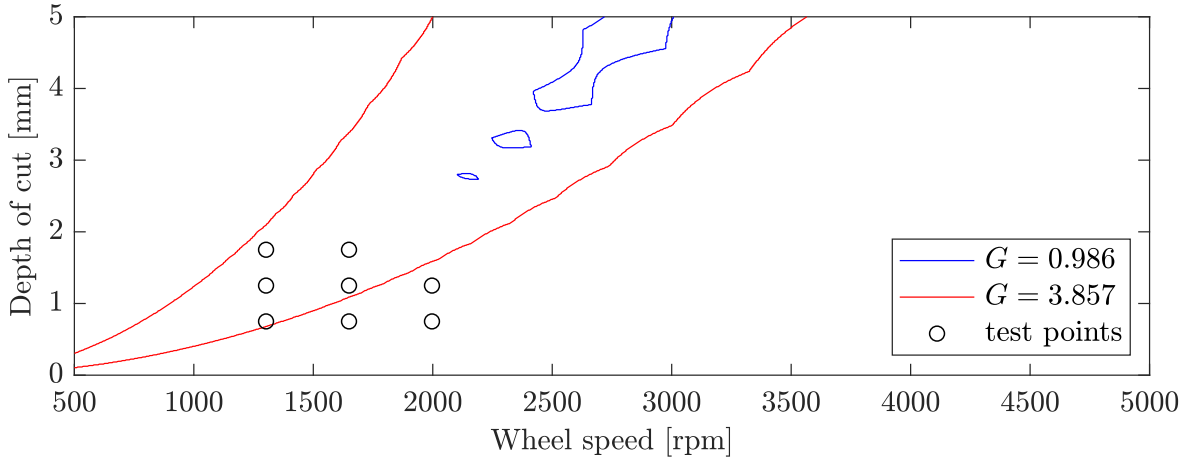

Figure 6.21: Theoretical stability boundaries and experimental test points for $R_g = 110$ mm and $v_w = 100$ mm/min

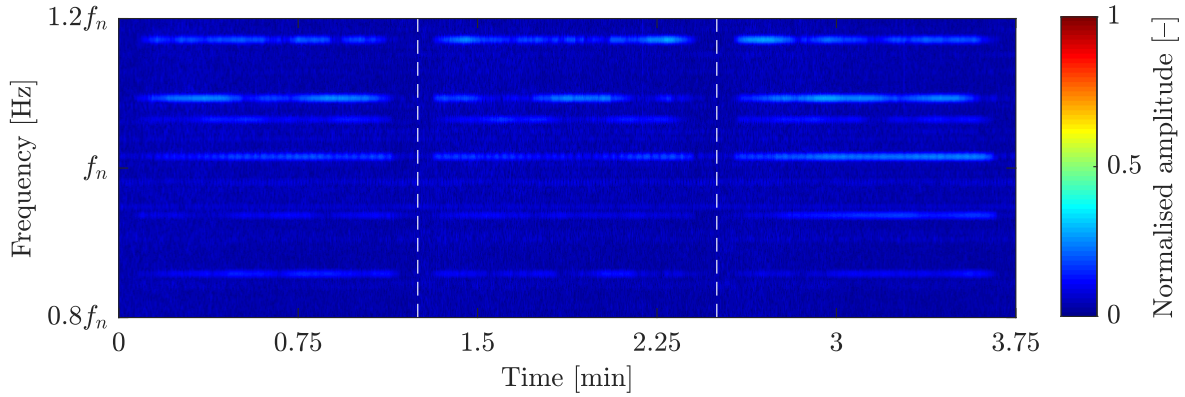

Figure 6.22: Evolution of the grinding force in the frequency domain for $v_g = 23$ m/s and $\delta_0 = 0.75$ mm – the three wheel passes are separated by dashed lines

undoubtedly clear that unstable scenarios are always expected, only the number of them can vary with the grinding ratio.

However, every experiment carried out using this new methodology produced stable results – even those that were predicted to be unstable by the chatter model under scrutiny. That is to say, the magnitude of the chatter-frequency component was insignificant in each case (e.g. Figure 6.22). It can be seen that none of the peaks around the expected location of the chatter frequency is large enough to indicate instability.

As this was a highly unexpected set of results, the author became suspicious of the new methodology employed. Removing and reclamping the test wheel before each pass (in order to use the cleaning wheel) turned out to have an adverse effect on the development of chatter. That is probably due to the fact that removing and reclamping the test wheel slightly changes the dynamics of the system between individual passes, which can be strong enough a disturbance that it is capable of breaking up the process of chatter development. Disturbing the regenerative effect is in fact a well-known method for suppressing chatter in machining [25, 86], however, the way it was achieved in this particular

case (i.e. stopping and restarting the machine after every pass) is obviously not a feasible approach to ensuring stable grinding operation. This explanation seems to be confirmed by the fact that repeating some of these experiments with recutting the same workpiece surface multiple times (just as in Section 6.3.2) produced unstable results. Nevertheless, this set of unsuccessful experiments served the purpose of narrowing down the experimental methodologies capable of generating and detecting chatter. Consequently, the author reverted to the previous approach described in Section 6.3.3, despite the fact that it took more time and cost more material to prepare the workpiece.

6.4.2 Creep-feed grinding (CFG)

This section presents and analyses a number of creep-feed grinding experiments performed using the methodology described in Section 6.3.3, which was tested and proved to be adequate for capturing wheel-related chatter in surface grinding. However, when it comes to selecting the initial test points, the flow of this investigation follows on from the unsuccessful experiments reported in Section 6.4.1, and builds on the data obtained there. Having measured the grinding forces corresponding to several other CFG cases as well, a thorough data analysis is performed in order to test the stability boundaries predicted by the proposed model. Finally, the results are summarised and presented at the end of the section.

6.4.2.1 New grinding wheel

Due to some expected yet unfavourable limitations with regard to both equipment and time, the author was unable to continue using the exact same type of grinding wheel as before, i.e., the one identified as GW-1 in Table 6.1. Two very similar grinding wheels were available to mitigate this issue, whose physical properties are listed in Table 6.9. The thicker wheel identified as GW-3 is approximately 37% heavier than GW-1, therefore, employing this wheel would inherently change the modal parameters of the structure. However, considering the modal characteristics of the system corresponding to GW-1 and GW-2 (discussed in Section 6.1) and the sensitivity of the stability boundaries to the natural frequency (presented in Section 6.2.2), it can be concluded that the difference between GW-1 and GW-3 in terms of their respective modal parameters is negligible as far as this study is concerned. The grinding wheel identified as GW-4 has the same thickness as GW-1, however, it uses slightly finer grains of the same shape (80/80 instead of 60/80,

Wheel identifier	Outer ⌀ [mm]	Inner ⌀ [mm]	Width [mm]	Grit number	Mass [kg]
GW-3	220	32	20	60/80	1.159
GW-4	220	32	15	80/80	0.835

Table 6.9: Physical properties of two additional 3M™ Cubitron™ II grinding wheels

which indicates a smaller and more consistent grain size). Practically speaking, either of these two new wheels is adequate to replace GW-1. Nevertheless, based on the fact that employing GW-3 would slightly alter the modal characteristics of the system, ideally calling for the modal analysis to be repeated, and that the grain size is a changeable parameter in the proposed model, the author decided to use GW-4 for the rest of his experiments.

6.4.2.2 Initial test points

Keeping in mind that even a small change in a low grinding ratio has the potential to significantly alter the predicted stability boundaries, the first challenge was to make sure that theoretically stable grinding scenarios can be realised in practice. The reason this is not a straightforward task is that the grinding ratio is – to some degree at least – an uncontrolled parameter in the experiments. That is to say, performing the same experiment over and over again can give different grinding ratios, and consequently, different stability boundaries as well. Therefore, considering the manner in which decreasing the grinding

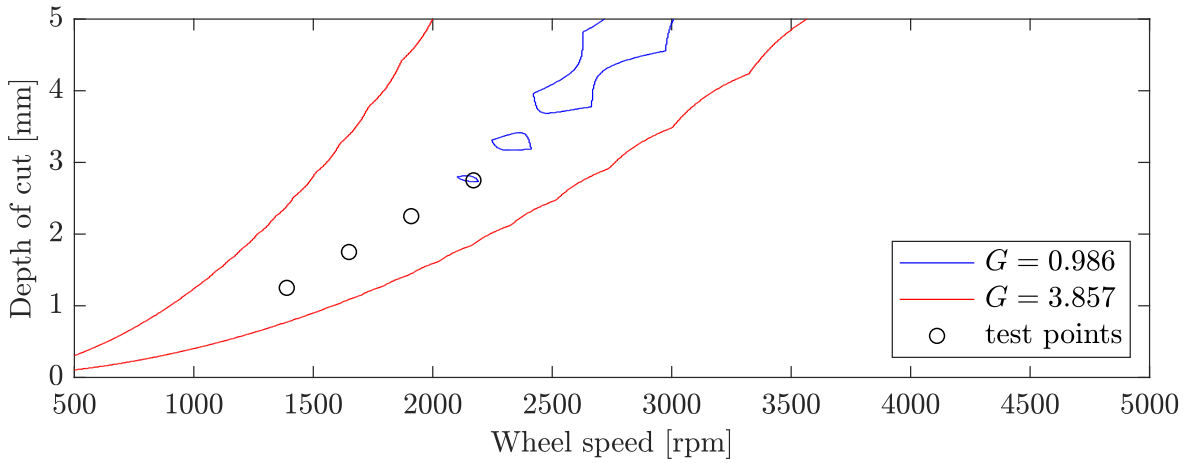

Figure 6.23: Initial test points selected to be theoretically stable

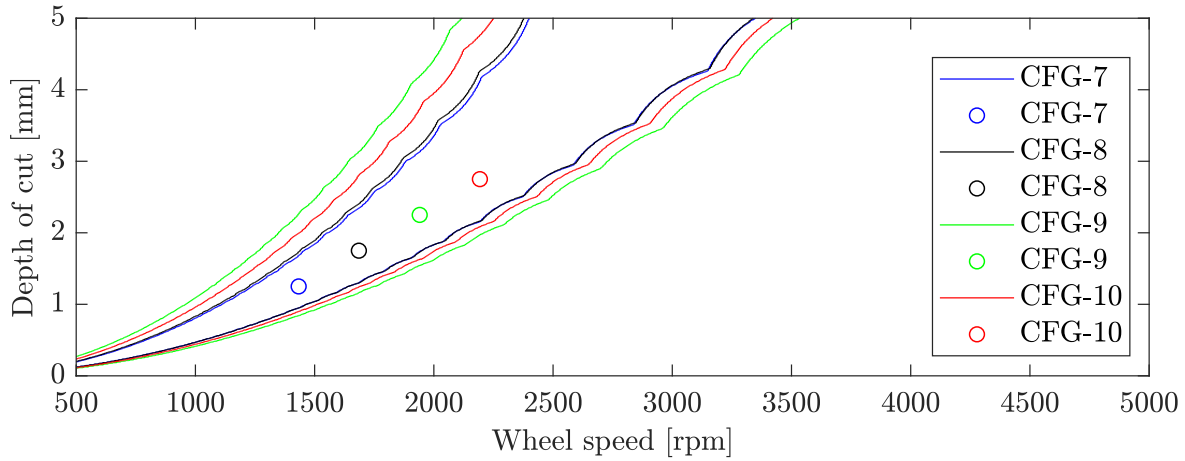

Figure 6.24: Initial test points confirmed to be theoretically stable

ratio reduces stability according to Figure 6.23, four test points were selected that are most likely to be stable (i.e. to remain stable for the longest as the G-ratio decreases), based on the stability boundaries calculated previously in Section 6.4.1. Since each test point corresponds to a different wheel radius and grinding ratio in reality, the predicted stability boundaries will be different in each case. For the sake of accuracy, this difference is taken into account in each scenario. Therefore, after performing the experiments corresponding to these four test points, measuring the wheel radii and calculating the grinding ratios, the actual stability boundaries were predicted. They are summarised in Figure 6.24, along with the test points themselves in matching colours. It can be seen that all four grinding processes are predicted to be stable, therefore, the first obstacle has been overcome: a number of practical grinding configurations have been identified that are expected to be stable according to the theoretical model.

6.4.2.3 Data analysis

The details of 20 more surface grinding experiments are listed in Table 6.10. Additionally, the stability properties of all 30 creep-feed grinding experiments are summarised in Figure 6.25 along with three sets of theoretical stability boundaries. Due to the fact that every experiment corresponds to a unique set of stability boundaries (since the wheel radius and the grinding ratio will be different in each case), it would be impractical to show every experiment in its own stability diagram. Nevertheless, it is useful to see the results of all creep-feed grinding experiments in a single figure, therefore, the wheel radius and the grinding ratio corresponding to the three sets of theoretical stability boundaries presented in Figure 6.25 have been chosen as follows. The wheel radius was set to 105 mm, which is the mean between the initial 110 mm and the minimum 100 mm (Section 6.2.2 provides more details on how the minimum wheel radius was determined). Since the stability

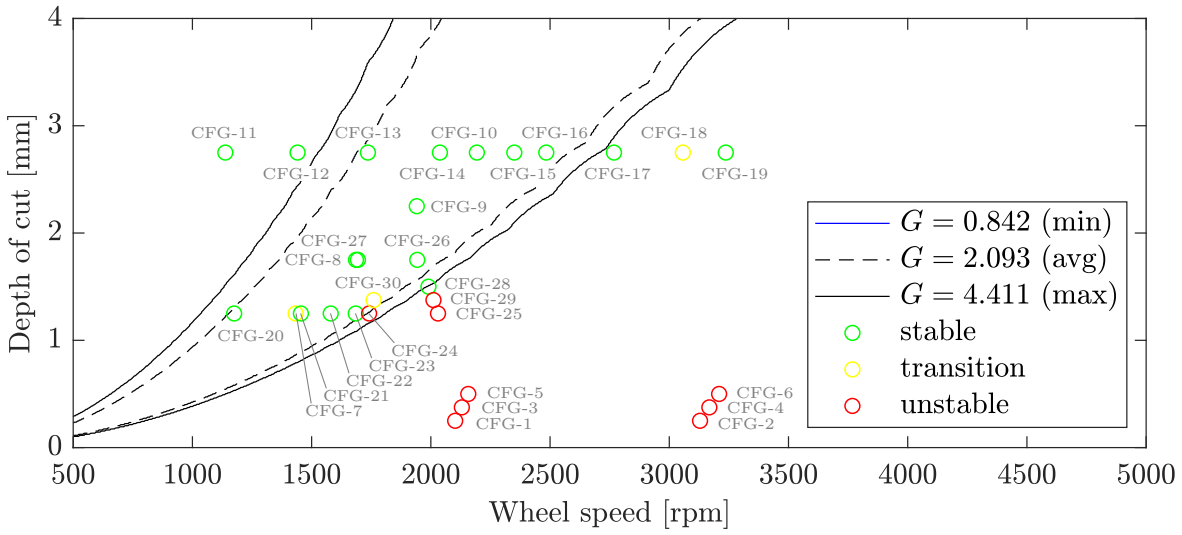

Figure 6.25: Theoretical (lines) and experimental (circles) stability properties of all creep-feed grinding tests (no stability boundary is visible for $G = 0.842$, because the entire parameter region presented above is unstable for this grinding ratio)

Case identifier	v_g [m/s]	δ_0 [mm] × № of passes	Q'_w [mm^2/s]	$R_{g,\text{before}}$ [mm]	$R_{g,\text{after}}$ [mm]	ω_g [rpm]	G [–]
CFG-7	16	1.25 × 3	2.08	106.622	106.260	1433	1.549
CFG-8	19	1.75 × 2	2.92	107.645	107.316	1686	1.575
CFG-9	22	2.25 × 1	3.75	108.251	108.134	1941	2.829
CFG-10	25	2.75 × 1	4.58	108.855	108.651	2193	1.973
CFG-11	13	2.75 × 2	4.58	109.046	108.088	1138	0.842
CFG-12	16	2.75 × 2	4.58	105.999	105.192	1441	1.027
CFG-13	19	2.75 × 2	4.58	104.537	103.786	1736	1.119
CFG-14	22	2.75 × 2	4.58	103.069	102.545	2038	1.625
CFG-15	25	2.75 × 2	4.58	101.584	101.089	2350	1.745
CFG-16	28	2.75 × 2	4.58	107.642	107.314	2484	2.483
CFG-17	31	2.75 × 2	4.58	106.930	106.653	2768	2.959
CFG-18	34	2.75 × 2	4.58	106.206	106.019	3057	4.411
CFG-19	37	2.75 × 2	4.58	109.164	108.962	3237	3.973
CFG-20	13	1.25 × 4	2.08	105.687	105.180	1175	1.489
CFG-21	16	1.25 × 4	2.08	105.020	104.468	1455	1.376
CFG-22	17	1.25 × 4	2.08	102.744	102.276	1580	1.659
CFG-23	18	1.25 × 4	2.08	102.001	101.574	1685	1.831
CFG-24	19	1.25 × 4	2.08	104.228	103.830	1741	1.922
CFG-25	22	1.25 × 4	2.08	103.492	103.121	2030	2.076
CFG-26	22	1.75 × 3	2.92	108.137	107.774	1943	2.132
CFG-27	19	1.75 × 3	2.92	107.130	106.620	1694	1.533
CFG-28	22	1.5 × 4	2.50	105.586	105.160	1990	2.127
CFG-29	22	1.375 × 4	2.29	104.443	104.081	2011	2.319
CFG-30	19	1.375 × 4	2.29	103.069	102.690	1760	2.245

Table 6.10: Additional creep-feed grinding tests (the first six are listed in Table 6.7)

boundaries do not vary significantly between $R_g = 110$ and 100 mm, the average of these two extreme values is able to represent the wheel radius during each experiment relatively accurately. The grinding ratio was set to three different values (hence the three sets of stability boundaries): the overall minimum and maximum (0.842 and 4.411), and the

average of all 30 creep-feed grinding experiments, which is 2.093. Presenting the results in this way provides an opportunity to see the stability properties of all 30 experiments in a single diagram without losing many of the details that characterise each experiment. Figure 6.25 shows the stability of each grinding experiment by a circle in colour. Stable and unstable processes are marked by green and red circles, respectively. However, there were some instances where it was ambiguous to decide whether the process was stable or unstable. In fact, these cases appeared to be marginally stable, transitioning from one state to the other, and are indicated by yellow circles in Figure 6.25. Before moving on to discussing the results in detail, three spectrograms are presented in Figure 6.26, corresponding to stable, transitional and unstable processes, in order to demonstrate how the stability of each experiment was assessed based on an inspection of the spectrogram.

It can be seen that CFG-23 is a stable grinding process throughout all four wheel passes, showing no sign of chatter in the presented time interval. The experiment identified as CFG-30 exhibits some transitional characteristics. Chatter seems to be developing, but the process is very slow – by the fourth wheel pass, the normalised amplitude is still moderate around the natural frequency. Experiment CFG-24 is clearly unstable. The rate at which instability occurs is significantly faster than in the case of CFG-30. The transition occurs during the third pass, and chatter is fully developed by the fourth. These experimental observations put two important aspects of grinding stability into focus. First, transitional behaviour suggests that the grinding parameters under investigation correspond to an unstable process that is very close to the stability boundary. That is why it appears to be stable for a long period of time. This inference prompts the question whether the processes tested and found to be stable are truly stable or they would eventually become unstable, provided that the experiments are run long enough. This is a valid point and will be discussed in Chapter 7. Second, instability happens at different rates depending on where the grinding process is located relative to the stability boundary. In order to investigate this idea of relative instability even further, and test its validity against experimental data, the spectrograms of three unstable processes situated at different distances from the stability boundary are presented in Figure 6.27 for closer examination.

It is clear that the phenomenon of relative instability is supported by the experiments. The test point located closest to the theoretical stability boundary (CFG-24, the one discussed earlier) begins its transition during the third pass, the second closest (CFG-29) between the first and second passes, and the test point that is farthest from the stability boundary (CFG-25) starts transitioning right at the beginning, during the first pass. This is a strong indication that a practical stability boundary exists away from CFG-25 in the directions of CFG-24 and CFG-29 – exactly the direction in which the theoretical stability boundary was predicted by the proposed chatter model. More details concerning the experimental results summarised in Figure 6.25 are now discussed in Section 6.4.2.4.

6.4.2.4 Results

Apart from the six unstable experiments discussed in detail in Section 6.3.3, two main conclusions can be drawn from Figure 6.25, corresponding to two groups of test points:

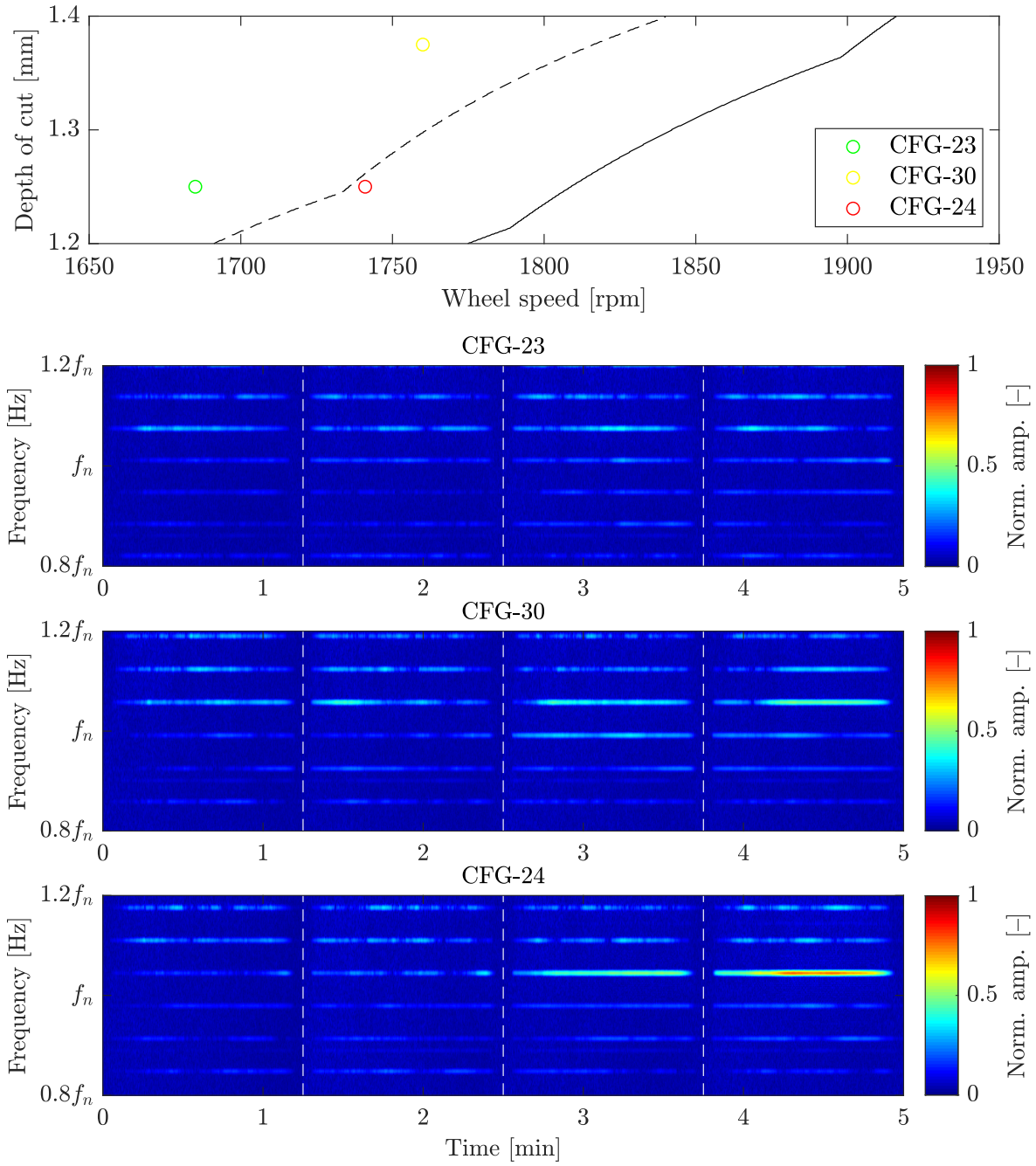

Figure 6.26: Stable, transitional and unstable grinding processes and their corresponding spectrograms – the four wheel passes are separated by dashed lines

those located between $\delta_0 = 1$ and 2 mm, and those at $\delta_0 = 2.75$ mm.

As it was stated in Section 6.4.2.3, the cluster of experimental data points in Figure 6.25 located between $\delta_0 = 1$ and 2 mm clearly indicate the existence of a practical stability boundary. Although it is important to keep in mind that the presented stability boundaries correspond to the average and maximum G-ratios of all creep-feed grinding tests performed, the evidence for a practical stability boundary is obvious, even if it does not coincide exactly with the theoretical predictions. The transition between stable

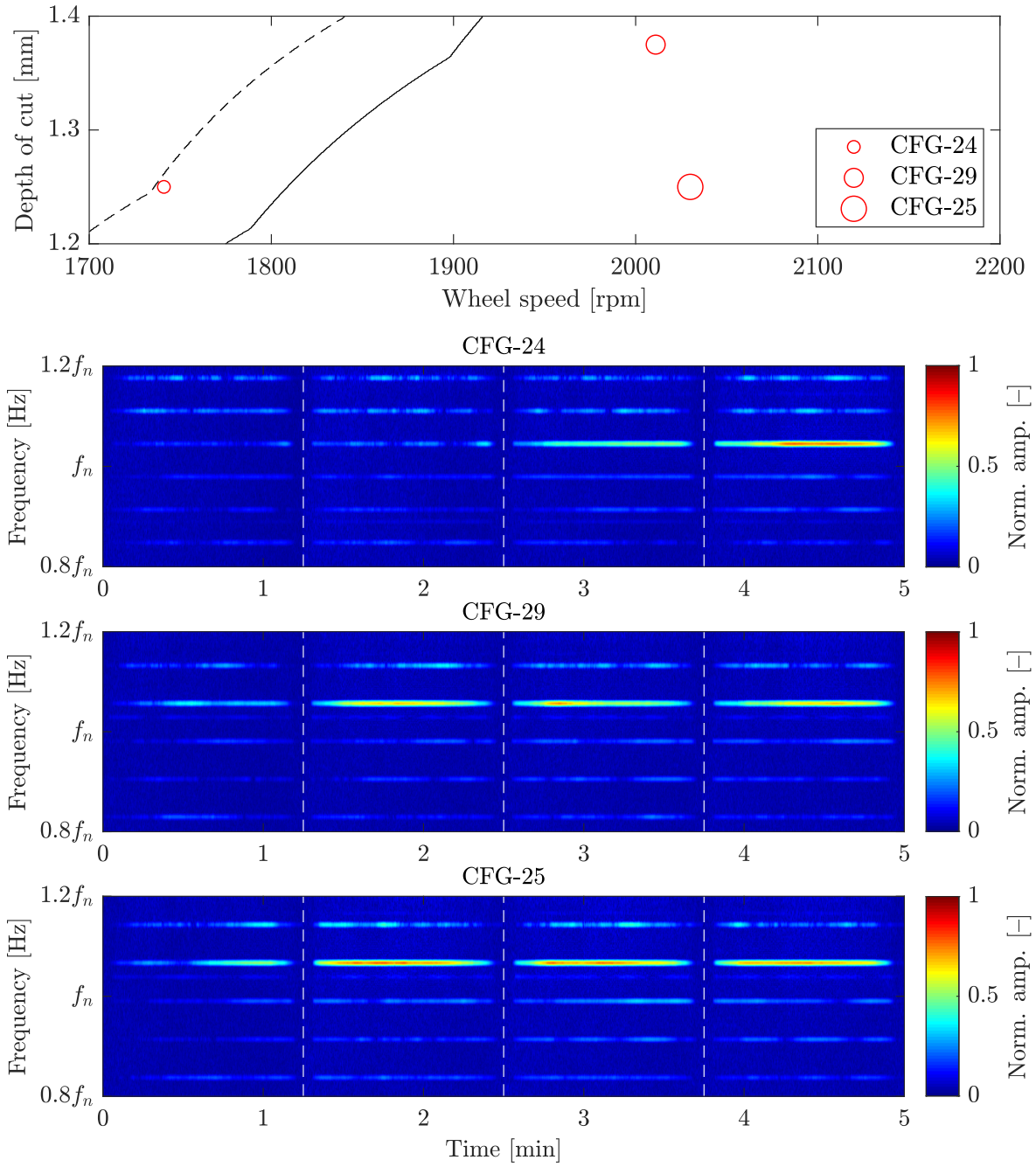

Figure 6.27: Unstable grinding processes and their spectrograms corresponding to different degrees of instability – the four wheel passes are separated by dashed lines

and unstable grinding can be seen mainly in two directions, which are marked by blue lines in Figure 6.28. One of the difficulties in finding the practical stability boundary is the variation of the grinding ratio between individual experiments. Since the grinding ratio changes the location of the stability boundary, different G-ratios result in different stability boundaries. Therefore, determining the experimental stability boundary with precision is possible only if the grinding ratio is kept under sufficient control. Based on the author's machining experiments, this is not always an easy task. The further analysis of the factors that influence the grinding ratio in practice and the conditions under which

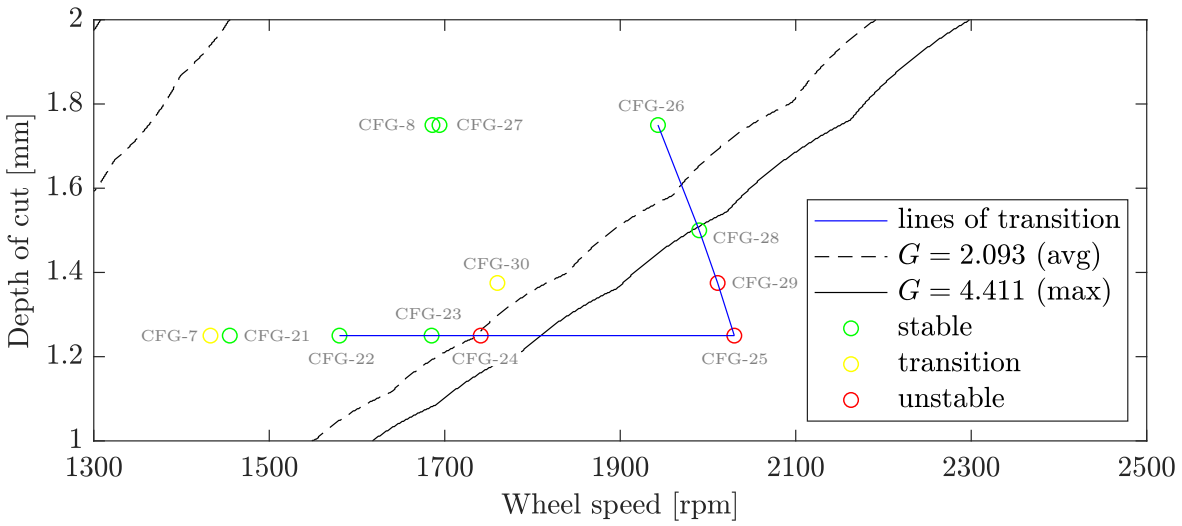

Figure 6.28: Two lines of transition between stable and unstable grinding, indicating the existence of a practical stability boundary

it can be kept approximately constant is outside the scope of this work, nevertheless, it can be a real challenge when it comes to grinding with low G-ratios. In summary of Figure 6.28, it can be concluded that a practical stability boundary has been found in a location that is qualitatively in agreement with the proposed chatter theory.

With regard to the chatter frequencies corresponding to the three unstable scenarios indicated in Figure 6.28, a somewhat unexpected phenomenon can be observed. The difference between the theoretical and experimental chatter frequencies is more significant for each test point than it was for the six shallow cuts (compare Tables 6.8 and 6.11). Furthermore, it can be noticed that the differences between the theoretical and experimental chatter frequencies are approximately equal to the respective wheel speeds. In order to investigate this issue more deeply, a number of simulations are presented in Figure 6.29. Keeping the wheel speed constant, the theoretical chatter frequencies are plotted as a function of the depth of cut for these three test points. It can be seen that, upon reaching a particular depth of cut, all three sets of predictions jump to a value that is significantly higher than the predictions before. Therefore, the difference that can be observed between the theoretical and experimental chatter frequencies also exists in the purely theoretical model itself. This phenomenon is further confirmed by Figure 5.15,

Case identifier	Chatter frequency			Peak ratio [–]
	Theory [Hz]	Experiment [Hz]	Difference [%]	
CFG-24	494.82	463.26	6.81	0.78
CFG-25	508.53	473.02	7.51	0.73
CFG-29	503.81	468.22	7.60	0.69

Table 6.11: Comparison between additional chatter frequencies (CFG)

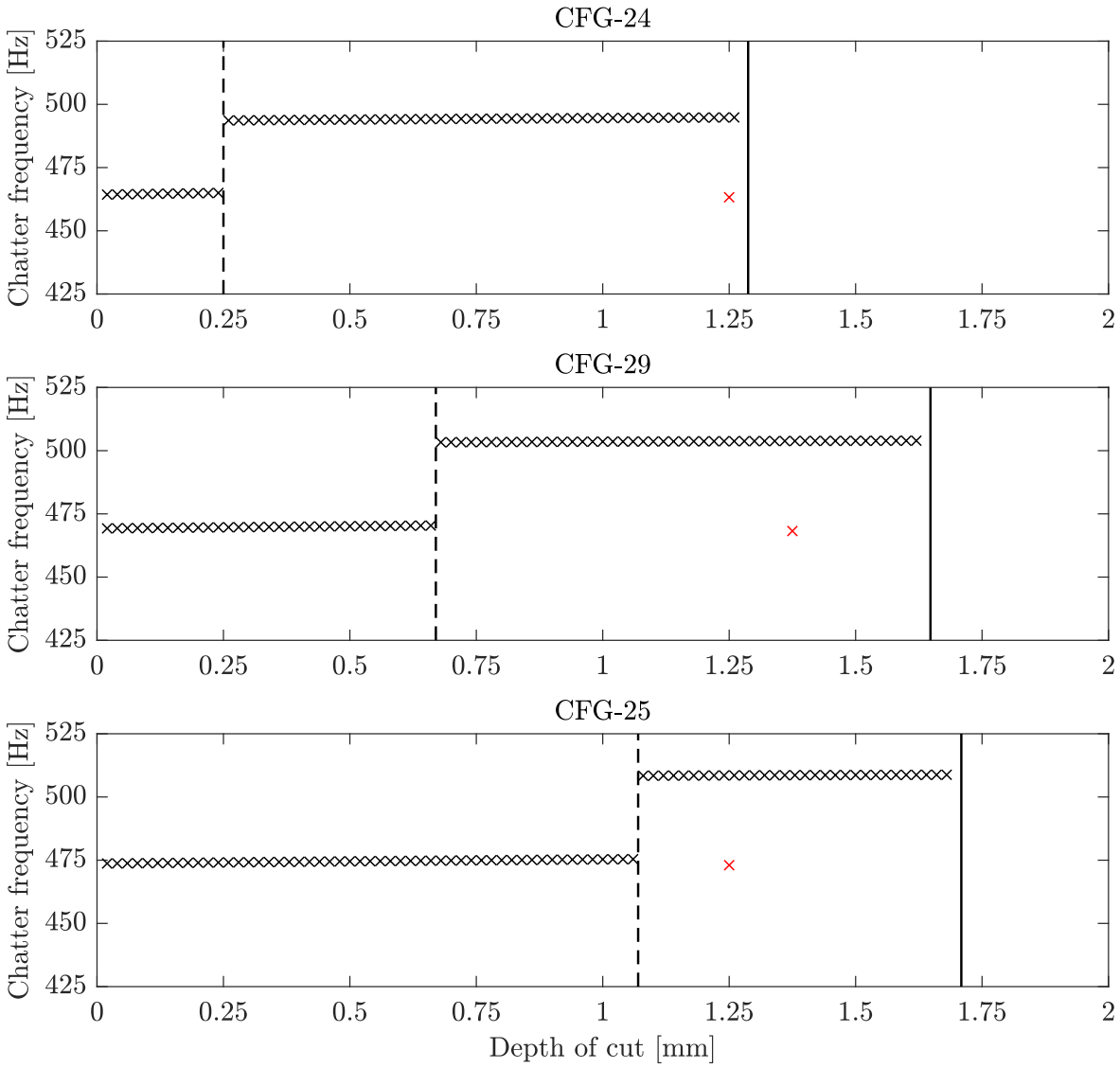

Figure 6.29: Predicted chatter frequencies against the depth of cut:
× simulation, × experiment, ——— stability boundary, – – – critical depth of cut

which shows that increasing the depth of cut at a given wheel speed can cause a jump to occur in the chatter frequency (or lobe number). It is also interesting to note that the depth of cut at which the jump happens depends on the relative stability of the process. Considering that CFG-24 is the least unstable and CFG-25 is the most unstable of the three cases according to Figure 6.27, and noting the distance between each experimental test point and the corresponding stability boundary in Figure 6.29, the proposed chatter theory suggests that the critical depth of cut at which the jump in chatter frequency occurs increases as the grinding process becomes more unstable. Nevertheless, it is clear that the location of the jump is incorrectly predicted by the model, and it is not obvious which assumptions are responsible for this error. Additional work is necessary to improve the chatter frequency predictions of the presented theory.

Concerning the test points at $\delta_0 = 2.75$ mm, a rather unexpected result can be observed:

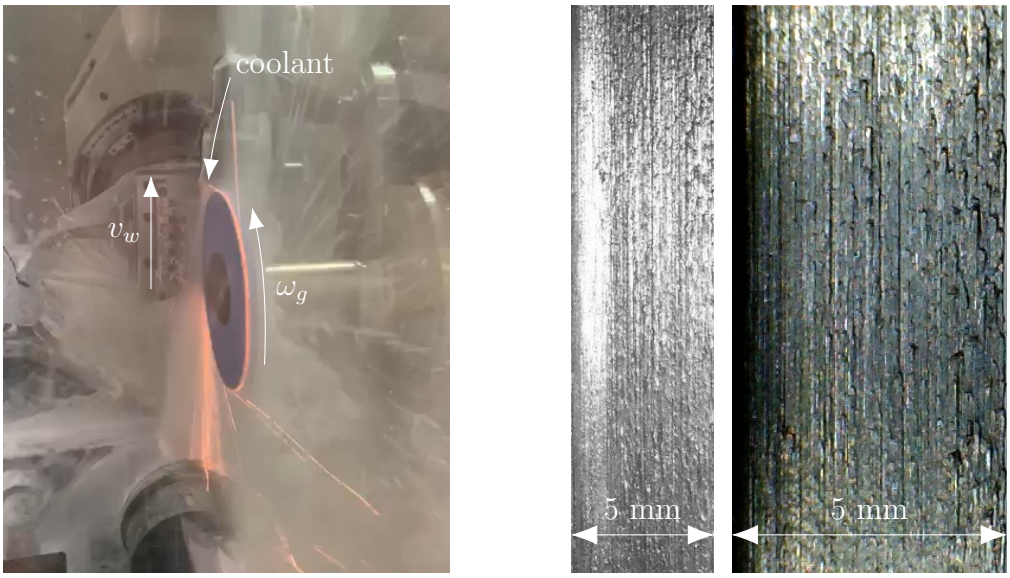

Figure 6.30: Hot workpiece material stuck to the circumference of the wheel during grinding (left) and the resulting surface finish at two different magnifications (right)

Figure 6.25 shows that every experiment turned out to be stable (with one exception of transitional behaviour), while a mixture of stable and unstable processes were predicted. There is no significant difference between these scenarios in terms of their respective spectrograms – each, except for the transitional one, corresponds to stable grinding. Even the transitional case is located between two stable experiments, suggesting no clear stability boundary at this particular depth of cut. Considering the fact that grinding is described in the literature as typically unstable with respect to wheel regeneration [25], this result was highly unexpected. However, having observed the grinding processes in question during cut, a reasonable explanation can be given as to why they were all stable. Due to the high depth of cut, so much heat was generated in the process (especially at higher wheel speeds) that the chips were slightly melted and got stuck to the grinding wheel. This phenomenon manifested itself as a constant glow around the circumference of the wheel throughout the entire process (as captured by Figure 6.30). Since wheel-related regenerative chatter is dependent on the wheel surface being able to regenerate and evolve, the process of surface regeneration and chatter development was probably stalled by workpiece material clogging up and covering the grinding wheel. Although the process was dynamically stable, such a grinding scenario is highly unfavourable and to be avoided in practice. That is because, due to workpiece material being stuck to the grinding wheel and covering its grits, chip formation is hindered, the grains are dragging the workpiece material instead of properly cutting it, workpiece material is continually being redeposited onto the machined surface, and the resulting surface finish is entirely unacceptable (as it is clearly visible in Figure 6.30). Therefore, it is potentially due to this phenomenon, which was not considered in the model, that there is a significant mismatch between the theoretical predictions and the experimental observations.

In conclusion, Figure 6.25 reveals three key pieces of information regarding the stability of the grinding experiments performed and the validity of the chatter theory proposed. First, the experiments between CFG-1 and CFG-6 were unstable processes as the author's

model had predicted. Second, the experiments between $\delta_0 = 1$ and 2 mm show clear lines of transition between stable and unstable operations, and therefore indicate the presence of a stability boundary, whose location is in qualitative agreement with the theoretically calculated stability boundary. And third, the test points at $\delta_0 = 2.75$ mm do not support the predicted results, due to an unexpected phenomenon that was not considered in the model. Therefore, the overall conclusion concerning Figure 6.25 is that the creep-feed grinding experiments performed by the author are largely in support of the proposed chatter theory and present a strong case for its validity.

6.5 Analysis of relative instability

As it was demonstrated in Chapter 5, the proposed model is capable of predicting the relative instability of a given grinding process based on the gain and phase margins of the system. The aim of this section is twofold: to calculate the relative instability of some of the experiments discussed in this chapter, and to compare them with the corresponding theoretical results. Due to the fact that creep-feed grinding (as an experimental methodology described in Sections 6.3 and 6.4) has been shown to be the most suitable configuration for testing the new chatter model, only CFG cases will be covered in this section.

In the first half of this analysis of relative instability, the first six CFG scenarios will be investigated. Transforming the horizontal axes in Figure 6.20 from specific material removed [mm^2] to actual grinding time [s], it is possible to measure the rate of chatter development, i.e., the rate at which the amplitude of the chatter-frequency component of the grinding force spectrum increases with time. This analysis provides valuable insight into the relative instability of each process. Although the fitted exponentials quantifying the rate of chatter development are rather inaccurate at times (as it was pointed out earlier in this chapter), they can still be used for a rudimentary approximation of relative instability. Considering that each fitted exponential has the form $F_x(t) = ae^{bt}$, the damping ratio of each process can be calculated according to the formula $b = -\zeta\omega_c$, where ζ is the damping ratio and ω_c is the chatter frequency in rad/s. This expression is based on elementary vibration theory (e.g. [156], pp. 28-33). Therefore, extracting the coefficients a and b along with the experimental chatter frequencies from the recorded data, it is possible to calculate the damping ratio corresponding to each of the six grinding scenarios presented in Figure 6.20. These results are summarised in Table 6.12.

It can be seen that the damping ratios are negative, which is indicative of instability. Also, it is noteworthy that the damping ratios are very low. In other words, instability developed very slowly. This observation corresponds not only to the first-hand experience of the author that it took quite a while for chatter to become detectable, but also to the position of the literature according to which wheel-related instability takes a long time to build up [25]. It is interesting to see that (apart from CFG-3 and CFG-6, the latter of which was already regarded as an anomaly earlier in Section 6.3.3.2) the damping ratios are not only of the same order of magnitude, but also quite close to one another. This means that these processes become unstable at relatively similar rates. With regard to

Case identifier	Fitted exponential: $F_x(t) = ae^{bt}$, $b = -\zeta\omega_c$		Chatter frequency		Damping ratio ζ [%]
	a [N]	b [rad/s]	f_c [Hz]	ω_c [rad/s]	
CFG-1	0.5897	0.06999	455.09	2859.4	−0.002448
CFG-2	0.5601	0.0681	468.90	2946.2	−0.002311
CFG-3	2.541	0.1141	460.82	2895.4	−0.003941
CFG-4	2.406	0.08221	474.55	2981.7	−0.002757
CFG-5	5.073	0.0863	466.54	2931.4	−0.002944
CFG-6	2.387	0.02801	480.73	3020.5	−0.000927

Table 6.12: Experimental damping ratios corresponding to the first six CFG cases (the graphs to which the exponentials are fitted are presented in Figure 6.20)

Table 6.12, it is important to keep in mind that the damping ratios listed there are only rudimentary approximations of relative instability because of two main reasons: (1) the fitted exponentials are not very accurate representations of the practical nature of chatter growth, i.e., they do not always fit the chatter-amplitude curves very well, and (2) the damping ratios were calculated assuming damped harmonic oscillations with negative damping, which is a rather simplistic approach.

After determining the experimental damping ratios, it is helpful to compare them with those predicted by the proposed theory in order to test the accuracy of the model. This can be done by calculating the phase margin in each case, and provided that it is expressed in degrees, dividing the phase margin by 100 gives a relatively good approximation of the theoretical damping ratio (i.e. $P_M = 100\zeta$ according to [155], p. 648). These results are summarised in the third column of Table 6.13. It is rather surprising to see how vastly

Case identifier	Experimental damping ratio [%]	Theoretical damping ratio [%]		
		$(0.6, 178)$	$(0.6, 17.8)$	$(0.6, 1.78)$
CFG-1	−0.002448	−59.4849	−10.7593	−5.1059
CFG-2	−0.002311	−41.4407	−33.973	−33.1883
CFG-3	−0.003941	−55.6265	−14.5101	−9.7682
CFG-4	−0.002757	−44.2191	−35.3523	−34.4213
CFG-5	−0.002944	−62.0563	−17.5389	−12.4579
CFG-6	−0.000927	−47.2764	−36.3642	−35.2082

Table 6.13: Comparison between experimental and theoretical damping ratios for three different wheel wear rates captured by (ΔA [%], Δu [J/mm^3]) pairs

different these values are from the experimental ones: the predicted damping ratios are at least four orders of magnitude larger than the measured ones. This means that the new model grossly overestimates the rate of stability loss. It is helpful to remember that an overly rapid rate of chatter development and stability loss was already encountered in Section 6.3.2.2 with reference to a couple of inaccurate chatter frequency predictions, and the two phenomena are probably connected. Considering the vast number of modelling assumptions made during the formulation of the theory (listed in Appendix B), this particular error can come from several potential sources.

One possible explanation is that the coefficient of dulling used in the theoretical analysis was too high, i.e., the wear rate of the grinding wheel was too fast. The coefficient of dulling was introduced by the author in Section 5.2.3 as a way of quantifying wheel wear by an increase in specific energy. According to Eq. (5.48), the coefficient of dulling depends on a number of parameters, such as the change in wear-flat area (ΔA) and the corresponding change in specific energy (Δu), the grinding ratio (G), and the geometry of abrasive grits (α and r_g). The grinding ratio and the grain geometry are relatively easy to determine, but measuring the relationship between the wear-flat area and the specific energy is a rather laborious task, which lies outside the scope of this work. Therefore, as it was explained in Section 5.3.4, the author utilised the experiments presented by Malkin and Guo (in Figure 5-19 on p. 142 of [11]) in order to calculate a practical estimate of the coefficient of dulling. However, the relationship between ΔA and Δu depends on the material properties of the wheel and the workpiece, which means that the accurate value of the coefficient of dulling related to the author's experiments is unknown. Therefore, the last two columns of Table 6.13 list a number of damping ratios corresponding to two other (ΔA, Δu) pairs, in order to see whether a more wear-resistant grinding wheel, or equivalently, a lower coefficient of dulling (namely one tenth and one hundredth of the original value) has any significant impact on the predicted damping ratios. Expectedly, the theoretical damping ratio changes with the coefficient of dulling: a lower coefficient of dulling corresponds to a smaller damping ratio (in an absolute sense) and thus to a slower loss of stability as a consequence. Nevertheless, the difference between the experimental and theoretical damping ratios remains substantial – the two are still at least three orders of magnitude apart. Another possible reason for such a major discrepancy is the effect of process damping, which was probably present in the experiments, yet it was unaccounted for in the model. However, considering the fact that the chatter frequencies and the stability boundaries are predicted remarkably accurately by the proposed model, the origin of this particular issue is not discussed any further in this thesis, but it is of high priority to address and clarify it in future research.

What can be said, however, is that both the measured and the originally predicted results indicate a certain degree of similarity relative to one another. In other words, the way the experimental damping ratios relate to each other is somewhat similar to the way the theoretical damping ratios relate to one another. For example, CFG-3 is more unstable than CFG-2 and CFG-4, both experimentally and theoretically. Although this correspondence between the measured and predicted results is clearly not true for any pair of grinding processes listed in Table 6.13, it still holds in a number of cases nonetheless. This observation warrants further analysis despite the fact that the theoretical model grossly overestimates the numerical value of the damping ratio. It would be interesting

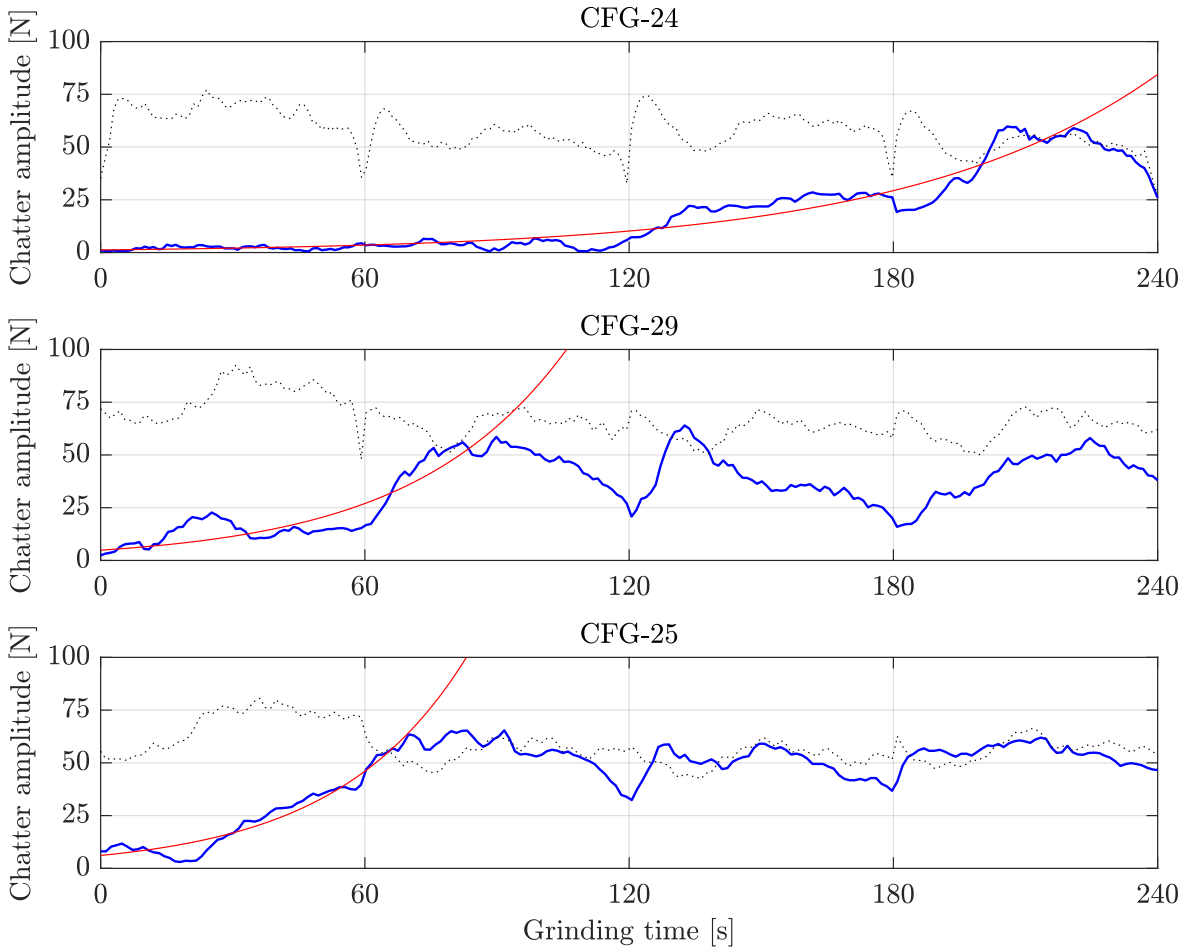

Figure 6.31: Variation in chatter amplitude for three CFG cases: ····· amplitude variation of the zero-frequency component, —— amplitude variation of the chatter-frequency component, —— exponential fitted to the chatter-frequency curve

to see whether the predictions exhibit the same qualitative trend as the experiments in the case of grinding processes whose relative instability properties can be measured with greater confidence than the ones just looked at.

As the first six CFG cases point to such an inference, three more scenarios are investigated now in order to test this hypothesis. These cases (CFG-24, CFG-25 and CFG-29) were presented in Figure 6.27 as three unstable processes with different degrees of instability. The advantage of looking at these three scenarios specifically is that their relative instability in relation to one another has already been established in Section 6.4.2.4. The following analysis aims to test the theoretical model against these three experimental scenarios using the original wheel wear rate (i.e. $\Delta A = 0.6\%$ and $\Delta u = 178$ J/mm^3). In order to measure the damping ratios corresponding to these three cases, a data analysis identical to that in Figure 6.20 has been performed and presented in Figure 6.31. It can be seen that the fitted exponentials somewhat inaccurately yet clearly reflect the same qualitative trend as that shown in Figure 6.27: CFG-24 is the least unstable and CFG-25 is the most unstable of the three grinding processes. The theoretical damping ratios are calculated based on the phase margin again, and tested against the corresponding ex-

Case identifier	Fitted exponential: $F_x(t) = ae^{bt}$, $b = -\zeta\omega_c$		Chatter frequency ω_c [rad/s]	Damping ratio ζ [%]	
	a [N]	b [rad/s]		Experiment	Theory
CFG-24	1.232	0.01762	2910.7	−0.000605	−0.9057
CFG-29	4.857	0.02859	2941.9	−0.000972	−5.9808
CFG-25	6.118	0.03364	2972.1	−0.001132	−10.0187

Table 6.14: Comparison between experimental and theoretical damping ratios for three CFG cases at the original wheel wear rate (i.e. $\Delta A = 0.6\%$ and $\Delta u = 178$ J/mm^3)

perimental results. This comparison is summarised in Table 6.14, where the three cases are listed in increasing order of relative instability. It is clear that the theoretical model significantly overestimates the experimental damping ratios, however, the predictions demonstrate the same trend in relative instability as that captured by the measurements. Therefore, although the new chatter model does not provide accurate results when it comes to the actual damping ratios, it gives a reasonably good approximation of the degree of instability in a relative sense, i.e., regarding the way the relative instability of a particular process relates to that of another.

In summary, it can be stated that the proposed theory faces some challenges in the area of relative instability. The numerical values of the damping ratios are not predicted correctly, nevertheless, the model provides useful information on how unstable a given grinding process is relative to another.

6.6 Summary of grinding experiments

After measuring the modal parameters of the structure and determining the stability and sensitivity of the actual grinding machine, the author designed and performed two sets of experiments in order to test the chatter frequencies and stability boundaries predicted by the proposed chatter theory.

In terms of the predicted chatter frequencies, they are in very good agreement with the practical results for a given wheel speed up to a certain depth of cut. According to Figure 6.25, nine unstable scenarios were tested: six at relatively low depths of cut and three at higher ones. The theoretical predictions corresponding to the six shallow cuts were very accurate – Table 6.8 shows that the difference between the predicted and measured chatter frequencies was around 1% in each case. However, the theoretical predictions corresponding to the three deep cuts were not so accurate – Table 6.11 demonstrates that the difference between the predicted and measured chatter frequencies was around 7% for each test point. Since this was a somewhat unexpected result, the author designed and ran a few more simulations (presented in Figure 6.29) in an attempt to find the origin of a potential problem. It was interesting to see the outcome of these simulations: for a given

wheel speed, the theoretical predictions are correct up to a certain depth of cut, above which they suddenly jump to a value that is significantly higher than the measured chatter frequency. The magnitude of this jump, or the difference between the two predictions before and after it, is equal to the rotational speed of the wheel. Considering Figure 5.15 as well, such a jump in chatter frequency is not entirely unexpected, but it does not take place in practice where it is predicted by the model. In terms of locating the source of this issue, it is not straightforward to identify the assumptions most likely to be responsible for this particular type of inaccuracy in the model. Further research is warranted to track down the origin of this error.

As for the predicted stability boundaries, their qualitative trend is clearly verified by the experiments. The measured test points revealed two lines of transition between stable and unstable grinding processes, indicating the existence of an experimental stability boundary, which matches the theoretical prediction relatively well. But considering the collective understanding of wheel regenerative chatter in the literature, the very fact that a stability boundary has been found is a substantial result in itself. This confirms the hypothesis that grinding can in fact be stable with regard to wheel regeneration. The practical implications of this conclusion are very promising when it comes to increasing productivity and preserving surface quality at the same time. Although both the wheel speed and the depth of cut have lower and upper limits in practice, it is nonetheless clear that a stable region has been found within these practical limits, which is at least uncommon if not unheard of as far as the literature is concerned.

Regarding relative instability, the predictions of the presented model have been falsified in one respect and verified in another. When it comes to the numerical values of the theoretical damping ratios, they are clearly shown to be inaccurate by the experiments. The stability boundary is reasonably accurate, but in the chatter regime the rate of exponential growth is much slower than expected. This suggests a form of non-linear energy dissipation. Energy dissipation because there is more damping (but no change in the oscillatory frequency), and non-linear because it is only present in the unstable regime and does not affect the stability boundary. This strongly suggests that ploughing effects (i.e. process damping) start to take hold. Nevertheless, in terms of assessing how unstable a given grinding process is relative to another, the proposed model provides qualitatively accurate results. This means that although the new chatter theory cannot predict a reliable damping ratio in an absolute sense, it is nonetheless capable of selecting the most favourable (i.e. the most stable or the least unstable) scenario from a number of grinding processes.

Overall, considering the simplicity of the model and the number of assumptions made during the formulation of the theory, it can be concluded that the experimental results are in remarkably good agreement with the predictions of the new chatter model. Practically speaking, the most important outcome of these experiments is the confirmation of theoretical stability, i.e., choosing the wheel speed and the depth of cut carefully, it is possible to avoid wheel regenerative chatter in single-pass surface grinding, and by extension, in multi-pass surface grinding as well, since the interruptions hinder rather than promote chatter development. Since the literature regards grinding as typically unstable with respect to wheel regeneration [25], this is a very significant result.

Chapter 7

Conclusions and future work

In this thesis, the dynamic stability of surface grinding was reviewed and investigated in great detail. Considering the role of the specific energy in process stability, a new chatter theory was formulated based on a novel description of the regenerative mechanism. The model developed by the author was tested against experimental data and found to be an accurate way of predicting grinding chatter.

The final chapter summarises the overall flow of this work, discusses the most important findings, and presents some potential directions for future research.

7.1 Summary and discussion

Starting with the broadest possible context, Chapter 1 gave a concise overview of modern manufacturing, tracking its origin and development in the course of human history. Having considered additive, formative and subtractive processes along with conventional and abrasive operations, Chapter 1 concluded with a short introduction to forced and self-excited machining vibrations, preparing the way for an in-depth literature review on the harmful phenomenon of regenerative machine tool chatter.

Chapter 2 provided a brief overview of self-excited vibrations in conventional machining, and a detailed, chronological review of regenerative chatter in grinding. It was found that, as a result of wheel wear, grinding processes can experience not only workpiece-related chatter, but wheel-related chatter as well. When it comes to this unique type of regeneration in grinding, the vast majority of papers in the literature attribute it to distributed radial wear or physical surface waves around the circumference of the grinding wheel. It was not until 2006 that a couple of researchers named Li and Shin proposed an alternative description of the regenerative mechanism. They postulated that wheel regenerative chatter is a consequence of two fundamentally distinct yet closely related phenomena. Preserving the significance of distributed radial wear or physical surface waves, their grinding chatter theory also included the possibility of distributed grit dullness or specific energy waves around the circumference of the grinding wheel.

With the help of their new model, the authors were able to shed some light on a number of experimental observations reported in the literature, which previous grinding chatter theories could not explain. However, despite Li and Shin's outstanding contribution to the field of grinding dynamics, grinding chatter research after 2006 has returned to the original, less accurate way of accounting for wheel regeneration, namely to a purely radial-wear-based approach.

In response to the knowledge gap revealed by the literature review, the present author proposed a new regenerative mechanism in Chapter 3, disregarding radial wear altogether and considering grit dullness alone in an attempt to assess its significance and also to find out why Li and Shin's improved model of wheel regeneration has not gained much traction in the literature. In order to isolate the problem of wheel regeneration, the author sought to consider a grinding process that cannot experience workpiece regeneration in practice. Single-pass surface grinding was found to be a suitable candidate for this purpose, because the two most common sources of workpiece-related instability (i.e. a rotating workpiece and multiple wheel passes) are absent in this configuration. Nevertheless, short workpiece regeneration (the type that occurs in milling) can still develop in single-pass surface grinding as a result of grits cutting the paths of previous grits in the grinding zone.

Chapter 4 was written to investigate the possibility of this phenomenon. It was found that this type of workpiece regeneration cannot happen in practice, because of the very large number of cutting edges on the wheel. Therefore, single-pass surface grinding was selected as a suitable process to isolate wheel regeneration and formulate a purely grit-dullness-based description of the regenerative mechanism. Furthermore, it is important to remember that the theoretical methodology derived and employed in this study is applicable to other stochastic problems as well, and thus provides a valuable contribution to the stability analysis of stochastic time-delay systems in general.

Chapter 5 presented the formulation of the new grinding chatter theory in detail. The primary results were stability charts and frequency diagrams. It has been found that the proposed model predicts stable operation for a certain range of wheel speeds and depths of cut, even though the literature states that grinding is typically unstable with respect to wheel regeneration. Therefore, this is a very promising theoretical result with potentially far-reaching practical implications. As for the predicted chatter frequencies, the presented model is in agreement with classical chatter theories in both conventional and abrasive machining when it comes to the ratio of the chatter frequency to the natural frequency, nevertheless, it gives only one chatter frequency for a particular unstable scenario. Regarding this result, the literature itself is divided, as both a single chatter frequency and multiple chatter frequencies have been predicted, measured and reported by various authors.

In order to test the new chatter theory, the author performed a number of surface grinding experiments to establish a case for or against the proposed model (Chapter 6). Since the theory predicts both stability boundaries and chatter frequencies, the experimental procedure was designed and carried out in such a way as to provide information about these two areas as well. Starting with the chatter frequencies, the measurements demonstrated that the predictions of the model are remarkably accurate for low depths of cut. However,

above a certain radial immersion, the theoretical chatter frequencies suddenly jump to a value that is significantly higher than the predictions before. The difference in chatter frequency before and after this jump is in fact equal to the rotational speed of the grinding wheel. However, the author's experimental observations did not support this prediction. Nevertheless, since such a jump in chatter frequency is consistent with the theory itself, it is reasonable to maintain the possibility that the jump exists in practice as well, but the model does not predict its location correctly. The reason for this particular inaccuracy is unclear, because it is difficult to associate this error with any of the modelling assumptions for certain. Concerning the stability boundaries, sufficient evidence has been found that the predicted boundaries accurately estimate the real lines of transition between stable and unstable surface grinding. This is a very significant result, because it means that chatter-free operation is possible for practical grinding parameters. The depths of cut for which the process was found to be stable is quite high (certainly higher than what is typical of finishing operations), but creep-feed grinding and high-efficiency deep grinding processes could benefit greatly from the predictions of this new theory. Also, the experiments demonstrated that stability is a relative concept in grinding, i.e., besides the stability boundaries themselves, the degree of instability is of great practical importance as well, providing valuable information about the amount of grinding time available in an actually unstable process that can still produce an acceptable surface finish. Considering the idea of relative instability, the rate of chatter development in the experiments was much slower than predicted, which suggests a form of non-linear energy dissipation in the system. The author strongly suspects that unmodelled ploughing effects (which amount to process damping) are responsible for this phenomenon.

Therefore, the proposed chatter model with the new regenerative mechanism has been validated to such a degree that it can be trusted in practical applications. Consequently, the regenerative mechanism of distributed grit dullness (even in the absence of distributed radial wear) is capable of describing and accounting for wheel regenerative chatter or wheel-related instability in single-pass surface grinding. Therefore, the phenomenon of specific energy waves is significant enough that neglecting it is not advised. This of course depends on the particular problem under investigation, but when it comes to a sophisticated description of wheel regenerative chatter, the variation of the specific energy (or cutting-force coefficient) is to be considered. It is somewhat puzzling why Li and Shin's theory has received so little attention in the literature. The author's best explanation is that the chatter models relying on a purely radial-wear-based approach were accurate enough for their intended purposes, and did not require the level of detail that Li and Shin's theory provides. Nevertheless, it was demonstrated in this thesis that, depending on the problem at hand, the regenerative mechanism of distributed grit dullness can be of major theoretical and practical significance.

Having discussed the main findings of this research at length, the following section summarises them in a clear and concise fashion.

7.2 Conclusions of the thesis

It can be concluded that:

1. Workpiece regeneration cannot lead to workpiece-related instability in single-pass surface grinding. This is because of the large number of cutting edges inherently involved in practical grinding processes. This result is the answer to the first research question in Table 3.1. This conclusion is drawn on the basis of a new mathematical model, which has been developed by the author and is described in Chapter 4. In solving this mathematical model, a new and alternative approach to handling stochastic time delays has been introduced (Sections 4.2.3 and 4.2.4). This poses a computationally efficient way to calculate the dynamic stability of stochastic time-delay systems in general.

2. Grit dullness alone, in the absence of radial wear, can lead to wheel-related instability in single-pass surface grinding. This finding is the answer to the second research question in Table 3.1. This conclusion is drawn on the basis of a new mathematical model, again developed by the author, and described in Chapter 5. The model has been experimentally validated using extensive machining experiments, signal processing and data analysis, as presented in Chapter 6.

This second conclusion raises some important issues from the perspective of both industrial users and academic researchers.

First, although the previous literature puts forth grinding as typically unstable with respect to wheel regeneration, this research has shown that stable parameter zones do in fact exist for large depths of cut. This is an unprecedented result not only in terms of novelty, but also in terms of industrial impact. Further work is needed to explore the parameter spaces in which this stability occurs, as it could pave the way for enhanced efficiency and productivity in industrial practice. However, further work is also needed to understand how this prediction is influenced by the underpinning modelling assumptions, and the extent to which these assumptions are valid.

Second, the model provides valuable information on chatter avoidance as well, i.e., which grinding parameters can be changed in order to stabilise an unstable system. This is very important, because depending on the nature of instability, changing certain grinding parameters has no stabilising effect on the process (Section 5.3.4). Again, the sensitivity of this result requires further exploration.

Third, the new theory suggests that increasing the grinding ratio to that of superabrasives results in stable machining not only for deep cuts, but for finishing operations as well. Further work is needed to experimentally validate the stable zones arising at low depths of cut (Figure 6.7a), as these parameter spaces can be of much benefit to industry. That is because process stability is crucial when it comes to taking shallow cuts in grinding, which are typically responsible for the final state of the workpiece. Furthermore, these stable regions are of interest to academia as well, indicating a closer relationship between superabrasive wheels and conventional cutting tools than previously thought.

7.3 Future work

As a result of reviewing the relevant literature, two main gaps in knowledge have been identified: (1) the relative significance of distributed radial wear and distributed grit dullness with regard to process stability has not yet been assessed, and (2) the dominance of distributed grit dullness and its capacity to generate wheel-related instability on its own has not yet been investigated. Since this thesis addressed only the second gap and concluded that the regenerative mechanism of distributed grit dullness can account for wheel-related chatter all by itself, the most natural, large-scale way to continue this work is to focus on the first gap and study how the two regenerative mechanisms compare with one another in terms of their relative dominance and stability predictions.

This direction of future research could also serve to assess the validity of the author's new approach depicted in Figure 3.1c. Although Li and Shin's model (shown in Figure 3.1b) is more realistic in the sense that it considers two separate but related effects of wheel wear as regenerative mechanisms, both of which are undeniably present in practice, these authors provided no information on the relative dominance between them. That work has been started by the present author, who isolated the lesser-known of these two mechanisms and began to study it on its own. The remaining suggestions for future research are concerned with the continuation and improvement of the new grinding chatter model developed in this thesis.

Regarding the first conclusion in Section 7.2, the theoretical result at the end of Chapter 4, proposing a computationally efficient way of dealing with stochastic time-delay systems in general, has some promising applications outside the field of grinding dynamics as well. Therefore, the formulation of a more complete theory is encouraged.

Concerning the second conclusion, there are a number of opportunities for future work. Although the proposed model has been validated to an extent that it is reliable in practice, considering the number of grinding experiments performed and reported in Chapter 6, it is clear that more experimental work is required to test more of the predicted results. Even though two very important lines of transition have been measured between stable and unstable processes, which coincide remarkably well with the lower stability boundary, more data points are needed to establish the transition in higher resolution.

Because of an unexpected phenomenon at large depths of cut, the experiments that were designed to test the upper stability boundary gave unreliable results. Therefore, another natural way to continue this work in the future is to reconsider the grinding parameters and retest the upper stability boundary.

Due to the observed phenomenon of relative stability, the question arose in Chapter 6 whether the grinding experiments judged to be stable were truly stable or they were simply not run long enough to show detectable signs of instability. Although the author kept the specific material removed approximately constant precisely for the sake of avoiding such a suspicion and therefore has much confidence that the stable processes will remain stable even if run for a longer time, it would still be reassuring to see this confirmed by experimental data. The difficulty of performing long machining experiments is that

the methodology described in Chapter 6 would require more than one block of workpiece material, which would involve the swapping of test pieces in between two wheel passes of the same experiment, and that may introduce some uncontrolled variations into the system. In light of the precautions taken by the author, the potential issue of stable operations turning out to be unstable is of minor concern, yet it is still worth checking in the future.

Another important topic of future work could be the establishment of a peak ratio threshold separating stable and unstable experiments that would allow an informed decision to be made with regard to grinding stability in practice. Although it is typically fairly straightforward to judge whether a process is stable or unstable just by looking at the corresponding spectrogram, it would still be helpful to have a clear and systematic way of characterising the stability of grinding experiments based on the measured peak ratio.

The new theory predicts a jump in the chatter frequency at a certain depth of cut (Figure 6.29). Although the experiments have shown that the location of this jump is predicted inaccurately by the current model, the jump itself is still expected in practice. Therefore, it would be useful to perform some tests designed to find the experimental location where the lobe number (chatter frequency per wheel speed) jumps from one integer to another. Regarding the validity of the proposed model at this stage, these are the main experimental directions for future work.

In terms of theoretical directions, there are some obvious ways to improve the current model by revisiting its assumptions listed in Appendix B. For example, similarly to Li and Shin's theory, distributed grit dullness can be considered along with distributed radial wear. This would provide an opportunity to compare the two models, and assess the significance of distributed grit dullness not only in an absolute sense, but relative to the effect of distributed radial wear as well. Or, regarding the grinding force expression, the idealised model can be replaced with a more sophisticated one, such as an empirical or even a stochastic grinding force model. Moreover, when it comes to the specific energy, the accuracy of the model can be improved by treating the three grinding mechanisms separately. This would allow for the effect of ploughing to be considered, which is probably responsible for the discrepancy between the theoretical and experimental results with regard to the rate of chatter growth. The self-sharpening property of grinding wheels can be taken into account as well, by allowing the specific energy to decrease or even drop instantly after a certain amount of grit wear, simulating the loss of a dull grain and the exposure of a sharp one. There are several other opportunities to improve the current theory by reconsidering more of the modelling assumptions. The ideas mentioned above are only a select few, addressing some of the most obvious ways to arrive at a more sophisticated grinding chatter theory.

And finally, concerning the sensitivity of the stability boundaries to the grinding ratio, it was interesting to see that increasing the G-ratio to extremely high values – pertaining to superabrasives in practice – causes a lobe-like stability structure to arise from the horizontal axis, indicating the fact that superabrasives can be stable even at low depths of cut, where conventional abrasives are typically unstable. This prediction has some very important practical implications in terms of stabilising finishing operations, which

are responsible for the surface quality and dimensional accuracy of the final product. Therefore, testing this theoretical result against experimental data would be yet another useful way to continue this work.

Bibliography

[1] Roser, C. (2016) "Faster, better, cheaper" in the history of manufacturing: From the Stone Age to lean manufacturing and beyond, Taylor & Francis, Abingdon.

[2] Chua, C. K. and Leong, K. F. (2014) 3D printing and additive manufacturing: Principles and applications, World Scientific, Singapore.

[3] Gibson, I., Rosen, D. W., and Stucker, B. (2014) Additive manufacturing technologies: 3D printing, rapid prototyping, and direct digital manufacturing (second edition), Springer, New York.

[4] Milewski, J. O. (2017) Additive manufacturing of metals: From fundamental technology to rocket nozzles, medical implants, and custom jewelry, Springer, New York.

[5] Conner, B. P., Manogharan, G. P., Martof, A. N., Rodomsky, L. M., Rodomsky, C. M., Jordan, D. C., and Limperos, J. W. (2014) Making sense of 3-D printing: Creating a map of additive manufacturing products and services. *Additive Manufacturing,* **1**, 64–76.

[6] Beaman, J. J., Atwood, C., Bergman, T. L., Bourell, D., Hollister, S., and Rosen, D. (2004) Additive/subtractive manufacturing research and development in Europe, World Technology Evaluation Center (WTEC), Inc., Baltimore, MD.

[7] Albert, M. (2011) Subtractive plus additive equals more than. *Modern Machine Shop,* **83**(9), 14.

[8] Jain, V. K. (2009) Advanced machining processes, Allied Publishers, New Delhi.

[9] Luo, X. and Qin, Y. (2018) Hybrid machining: Theory, methods, and case studies, Academic Press, London.

[10] Seah, K. H. W., Li, X., and Lee, K. S. (1995) The effect of applying coolant on tool wear in metal machining. *Journal of Materials Processing Technology,* **48**(1-4), 495–501.

[11] Malkin, S. and Guo, C. (2008) Grinding technology: Theory and applications of machining with abrasives (second edition), Industrial Press, New York.

[12] Walker, J. R. (2004) Machining fundamentals: From basic to advanced techniques (eighth edition), Goodheart-Willcox, Tinley Park.

[13] Kibbe, R. R., Neely, J. E., Meyer, R. O., and White, W. T. (2005) Machine tool practices, Prentice Hall, New Jersey.

[14] Davim, J. P. (2008) Machining: Fundamentals and recent advances, Springer-Verlag, London.

[15] Wikimedia Commons (File: Leonardo machine for grinding convex lenses.JPG).

[16] Lynch, A. J. and Rowland, C. A. (2005) The history of grinding, Society for Mining, Metallurgy & Exploration (SME), Littleton, Colorado.

[17] Jacobs, F. B. (1919) Abrasives and abrasive wheels, their nature, manufacture and use, Henley, New York.

[18] Woodbury, R. S. (1959) History of the grinding machine: A historical study in tools and precision production, MIT Press, Cambridge, MA.

[19] Coes, L. (1971) Abrasives, Springer-Verlag, New York.

[20] Ueltz, H. F. G. (1972) Abrasive grains: Past, present and future. In *Proceedings of the International Grinding Conference,* pp. 1–33.

[21] Lewis, K. B. and Schleicher, W. F. (1976) The grinding wheel: A textbook of modern grinding practice, Grinding Wheel Institute, Cleveland, OH.

[22] Kalpakjian, S. (1984) Manufacturing processes for engineering materials, Addison-Wesley, Reading, MA.

[23] King, R. I. and Hahn, R. S. (2012) Handbook of modern grinding technology, Springer, New York.

[24] Rowe, W. B. (2013) Principles of modern grinding technology, William Andrew, New York.

[25] Inasaki, I., Karpuschewski, B. A., and Lee, H. S. (2001) Grinding chatter – Origin and suppression. *CIRP Annals,* **50**(2), 515–534.

[26] Rao, B. K. N. (1996) Handbook of condition monitoring, Elsevier, Amsterdam.

[27] Carden, E. P. and Fanning, P. (2004) Vibration based condition monitoring: A review. *Structural Health Monitoring,* **3**(4), 355–377.

[28] Vachtsevanos, G. J., Lewis, F., Hess, A., and Wu, B. (2006) Intelligent fault diagnosis and prognosis for engineering systems, Wiley, New Jersey.

[29] Widodo, A. and Yang, B. S. (2007) Support vector machine in machine condition monitoring and fault diagnosis. *Mechanical Systems and Signal Processing,* **21**(6), 2560–2574.

[30] Randall, R. B. (2011) Vibration-based condition monitoring: Industrial, aerospace and automotive applications, John Wiley & Sons, New Jersey.

[31] Taylor, F. W. (1906) On the art of cutting metals, American Society of Mechanical Engineers (ASME), New York.

[32] Tobias, S. A. (1965) Machine-tool vibration, Wiley, New Jersey.

[33] Stépán, G. (1989) Retarded dynamical systems: Stability and characteristic functions, Longman, Harlow.

[34] Tlusty, J. (2000) Manufacturing processes and equipment, Prentice Hall, New Jersey.

[35] Altintas, Y. (2012) Manufacturing automation: Metal cutting mechanics, machine tool vibrations, and CNC design, Cambridge University Press, Cambridge.

[36] Wiercigroch, M. and Budak, E. (2001) Sources of nonlinearities, chatter generation and suppression in metal cutting. *Philosophical Transactions of the Royal Society of London. Series A: Mathematical, Physical and Engineering Sciences,* **359**(1781), 663–693.

[37] Arnold, R. (1946) Cutting tools research: Report of subcommittee on carbide tools: The mechanism of tool vibration in the cutting of steel. *Proceedings of the Institution of Mechanical Engineers,* **154**(1), 261–284.

[38] Hahn, R. S. (1953) Metal-cutting chatter and its elimination. *Transactions of the ASME,* **75**(6), 1073.

[39] Doi, S. and Kato, S. (1955) Chatter vibration of lathe tools. *Transactions of the ASME,* **78**, 1127–1134.

[40] Tobias, S. A. and Fishwick, W. (1958) Theory of regenerative machine tool chatter. *The Engineer,* **205**(7), 199–203.

[41] Tlusty, J. and Polacek, M. (1963) The stability of the machine tool against self-excited vibration in machining. In *Proceedings of the International Research in Production Engineering,* pp. 465–474.

[42] Merritt, H. E. (1965) Theory of self-excited machine-tool chatter. *ASME Journal of Engineering for Industry,* **87**, 447–454.

[43] Altintas, Y. and Budak, E. (1995) Analytical prediction of stability lobes in milling. *CIRP Annals,* **44**(1), 357–362.

[44] Altintas, Y. and Weck, M. (2004) Chatter stability of metal cutting and grinding. *CIRP Annals,* **53**(2), 619–642.

[45] Budak, E., Altintas, Y., and Armarego, E. J. A. (1996) Prediction of milling force coefficients from orthogonal cutting data. *Journal of Manufacturing Science and Engineering,* **118**(2), 216–224.

[46] Budak, E. and Altintas, Y. (1998) Analytical prediction of chatter stability in milling – Part I: General formulation. *Journal of Dynamic Systems, Measurement, and Control,* **120**(1), 22–30.

[47] Budak, E. and Altintas, Y. (1998) Analytical prediction of chatter stability in milling – Part II: Application of the general formulation to common milling systems. *Journal of Dynamic Systems, Measurement, and Control,* **120**(1), 31–36.

[48] Budak, E. (2006) Analytical models for high performance milling. Part I: Cutting forces, structural deformations and tolerance integrity. *International Journal of Machine Tools and Manufacture,* **46**(12-13), 1478–1488.

[49] Budak, E. (2006) Analytical models for high performance milling. Part II: Process dynamics and stability. *International Journal of Machine Tools and Manufacture,* **46**(12-13), 1489–1499.

[50] Budak, E. (2003) An analytical design method for milling cutters with nonconstant pitch to increase stability, Part I: Theory. *Journal of Manufacturing Science and Engineering,* **125**(1), 29–34.

[51] Budak, E. (2003) An analytical design method for milling cutters with nonconstant pitch to increase stability, Part 2: Application. *Journal of Manufacturing Science and Engineering,* **125**(1), 35–38.

[52] Koenigsberger, F. and Tlusty, J. (2016) Machine tool structures, Pergamon Press, Oxford.

[53] Tlusty, J. and Ismail, F. (1981) Basic non-linearity in machining chatter. *CIRP Annals,* **30**(1), 299–304.

[54] Tlusty, J. and Ismail, F. (1983) Special aspects of chatter in milling. *Journal of Vibration, Acoustics, Stress, and Reliability in Design,* **105**(1), 24–32.

[55] Tlusty, J. (1986) Dynamics of high-speed milling. *Journal of Engineering for Industry,* **108**(2), 59–67.

[56] Ema, S. and Marui, E. (2000) Suppression of chatter vibration of boring tools using impact dampers. *International Journal of Machine Tools and Manufacture,* **40**(8), 1141–1156.

[57] Ema, S., Fujii, H., and Marui, E. (1988) Chatter vibration in drilling. *Journal of Engineering for Industry,* **110**(4), 309–314.

[58] Kato, S. and Marui, E. (1974) On the cause of regenerative chatter due to workpiece deflection. *Journal of Engineering for Industry,* **96**(1), 179–186.

[59] Ema, S. and Marui, E. (2003) Theoretical analysis on chatter vibration in drilling and its suppression. *Journal of Materials Processing Technology,* **138**(1-3), 572–578.

[60] Ema, S. and Marui, E. (1998) Suppression of chatter vibration in drilling. *Journal of Manufacturing Science and Engineering,* **120**(1), 200–202.

[61] Marui, E., Kato, S., Hashimoto, M., and Yamada, T. (1988) The mechanism of chatter vibration in a spindle-workpiece system: Part 1 – Properties of self-excited chatter vibration in spindle-workpiece system. *Journal of Engineering for Industry,* **110**(3), 236–241.

[62] Marui, E., Kato, S., Hashimoto, M., and Yamada, T. (1988) The mechanism of chatter vibration in a spindle-workpiece system: Part 2 – Characteristics of dynamic cutting force and vibration energy. *Journal of Engineering for Industry,* **110**(3), 242–247.

[63] Soliman, E. and Ismail, F. (1997) Chatter suppression by adaptive speed modulation. *International Journal of Machine Tools and Manufacture,* **37**(3), 355–369.

[64] Ismail, F. and Ziaei, R. (2002) Chatter suppression in five-axis machining of flexible parts. *International Journal of Machine Tools and Manufacture,* **42**(1), 115–122.

[65] Ahmadi, K. and Ismail, F. (2010) Experimental investigation of process damping nonlinearity in machining chatter. *International Journal of Machine Tools and Manufacture,* **50**(11), 1006–1014.

[66] Ahmadi, K. and Ismail, F. (2011) Analytical stability lobes including nonlinear process damping effect on machining chatter. *International Journal of Machine Tools and Manufacture,* **51**(4), 296–308.

[67] Insperger, T., Mann, B. P., Stépán, G., and Bayly, P. V. (2003) Stability of up-milling and down-milling, Part 1: Alternative analytical methods. *International Journal of Machine Tools and Manufacture,* **43**(1), 25–34.

[68] Insperger, T., Stépán, G., Bayly, P. V., and Mann, B. P. (2003) Multiple chatter frequencies in milling processes. *Journal of Sound and Vibration,* **262**(2), 333–345.

[69] Gradišek, J., Kalveram, M., Insperger, T., Weinert, K., Stépán, G., Govekar, E., and Grabec, I. (2005) On stability prediction for milling. *International Journal of Machine Tools and Manufacture,* **45**(7-8), 769–781.

[70] Mann, B. P., Insperger, T., Bayly, P. V., and Stépán, G. (2003) Stability of up-milling and down-milling, Part 2: Experimental verification. *International Journal of Machine Tools and Manufacture,* **43**(1), 35–40.

[71] Zatarain, M., Munoa, J., Peigné, G., and Insperger, T. (2006) Analysis of the influence of mill helix angle on chatter stability. *CIRP Annals,* **55**(1), 365–368.

[72] Insperger, T. and Stépán, G. (2000) Stability of the milling process. *Periodica Polytechnica Mechanical Engineering,* **44**(1), 47–57.

[73] Bayly, P. V., Mann, B. P., Schmitz, T. L., Peters, D. A., Stépán, G., and Insperger, T. (2002) Effects of radial immersion and cutting direction on chatter instability in end-milling. In *ASME 2002 International Mechanical Engineering Congress and Exposition,* pp. 351–363.

[74] Kalmár-Nagy, T., Stépán, G., and Moon, F. C. (2001) Subcritical Hopf bifurcation in the delay equation model for machine tool vibrations. *Nonlinear Dynamics,* **26**(2), 121–142.

[75] Stépán, G. (2001) Modelling nonlinear regenerative effects in metal cutting. *Philosophical Transactions of the Royal Society of London. Series A: Mathematical, Physical and Engineering Sciences,* **359**(1781), 739–757.

[76] Stépán, G. (1998) Delay-differential equation models for machine tool chatter. *Dynamics and Chaos in Manufacturing Processes,* pp. 165–192.

[77] Stépán, G. and Kalmár-Nagy, T. (1997) Nonlinear regenerative machine tool vibrations. In *Proceedings of the 1997 ASME Design Engineering Technical Conference on Vibration and Noise,* Sacramento, CA: pp. 1–11.

[78] Schmitz, T. L. and Smith, K. S. (2014) Machining dynamics, Springer, New York.

[79] Schmitz, T. L. (2003) Chatter recognition by a statistical evaluation of the synchronously sampled audio signal. *Journal of Sound and Vibration,* **262**(3), 721–730.

[80] Hanna, N. H. and Tobias, S. A. (1974) A theory of nonlinear regenerative chatter. *Journal of Engineering for Industry,* **96**(1), 247–255.

[81] Ota, H. and Kono, K. (1974) On chatter vibrations of machine tool or work due to regenerative effect and time lag. *Journal of Engineering for Industry,* **96**(4), 1337–1346.

[82] Kondo, E., Ota, H., and Kawai, T. (1997) A new method to detect regenerative chatter using spectral analysis, Part 1: Basic study on criteria for detection of chatter. *Journal of Manufacturing Science and Engineering,* **119**(4A), 461–466.

[83] Ota, H., Kondo, E., and Yamada, T. (1989) Regenerative chatter vibrations of turning workpieces: Two degrees of freedom and their stability criteria. *JSME International Journal, Series 3: Vibration, Control Engineering, Engineering for Industry,* **32**(1), 142–149.

[84] Insperger, T., Stépán, G., and Turi, J. (2007) State-dependent delay in regenerative turning processes. *Nonlinear Dynamics,* **47**(1-3), 275–283.

[85] Eynian, M. and Altintas, Y. (2009) Chatter stability of general turning operations with process damping. *Journal of Manufacturing Science and Engineering,* **131**(4).

[86] Munoa, J., Beudaert, X., Dombóvári, Z., Altintas, Y., Budak, E., Brecher, C., and Stépán, G. (2016) Chatter suppression techniques in metal cutting. *CIRP Annals,* **65**(2), 785–808.

[87] Tóth, M. (2014) Vibration analysis of milling processes (master's thesis), Budapest University of Technology and Economics, Budapest, Hungary.

[88] Driver, R. D. (1977) Ordinary and delay differential equations, Springer, New York.

[89] Ehmann, K. F., Kapoor, S. G., DeVor, R. E., and Lazoglu, I. (1997) Machining process modeling: A review. *Journal of Manufacturing Science and Engineering,* **119**(4B), 655–663.

[90] Quintana, G. and Ciurana, J. (2011) Chatter in machining processes: A review. *International Journal of Machine Tools and Manufacture,* **51**(5), 363–376.

[91] Insperger, T., Lehotzky, D., and Stépán, G. (2015) Regenerative delay, parametric forcing and machine tool chatter: A review. *IFAC-PapersOnLine,* **48**(12), 322–327.

[92] Insperger, T. and Stépán, G. (2002) Semi-discretization method for delayed systems. *International Journal for Numerical Methods in Engineering,* **55**(5), 503–518.

[93] Insperger, T. and Stépán, G. (2011) Semi-discretization for time-delay systems, Springer, New York.

[94] Merdol, S. D. and Altintas, Y. (2004) Multi frequency solution of chatter stability for low immersion milling. *Journal of Manufacturing Science and Engineering,* **126**(3), 459–466.

[95] Bachrathy, D. and Stépán, G. (2013) Improved prediction of stability lobes with extended multi frequency solution. *CIRP Annals,* **62**(1), 411–414.

[96] Stone, B. (2014) Chatter and machine tools, Springer, Switzerland.

[97] Hahn, R. S. (1954) On the theory of regenerative chatter in precision-grinding operations. *Transactions of the ASME,* pp. 593–597.

[98] Landberg, P. (1957) Experiments on grinding. *Microtecnic,* **11**(1), 18–26.

[99] Gurney, J. P. (1965) An analysis of surface wave instability in grinding. *Journal of Mechanical Engineering Science,* **7**(2), 198–209.

[100] Snoeys, R. and Brown, D. (1969) Dominating parameters in grinding wheel—and workpiece regenerative chatter. In *Proceedings of the 10th International Conference on Machine Tool Design and Research,* pp. 325–348.

[101] Thompson, R. A. (1974) On the doubly regenerative stability of a grinder. *Journal of Engineering for Industry,* **96**(1), 275–280.

[102] Thompson, R. A. (1977) On the doubly regenerative stability of a grinder: The combined effect of wheel and workpiece speed. *Journal of Engineering for Industry,* **99**(1), 237–241.

[103] Thompson, R. A. (1986) On the doubly regenerative stability of a grinder: The theory of chatter growth. *Journal of Engineering for Industry,* **108**(2), 75–82.

[104] Thompson, R. A. (1986) On the doubly regenerative stability of a grinder: The mathematical analysis of chatter growth. *Journal of Engineering for Industry,* **108**(2), 83–92.

[105] Thompson, R. A. (1992) On the doubly regenerative stability of a grinder: The effect of contact stiffness and wave filtering. *Journal of Engineering for Industry,* **114**(1), 53–60.

[106] Thompson, R. A. (1971) The dynamic behavior of surface grinding: Part 1 – A mathematical treatment of surface grinding. *Journal of Engineering for Industry,* **93**(2), 485–491.

[107] Thompson, R. A. (1971) The dynamic behavior of surface grinding: Part 2 – Some surface grinding tests. *Journal of Engineering for Industry,* **93**(2), 492–497.

[108] Li, H. and Shin, Y. C. (2006) Wheel regenerative chatter of surface grinding. *Journal of Manufacturing Science and Engineering,* **128**(2), 393–403.

[109] Inasaki, I. and Yonetsu, S. (1968) Surface waves generated on the grinding wheel. *Bulletin of JSME,* **11**(47), 922–929.

[110] Inasaki, I. and Yonetsu, S. (1969) Surface waves generated on the grinding wheel (Report 2, Consideration on the generation of waves). *Bulletin of JSME,* **12**(52), 918–922.

[111] Chung, K. W. and Liu, Z. (2011) Nonlinear analysis of chatter vibration in a cylindrical transverse grinding process with two time delays using a nonlinear time transformation method. *Nonlinear Dynamics,* **66**(4), 441–456.

[112] Yan, Y., Xu, J., and Wang, W. (2012) Nonlinear chatter with large amplitude in a cylindrical plunge grinding process. *Nonlinear Dynamics,* **69**(4), 1781–1793.

[113] Kim, P., Jung, J., Lee, S., and Seok, J. (2013) Stability and bifurcation analyses of chatter vibrations in a nonlinear cylindrical traverse grinding process. *Journal of Sound and Vibration,* **332**(15), 3879–3896.

[114] Yan, Y., Xu, J., and Wiercigroch, M. (2015) Non-linear analysis and quench control of chatter in plunge grinding. *International Journal of Non-Linear Mechanics,* **70**, 134–144.

[115] Yan, Y., Xu, J., and Wiercigroch, M. (2016) Regenerative chatter in self-interrupted plunge grinding. *Meccanica,* **51**(12), 3185–3202.

[116] Yan, Y., Xu, J., and Wiercigroch, M. (2017) Regenerative chatter in a plunge grinding process with workpiece imbalance. *The International Journal of Advanced Manufacturing Technology,* **89**(9-12), 2845–2862.

[117] Yan, Y., Xu, J., and Wiercigroch, M. (2018) Stability and dynamics of parallel plunge grinding. *The International Journal of Advanced Manufacturing Technology,* **99**(1-4), 881–895.

[118] Yoshikawa, H. and Sata, T. (1963) Study on wear of grinding wheels. *Journal of Engineering for Industry,* **85**(1), 39–42.

[119] Malkin, S. (1968) The attritious and fracture wear of grinding wheels (PhD thesis), Massachusetts Institute of Technology, Cambridge, MA.

[120] Malkin, S. and Cook, N. H. (1971) The wear of grinding wheels: Part 1 – Attritious wear. *Journal of Engineering for Industry,* **93**(4), 1120–1128.

[121] Malkin, S. and Cook, N. H. (1971) The wear of grinding wheels: Part 2 – Fracture wear. *Journal of Engineering for Industry,* **93**(4), 1129–1133.

[122] Li, H. N. and Axinte, D. (2016) Textured grinding wheels: A review. *International Journal of Machine Tools and Manufacture,* **109**, 8–35.

[123] Kannappan, S. and Malkin, S. (1972) Effects of grain size and operating parameters on the mechanics of grinding. *Journal of Engineering for Industry,* **94**(3), 833–842.

[124] Malkin, S. (1975) Specific energy and mechanisms in abrasive processes. In *Proceedings of the Third North American Metalworking Research Conference,* pp. 453–465.

[125] Malkin, S. (1976) Selection of operating parameters in surface grinding of steels. *Journal of Engineering for Industry,* **98**(1), 56–62.

[126] Inasaki, I. and Yonetsu, S. (1977) Regenerative chatter in grinding. In *Proceedings of the 18th International Machine Tool Design and Research Conference,* London: pp. 423–429.

[127] Shimizu, T., Inasaki, I., and Yonetsu, S. (1977) Studies on the forced vibration during grinding. *Bulletin of the JSME,* **20**(142), 475–482.

[128] Werner, G. (1978) Influence of work material on grinding forces. *CIRP Annals,* **27**(1), 243–248.

[129] Yan, Y. and Xu, J. (2013) Suppression of regenerative chatter in a plunge-grinding process by spindle speed. *Journal of Manufacturing Science and Engineering,* **135**(4).

[130] Yan, Y., Xu, J., and Wiercigroch, M. (2016) Regenerative and frictional chatter in plunge grinding. *Nonlinear Dynamics,* **86**(1), 283–307.

[131] Jalili, M. M., Fazel, R., and Abootorabi, M. M. (2017) Simulation of chatter in plunge grinding process with structural and cutting force nonlinearities. *The International Journal of Advanced Manufacturing Technology,* **89**(9-12), 2863–2881.

[132] Yan, Y., Xu, J., and Wiercigroch, M. (2017) Influence of workpiece imbalance on regenerative and frictional grinding chatters. *Procedia IUTAM,* **22**, 146–153.

[133] Chen, Y., Chen, X., Xu, X., and Yu, G. (2018) Quantitative impacts of regenerative vibration and abrasive wheel eccentricity on surface grinding dynamic performance. *The International Journal of Advanced Manufacturing Technology,* **96**, 2271–2283.

[134] Mishra, V. K. and Salonitis, K. (2013) Empirical estimation of grinding specific forces and energy based on a modified Werner grinding model. *Procedia CIRP,* **8**, 287–292.

[135] Lichun, L., Jizai, F., and Peklenik, J. (1980) A study of grinding force mathematical model. *CIRP Annals – Manufacturing Technology,* **29**(1), 245–249.

[136] Durgumahanti, U. P., Singh, V., and Rao, P. V. (2010) A new model for grinding force prediction and analysis. *International Journal of Machine Tools and Manufacture,* **50**(3), 231–240.

[137] Sun, C., Niu, Y., Liu, Z., Wang, Y., and Xiu, S. (2017) Study on the surface topography considering grinding chatter based on dynamics and reliability. *The International Journal of Advanced Manufacturing Technology,* **92**(9-12), 3273–3286.

[138] Sun, C., Liu, Z., Lan, D., Duan, J., and Xiu, S. (2018) Study on the influence of the grinding chatter on the workpiece's microstructure transformation. *The International Journal of Advanced Manufacturing Technology,* **96**(9-12), 3861–3879.

[139] Hou, Z. B. and Komanduri, R. (2003) On the mechanics of the grinding process – Part I. Stochastic nature of the grinding process. *International Journal of Machine Tools and Manufacture,* **43**(15), 1579–1593.

[140] Chang, H. C. and Wang, J. J. J. (2008) A stochastic grinding force model considering random grit distribution. *International Journal of Machine Tools and Manufacture,* **48**(12-13), 1335–1344.

[141] Stępień, P. (2009) A probabilistic model of the grinding process. *Applied Mathematical Modelling,* **33**(10), 3863–3884.

[142] Nakayama, K., Brecker, J., and Shaw, M. C. (1971) Grinding wheel elasticity. *Journal of Engineering for Industry,* **93**(2), 609–613.

[143] Saini, D. P. and Brown, R. H. (1980) Elastic deflections in grinding. *CIRP Annals – Manufacturing Technology,* **29**(1), 189–194.

[144] Kumar, K. V. and Shaw, M. C. (1981) The role of wheel-work deflection in grinding operations. *Journal of Engineering for Industry,* **103**(1), 73–78.

[145] Rowe, W. B., Morgan, M. N., Qi, H. S., and Zheng, H. W. (1993) The effect of deformation on the contact area in grinding. *CIRP Annals – Manufacturing Technology,* **42**(1), 409–412.

[146] Qi, H. S., Mills, B., and Rowe, W. B. (1994) An analysis of real contact length in abrasive machining processes using contact mechanics. *Wear,* **176**(1), 137–141.

[147] Aslan, D. and Budak, E. (2014) Semi-analytical force model for grinding operations. *Procedia CIRP,* **14**, 7–12.

[148] Aslan, D. and Budak, E. (2015) Surface roughness and thermo-mechanical force modeling for grinding operations with regular and circumferentially grooved wheels. *Journal of Materials Processing Technology,* **223**, 75–90.

[149] Wiederkehr, P., Siebrecht, T., and Potthoff, N. (2018) Stochastic modeling of grain wear in geometric physically-based grinding simulations. *CIRP Annals,* **67**, 325–328.

[150] Li, Z., Zhang, F., Luo, X., Guo, X., Cai, Y., Chang, W., and Sun, J. (2018) A new grinding force model for micro grinding RB-SiC ceramic with grinding wheel topography as an input. *Micromachines,* **9**(8), 368–385.

[151] Snoeys, R., Peters, J., and Decneut, A. (1974) The significance of chip thickness in grinding. *CIRP Annals,* **23**(2), 227–237.

[152] Sims, N. D. (2017) Multi-frequency chatter analysis using the shift theorem. *Procedia IUTAM,* **22**, 3–9.

[153] Insperger, T. and Stépán, G. (2004) Updated semi-discretization method for periodic delay-differential equations with discrete delay. *International Journal for Numerical Methods in Engineering,* **61**(1), 117–141.

[154] Sims, N. D., Mann, B. P., and Huyanan, S. (2008) Analytical prediction of chatter stability for variable pitch and variable helix milling tools. *Journal of Sound and Vibration,* **317**(3-5), 664–686.

[155] Dorf, R. C. and Bishop, R. H. (2011) Modern control systems (thirteenth edition), Pearson, Harlow.

[156] Thomson, W. (1988) Theory of vibration with applications (third edition), Prentice Hall, New Jersey.

[157] Nyquist, H. (1932) Regeneration theory. *The Bell System Technical Journal,* **11**(1), 126–147.

[158] James, H. M., Nichols, N. B., and Phillips, R. S. (1947) Theory of servomechanisms, McGraw-Hill, New York.

[159] Rugh, W. J. (1996) Linear system theory, Prentice Hall, New Jersey.

[160] Desoer, C. and Wang, Y. T. (1980) On the generalized Nyquist stability criterion. *IEEE Transactions on Automatic Control,* **25**(2), 187–196.

[161] Yan, Y., Xu, J., and Wiercigroch, M. (2014) Chatter in a transverse grinding process. *Journal of Sound and Vibration,* **333**(3), 937–953.

[162] Li, H. and Shin, Y. C. (2006) A time-domain dynamic model for chatter prediction of cylindrical plunge grinding processes. *Journal of Manufacturing Science and Engineering,* **128**(2), 404–415.

[163] Hahn, R. S. (1993) Ceramic grinding with self-sharpening diamond wheels subjected to wheel-regenerative chatter. In *Proceedings of the 5th International Grinding Conference,* Paper MR93-344:1–12.

Appendix A

The Nyquist stability criterion

The Nyquist criterion is a robust method for assessing the stability properties of a dynamical system in the frequency domain. It was developed by Harry Nyquist in 1932, and remains a fundamental approach to investigating the stability of linear control systems to this day [157]. It can be applied in five steps as follows.

1. Initially, the mathematical description of the problem is required in the form of either a governing equation of motion or a number of expressions defining individual relationships between the system variables. This is typically calculated in the time domain first, and constitutes the starting point of the Nyquist stability criterion.

2. Since the Nyquist criterion operates in the frequency domain, the time-domain representation of the system has to be transformed into the frequency domain. This is usually done by the Laplace transform.

3. Based on the frequency-domain representation of the system, a block diagram can be constructed describing the flow of information between individual process variables. In dynamical systems that can be stable or unstable depending on the actual process parameters used, the block diagram typically contains a feedback loop, indicating that the current state of the system is influenced by its previous state as well.

4. Considering the block diagram, the open-loop transfer function of the system is fairly straightforward to determine. When it comes to the Nyquist stability criterion, the open-loop transfer function is typically calculated for a negative feedback loop. Since it is the sole direct input of the Nyquist criterion, the open-loop transfer function is all that is needed to assess the stability of the system.

5. The Nyquist stability criterion is based on Cauchy's theorem, more commonly known as the principle of the argument [158, 159]. According to Dorf and Bishop's summary of the theorem in [155], p. 629, it can be stated as follows: "If a contour Γ_s in the s-plane encircles Z zeros and P poles of $F(s)$ and does not pass through any poles or zeros of $F(s)$ and the traversal is in the clockwise direction along the contour, the corresponding contour Γ_F in the $F(s)$-plane encircles the origin of the $F(s)$-plane

$N = Z - P$ times in the clockwise direction." A graphical illustration of Cauchy's theorem is presented in Figure A.1.

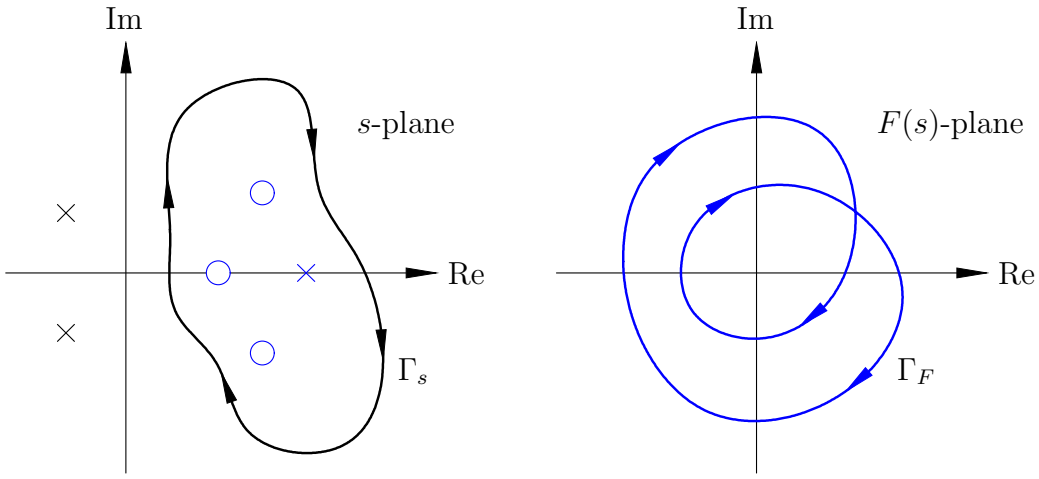

Figure A.1: A visual illustration of Cauchy's theorem ($Z = 3$, $P = 1$, $N = 2$)

In the statement above, $F(s)$ is the characteristic function, which gives the characteristic equation of the negative feedback system in the form

$$F(s) = 1 + T_o(s) = 0, \tag{A.1}$$

where $T_o(s)$ is the open-loop transfer function. Since the characteristic function is the denominator of the closed-loop transfer function, the system is stable if and only if $F(s)$ has no zeros with positive real parts. Due to the fact that the zeros of $F(s)$ can be not only difficult to calculate but also infinite in number, it is often impractical or even impossible to compute them directly. Therefore, the Nyquist criterion was developed to determine process stability without having to calculate all the zeros of $F(s)$. According to Cauchy's theorem, if the contour Γ_s is chosen in such a way that it encloses the entire right-hand side of the s-plane, the contour Γ_F in the $F(s)$-plane will provide sufficient information to determine the number of zeros of $F(s)$ with positive real parts, assuming that the number of poles of $F(s)$ encircled by Γ_s is known. And since the poles of $F(s)$ are typically much easier to compute than its zeros, this is a major reduction in the complexity of the stability analysis. Therefore, the Nyquist stability criterion is a special application of Cauchy's theorem, in which case Γ_s and Γ_F are called the Nyquist contour and the Nyquist plot, respectively.

Note: As illustrated in Figure A.2, the Nyquist contour consists of two parts: (1) the imaginary axis and (2) a semicircular arc of infinite radius that encloses the entire right-hand side of the s-plane. The infinite semicircle part of the Nyquist contour is usually disregarded in numerical simulations, as it typically maps to a single point in the Nyquist plot (according to [155], pp. 632-633).

Since Eq. (A.1) shows that the only difference between the characteristic function $F(s)$ and the open-loop transfer function $T_o(s)$ is an offset of one, it is possible to reformulate Cauchy's theorem for $T_o(s)$. In that case, it is not the encirclements of the origin of the $F(s)$-plane that are to be counted, but the encirclements of the $(-1, 0)$ point of the $T_o(s)$-plane. Every other aspect of the analysis is the same.

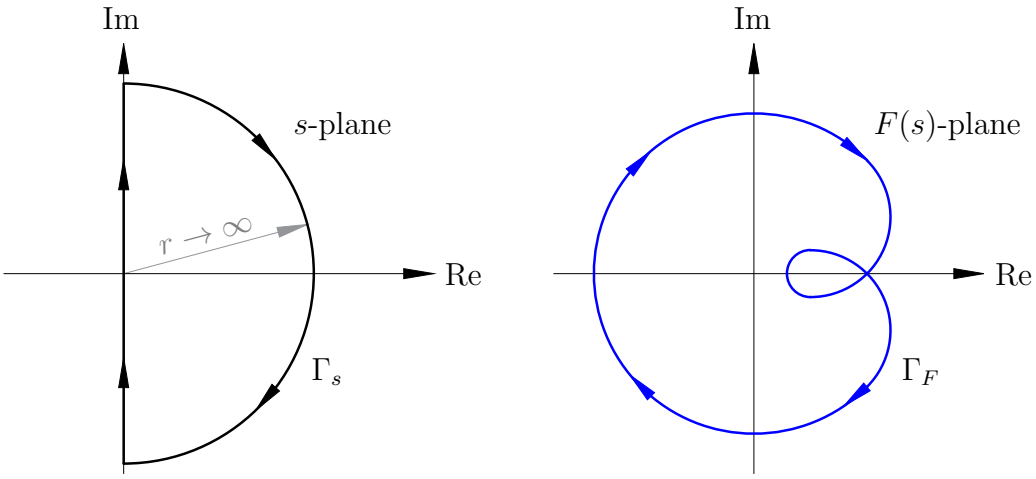

Figure A.2: Nyquist contour (left) and Nyquist plot (right)

According to [155], p. 633, the Nyquist criterion can be summarised as follows: "A feedback control system is stable if and only if, for the Nyquist plot of $T_o(s)$, the number of anticlockwise encirclements of the $(-1, 0)$ point is equal to the number of poles of $T_o(s)$ with positive real parts." That is because for a stable system $Z = 0$, so the condition for stability becomes $N = -P$, where the negative sign indicates anticlockwise encirclements of the $(-1, 0)$ point.

It is important to note that the Nyquist stability criterion can be extended to Multiple-Input-Multiple-Output (MIMO) systems as well. The result is the generalised Nyquist criterion [160], according to which the characteristic function can be calculated as

$$F(s) = \det(\mathbf{I} + \mathbf{T}_o(s)), \tag{A.2}$$

where $\mathbf{I}$ is the identity matrix and $\mathbf{T}_o(s)$ is the open-loop transfer function matrix. The rest of the analysis is identical to that of a Single-Input-Single-Output (SISO) system.

Appendix B

Summary of modelling assumptions

Throughout the formulation of the new grinding chatter theory presented in Chapter 5, the following modelling assumptions have been made:

1. A single-degree-of-freedom mechanical model of single-pass surface grinding is considered. Relative vibration between the wheel and the workpiece is allowed only in the direction of the depth of cut (i.e. normal to the workpiece surface). That is because wheel vibration in this direction has a direct effect on surface quality and dimensional accuracy. Wheel vibration in the direction of the feed rate (i.e. tangential to the workpiece surface) may have some effect on wheel vibration in the normal direction, but it is assumed to be small. This justification for single-degree-of-freedom modelling is largely based on Gurney's reasoning, who considered cylindrical plunge grinding and captured the relative motion between the wheel and the workpiece with a single variable [99]. A more sophisticated description of the wheel and the workpiece may necessitate the employment of two absolute coordinates instead of a single relative one (as in the work of Yan et al. on cylindrical traverse grinding [161]), but the dominance of normal vibrations is widely accepted in chatter modelling. ⟨*used on p. 66*⟩

2. A two-dimensional model of surface grinding is considered. This is a reasonable simplification since no grinding parameter varies significantly in the axial direction of the wheel. Such two-dimensional approaches are utilised in many grinding chatter theories, because they are sophisticated enough to describe the regenerative effect relatively accurately [100, 106, 108, 161, 162]. Nevertheless, more advanced grinding chatter theories have been developed as well, typically to capture self-excited vibration alongside some other complicating factor (e.g. workpiece imbalance). For example, the three-dimensional model of external cylindrical plunge grinding created by Yan, Xu and Wiercigroch is often used in their publications [116, 130, 132]. ⟨*used on p. 66*⟩

3. Linear damping and stiffness characteristics are assumed in the model. Therefore, each of these two components (i.e. dashpot and spring) is described by a single constant (c and k) in Figure 4.1. This is a typical approach in grinding chatter theory. Even non-linear models tend to make this assumption, focusing on other sources of non-linearities, such as the grinding force and large-amplitude vibrations [111–114]. ⟨*used on p. 66*⟩

4. Workpiece regeneration is neglected based on the findings reported in Chapter 4. According to the author's understanding of the relevant literature, the kind of short workpiece regeneration that is typical in milling (which is the only type that can occur in single-pass surface grinding) is scarcely, if ever, considered in grinding chatter theories. The phenomenon of workpiece regeneration is usually taken into account on a significantly larger time scale, such as the rotational or linear period of the workpiece in cylindrical grinding [101] or multi-pass surface grinding [106], respectively. Therefore, the regenerative effect in the proposed model is restricted to wheel regeneration alone. ⟨*used on p. 65*⟩

5. Distributed radial wear is neglected, i.e., a perfectly circular wheel is assumed throughout the entire grinding process. Therefore, the only mechanism responsible for wheel regeneration is the presence of distributed grit dullness characterised by specific energy waves around the circumference of the grinding wheel. This is a significant departure from mainstream grinding chatter research. A combination of these two sources of wheel regeneration (i.e. distributed radial wear and distributed grit dullness) was addressed in the work of Li and Shin [108], apart from which the literature focuses predominantly on distributed radial wear as the sole source of wheel regeneration in grinding (as presented in detail in Section 2.2). ⟨*used on p. 67*⟩

6. Individual cutting edges are not treated separately in the grinding force model, i.e., the formulation of the cutting force is based on the depth of cut instead of the chip thickness. This is a typical approach in grinding force modelling, although there are several chip-thickness-based methods as well (a few of which are mentioned in Section 2.2.4) that seek to capture the behaviour of individual cutting edges. Such models pay much attention to the accurate formulation of a single-grit force expression, then summarise them over all active grains in the grinding zone. ⟨*used on p. 66*⟩

7. Grains are modelled as evenly distributed triangles around the circumference of the grinding wheel. The grits are assumed to be straight and elongated in the axial direction of the wheel, in accordance with the two-dimensional nature of the model (Assumption 2). This approach is used only for the calculation of two parameters: the grit-passing period and the coefficient of dulling, i.e., the grinding force model remains a depth-of-cut-based one, as it was stated in Assumption 6. When it comes to grain models, triangular shapes are often employed, but rounded profiles are also used in process modelling [141]. An irregular grit distribution is typically considered in stochastic force models alone, which are rarely applied to grinding chatter problems (as discussed in Section 2.2.4.3 and summarised in Table 2.3). ⟨*used on p. 85*⟩

8. An idealised grinding force model is employed, which is one of the simplest ways to calculate the grinding force (more details on idealised grinding force models can be found in Section 2.2.4.1). The number of empirical constants is reduced to a minimum, and the stochastic nature of the process is neglected. As it was shown in Section 2.2.4, this is not the most widely used type of force model in chatter research, but the simplicity of this approach makes it easier to focus on the new regenerative mechanism, which is the primary objective of this work. ⟨*used on p. 66*⟩

9. The model makes no distinction between the three grinding mechanisms (i.e. sliding, ploughing and chip formation), so they are not treated separately in the formulation

of the specific energy. Similarly to Assumption 8, this modelling choice serves the purpose of shifting the focus towards the new regenerative mechanism by simplifying a secondary aspect of the problem. Nevertheless, most grinding chatter theories use empirical force models (according to Table 2.3), which tend to distinguish between the three grinding mechanisms. Consequently, depending on the sophistication of the empirical force model to which it is compared, this particular simplification constitutes a certain degree of departure from typical chatter research. ⟨*used on p. 66*⟩

10. The grinding force is calculated by integrating the specific energy distribution in the cutting zone according to two averaging methods: the arithmetic mean and the weighted mean. Since this approach is closely tied to the novelty of the thesis, it does not appear in the literature in analytical form. The work of Li and Shin [108] bears the closest resemblance to it, but theirs is a numerical model that was created by discretising the circumference of the grinding wheel. In contrast, the current theory assumes a continuous specific energy distribution around the circumference of the grinding wheel (based on the large number of cutting edges inherently involved in the process) and addresses the problem in an analytical fashion. ⟨*used on p. 74*⟩

11. Of the two averaging methods mentioned in Assumption 10, the arithmetic mean is chosen for its simplicity to assess stability. The weighted mean is not investigated in detail in this thesis, however, a simple simulation is presented here to compare the two approaches. Figure B.1 shows the specific energy distribution around the circumference of the grinding wheel for both averaging methods. Three main observations are made regarding these results: (1) both methods predict instability for the grinding parameters considered, (2) the number of specific energy waves on the wheel is slightly different in the two cases (five and six for the arithmetic mean and weighted mean

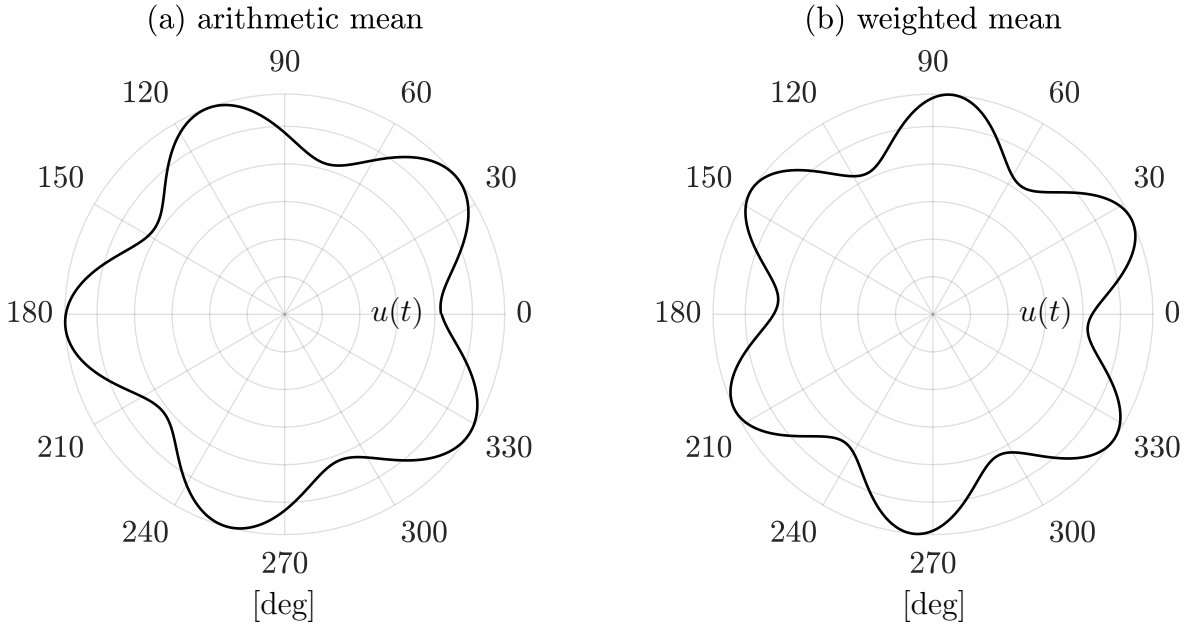

Figure B.1: Specific energy distribution around the circumference of the grinding wheel for two ways of averaging the specific energy in the cutting zone ($\omega_g = 3100$ rpm, $\delta_0 = 21$ mm, every other parameter is listed in Table 5.2)

approaches respectively), which is directly related to the theoretical chatter frequency, and (3) the rate of chatter development predicted by each method is significantly different: the arithmetic mean produced detectable instability (i.e. a chatter amplitude of approximately 20 N in the grinding force spectrum) after 1.39 minutes of grinding time, whereas the weighted mean took 2.65 hours of grinding time to reach the same level of unstable vibration. Since the two approaches show not only similarities but considerable differences as well, the in-depth analysis of the weighted mean method is encouraged in future research. ⟨*used on p. 79*⟩

12. The ratios between the cutting force components (i.e. $\mu = F_t/F_n$ and $\mu_x = F_x/F_t$) are assumed to remain constant throughout the entire machining process. In other words, the cutting force components are assumed to grow in proportion to one another. Since the ratios between the cutting force components change in the presence of grinding burn (as demonstrated in [11], p. 126), this assumption means that grinding burn cannot be adequately accounted for by the proposed model. However, this limitation is typical in chatter theories, as the effect of grinding burn is usually neglected. ⟨*used on p. 67*⟩

13. The specific energy is a single-variable function of time. At the current time, it corresponds to the grain that is just leaving the grinding zone (as illustrated in Figure 5.1). This modelling choice simplifies the description of the specific energy (which varies in both space and time) without limiting the accuracy of the model. Therefore, strictly speaking, this is not so much an assumption as an important aspect of modelling to keep in mind. More details can be found in Section 5.1.2. ⟨*used on p. 68*⟩

14. The specific energy function is constant along the axial direction of the grinding wheel. This assumption is a direct consequence of the two-dimensional description of the grinding system (Assumption 2). ⟨*used on p. 68*⟩

15. The self-sharpening property of the grinding wheel is neglected. This assumption is often made in chatter analysis, although some models take the self-sharpening effect into account (e.g. [163]). With regard to the current theory, this means that the specific energy never decreases. It increases inside the grinding zone as a result of grit wear, and remains constant outside. ⟨*used on p. 68*⟩

16. The relationship between the material removal rate and the specific energy increase is assumed to be linear, just as in Li and Shin's model [108]. ⟨*used on p. 72*⟩

17. Wheel vibration does not change the chip thickness, only the depth of cut. This corresponds to the fact that the grinding force is based on the depth of cut instead of the chip thickness (Assumption 6). Furthermore, wheel vibration affects the depth of cut as if the yet-to-be-ground workpiece surface were oscillating relative to a stationary grinding wheel (according to Figure 5.2). This assumption simplifies the formulation of the time-varying cutting force expression. Such a description is not particularly common in grinding chatter research, but it is still capable of accounting for the regenerative effect. Therefore, it is a compromise between accuracy and simplicity. ⟨*used on p. 69*⟩

18. The grinding parameters pertaining to the cutting zone (e.g. depth of cut, entering and exiting angles, contact angle, etc.) are assumed to be their steady-state versions when

it comes to calculating the specific energy distribution in the grinding zone and the resulting cutting force. This assumption is rather substantial, but it does not eliminate the regenerative effect from the model. The grinding force can still vary, because the specific energy distribution in a nominal-sized cutting zone is still influenced by the depth-of-cut-dependent material removal rate. In other words, the grinding zone is assumed to be of nominal size only in the calculation of the cutting force. That is to simplify the grinding force expression in order to avoid having to deal with the complexities of a non-linear force model. ⟨*used on p. 73*⟩

19. Because of the filtering effect, the Nyquist contour is calculated only up to $\pm 2\pi/\tau_{c,0}$, which is the frequency corresponding to the nominal contact time (i.e. the amount of time a grain takes to pass through the contact zone under steady-state grinding conditions). Since wave patterns with a higher frequency are unlikely to form, the Nyquist contour is capped at this critical frequency. This is a reasonable simplification considering the practical limitations of wave formation on the grinding wheel. ⟨*used on p. 79*⟩

Appendix C

MATLAB code for stability analysis

The following code calculates the stability boundaries of single-pass surface grinding based on the author's new theory presented in Chapter 5.

```
clear;clc

%% Grinding parameters according to Table 5.2:

% Modal parameters of the wheel:
m = 1; % modal mass [kg]
zeta = 0.01; % damping ratio [1]
wn = 300*2*pi; % natural frequency [rad/s]=[Hz]*2*pi

% Wheel and workpiece parameters:
Rg = 100/1000; % wheel radius [m]
w = 20/1000; % grinding width [m]
Z = 10000; % number of cutting points on the wheel [1]
Cd = 4e21; % coefficient of dulling [J/m^3/m^2]
mu = 0.4; % coefficient of friction (=Ft/Fn) [1]
vw = 56/1000/60; % workpiece feed [m/s]=[mm/min]/1000/60

%% Limits and resolution of the stability map:

wg_min = 500/60*2*pi; % minimum wheel speed [rad/s]=[rpm]/60*2*pi
wg_max = 5000/60*2*pi; % maximum wheel speed [rad/s]=[rpm]/60*2*pi
wg_n = 1000; % wheel speed resolution [1]
wg_v = linspace(wg_min,wg_max,wg_n); % vector of wheel speeds

doc_min = 0.03/1000; % minimum depth of cut [m]
doc_max = 30/1000; % maximum depth of cut [m]
doc_n = 500; % depth of cut resolution [1]
doc_v = linspace(doc_min,doc_max,doc_n); % vector of depths of cut
```

```
X = zeros(wg_n,doc_n); % x-axis of the stability map (wheel speed)
Y = zeros(wg_n,doc_n); % y-axis of the stability map (depth of cut)
enc = zeros(wg_n,doc_n); % encirclements of the (0,0) position

%% Numerical simulation:

for wg_k = 1 : wg_n % for-loop for the wheel speeds
for doc_k = 1 : doc_n % for-loop for the depths of cut

% Calculated parameters:
wg = wg_v(wg_k); % current wheel speed [rad/s]
doc = doc_v(doc_k); % current depth of cut [m]
Tg = 2*pi/wg; % wheel period [s]
tau_g = Tg/Z; % grit-passing period [s] (regular grain distribution)
vg = wg*Rg; % wheel circumferential speed [m/s]
phi_c0 = acos(1-doc/Rg); % nominal contact angle [rad]
tau_c0 = phi_c0/wg; % nominal grit contact time [s]
cos_a = (1+cos(phi_c0))/2; % cos of the grinding force angle
sin_a = sqrt(1-cos_a^2); % sin of the grinding force angle
mux = -sin_a + 1/mu*cos_a; % =Fx/Ft (up-grinding)
wmax = 2*pi/tau_c0; % limit frequency due to the filtering effect

% Generation of the Nyquist contour according to Figure 5.7:
eps = 1e-3; % detour radius around each pole (tending to zero)
n_w = 150; % base frequency resolution (within wg)
dw = (wg-2*eps)/n_w; % frequency step size [rad/s]
n_a = 25; % base angular resolution (within pi/2)
da = pi/2/n_a; % angular step size [rad]

% Creating the base Nyquist element between two poles:
ang = (da:da:pi/2-da); % angle vector
uha_x = eps*cos(ang); % upper half-arc (x)
uha_y = eps*sin(ang); % upper half-arc (y)
lha_x = eps*cos(fliplr(-ang)); % lower half-arc (x)
lha_y = eps*sin(fliplr(-ang))+wg; % lower half-arc (y)
mid_x = linspace(0,0,n_w+1); % middle part (x)
mid_y = (eps:dw:wg-eps); % middle part (y)
base_x = [uha_x,mid_x,lha_x]; % base Nyquist element (x)
base_y = [uha_y,mid_y,lha_y]; % base Nyquist element (y)

% Building the Nyquist contour from its base elements:
kmax = floor(wmax/wg); % kmax*wg is just below (or equal to) wmax
s_x = base_x;
s_y = base_y;
for k = 1 : kmax-1
  s_x = [s_x,base_x];
  s_y = [s_y,base_y+k*wg];
end
```

```
% Completing the Nyquist contour all the way to wmax:
s_x = [s_x,uha_x,linspace(0,0,round((wmax-(kmax*wg+eps))/dw))];
s_y = [s_y,uha_y+kmax*wg,linspace(kmax*wg+eps,wmax,round((wmax-...
      (kmax*wg+eps))/dw))];
% Including negative frequencies (going from negative to positive):
s_x = [fliplr(s_x),s_x];
s_y = [-fliplr(s_y),s_y];
% Total length of the Nyquist contour:
s_n = length(s_x);

% Stability analysis:
F = zeros(1,s_n/2); % half of the char. func. (due to symmetry)
for s_k = 1 : s_n/2
  s = s_x(s_k)+1i*s_y(s_k); % complex Laplace frequency
  J = Cd*vw*tau_g/(1-exp(-s*Tg)); % Eq.(5.36)
  Ha = mux*doc*w*vw/tau_c0/vg*exp(-s*Tg)*(exp(s*tau_c0)-1)/s; % Eq.(5.37)
  G = 1/m/(s^2+2*zeta*wn*s+wn^2); % Eq.(5.39)
  F(s_k) = 1 + J*Ha*G; % Eq.(5.42)
end
F2 = [F,fliplr(conj(F))]; % completing the characteristic function

X(wg_k,doc_k) = wg*60/2/pi; % x-axis: wheel speed [rpm]
Y(wg_k,doc_k) = doc*1000; % y-axis: depth of cut [mm]
enc(wg_k,doc_k) = encirclements(F2); % encirclements around (0,0)
end % end of the for-loop for doc
disp(wg_k/wg_n*100) % counter
end % end of the for-loop for wg

%% Stability boundaries:

figure
contour(X,Y,enc,[1,1],'k')
pbaspect([2 1 1])
xlim([wg_min*60/2/pi,wg_max*60/2/pi])
ylim([doc_min*1000,doc_max*1000])
xlabel('Wheel speed [rpm]')
ylabel('Depth of cut [mm]')
```

```
%% The ‘‘encirclements’’ function:

function enc = encirclements(F) % F = characteristic function
L = length(F);
% Potential origin-crossing (1st test):
if sum(F==0) > 0 % if there is at least one F=0
  disp(‘Origin-crossing!’)
  enc = NaN;
  return
end
ph = angle(F); % phase angle of each element of F: (-pi,+pi]
dph = zeros(3,L); % phase angle differences
  dph(1,1:end-1) = -diff(ph);
  dph(1,end) = ph(end)-ph(1);
  dph(2,:) = dph(1,:)+2*pi;
  dph(3,:) = dph(1,:)-2*pi;
% Potential origin-crossing (2nd test):
int = (-pi<dph)&(dph<pi); % permissible interval
if sum(sum(int,1)) < L % if there is at least one empty set
  disp(‘Origin-crossing!’)
  enc = NaN;
  return
end
DPH = sum(dph.*int,1); % real phase angle differences
enc = round(sum(DPH)/(2*pi)); % rounded to avoid numerical inaccuracies
end
```